# The geochemistry of Re and Os in ultramafic rocks from the Pyrenees and Massif Central, France.

## Thesis

UNRESTRICTED

# THE GEOCHEMISTRY OF RE AND OS IN ULTRAMAFIC ROCKS FROM THE PYRENEES AND MASSIF CENTRAL, FRANCE

A THESIS SUBMITTED FOR THE DEGREEE OF DOCTOR OF PHILOSOPHY


**OLIVER MARCUS BURNHAM**
**B.A. (Hons) Cantab 1988**

Department of Earth Sciences
Open University


May 1995



Date of submission : 10th May 1995
Date of award : 7th September 1995

"Son, be not over hasty, I exalt our med'cine,
By hanging him in *balneo vaporoso*,
And giving him solution; then congeal him;
And then dissolve him; then again congeal him;
For look, how oft I iterate the work,
So many times, I add unto his virtue."

*(The Alchemist, II iii 102-107)*

# Abstract

The Re and Os contents and Os isotopic compositions of spinel peridotites derived from the continental mantle lithosphere underlying central and south-western France were investigated with the dual aims of determining the factors which control the behaviour of the elements during geological processes and investigating the early evolution of a region of non-cratonic lithosphere. Samples were obtained from the orogenic massifs of the N.E. Pyrénées and a suite of mantle xenoliths erupted by the basalts of the Massif Central.

Before the Re-Os isotope study could be carried out, methods for the determination of Re and Os abundances and Os isotope ratios in samples possessing low concentrations of these elements had to be established. Initially a procedure using ICP-MS for the final analysis was employed, however, in view of its significantly better precision, most analyses were eventually performed by N-TIMS. Whilst within-run precisions of better than 1‰ could be routinely obtained for $^{187}Os/^{188}Os$ ratios determined by the N-TIMS technique, owing to an unidentified interference, the uncertainty in the sample ratios was closer to 1%.

Thermochemical calculations of the stabilities of the oxide and sulphide species of Re, Os and the other Pt-group elements (PGE) confirm that the base-metal sulphide phase present in most mantle peridotites should dominate the geochemistry of Re and Os, both within the mantle and during the transport of the peridotites to the surface. Modelling of the Re abundances in the N.E. Pyrenean massifs indicates that, during melting, Re is significantly less compatible in the mantle sulphide phase than the PGE, with a sulphide-silicate partition coefficient similar to that of Cu.

Modelling of the whole-rock elemental compositions of the peridotites collected from the N.E. Pyrénées and Massif Central indicates that the range of compositions may be consistent with a process of two component mixing or unmixing, involving either the extraction of a melt from a fertile mantle source or the refertilisation of depleted mantle material. Although the two processes cannot be resolved using the available lithophile element data, the whole-rock S contents of the Pyrenean peridotites favour a model involving variable degrees of melt extraction. Modelling of the HREE contents of the peridotites of the Pyrenean massifs indicates that such melting may have occurred close to the spinel-garnet phase transition.

The $^{187}Os/^{188}Os$ ratios of peridotites from both the N.E. Pyrénées and Massif Central range from values close to those estimated for the bulk-Earth mantle (0.12711; Walker *et al.*, 1994) to ~0.1193. Minimum model ages calculated from these ratios show that parts of the French mantle lithosphere have been stable since at least the mid-Proterozoic. These model ages are consistent with a ~2 Ga Re-Os isochron age obtained for the peridotites of the N.E. Pyrénées and coincide with both U-Pb and Nd model-ages for the western European basement. Given the postulated susceptibility of non-cratonic mantle lithosphere to delamination processes during periods of tectonic activity, the observed preservation of such mantle since the early Proterozoic is noteworthy, indicating that delamination either does not affect the whole mantle lithosphere, or may be less common than originally thought. This study also shows that the evolution of the crust and mantle components of non-cratonic continental lithosphere may be coupled, indicating a causative link between their formations.

# Acknowledgments

Whilst pursuing this research project I benefited from the help, guidance and companionship of numerous people both at the O.U. and elsewhere, for which I shall be forever grateful and to whom I would like to express my thanks.

First of all, I thank Nick Rogers and Phil Potts, my supervisors, for the words of advice they offered me throughout the project and for the rapid return of early drafts of chapters. I also gratefully acknowledge the NERC grant which enabled me to carry out the research. I must compliment Nick for his powers of persuasion, pandering, as he did, to my sense of adventure and convincing me that this project was not as great a folly as it initially appeared. I also thank Hilary Downes at Birkbeck College for the Massif Central xenolith material used in the project.

I also owe many thanks to those who helped with the technical aspects of the project: I thank Conrad Grégoire of the Geological Survey of Canada for his time and patience during my initial experimentations with Os distillations and ICP-MS analysis; Kym Jarvis, John Williams and Julian Wills of the NERC ICP-MS facility for their time and efforts during the development of the ICP-MS technique; Andy Smith at Leicester for total C and S determinations; John Watson and Pete Webb at the O.U. for XRF analysis and access to numerous reference materials; Kay Chambers for thin sections and Phil Bland for the use of the camera on which the micrographs were shot. For help in the field, I would especially like to thank Phil G.; he was an excellent chauffeur, guide, cook and drinking partner, all for a few sous per day.

I am specially grateful to Graham Pearson and Charlie Gowing for services above and beyond the call of duty. Graham's endless advice (tempered with considerable Yorkshire practicality) about N-TIMS analysis, processes within the mantle lithosphere and which pubs served the best beers was most gratefully received, as were Charlie's numerous words of advice concerning the analysis of the Pt-group elements at low levels and the setting up of a laboratory.

I would like to thank all those who also worked in the radiogenic laboratory, both for their on-going company and for the numerous lab. parties to celebrate birthdays, thesis submissions, successful *vivas*, grant awards or simply the fact that there had not been a lab. party for some time. For all-round help in the laboratory, encouragement, gossip and her hospitality to the waifs and strays of the department, I would particularly like to thank Mabs Johnston, without whose presence life in the radiogenic laboratory would not have been half the fun its was.

Thanks go to all those who have shared accommodation with me in Milton Keynes: Reza Zemani, for taking me in at such short notice at the start of the project; Josanne and John, for

helping me throw the most significant party in my whole time in M.K. and Jessica, Sam and Martin for putting up with my compulsive tidiness in the kitchen. I also thank all those who shared an office with me (Arlëne, John, Charlie, Mark, Yiming, Jason, Fran, Kate and Jessica) and apologise for all the sudden outbursts, ravings and gratuitous questions. Particular thanks go to Arlëne for four years of fun, friendship and fondues.

For maintaining my insanity throughout the later parts of the project I thank the Village: in particular Vaurien, Rhiannon, Aelthric, Rowan, Keirik and Thorrun.

Whilst enormous thanks go to my parents, to my mother for her support (financial, emotional and intellectual) throughout the project and to my father for encouraging my early tendencies to explore and research, most of all I want to thank Jo for her love and patience through both the good times and the bad: I thank her for not giving me an excuse to quit when I may have wanted it, but giving me the incentive to finish when I was in need.

# Table of Contents

# List of Figures

## CHAPTER 1



## CHAPTER 2



## CHAPTER 3

## CHAPTER 4

## CHAPTER 5

## CHAPTER 6

# List of Tables

## CHAPTER 5



## APPENDICES

# List of Plates

## CHAPTER 3



## CHAPTER 4

# Chapter 1

# Re-Os Isotope Systematics and the Continental Mantle Lithosphere

## 1.1 The Re-Os Isotope System

In 1948, Naldrett & Libby discovered that the element Re was a weak natural ß-emitter, its major isotope, $^{187}Re$, decaying to form a minor isotope of Os according to the equation

$$^{187}Re \rightarrow {}^{187}Os + \beta^- + \bar{\nu} + Q \qquad \textbf{(Eqn. 1.1)}$$

Although initial attempts to quantify the half-life of $^{187}Re$ were unsuccessful, owing to the low end-point energy of the emitted beta radiation (~2.5 keV), values obtained using the Os isotope ratios of molybdenites of known age, iron and chondrite meteorites and concentrated laboratory solutions of Re all yielded estimates of ~43 Ga (Hirt *et al.*, 1963; Luck *et al.*, 1980; Luck & Allègre, 1983; Lindner *et al.*, 1986, 1989). While the long half-life of $^{187}Re$ alone demonstrates that the Re-Os isotope system has potential applications in both geochronology and cosmochronology, falling as it does within the range of half-lives of the well-established Rb-Sr, Sm-Nd and U-Pb techniques, the unusual geochemistry of the two elements indicate that the Os isotope systematics of mantle rocks and mantle-derived melts may provide a unique perspective on a variety of geological processes.

### 1.1.1 Geochemistry of Re and Os

Although considerable uncertainty exists concerning the detailed behaviour of Re and Os during geological processes, the two elements appear to be predominantly either siderophile or chalcophile under most conditions, consistent with their positions in Groups VIIB and VIIIB of the periodic table. The siderophile / chalcophile natures of the two elements suggest that they may be used to investigate a range of geochemical processes which are either inaccessible to the established incompatible element isotopic techniques (owing to their low concentrations or the effects of subsequent alteration) or may have affected the sulphide,

metal or silicate phases differently. Such processes would include those within the mantle lithosphere, where the concentrations of both Re and Os are relatively high compared to those in crustal rocks and sulphide phases are present in all but the most depleted harzburgites (Lorand, 1991).

| Sample Type | Re (ppb) | Os (ppb) | Re/Os |
|---|---|---|---|
| Meteorites | | | |
| Basaltic Achondrites [a] | 0.0004 - 0.0313 | 0.004 - 0.358 | 0.07 - 0.22 |
| Chondrites [a] | 25 - 48 | 314 - 585 | 0.095 - 0.125 |
| C1 Chondrite [b] | 35.8 | 517 | 0.069 |
| Irons [c,d] | 240 - 4800 | 13 - 65000 | 0.061 - 0.21 |
| Mantle Rocks | | | |
| Ultramafic Xenoliths [e,f] | b.d.l. - 0.264 | 1.1 - 6.9 | 0.002 - 0.074 |
| Orogenic Peridotites [g] | 0.019 - 0.45 | 3.2 - 6.7 | 0.004 - 0.089 |
| Primitive Mantle Estimate [b] | 0.26 | 3.1 | 0.083 |
| Pyroxenite Layers [g] | 0.19 - 1.56 | 0.005 - 1.15 | 0.97 - 56 |
| Igneous Rocks | | | |
| Komatiites [h] | 0.54 - 1.27 | 1.0 - 2.2 | 0.36 - 1.33 |
| Ocean Island Basalts [i,j] | 0.008 - 1.621 | 0.001 - 0.750 | 0.4 - 202 |
| MORB [k] | 0.322 - 1.17 | 0.002 - 0.25 | 2.6 - 49 |
| Kimberlites [f] | 0.13 - 1.73 | 0.66 - 1.91 | 0.07 - 2.7 |
| Granites / Granitic Gneisses [l,m] | 0.04 | 0.01 - 0.02 | 2.24 - 4.65 |
| | 0.076 - 0.125 | 0.004 - 0.007 | 17.5 - 22.6 |
| Sediments | | | |
| Terrigenous Sediments [n] | – | 0.015 - 0.09 | – |
| Pelagic Clay [o,p] | b.d.l. - 0.1 | 0.14 | < 1.4 |
| Black Shales [q] | 21 - 85 | 0.23 - 0.69 | 95 - 290 |
| Ave. Continental Crust [o] | 0.4 - 0.6 | 0.05 | ~400 |

**Table 1.1** Re and Os concentrations of meteorites and terrestrial rocks. References: [a] Birck & Allègre, 1994; [b] Morgan, 1986; [c] Luck & Allègre, 1983; [d] Morgan *et al.*, 1992; [e] Morgan *et al.*, 1981; [f] Walker *et al.*, 1989a; [g] Reisberg *et al.*, 1991; [h] Walker *et al.*, 1988; [i] Reisberg *et al.*, 1993; [j] Hauri & Hart, 1993; [k] Roy-Barman & Allègre, 1994; [l] Walker *et al.*, 1989b; [m] Walker *et al.*, 1991; [n] Esser & Turekian, 1993; [o] Koide *et al.*, 1987; [p] Esser & Turekian, 1988; [q] Ravizza *et al.*, 1991.

The two most striking features of the mantle geochemistry of Re and Os are firstly their extremely low concentrations relative to those of meteorites (< 1%), yet chondritic ratios in undepleted peridotite samples and secondly the intense fractionation of Re from Os during mantle melting processes, leading to a difference of several orders of magnitude in the Re/Os ratios of mantle-melts and their residues (Table 1.1 and Figure 1.1).

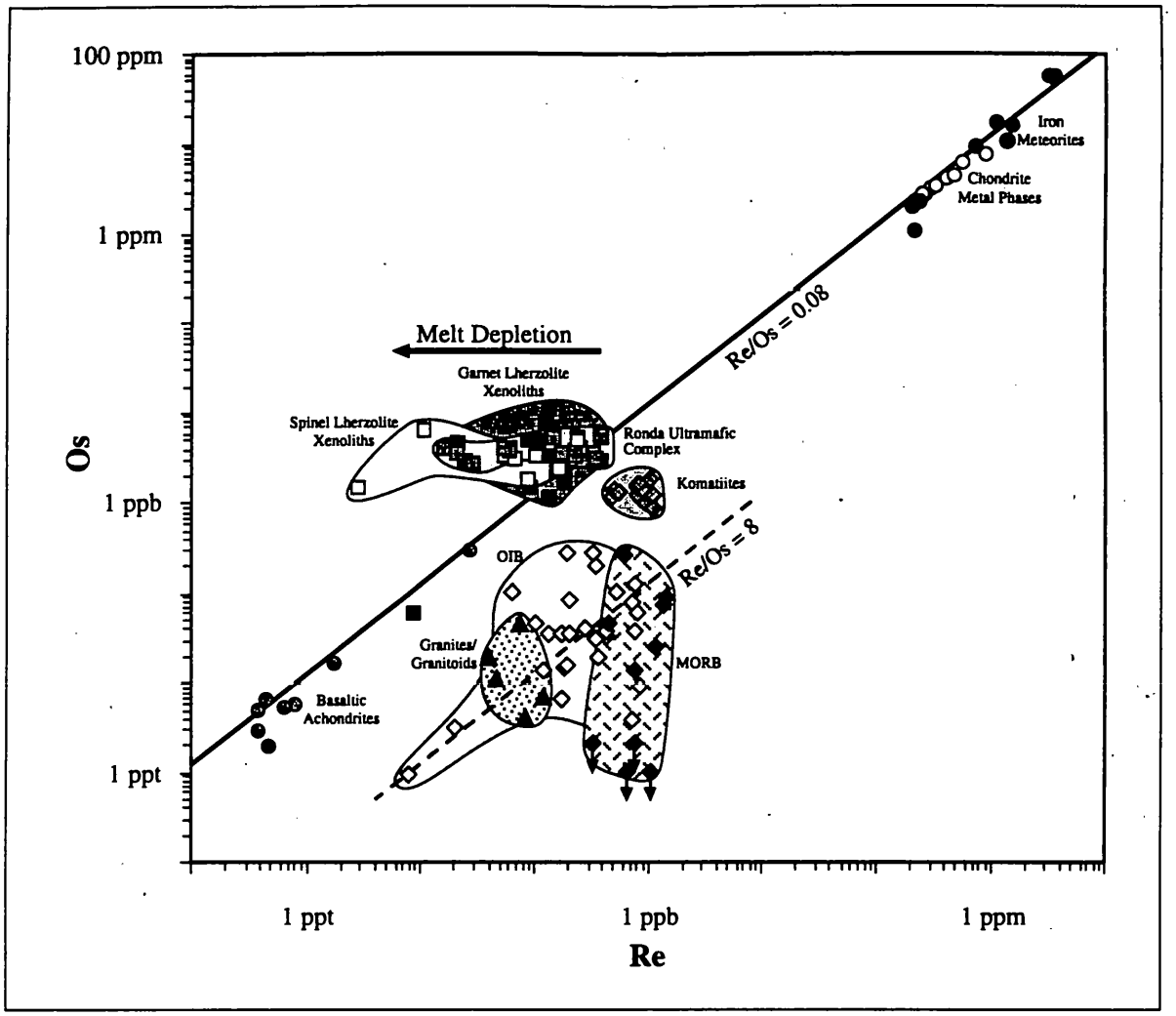


**Figure 1.1** Os *vs.* Re abundances in meteorites, mantle samples and mantle derived melts demonstrating the chondritic Re/Os ratios in the mantle, but extreme fractionation of Re from Os during melting. Sources of data are given in Table 1.1. Additional data: MORB, Hertogen *et al.* (1980); OIB, Martin (1991).

### *Re and Os Abundances in Meteorites and the Earth's Mantle*

Although the significant depletions of Re and Os in the upper mantle relative to meteorites are similar to those observed for the other highly siderophile elements (e.g. the Pt-group elements, Au and Ge; Arculus & Delano, 1981), and may be interpreted as the result of the extraction of these elements into the metallic core during its differentiation from the mantle, the roughly chondritic ratios between the Re and Os abundances of undepleted mantle material (in addition to chondritic ratios between the other siderophile elements) are inconsistent with the range of silicate-metal distribution coefficients determined for the elements (Kimura *et al.*, 1974; Jones & Drake, 1986). The preservation of chondritic ratios between the highly siderophile elements has been used to suggest that, following core-mantle separation, small amounts of meteoritic material were added to the Earth's mantle,

establishing the current siderophile element abundances (e.g. Kimura *et al.*, 1974; Chou, 1978; Jagoutz *et al.*, 1979; Arculus & Delano, 1981).

By comparing the noble metal patterns of a number of mantle xenoliths with those of different groups of meteorites, Morgan (1986) determined that the added material may have had a siderophile composition similar to that of the CM2 chondrites. Although this model can account for the relative abundances of most of the siderophile elements, it is inconsistent with estimates of the Re/Os ratio of the mantle, both from ultramafic xenoliths Morgan (1986) and from the mantle-evolution curve defined using the Os isotopic compositions of mantle-derived Os-bearing alloys of known age (Figure 1.2; Allègre & Luck, 1980; Luck & Allègre, 1991). Although it is possible that the material added during the late-stage accretion event was a mixture of meteorites possessing a range of Re/Os ratios (e.g. predominantly material resembling the CM2 chondrites, but with a component of H-type material which raised the Re/Os ratio to the bulk mantle value proposed by Allègre & Luck (1980)), the range of Os isotope ratios found in recently erupted basalts does not sufficiently constrain the Re/Os ratio of the mantle source, so that the exact type of meteoritic material may be accurately determined.

***Fractionation of Re/Os Ratios During Mantle Melting***

Whilst the Re/Os ratios of undepleted mantle material do not seem to be significantly fractionated relative to the range of Re/Os found in chondrites, during mantle melting the two elements appear to behave quite differently, leading to potentially extreme fractionation of the Re/Os ratio. During most degrees of partial melting Re behaves as a mildly incompatible element, with melt concentrations slightly greater than those in the mantle source. In contrast, for low to moderate degrees of melting, Os appears to be highly compatible in the mantle residue, with melt concentrations 2 - 3 orders of magnitude less than those in the source (Table 1.1). At higher degrees of melting, such as those required for the production of komatiites, however, the compatibility of Os appears to decrease and magmas may contain ppb-levels of Os.

To demonstrate the consequences of the contrasting compatibilities of Re and Os during mantle melting, the evolution of the Re-Os isotope systematics of some hypothetical melts and residues are illustrated in Figure 1.2. On account of the compatibility of Os during

mantle melting, the Re/Os ratios of most magmas are significantly greater than those of the mantle source, leading to the rapid growth of their $^{187}Os/^{188}Os$ ratios. Because such melts ultimately form either the oceanic or continental crust, almost all crustal rocks are characterised by low Os and mantle-like Re contents, leading to highly radiogenic average crustal $^{187}Os/^{188}Os$ ratios (e.g. 10 - 11 for the average continental crust; Esser & Turekian, 1993). In contrast to the melt, the depleted mantle residue evolves with a Re/Os ratio less

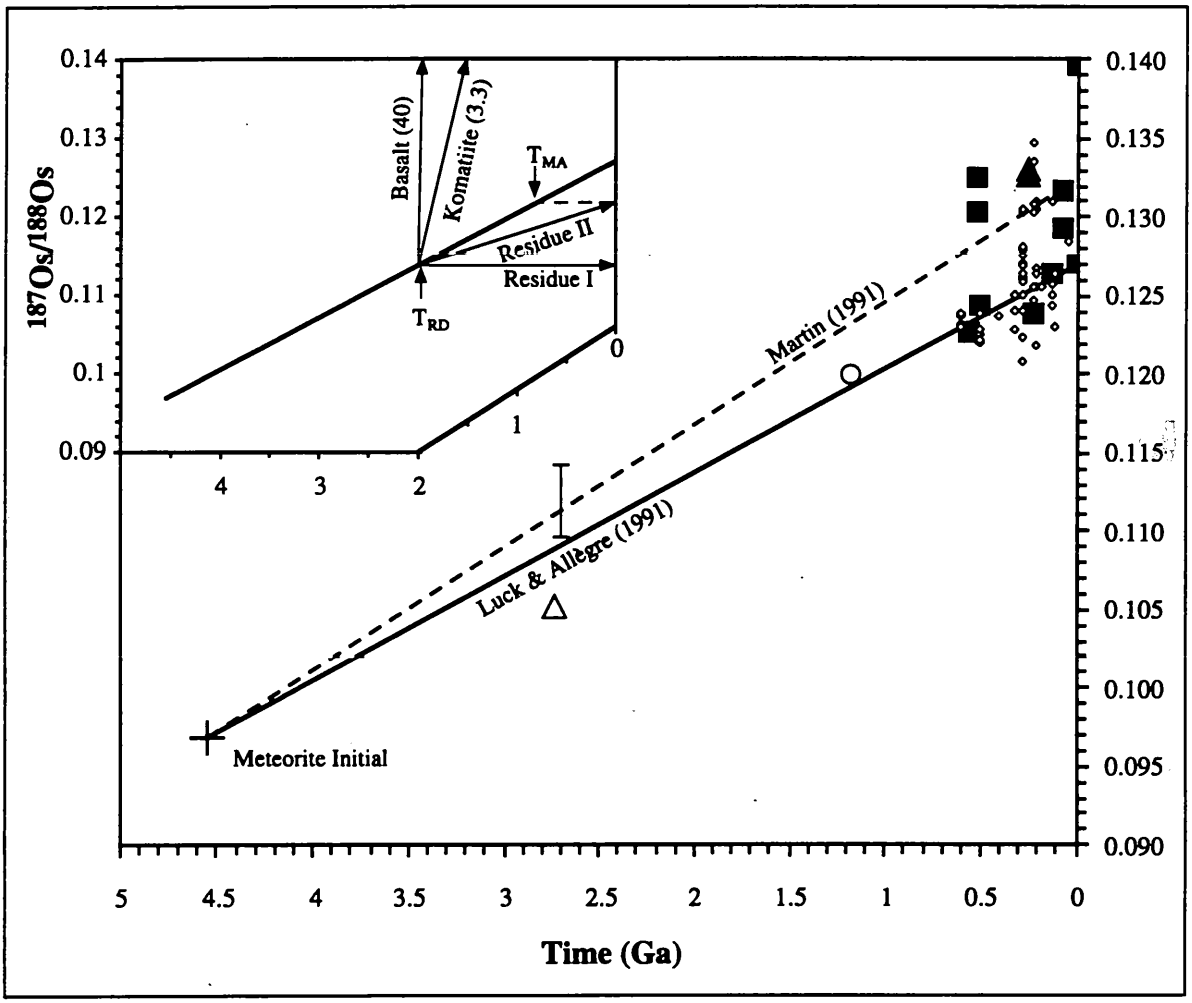


**Figure 1.2** Evolution of the mantle $^{187}Os/^{188}Os$ ratio through time showing two possible single-stage curves. Heavy solid line, mantle evolution curve of Luck &Allègre (1991), corresponding to a present day $^{187}Os/^{188}Os$ ratio of 0.12697 ($^{187}Os/^{186}Os$ = 1.055) and $^{187}Re/^{188}Os$ of 0.4 ($^{187}Re/^{186}Os$ = 3.32); heavy dashed line, plume-source mantle evolution curve of Martin (1991), corresponding to a present day $^{187}Os/^{188}Os$ ratio of 0.1324 ($^{187}Os/^{186}Os$ = 1.10) and $^{187}Re/^{188}Os$ of 0.49 ($^{187}Re/^{186}Os$ = 4.1). △, Pyke Hill komatiites, (Walker *et al.*, 1988); ○, Ronda Ultramafic Complex (Reisberg *et al.*, 1991); ■, osmiridium alloys and ophiolites used by Luck & Allègre (1991); ◇, osmiridium alloys associated with ultramafic intrusions (Hattori & Hart, 1991); ▲, Noril'sk, Talnakh and Kharaelakh intrusions, Siberia (Walker *et al.*, 1994); bar, chromites of the Stillwater Complex, Montana (Marcantonio *et al.*, 1993).
The inset illustrates the calculated evolution of the $^{187}Os/^{188}Os$ ratios in two mantle melts and their residues, formed at 2 Ga (melt $^{187}Re/^{188}Os$ ratios in parentheses). Residue I produced by the extraction of 30-40% komatiitic melt, entirely depleting the mantle in Re ($^{187}Re/^{188}Os_{residue}$ = 0), whilst Residue II formed by the extraction of ~15% basalt ($^{187}Re/^{188}Os_{residue}$ = 0.24). Residue II is used to illustrate the two model ages ($T_{RD}$ and $T_{MA}$).

than that of the original source, leading to a $^{187}Os/^{188}Os$ ratios less than that of the bulk Earth. In an extreme case, the Re contained within the mantle source may be wholly removed by large degrees of melt extraction, resulting in no evolution of the $^{187}Os/^{188}Os$ ratio in the residue with time and the preservation of the $^{187}Os/^{188}Os$ ratio of the source prior to melting.

Owing to the relatively high abundances of Os in mantle rocks compared with those in both the continental crust and mantle-derived melts, the Os isotopic compositions of mantle fragments transported to the surface are thought to be relatively insensitive to contamination by the host lavas or fluids originating from the crust through which they pass. This differs greatly from the observed behaviour of the Rb-Sr, Sm-Nd and U-Pb isotope systems, in which the whole-rock budgets of Sr, Nd and Pb in mantle peridotites are dominated by interactions with such fluids on account of their considerably greater incompatible-element concentrations. Any variations in the Os isotopic composition of mantle peridotites, therefore, should reflect previous episodes of Re-loss, which may be correlated with melt removal, rather than later metasomatic disturbance (Walker *et al.*, 1989a; Reisberg *et al.*, 1991).

### 1.1.2 Mantle Evolution Models

The foundations of modern Re-Os studies of the mantle were laid by Allègre & Luck (1980), who used the Os isotopic compositions of Os-bearing alloys from ultramafic bodies of known age to define a mantle evolution line, corresponding to near linear growth in the $^{187}Os/^{186}Os$ ratio from an initial value of 0.805 at 4.55 Ga to a present-day ratio of ~1.04 ($^{187}Os/^{188}Os$ = 0.0969 to 0.1252). Although Luck & Allègre (1991) later revised the present day value of the $^{187}Os/^{186}Os$ ratio to 1.05 - 1.06 (0.1264 - 0.1276), their mantle evolution curve was unable to account for the high Os isotope ratios determined in ocean island basalts ($^{187}Os/^{188}Os \geq 0.1324$: Martin, 1991; Hauri & Hart, 1993: Reisberg *et al.*, 1993). The discovery of such radiogenic ratios in OIB has led to considerable debate concerning about which evolution line should be used in the modelling of mantle-derived rocks.

Martin (1991) observed that ocean island basalts possessing radiogenic Os isotope ratios were also characterised by high $^{3}He/^{4}He$ ratios (indicative of a potentially primitive mantle

source) and proposed that the average silicate earth was actually characterised by a present-day $^{187}Os/^{186}Os$ ratio close to 1.10 ($^{187}Os/^{188}Os = 0.1324$), implying that the osmiridium alloys analysed by Allègre & Luck (1980) were derived from a mantle source characterised by low time-averaged Re/Os ratios. Although this conclusion is not inconsistent with the range of $^{187}Os/^{188}Os$ ratios found in carbonaceous chondrites (0.1204 - 0.1348; Walker & Morgan, 1989), it is probable that the high $^{187}Os/^{188}Os$ ratios found in OIBs reflect either the recycling of old basaltic crust into the magma source (Hauri & Hart, 1993; Roy-Barman & Allègre, 1995) or the assimilation of $^{187}Os$-rich marine sediments from the volcanic piles traversed by the magmas (Reisberg *et al.*, 1993). The more recent determination of high $^{3}He/^{4}He$ ratios, yet unradiogenic Os isotope ratios in basalts analysed from Samoa Island (Farley *et al.*, 1992; Hauri & Hart, 1993) also argues against Martin's connection between high $^{187}Os/^{188}Os$ ratios and magmas derived from a primitive reservoir.

In order to constrain better the evolution of the mantle over geological time it may be necessary to perform more analyses of mantle-derived samples and chondritic meteorites. In the meantime, however, on the basis of ocean island basalt data, it does not appear necessary to assume that the primitive mantle evolution curve differs significantly from that suggested by Luck & Allègre (1991), whose values will be used during the discussion of the data obtained in this study.

### 1.1.3 Model Ages and $\gamma_{Os}$

From Figure 1.2 it may be seen that two model ages may be defined for a sample, the bulk-earth mantle model age, $T_{MA}$, and the Re-depletion model age $T_{RD}$. The $T_{MA}$ model age was first used by Allègre & Luck (1980) and is analogous to the $T_{DM}$ model age used in Nd and Sr isotope systematics. It assumes that the sample was derived from the mantle by a single-stage process and uses the measured Re/Os ratio to extrapolate the Os isotopic composition of the sample back to that of the chondritic mantle reservoir, according to the equation

$$T_{MA} = \frac{1}{\lambda_{Re}} \cdot \ln\left(\frac{(^{187}Os/^{188}Os)_{mantle} - (^{187}Os/^{188}Os)_{sample}}{(^{187}Re/^{188}Os)_{mantle} - (^{187}Re/^{188}Os)_{sample}} + 1\right) \quad \textbf{(Eqn. 1.2)}$$

where $(^{187}Os/^{188}Os)_{mantle} = 0.127$ and $(^{187}Re/^{188}Os)_{mantle} = 0.40$, corresponding to the values used in the mantle evolution model of Luck & Allègre (1991), and $\lambda_{Re}$ is the decay constant of $^{187}Re$ ($1.64 \times 10^{-11}$; Lindner *et al.*, 1989).

Although $T_{RD}$ is calculated in a similar way to $T_{MA}$, it presumes that the $^{187}Re/^{188}Os$ ratio of the sample is zero (Walker *et al.*, 1989a). For mantle peridotites this assumption would be valid if either the sample had been entirely depleted in Re by large degrees of melt extraction or only low-Re phases (such as Os alloys) were analysed. Under such circumstances $T_{RD}$ should approach $T_{MA}$, however, if any Re is present in the samples, then $T_{RD}$ will represent a minimum model age for the depletion of Re in mantle peridotites. Although the $T_{MA}$ model age may be affected by recent Re addition to mantle peridotites (either within the mantle lithosphere or during transport to the surface), giving erroneously old or even future ages, the $T_{RD}$ model age will always give a minimum estimate of the time of melt removal because it is independent of the Re/Os ratio determined in the sample.

In order to describe the Os isotopic composition of a sample at a particular time, Walker *et al.* (1989a) also defined a parameter, $\gamma_{Os}$, which compares the $^{187}Os/^{188}Os$ ratio of the sample with that of the reference mantle. The $\gamma_{Os}$ parameter is calculated in an analogous way to the $\varepsilon$ parameter of the Sm-Nd and Rb-Sr isotope systems, however, in view of the greater variation in the Os isotope ratios of samples, it describes the percentage difference from the reference value.

### 1.1.4 Purposes of this Study

One of the principal aims of this study is to determine the factors which may affect the behaviour of Re and Os during processes both within the mantle and during the transport of the samples to the surface, in order to facilitate the interpretation of the Re-Os isotope systematics of mantle-derived samples. In particular the controls on their partitioning during melt extraction and subsequent interaction with magmatic fluids will be addressed, using both thermochemical calculations and existing experimentally obtained partition coefficients (Chapter 2). Previous observations of the partitioning of Re and Os during magmatic processes have suggested that their behaviour may be a function of temperature, percentage of partial melting or the nature of the trace phases that remain in the mantle residue after melt extraction (Walker *et al.*, 1989a). However, experimentally obtained partition coefficients of Re and Os between basaltic melts and various mantle phases have yielded conflicting conclusions regarding which phases or phases are responsible for the elements' behaviour.

Base-metal sulphides, chrome-spinel, olivine, clinopyroxene and discrete Pt-group minerals have all been suggested as potential hosts.

The results of the discussion of the thermochemical and experimental partitioning data will be tested using the Re and Os abundances of peridotites originating from both orogenic massifs and a suite of ultramafic xenoliths (Chapter 5). In view of the suggested role of base-metal sulphides in the partitioning of Re and Os during mantle melting and the recognised chalcophile nature of the elements, the determined Re and Os abundances in the peridotite samples will be discussed in parallel with their chalcophile compositions.

Because the analytical techniques required for the determination of Re and Os are far from routine, a discussion of the methods used in this study is included as a separate chapter of this thesis (Chapter 3). It outlines the various methods by which samples were prepared for Re and Os analysis and describes the two instrumental techniques used during the study (ICP-MS and N-TIMS), concluding with a comparison of the results obtained using the different instruments.

## 1.2 The Continental Mantle Lithosphere

The continental lithosphere may be defined as the rigid outer layer of the Earth which cools by conduction and is mechanically and chemically distinct from the underlying convecting asthenosphere. It may be divided into two major components, an upper (crustal) component, characterised by metamorphic, igneous and sedimentary rocks possessing extremely diverse chemical compositions and mineralogies, and a lower (mantle) component comprising relatively buoyant refractory peridotite produced by the extraction of melts from the more fertile underlying asthenosphere.

### 1.2.1 Evolution of the Continental Mantle Lithosphere Through Time

In order to interpret the rate and mechanisms by which the present regions of continental lithosphere have grown through geological time, it is important to understand the processes responsible for the formation and evolution of both the crust and mantle components of the lithosphere and the relationship between the processes occurring in the two layers. Although the evolution of the continental crustal lithosphere is moderately well constrained for most regions, neither the timing nor the processes associated with the stabilisation of the

underlying mantle lithosphere are particularly well understood. Direct attempts to date lithospheric mantle material using conventional isotopic systems, in which both parent and daughter isotopes are incompatible elements, have met with a number of problems:

Firstly, much of the lithospheric mantle is above the closure temperatures of the isotope systems commonly used in geochronology, resulting in the diffusive exchange of isotopes between minerals and mineral isochrons that record the cooling of the peridotites following their removal from the mantle lithosphere, rather than the time at which they were extracted from the convecting mantle (e.g. 21 - 24 Ma cpx-gt isochron ages for the Ronda massif which date its crustal emplacement: Reisberg *et al.*, 1989).

Secondly, on account of the incompatibility of the elements during partial melting, both the parent and daughter isotopes of the Sm-Nd, Rb-Sr and U-Pb isotope systems are severely depleted in the mantle residue, and extensive hand-picking of minerals is required in order to obtain sufficient material for analysis.

Thirdly, the relatively cool temperatures in the continental mantle lithosphere may "trap" incompatible element enriched melts or fluids produced by low degrees of partial melting, leading to enrichment of the mantle peridotites. Such enrichment would obscure the older isotope signatures of the incompatible elements, which may have recorded the initial melt depletion event.

Finally, during transport of fragments of the mantle lithosphere to the surface, as either ultramafic xenoliths or tectonic slices of mantle material, the peridotites may interact with incompatible-element enriched fluids, further disrupting the incompatible-element isotope compositions. For ultramafic xenoliths, this fluid would be represented by the host basalts, whilst for tectonically emplaced orogenic peridotite massif, the fluids may originate from the crust through which they passed.

In order to overcome these problems, investigation of the formation and evolution of the continental mantle lithosphere requires an isotope system whose elements are either compatible in the mantle residue, or are not significantly enriched in the metasomatic fluids. Such criteria appear to be satisfied by the geochemistry of the Re-Os isotope system, leading to several Re-Os isotope studies of the continental mantle lithosphere underlying both ancient cratonic regions, using kimberlite-borne ultramafic xenoliths (Walker *et al.*, 1989a; Pearson

*et al.*, 1995a; Carlson & Irving, 1994), and regions of younger crustal ages, as sampled by tectonically emplaced slices of mantle material (Reisberg *et al.*, 1991) and ultramafic xenoliths (Luck & Allègre, 1991; Pearson *et al.*, 1994).

### 1.2.2 Crust-Mantle Coupling

Re-Os isotope studies of the mantle lithosphere below both the Archaean Kaapvaal and Siberian cratons have yielded similar $T_{RD}$ model ages to those of the overlying crust (Pearson *et al.*, 1995a), demonstrating that the stabilisation of their deep lithospheric mantle keels probably coincided with a period of major crustal generation or stabilisation in the two regions and possibly indicating a causative link between the generation of mantle and crust during the Archaean. Similar studies of the lithosphere below a tectonically stable area of Early Proterozoic crust adjacent to Kaapvaal craton also yield similar model ages to the overlying crust (Pearson *et al.*, 1994), indicating crust-mantle coupling over a considerable period in southern Africa.

In the only systematic study of the Re-Os isotope systematics of mantle lithosphere not directly associated with an ancient cratonic region, Reisberg *et al.* (1991) determined a mid-Proterozoic isochron age for the peridotites of the Ronda Ultramafic Complex, southern Spain. However, no connection was made between the evolution of the crust in the region and the age determined for the underlying mantle, preventing the link between the generation of crust and the stabilisation of the underlying mantle lithosphere from being extended to younger crustal regions. In view of the large areal extent of post-Archaean basement (>95% of the total area of the continents, Hurley & Rand, 1969), the coincident generation of both the crust and mantle in young crustal regions would have important implications for the evolution of continental lithosphere through time.

Whilst the geological ages of Archaean crustal rocks appear to match their Nd model ages, indicating limited crustal recycling during the Archaean (Allègre & Ben Othman, 1980; Ben Othman *et al.*, 1984b), the incompatible element isotope systematics of most post-Archaean basement rocks appear to have been disturbed during one or more periods of deformation subsequent to their initial generation. By studying the Re-Os isotope systematics of the mantle lithosphere underlying regions of post-Archaean crust, it may be possible to determine whether the mantle lithosphere maintains a record of the initial melt

extraction event, which may have coincided with the stabilisation of the CML, or whether, during the deformation processes, the crust and mantle have become decoupled due to processes such as delamination and lithospheric recycling (Bird, 1978; Houseman *et al.*, 1981; Platt & Vissers, 1989). Owing to its generally more fertile composition and higher FeO contents, mantle lithosphere which stabilised since the Archaean may be expected to be less buoyant than that which constitutes the cratonic keels (Maaloe & Aoki, 1977; Jordan, 1978; Hawkesworth *et al.*, 1990), hence may be more susceptible to either delamination or thermal erosion, leading to the replacement of old mantle lithosphere by younger material.

### 1.2.3 Purposes of this Study

By determining the Re-Os isotope systematics of mantle peridotites originating from the continental mantle lithosphere underlying south-western and central France, this study will investigate the link between the age of the mantle lithosphere in the region and existing estimates for the age of the crust, obtained using the Rb-Sr, Sm-Nd and U-Pb isotope systems (Chapter 5). Comparison of the $^{187}Os/^{188}Os$ ratios of the French continental mantle lithosphere at the time of its stabilisation with the mantle evolution curves of Luck & Allègre (1991) may also enable the Os isotopic characteristics of its mantle source to be constrained.

Although the investigation of samples collected from well characterised locations should enable the results of the Re-Os isotope study to be interpreted within existing models for the evolution of the continental mantle lithosphere in the region, the interpretation of their Re-Os isotope systematics will be preceded by a discussion of the process or processes responsible for the range of elemental and isotopic compositions observed in the samples (Chapter 4).

# Chapter 2

# Behaviour of Re and Os During Mantle Processes

## 2.1 Introduction

In order to interpret the Re-Os isotope systematics of mantle rocks, it is necessary to understand how the two elements behave during processes within the mantle and during the transport of mantle rocks to the surface. In particular, it is necessary to appreciate how Re and Os may be affected by a) the extraction of mafic melts, b) interaction with the magmatic or volatile-rich fluids which may be responsible for metasomatism of the mantle lithosphere, and c) alteration of mantle peridotite either *en route* to the surface or subsequent to emplacement.

This chapter discusses the factors which may dictate how the elements behave during these different processes. It focuses on theoretical arguments (based on rudimentary thermochemical calculations of the relative stabilities of Re, Os and the other Pt-group elements (PGE) as pure metals, sulphides or oxides), as well as previous experimental investigations, including studies of the partitioning of the PGE between a variety of potential host phases. Critical to both approaches is the range of physical conditions expected in the continental mantle lithosphere, in particular the sulphur and oxygen fugacities ($f_{S_2}$ and $f_{O_2}$), and the behaviour of the mantle phases which may host the elements.

Because Os is one of the Pt-group elements, its behaviour during magmatic processes has been studied in considerably more detail than that of Re. Over the last decade, interest in the PGE has resulted in a number of laboratory and field studies into their partitioning behaviour both during normal magmatic processes and during the formation of economic PGE deposits. Whilst these studies suggested that the PGE may be hosted by a number of different mantle phases (including spinel, clinopyroxene, olivine), detailed analysis of Pd, Ir and Au abundances in the consituent minerals of mantle-derived spinel lherzolite xenoliths suggests that the majority of the PGE are most likely present in an intergranular component

(Mitchell & Keays, 1981). In view of the recognised chalcophile nature of the PGE and the apparent absence of discrete Pt-group minerals, Mitchell & Keays suggested that the PGE reside predominantly in solid solution in the intergranular base-metal sulphide (BMS) phases present in the mantle.

On account of its low economic importance and low abundance, Re has rarely been analysed in mantle samples, let alone in individual minerals. However, it is generally assumed that Re behaves as a chalcophile element during magmatic processes, as demonstrated by the high concentrations of Re found in molybdenite ores (~$MoS_2$) and its correlation with sulphur in the suite of mantle xenoliths analysed by Morgan *et al.* (1981).

Despite these studies, the behaviour of the PGE and Re during mantle processes remains poorly understood, primarily owing to difficulties in their routine analysis at the low concentrations in which they are encountered in non-mineralised rocks. Whilst they are far from quantitative, the thermochemical calculations included in this chapter suggest that under normal mantle conditions both Re and Os should be present predominantly in the base-metal sulphide phase, consistent with both experimental and field observations.

## 2.2 Mantle Conditions

In contrast to the elements which figure in most of the other commonly applied isotope systems, both Re and Os exhibit strong chalcophile and siderophile behaviour, with high metal-silicate and sulphide-silicate partition coefficients (e.g. Jones & Drake, 1986; Kimura *et al.*, 1974; Bezmen *et al.*, 1994; Peach *et al.*, 1994). In order to discuss the mantle behaviour of Re and Os (as well as the other PGE), therefore, it is necessary to constrain the redox state and activity of sulphur in the mantle during the processes of interest. Under strongly reducing conditions, when (Fe,Ni) metal phases may be present, these elements would be expected to partition into the metal phase, however, under more oxidising conditions, when such phases should be unstable relative to oxide or silicate phases, the behaviour of the PGE is less clear and may depend on the availability of sulphur.

### 2.2.1 Oxygen Fugacity

In their review of estimates of the redox state of the upper mantle, Arculus & Delano (1987) concluded that the mantle appears to exhibit a significant range of oxygen fugacities

($f_{O_2}$), which extend from those for the iron-wüstite (IW) buffer to slightly more oxidised values than those for the fayalite-magnetite-quartz (FMQ) buffer. Whilst the mantle source of MORB magmas exhibits the entire range of redox conditions documented in the upper mantle (with FMQ-4 ≤ log $f_{O_2}$ ≤ FMQ+1; Wood *et al.*, 1990), with a peak at approximately two log units below the FMQ buffer (Carmichael, 1991), the redox state of peridotites sampled from the shallow CML appears to be less variable, with $f_{O_2}$ values bracketing the FMQ buffer (FMQ-1.7 ≤ log $f_{O_2}$ ≤ FMQ+1.2; Mattioli *et al.*, 1989; Wood & Virgo, 1989; Wood *et al.*, 1990). For simplicity during the calculations and discussions of this chapter, the oxygen fugacity of the CML is assumed to be close to that for the FMQ buffer.

### 2.2.2 Sulphur Fugacity

Compared to the considerable work undertaken to investigate the oxygen activity in the upper mantle, until recently, little interest has been shown in the activity and behaviour of sulphur in the mantle.

In most mantle peridotite samples the sulphide component occurs as polyphase aggregate grains, with compositions lying within the Cu-Fe-Ni-S system. Although the sulphide minerals commonly show evidence of alteration following their separation from the mantle (either by serpentinisation or oxidation), where the grains are enclosed within silicate minerals they are predominantly present as an assemblage of Ni-rich pentlandite ± pyrite ± Fe-poor pyrrhotite ± chalcopyrite (Garuti *et al.*, 1984; Lorand, 1989b). Experimentally determined phase equilibria suggest that such an assemblage may have originated from the unmixing of a high temperature mono-sulphide solid solution (MSS), which crystallised from an immiscible liquid sulphide phase (Kullerud *et al.*, 1969; Craig & Kullerud, 1969).

The sulphur fugacity of mantle rocks may be determined from either a) the composition of particular sulphide phases (e.g. the Fe/Ni ratios of pentlandite or the metal/S ratios in pyrrhotite) or b) the observed sulphide mineral assemblage, in which minerals with high metal:sulphur ratios are stabilised at high $f_{S_2}$. Using the phase assemblage and the compositions of the individual sulphide minerals present in unfractured silicate grains of the N.E. Pyrenean peridotite massifs, Lorand (1989b) estimated that the minerals were exsolved from MSS at ~400 °C and $f_{S_2}$ between $10^{-7}$ and $10^{-9}$ bar.

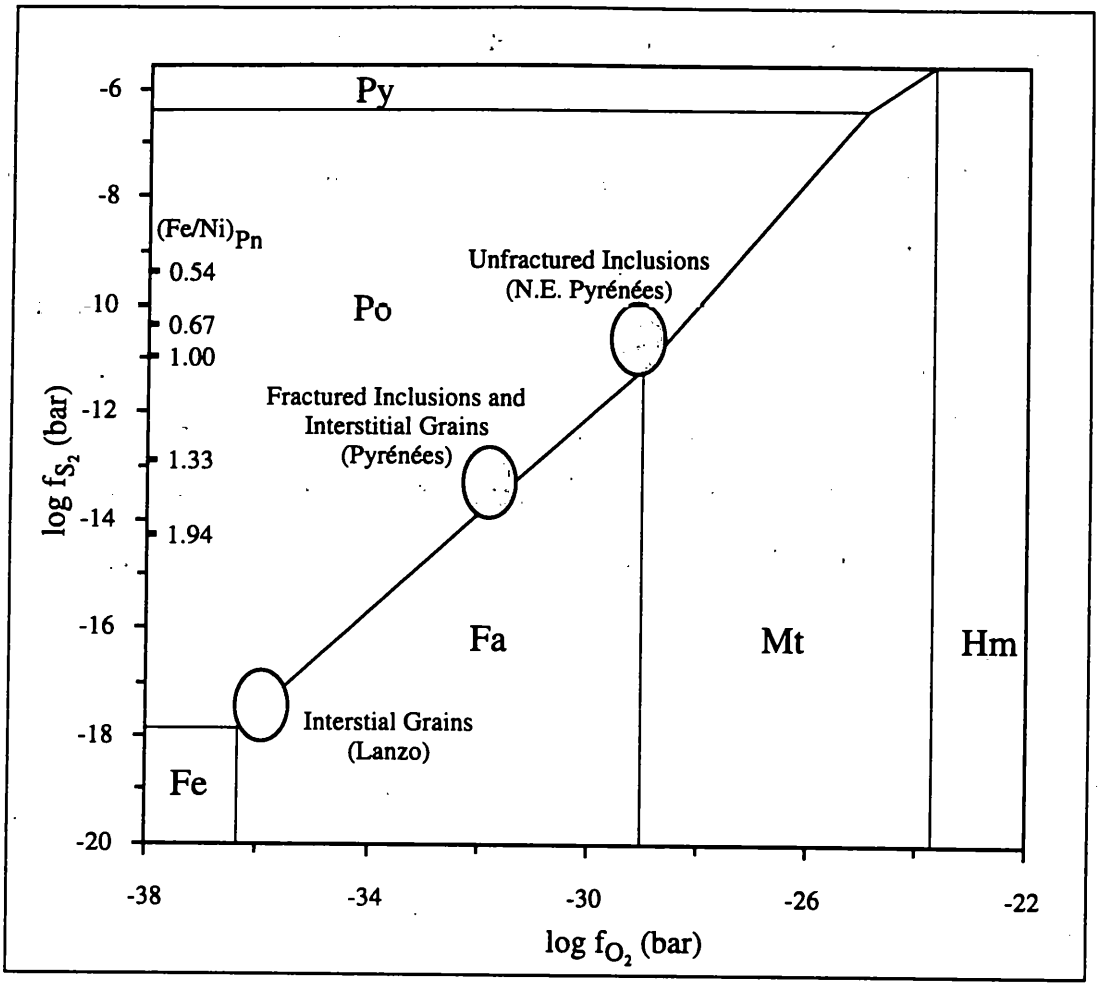


**Figure 2.1** $fS_2$ - $fO_2$ conditions recorded by the main sulphide assemblages occurring in orogenic peridotite massifs, plotted relative to the $fS_2$ and $fO_2$ buffers of the Fe-O-S-Si system at 400°C. Inclusion data after Lorand (1991), thermodynamic data for $fS_2$ and $fO_2$ buffers from Shi (1992) and Shi & Saxena (1992), Ni/Fe ratios of pentlandite from Kaneda *et al.* (1986). Fe = native iron, Fa = fayalite, Mt = magnetite, Hm = haematite, Po = pyrrhotite, Pn = pentlandite and Py = pyrite.

Whilst the sulphur fugacity in an oxygen-free system may be buffered solely by reactions between sulphide phases, in systems containing both oxide and sulphide phases, $fS_2$ and $fO_2$ are interdependent and will be controlled by divariant reactions between the two phases. Figure 2.1 shows the fields of the various phases in the Fe-O-S-Si system. If a Ni-Fe sulphide phase is to coexist with the silicate and oxide phases present in the mantle, then the $fS_2$-$fO_2$ conditions must lie along the phase boundary defined by either the Fa-Po+Qz or Mt-Po reactions. Because the proportion of silicate and oxide phases in the mantle greatly outweigh that of the BMS phase, the sulphur fugacity of the mantle should be dictated by its $fO_2$. If the oxygen fugacity of the mantle is buffered at values close to those for the FMQ buffer, then its $fS_2$ should generally lie close to the fayalite+pyrrhotite-magnetite-quartz (FPoMQ) invariant reaction at most temperatures and pressures, as demonstrated by the

values of $f_{S_2}$ determined by Lorand (1989b), when plotted in Figure 2.1. Extrapolation of the FPoMQ buffer to mantle solidus temperatures (~1200°C) indicates that the sulphur fugacity of the Pyrenean peridotite massifs may have been in the range 0.1 - 10 bar during melt extraction.

In contrast to the inclusions in unfractured silicate grains, the phase assemblages and mineral compositions in many of the interstitial sulphide grains found within mantle peridotites record a history of decreasing $f_{S_2}$, consistent with the buffering of $f_{S_2}$ by the low values of $f_{O_2}$ present during serpentinisation (Figure 2.1).

## 2.3 Thermochemical Calculations

### 2.3.1 Introduction

Before the partitioning of Re and Os during mantle processes can be usefully discussed, it is necessary to determine what mantle phase or phases is most likely to host the elements, so that the relevant partition coefficients may be considered. In their study of the distribution of Au, Pd and Ir in spinel lherzolite xenoliths, Mitchell & Keays (1981) reported that, out of the silicate and oxide phases present in the peridotites, spinel exhibited the highest PGE abundances whilst olivine generally contained the lowest. Mass balance calculations, based on the PGE contents of the minerals analysed and their modal abundances, however, demonstrated that the silicate and oxide phases could account for only 20 - 40% of the determined whole-rock PGE abundances, leading Mitchell & Keays to conclude that the bulk of the PGE must be present in the intergranular component. Although this marked a step forward in our understanding of the behaviour of PGE in the mantle, several questions remained regarding the principal phase hosting the PGE: i.e. are they present in solid solution in the mantle base-metal sulphide phase? do they form discrete Pt-group sulphide minerals? or could they be present as alloy phases, reflecting the highly siderophile character of the elements?

Using thermochemical data for the metals, sulphides and oxides of the PGE and Re, the conditions under which discrete PGE minerals may coexist with the metals were calculated at temperatures, pressures and values of $f_{S_2}$-$f_{O_2}$ characteristic of the CML. Using data for the mixing behaviour of the oxides and sulphides of the PGE and Re in particular mineral

phases, the solubilities of the elements in some mantle minerals were also calculated under lithospheric mantle conditions. Because suitable mixing data for the PGE and Re species in mantle minerals were limited, it was necessary to infer several of the required values from experiments involving either only a sub-set of the PGE or related mineral phases. The thermodynamic data and equations used in these calculations are outlined in Appendix B.

### 2.3.2 The Role of Sulphide Phases

Figure 2.2 shows the calculated sulphur fugacities necessary for the coexistence of the PGE and Re as pure metal and sulphide species at 10 kbar pressure, plotted as a function of temperature. In the calculations it was assumed that both the metal and sulphide species were present as pure components (i.e. $a_i=1$ for all solid species). For comparison, the iron-pyrrhotite (IPo), fayalite+pyrrhotite-magnetite-quartz (FPoMQ), pyrrhotite-pyrite (PoPy) and buffers are also plotted at high pressure, using data from Shi (1992) and Shi & Saxena (1992). Although several of the PGE form more than one sulphide species, depending on the value of $f_{S_2}$ (e.g. $Ir_2S_3$ and $IrS_2$ or PtS and $PtS_2$), for clarity, only the sulphide formed at the lowest values of $f_{S_2}$ is shown in the figure.

The calculations suggest that at low to moderate temperatures and values of $f_{S_2}$ close to those for the FPoMQ buffer, most of the PGE sulphides should be stable relative to the metals. At higher temperatures ($T > 800°C$) the stability of $OsS_2$, $Ir_2S_3$ and PdS is reduced and the elements should occur as metallic phases.

Although these calculations indicate that the majority of the PGE may exist as discrete PGE sulphide phases under lithospheric mantle conditions, the free energy of the PGE sulphide species may be further reduced by their dissolution in the mantle base-metal sulphide phase, on account of the increased entropy of the system. Consequently, before a discrete PGE or Re mineral phase may form, the BMS phase would have to be saturated with respect to the relevant element. Hence, in order to determine whether the PGE or Re may be present in discrete phases within the mantle, it is first necessary to determine the solubilities of the PGE and Re in the BMS phase.

The solubility of each of the PGE in the BMS phase is dictated by both its activity ($a_{MS_{2x}}$) and the ideality of the PGE/base-metal sulphide mixture, as described by its activity

coefficient, $\gamma_{MS_{2x}}$. Although $\gamma_{MS_{2x}}$ may vary as a function of mineral composition and PGE concentration, for the dissolution of only trace quantities of PGE in the BMS phase Henry's law should apply, such that it may be considered to be constant over the concentration range of interest.

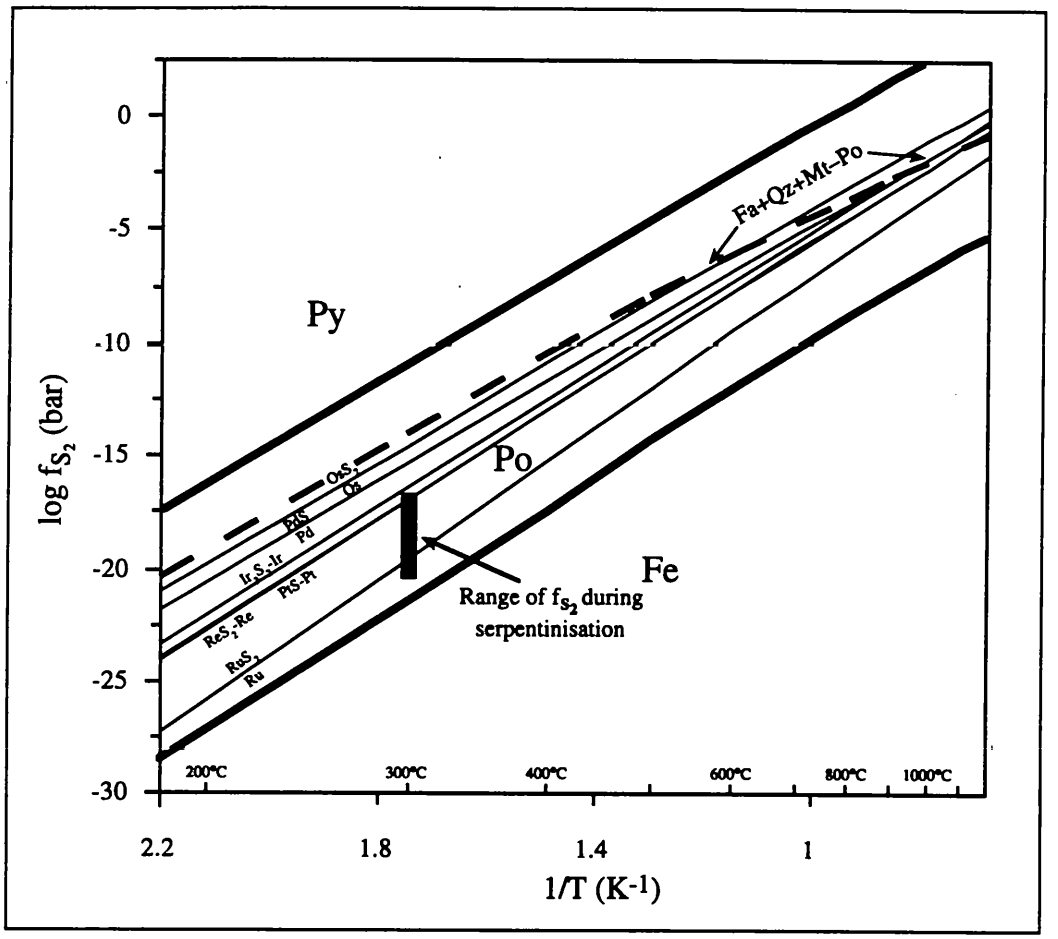


**Figure 2.2** Log $f_{S_2}$–T plot illustrating the sulphur fugacities required to stabilise the Pt-group elements as discrete sulphide minerals at 10 kbar pressure (thin lines). Thicker lines denote the univariant Po($Fe_{0.877}S$)-Py and Tr (FeS)-Fe reactions which buffer $f_{S_2}$ and the Fa+Qz+Mt–Po invariant reaction, by which $f_{S_2}$ is buffered in the continental mantle lithosphere, assuming $f_{O_2} \approx$ FMQ, dashed. Sources of thermodynamic data: the Pt-group metals and their sulphides, Barin & Knacke (1973) and Barin *et al.* (1977); phase relations in the Fe-O-S-Si system, Shi (1992) and Shi & Saxena (1992). Abbreviated phase names are the same as in Figure 2.1.

Experiments by Malevskiy *et al.* (1977) demonstrated that the PGE are highly soluble in pyrrhotite of a similar composition to that which is present in the mantle BMS inclusions (~$Fe_{0.875}S$). If the experimentally determined solubilities of the PGE in pyrrhotite reflect those in the BMS phase under similar conditions, then the experiments of Malevskiy *et al.* may be used to calculate activity coefficients for the PGE, from which their solubilities under different mantle conditions may be determined.

In the experiments, involving all six PGE, only Os, Ru and Pd appeared to reach saturation in the metal-poor pyrrhotite, in which the dissolved PGE were in equilibrium with the pure PGE sulphides. Using the determined noble metal concentrations in the pyrrhotite, an activity coefficient of ~470 may be calculated for the dissolution of $OsS_2$ in the BMS phase, whilst a value of ~60 may be calculated for both $RuS_2$ and PdS. Because no separate Pt-group minerals were observed in experimental charges containing up to 10 wt% Ir or Rh, both elements would appear to be highly soluble in the pyrrhotite phase. Maximum estimates of the activity coefficients of $Rh_2S_3$ and $Ir_2S_3$, calculated from the experiments containing the highest Rh and Ir contents, would be ~20 and 50, respectively. Although these significantly lower activity coefficients are inconsistent with the orthorhombic structure of the pure $Rh_2S_3$ and $Ir_2S_3$ minerals proposed by Parthé *et al.* (1967), the formation of RhSe with a niccolite structure suggests that the Rh sulphide species may be able to adopt a structure similar to that of pyrrhotite more easily than the other PGE (whose selenides all possess similar structures to their sulphides; Berlincourt, 1981).

In view of the high solubility of $ReS_2$ in molybdenite ($MoS_2$) and the similarity between the hexagonal lattice structures of molybdenite and pyrrhotite, the activity coefficient of $ReS_2$ in pyrrhotite may be similar to or lower than that of $Ir_2S_3$ (both elements possessing similar atomic radii) and Re should also be highly soluble in the base-metal sulphide phase.

Although the PGE and Re appear to possess activity coefficients greater than unity for the dissolution of their sulphides in pyrrhotite, the estimated values of $\gamma_{MS_{2x}}$ are not so high as to counteract the high activities of the PGE and Re sulphide species under mantle $f_{S_2}$-P-T conditions, as estimated from the thermochemical calculations. Consequently, the bulk of the PGE and Re may be able to dissolve in the BMS phase of the mantle peridotites and no discrete Pt-group or Re minerals would be expected under normal mantle conditions. Even at temperatures close to the peridotite solidus ($T \geq 1200°C$) the calculated solubility of Os in the BMS phase at 10 kbar is > 50 ppm, which is more than sufficient for the ppb concentrations of Os present in the mantle to dissolve in the 0.05% BMS phase present in most fertile peridotites.

At the lower sulphur fugacities estimated for the serpentinisation of the N.E. Pyrenean peridotite massifs (i.e. $10^{-17}$ - $10^{-20}$ bar at 300°C; Lorand, 1989b), the activities of the PGE

sulphide species will be considerably reduced relative to their values in the unaltered peridotites, leading to a reduction in the solubilities of the elements in the BMS phase. Whilst the reduced solubility is insufficient to affect the behaviour of most of the PGE, the solubilities of Os and Ir would be reduced to 15 ppb - 15 ppm and 25 ppb - 750 ppm respectively, resulting in their partial or complete exsolution during alteration. Under the reducing conditions associated with such alteration, neither $OsS_2$ nor $Ir_2S_3$ should be stable relative to the metals (Figure 2.2), hence, the elements would be exsolved as alloy phases, rather than PGE sulphides.

***PGE and Re Sulphide Solubility During Melt Extraction***

Because the base-metal sulphide phase is a liquid at peridotite solidus temperatures, in addition to considering the solubility in the solid BMS phase, it is necessary to consider the solubility of the PGE and Re in a liquid sulphide phase before discussing the behaviour of Re and Os during the extraction of silicate melts. Too little is known of the melt structure in liquid sulphides at high temperatures to estimate relative activity coefficients based on the similarity of sulphide structures (as was attempted for solid BMS, above). However, measurements of the partitioning of the noble metals between liquid Fe-Ni-Cu sulphide and crystallising MSS suggest that the activity coefficients of the PGE may vary slightly between the two phases (Fleet *et al.*, 1993): Os, Ru, Ir and Rh all appear to be more compatible in the MSS phase ($D_{liq/MSS}$ = 0.23 - 0.33), whilst Pt and Pd both partition into the liquid ($D_{liq/MSS} \approx 4.8$). Because the activity of the sulphide species in both solid and liquid phases should be equal, the determination of partition coefficients less than unity for Os, Ru, Rh and Ir indicates that their activity coefficients in the liquid phase are greater than those in the solid BMS phase. The three or four fold increase in $\gamma_{MS_2}$ calculated for Os, Ir, Ru and Rh, however, is insufficient to reduce the solubility of the elements in the sulphide phase such that discrete Pt-group minerals would be exsolved during melting of the solid BMS.

In conclusion, although discrete sulphide minerals of all the PGE and Re may be stable relative to the metal under lithospheric mantle conditions, thermochemical calculations suggest that complete dissolution of the metals in the mantle base-metal sulphide phase should occur instead, both in the solid MSS at low temperatures and in the sulphide liquid present during silicate melt extraction. Under conditions of low $f_{S_2}$, e.g. during

serpentinisation of mantle peridotites, the majority of the PGE and Re should remain in the sulphide solid solution, however both Os and Ir may exsolve to form alloy phases. Although the presence of Ir-Os alloys in mantle peridotite samples may have consequences for the way in which they are prepared for analysis, the inert nature of the alloy phase should not result in an increase in Os mobility during serpentinisation. Consequently, Os isotopic data obtained on moderately serpentinised samples may be interpreted with reasonable confidence, despite the effects of such alteration on the lithophile major and trace elements.

### 2.3.3 The Role of Oxide Phases

Figure 2.3 illustrates the values of $f_{O_2}$ at which the refractory oxides of the PGE and Re may coexist with the metals. It illustrates that, under lithospheric mantle conditions (characterised by $f_{O_2}$ close to that for the FMQ buffer), pure oxides of the PGE should decompose to the metals. The calculated values of $f_{O_2}$ required for the coexistence of metallic Re and $ReO_2$, however, suggest that $ReO_2$ may exist stably under conditions of high temperature and values of $f_{O_2}$ close to the upper limit observed in the continental mantle lithosphere.

Just as the free energy of the PGE and Re sulphides may be reduced by dissolution of the elements in the BMS phase, however, it is possible that oxides of noble metals may be stabilised by dissolution in mantle oxide phases, the most abundant of which is spinel. Although spinel *sensu stricto* has the composition $MgAl_2O_4$, the substitution of $Fe^{2+}$ for Mg and $Cr^{3+}$ or $Fe^{3+}$ for Al, and the presence of traces of Ti; Ni and Mn, suggest that the mineral may accept cations with a range of sizes and oxidation states. The similarity between the ionic radii of $Re^{4+}$, $Os^{4+}$, $Ru^{4+}$, $Ir^{4+}$ (r = 0.6 - 0.63 Å), $Rh^{3+}$ (r = 0.665 Å) and $Pd^{2+}$ and $Pt^{2+}$ (r = 0.80 - 0.86 Å) and those of octahedrally-coordinated $Ti^{4+}$ and high-spin $Fe^{3+}$ and $Fe^{2+}$ (r = 0.605, 0.645 Å and 0.78 Å; Shannon, 1976) would suggest that the PGE and Re may be able to substitute for either Ti or Fe in mantle spinels.

Whilst the solubilities of Re and Os in spinel have not been ascertained, the solubilities of Ru, Rh and Pd in Al-spinel were determined experimentally by Capobianco & Drake (1990). Although the PGE-bearing spinel grains were in equilibrium with pure PGE oxides in some of these experiments (permitting the assumption of $a_{MO_{2x}} \approx 1$), in others only dissolved PGE species were present. Where no pure PGE oxides were present,

thermochemical data for the PGE and their oxides and details of the conditions under which the experiments were conducted (e.g. $f_{O_2}$ and T) were required in order to estimate the activities of the PGE oxide species dissolved in the spinels, from which activity coefficients could be calculated (using the equations in Appendix B). On account of the similar (rutile) structures of pure $RuO_2$, $OsO_2$ and $ReO_2$ and the similarity of the elements' ionic radii, $\gamma_{OsO_2}$, $\gamma_{ReO_2}$ and $\gamma_{RuO_2}$ may be comparable, enabling the solubilities of Re and Os in spinels to be calculated under mantle conditions, employing the values derived for $\gamma_{RuO_2}$.

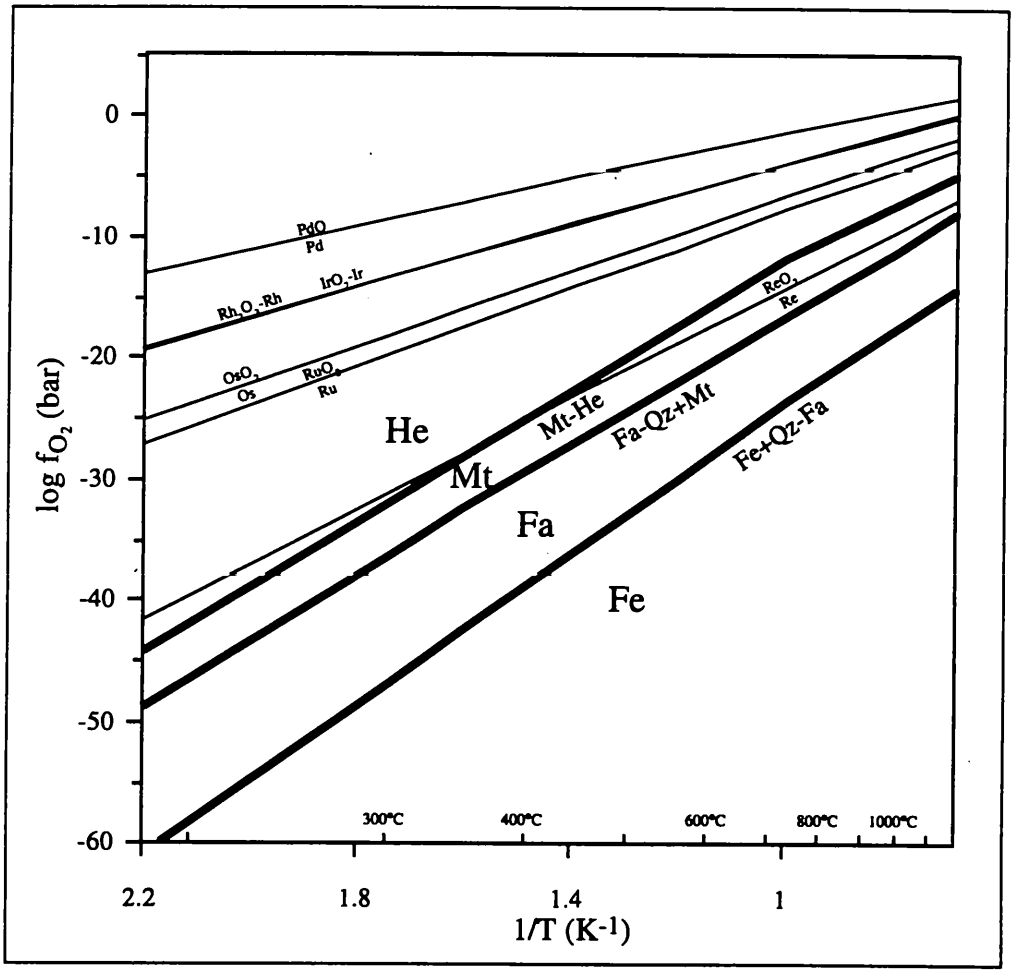


**Figure 2.3** Log $f_{O_2}$–T plot demonstrating that the oxygen fugacities necessary to stabilise the Pt-group elements as discrete oxide minerals at 10 kbar are all considerably higher than those expected in the lithospheric mantle ($f_{O_2}$ ≈ FMQ). Thicker lines denote the Fe+Qz–Fa, Fa–Qz+Mt and Mt–Hm univariant buffers. Sources of thermodynamic data: Pt-group metals and their oxides, Barin & Knacke (1973) and Barin *et al.* (1977); phase relations in the Fe-O-Si system, Shi (1992) and Shi & Saxena (1992). Abbreviations are the same as in Figure 2.1.

Using the concentration data of Capobianco & Drake (1990), the calculated activity coefficients of $RhO_{1.5}$ and $RuO_2$ in spinel at 1290 - 1300°C are 265 and 7.1, respectively. Although they did not report the solubility of Pd at a similar temperature, Capobianco &

Drake (1990) showed that, in spinels equilibrated at 1450°C and $f_{O_2} \approx 1$ bar, its concentration was below the detection limit of the microprobe (~25 ppm), suggesting an activity coefficient in excess of 4500.

| Temp. | $f_{O_2}$ | Solubility in Spinel (ppm) | | | | | |
|---|---|---|---|---|---|---|---|
| (°C) | (bar) | Os | Ir | Ru | Rh | Pd | Re |
| 1275 | -6.9 | 16.4 ppb | 606 ppt | 101.9 ppb | 1206 ppb | <14.1 ppb | 1543 ppm |
| 1000 | -10.8 | 224.3 ppt | 2.5 ppt | 1.7 ppb | 29.4 ppb | <0.5 ppb | 226 ppm |
| 800 | -14.8 | 4.4 ppt | 0.016 ppt | 39 ppt | 0.9 ppb | <25 ppt | 52 ppm |

**Table 2.1** Variation in the solubility of the PGE and Re in Al-spinel as a function of temperature, calculated for $f_{O_2}$ close to the FMQ buffer and P ≈ 10 kbar. PGE and Re concentrations calculated using the oxide activities calculated at the temperature of interest and activity coefficients determined from the data of Capobianco & Drake (1990). Sources of thermochemical data and the methods used in the calculations are documented in Appendix B.

If the activity coefficients of the PGE oxides are assumed not to vary greatly as a function of temperature or pressure, the solubilities of the PGE and Re in Al-spinel under mantle conditions may be calculated over a range of mantle temperatures (Table 2.1). While these solubility estimates are likely to represent maximum values, for mantle containing approximately 3% spinel and PGE abundances close to bulk mantle estimates, they suggest that the entire Re, Rh (and possibly Ru) contents of the mantle may dissolve in the spinel phase. For a mantle Os content of 3.5 ppb, however, less than 15% of the total Os could be dissolved before the element reached saturation.

If the temperature of the system is reduced, the solubility of the PGE in the spinel phase also decreases (consistent with the increasing difference between the oxygen fugacity for the FMQ buffer and those required to stabilise the PGE as oxides, Figure 2.3). For a reduction of less than 500°C, the solubilities of the PGE may decrease by 3 - 4 orders of magnitude. Consequently, any PGE present in solid-solution in spinel at high temperature would be exsolved during cooling. If no other phase is present into which the PGE can partition, then the exsolved PGE may form either mineral inclusions within the spinel grains, or migrate to grain boundaries to form the intergranular component noted by Mitchell & Keays (1981). In the absence of sulphur, such inclusions would be mostly PGE alloys.

In conclusion, at oxygen fugacities close to those for the FMQ buffer, the PGE and Re cannot exist as discrete, pure oxide minerals, but may be present at low concentrations in the

Al-spinel present in most mantle peridotites. The order of increasing solubility of the PGE and Re in the spinel phase is predicted to be Ir<Pd≤Os<Ru<Rh<<Re. At temperatures close to the anhydrous peridotite solidus, Re, Rh (and possibly Ru) may be sufficiently soluble in the spinel phase for complete dissolution of the elements in the oxide phase. However, with decreasing temperature, the solubility of the PGE decreases considerably, such that at 800°C only Re may be significantly soluble. Decreasing temperature may result in the exsolution of dissolved PGE from the spinel grains, producing discrete inclusions of PGM within the mineral grains, which may be transferred to the grain boundaries during subsequent deformation and recrystallisation of the mantle peridotite.

### 2.3.4 Relative Concentrations in Sulphide and Oxide phases

In the preceding sections, calculations based on thermochemical data suggested that, under lithospheric mantle conditions, some or all of the PGE and Re may be sufficiently soluble in the mantle oxide or sulphide minerals for the elements to be wholly dissolved in either phase. Because both spinel and BMS are present in most mantle peridotites, partitioning of the elements between the two phases will dictate the relative concentration in each mineral. Using similar data to that used for the calculation of mineral solubilities, it was possible to estimate sulphide/spinel partition coefficients for Re and the four PGE for which thermochemical data were available for both sulphide and solid oxide species (employing the equations defined in Appendix B).

#### *Partitioning of the PGE and Re between Spinel and Sulphide*

Spinel-sulphide partition coefficients for Os, Ir, Ru, Pd and Re were calculated at a total pressure of 10 kbar, $f_{S_2}$-$f_{O_2}$ conditions close to those for the FPoMQ buffer and a range of temperatures (Table 2.2). Os, Ir, Ru and Re were all assumed to dissolve as dioxide or disulphide species, but Pd was assumed to be present as either PdO or PdS.

The calculated partition coefficients indicate that, despite the high solubility of the PGE and Re in spinel at high temperature, the elements should partition predominantly in to the BMS phase. From estimates of the relative abundances of the two host phases in the upper mantle (~3% spinel and 0.05% BMS), the calculated proportion of the PGE and Re present in the spinel phase at 1100°C varies from less than 0.2 to ~40 ppm of the total mantle

abundance (for Ir and Re respectively). With falling temperature, the value of $D_{spinel/BMS}$ decreases considerably. Thus, any PGE or Re dissolved in the spinel at high temperature should increasingly partition into the sulphide phase as temperature decreases, further reducing the role of spinel in the mantle behaviour of the PGE and Re.

| Temp (°C) | $fS_2$ (bar) | $fO_2$ (bar) | $D_{spinel/BMS}$ (x $10^{-9}$) | | | | |
|---|---|---|---|---|---|---|---|
| | | | Os | Ir | Ru | Pd | Re |
| 1200 | -0.8 | -7.8 | 1200 | 24 | 53 | 1.1 | 3100 |
| 1100 | -1.3 | -9.3 | 170 | 2.9 | 6.6 | 0.14 | 600 |
| 1000 | -1.9 | -10.9 | 17 | 0.25 | 0.6 | 0.012 | 90 |
| 850 | -3.1 | -13.8 | 0.41 | 0.0043 | 0.011 | 0.00022 | 4.0 |

**Table 2.2** Calculated spinel/BMS partition coefficients for selected PGE and Re under mantle conditions of 10 kbar and $fO_2$ and $fS_2$ close to those for the FPoMQ buffer. Values rounded to two significant figures. Sources of thermochemical data and activity coefficients are the same as those used in Table 2.1. Methods used to calculate $D_{spinel/BMS}$ are documented in Appendix B.

### 2.3.5 Applicability of Thermodynamic Calculations and Conclusions

Although solubilities and partition coefficients have been calculated for the PGE and Re, for several reasons the values obtained should be considered as estimates only. Firstly, in extrapolating the thermochemical data to temperatures and pressures similar to those of the mantle, all solid phases were treated as incompressible solids and it was assumed that no phase changes occurred. Although the structures of Ir and Pd metal were recognised to change with increasing temperature no other phase changes were noted in the metals, sulphides or oxides of the PGE and Re in the temperature range 298 - 1400°C. These compounds are, however, poorly studied and little information was available concerning their behaviour under non standard conditions, particularly at high pressures.

Secondly, the accuracy of the free energy values used for the calculation of the mineral solubilities and partition coefficients is estimated at between 0.5 and 2%. Such uncertainties may lead to relative errors in the calculated mineral solubilities and values of $D_{spinel/BMS}$ of between ± 25% and a factor of 2 - 3, depending on the element and species concerned.

Thirdly, all activity coefficients were determined at atmospheric pressures. If the sulphide and spinel phases are not wholly incompressible, then with increasing pressure the structure of the minerals may alter, resulting in changes in the activity coefficients.

Finally, the assumption that $\gamma_{OsO_2}$, $\gamma_{ReO_2}$ and $\gamma_{ReS_2}$ may be comparable with $\gamma_{RuO_2}$ and $\gamma_{IrS_2}$ and that activity coefficients determined in pyrrhotite are applicable to MSS introduces further potential inaccuracies to the modelling. In the absence of more appropriate experimental values, however, such approximations may represent the only way to approach such calculations.

Notwithstanding these points, the calculations based on thermochemical data may be used to make a number of observations concerning the behaviour of the PGE and Re during mantle processes:

i) Provided a base-metal sulphide phase exists in the mantle peridotite, the Pt-group elements should be almost entirely dissolved in the BMS phase and should not be present as discrete Pt-group minerals.

ii) In contrast to the PGE, an oxide of Re may be relatively stable under mantle conditions and may either coexist with the metal at temperatures close to the anhydrous peridotite solidus, or dissolve entirely in the spinel phase present in the mantle. Despite the high solubility of Re in spinel, the considerably greater solubility estimated for the element in the base-metal sulphide phase would suggest that little of it should partition into spinel, provided a BMS phase is present.

iii) Under conditions of low $f_{S_2}$-$f_{O_2}$, Os and Ir may be partially present as discrete alloy grains. Whilst such $f_{S_2}$-$f_{O_2}$ conditions are relatively common during the low-temperature serpentinisation of peridotites, they do not appear to characterise most melting environments. Consequently, the partitioning of Ir and Os during mantle melting should be controlled predominantly by partitioning between the base-metal sulphide and silicate melts.

### 2.3.6 Volatile PGE and Re Species and Transport in a Vapour Phase

In addition to the refractory oxides and sulphides discussed above, the PGE and Re form a number of volatile species which may be present in magmatic or metasomatic fluids. Although the principle volatile species are oxides, containing the PGE in their highest oxidation states (e.g. $OsO_4$, $Re_2O_7$, $IrO_3$ and $PtO_2$), many of the PGE and Re may also form volatile halide and oxy-halide compounds.

Using similar thermochemical arguments to those employed in Sections 2.3.2 and 2.3.3, Wood (1987) calculated the activities of the PGE in hydrous magmatic fluids ($f_{H_2O}$=1 kbar),

demonstrating that, at oxygen fugacities close to those for the FMQ buffer and temperatures up to 1330°C, the concentrations of Os, Ir, Ru and Pt in the fluid do not exceed 1 ppt. These calculations suggested that, despite the volatility of many of the higher PGE oxides, the transport of the PGE as oxide species in the vapour phase should be minimal under lithospheric mantle conditions.

A similar calculation may be performed for $Re_2O_7$, using the data listed in Appendix B. From studies of the vapour transport of W and Mo in magmatic fluids and the enrichment of Re in the molybdenites precipitated from these fluids, it is probable that Re is present predominantly as a hydrated oxide ($HReO_4$) during vapour transport, rather than as $Re_2O_7$ (Bernard *et al.*, 1990). Although it is not possible to take into account the effects of hydration on the stability of the heptoxide, the calculated concentrations of Re in hydrous metasomatic fluids are also low, implying that appreciable transport of the element also should not occur under mantle conditions.

The formation of volatile halide and oxy-halide compounds by most of the PGE and Re suggests that fluid transport of the PGE may be possible in halide-rich fluids. It has been proposed that such fluids may account for the mobilisation of the PGE in the Bushveld, Stillwater and similar complexes and for Os mobility in some mafic and ultramafic amphibolites, which contain evidence for noble metal mineralisation (Boudreau & McCallum, 1986; Walker *et al.*, 1989b). Calculations by Wood (1987) suggested that, whilst the presence of chlorine in the fluid may increase the volatility of Pd and Ru significantly, chloride fugacities in excess of 100 bar would be required before the concentrations of $PdCl_2$ and $RuCl_3$ in the fluids would exceed 1 ppt. Although such chloride fugacities may be reasonable for volatile-rich magmatic fluids associated with mineralisation, it is unclear what values of $f_{HCl}$ would be necessary to mobilise Re and Os and whether such fugacities may be present in mantle metasomatic fluids.

In summary, the existence of volatile rhenium or osmium oxides and their transport by metasomatic fluids is not to be expected under normal lithospheric mantle conditions, although some mobility may be possible in crustal fluids containing high halide concentrations, such as those associated with noble-metal mineralisation.

## 2.4 Experimentally Derived Partition Coefficients

Over the last decade a number of partitioning experiments have been carried out in order to ressolve the debate concerning the mineral or minerals which dictate the behaviour of the PGE during magmatic processes. These experiments investigated the partitioning of the PGE between mafic silicate melts and a variety of mineral phases, including olivine, clinopyroxene, spinel, base-metal sulphides and PGE alloys. From the results of the thermochemical calculations in Section 2.3, partitioning between the silicate melt and base-metal sulphides would be expected to exert the strongest control on the behaviour of the PGE during mantle melting. However, if basaltic melts fractionate in the absence of a sulphide phase, or the sulphide phase is removed from the mantle source by sufficiently high degrees of melting, then other phases may also influence the behaviour of the PGE.

Although many of the partitioning experiments included several of the PGE, few analysed Os and fewer still Re. Whilst the partitioning of Os may resemble that of Ir (which is frequently included in partitioning studies on account of its relative ease of analysis), the behaviour of Re is less easy to deduce from PGE partitioning experiments, because no clear link has been ascertained between the abundances of Re and any particular PGE. Consequently, except where specifically analysed, the partitioning behaviour of Re cannot be addressed from the results of the majority of the experiments.

### 2.4.1 Olivine

On the assumption that olivine was the only fractionating phase, the direct correlation of Os, Ir and Ru abundances with the MgO contents of komatiites from the Gorgona and Alexo volcanic suites led Brügmann *et al.* (1987) to the conclusion that these elements were compatible in olivine, with partition coefficients in the range 1.6 - 1.8. The correlation of Os, Ir and Ru with MgO contrasted with the behaviour of Pd, Cu and Au, whose increasing abundances with decreasing MgO content were consistent with almost perfect incompatibility. To account for the contrasting compatibility of different PGE, Brügmann *et al.* (1987) proposed that the similarity between the ionic radii of $Os^{2+}$, $Ir^{2+}$ and $Ru^{2+}$ and $Fe^{2+}$ and $Mg^{2+}$ enabled them to substitute for Fe and Mg in olivine, whilst the dissimilar ionic radii and charges of the most stable ions of Au ($Au^{+}$ and $Au^{3+}$) precluded it from partitioning into the mineral.

Few reports, if any, exist of compounds containing divalent Os, Ir or Ru and no ionic radii for such ions could be found in the reference cited by Brügmann *et al.* (Shannon, 1976). From the ionic radii of the trivalent and tetravalent ions of these elements, the divalent ions would, in fact, be expected to have ionic radii considerably greater than those of either $Mg^{2+}$ or $Fe^{2+}$. Consequently, the suggestion by Brügmann *et al.*, that Os, Ir or Ru partition into olivine as divalent ions, is viewed with suspicion and the solid solution of these elements in olivine is rejected as the cause of their apparent compatibility during melting and crystallisation processes. This conclusion is supported by the observations of Mitchell & Keays (1981), who found that the Ir content of olivines from mantle xenoliths was no greater than that of the coexisting minerals.

### 2.4.2 Clinopyroxene

Despite the important role of clinopyroxene in the partitioning of lithophile trace elements during magmatic processes, only one experimental study has been published in which the partitioning of a PGE between a basaltic melt and clinopyroxene phase was investigated (Watson *et al.*, 1987). Because this study aimed to investigate the role of clinopyroxene in the partitioning of a number of isotopic parent-daughter pairs, the compatibilities of both Re and Os were investigated. Although the results of the study were of a purely reconnaissance nature, with some uncertainty introduced through the dissolution of the Re and Os in the Pt containers, the calculated partition coefficients of 0.035±5 and 0.07±4 for Re and Os respectively indicate that neither element should be compatible in the mantle clinopyroxene phase, hence the mineral should exert negligible control on the behaviour of the elements during mantle processes.

### 2.4.3 Spinel

The frequent association of high Os, Ir and Ru abundances with spinel in layered mafic complexes (e.g. Gijbels *et al.*, 1974), ophiolites (Oshin & Crocket, 1982; Page & Talkington, 1984; Cocherie *et al.*, 1989) and mantle xenoliths (Mitchell & Keays, 1981) and the apparently compatible behaviour of these elements during magmatic processes has led to the proposal that these elements may partition into spinel minerals under sulphur undersaturated conditions. Whilst several authors have suggested that the Ir-group of the PGE (IPGE; Ir, Os and Ru) may dissolve in the spinel phase (e.g. Agiorgitis & Wolf, 1978:

Oshin & Crocket, 1982), others have proposed that the spinels have either nucleated on discrete PGE mineral grains or merely co-precipitated with PGE minerals as early formed phases (e.g. Prichard *et al.*, 1981; Stockman & Hlava, 1984; Tarkian *et al.*, 1991). Although nucleation of spinels by discrete PGM would have negligible consequences for the partitioning of the PGE during partial melting, solid solution of the PGE in spinel may significantly affect their behaviour during melting.

In order to investigate the role of spinel in the fractionation of the PGE during partial melting or crystallisation processes, partitioning experiments between silicate melt and Al-spinel or magnetite were carried out by Capobianco & Drake (1990) and Capobianco *et al.* (1994), the data from which were used in the thermochemical calculations of Section 2.3. In the absence of sulphur and at high oxygen fugacities used in the experiments, the partitioning behaviour of Ru, Rh and Pd were found to differ significantly, with Ru and Rh appearing to be considerably more compatible in the oxides than Pd. If the compatibility of the PGE in the second-row of the transition metals is mirrored by those in the third row, the experiments would predict that both Os and Ir should partition into spinels, leading to fractionation of the PGE. Because the experiments were performed under sulphur absent conditions and at oxygen fugacities considerably higher than those which may occur in the continental mantle lithosphere, however, it is not wholly clear from the experimental data alone whether such partitioning would occur under more realistic geological conditions.

### 2.4.4 Sulphides

On account of their recognised chalcophile nature, numerous experiments have been performed in order to measure liquid sulphide-liquid silicate partition coefficients for the PGE. Using these experimentally derived values many authors hoped to determine whether sulphide-silicate melt partitioning could account for the fractionation of the PGE commonly observed in mantle-derived melts. To date, no single set of sulphide-silicate melt partition coefficients has been able to account for the behaviour of the PGE in mafic and ultramafic rocks. Not only do estimates of $D_{sul/sil}$ for the same element vary over several orders of magnitude between partitioning studies performed by different authors (e.g. $D^{Ir} = 3 \times 10^3$ and $D^{Pd} = 2 \times 10^3$ in the the study by Fleet *et al.*, 1991, but $D^{Ir} \approx 3 \times 10^5$ and $D^{Pd} \approx 6 \times 10^4$ in the study by Bezmen *et al.*, 1994), but the order of estimated "compatibility" of the PGE

observed in magmatic sulphide deposits (i.e. $D^{Os}>D^{Ir}>D^{Ru}>D^{Rh}>D^{Pt}>D^{Pd}$) is not reflected in the partition coefficients determined in most experimental studies, (e.g. $D^{Ir} > D^{Pd} > D^{Rh} > D^{Ru} > D^{Os}$, Bezmen *et al.*, 1994; $D^{Pd} > D^{Ir}$ ($>>D^{Pt}$), Peach *et al.*, 1990 and $D^{Ir} \approx D^{Pd} \approx 3.5 \times 10^4$, Peach *et al.*, 1994).

Although the reasons for the variation in the partition coefficients determined by the different studies remain uncertain, the high partition coefficients determined in all the experiments confirm that the base-metal sulphide phase probably dominates the partitioning behaviour of the PGE. Despite the low modal abundance of sulphides in the mantle, the high values of $D_{sul/sil}$ should result in compatible behaviour during melting: for mantle peridotite containing 0.05% BMS in equilibrium with a silicate melt, the calculated peridotite-melt bulk distribution coefficient for an element with $D_{sul/sil} \approx 10^4$ would be ~5.

### 2.4.5 Alloys

Under conditions of low $f_{O_2}$ and $f_{S_2}$, the PGE may be present as metallic phases, either dissolved in Fe-Ni alloys or as discrete Pt-group minerals. Partitioning experiments performed at oxygen fugacities close to those for the iron+quartz-fayalite buffer and with metallic phases present (e.g. Jones & Drake, 1986; Fleet *et al.*, 1991) suggest that metal-silicate liquid partition coefficients for the PGE are considerably higher than those observed between sulphide and silicate liquids, with values in the range $10^5$ - $10^6$ calculated for Re, Ir and Pt (Jones & Drake, 1986).

As a consequence of the large partition coefficients of the PGE between alloy phases and silicate melts, such phases would exert a strong influence on the partitioning behaviour of the PGE and Re. However, at the oxygen and sulphur fugacities estimated for the mantle lithosphere, Fe-Ni alloys should not be stable relative to more oxidised phases, hence any alloy phase will be composed predominantly of the PGE. In view of the low PGE concentrations in mantle peridotites, the modal proportion of such alloys would be very small, counteracting the high distribution coefficients and potentially leading to low bulk distribution coefficients.

### 2.4.6 Conclusions of Partitioning Studies

Despite numerous experiments to determine partition coefficients between the PGE and mantle phases, there remains considerable debate about the phases which control the

behaviour of the PGE during melting and crystallisation processes. Although olivine and clinopyroxene can be rejected as potentially important phases, spinel, base-metal sulphides and alloy phases may all exert some influence on the behaviour of the PGE under different conditions. Partitioning experiments demonstrate that all the the PGE are highly compatible in a base-metal sulphide phase, which probably dominates the partitioning of the PGE during mantle melting, however the compatibility of Ru and Rh in spinel phases would suggest that significant fractionation of the PGE may occur during spinel-silicate melt interactions.

## 2.5 The Observed Behaviour of the PGE and Re during Mantle Processes

As mentioned above, the economic importance and apparently coherent behaviour of the Pt-group elements have resulted in considerably greater study of their behaviour than of that of Re. Over the last decade a number of studies have determined the abundances of either most or all of the PGE in peridotite and pyroxenite samples collected from a number of orogenic massifs or suites of xenoliths contained within intraplate volcanic rocks (e.g. Mitchell & Keays, 1981; Garuti *et al.*, 1984; Morgan, 1986; Lorand, 1989a, 1989c, 1991; Lorand *et al.*, 1993). In only one of these studies was Re analysed (Morgan, 1986). On account of the low number of studies of mantle rocks in which Re has been determined in addition to the PGE in mantle rocks, most of the observations of the behaviour of Re in the mantle must be deduced from the abundances of Re in erupted magmas (e.g. Hertogen *et al.*, 1980) or from studies of the Re-Os isotope systematics in mantle peridotites and mantle-derived melts (e.g. Walker *et al.*, 1988; Martin, 1989, 1990; Reisberg, 1991).

### 2.5.1 Behaviour of Re during Mantle Melting and Fractionation

***Mantle Melting***

In a study of the abundances of siderophile elements in a collection of spinel peridotite xenoliths originating from alkali basalts in the western United States, Central America, Alaska and Australia, Morgan (1986) noted that the Re abundances of the peridotites exhibited a linear decrease with increasing degrees of depletion in major elements (Figure 2.4). By extrapolating this trend to zero melt depletion, he calculated that the Re

concentration in undepleted mantle material was approximately 0.26 ppb (~0.0071 x chondrite), consistent with the value (0.25 ± 0.02) independently estimated by Allègre & Luck (1980) as part of their determination of the mantle evolution curve. The decreasing Re abundances in the xenoliths suggested that during partial melting Re behaves as an incompatible element and partitions into the silicate melt phase, as demonstrated by the high Re abundances observed in many mantle melts (e.g. 0.3 - 1.4 ppb in MORB; Roy-Barman & Allègre, 1994).

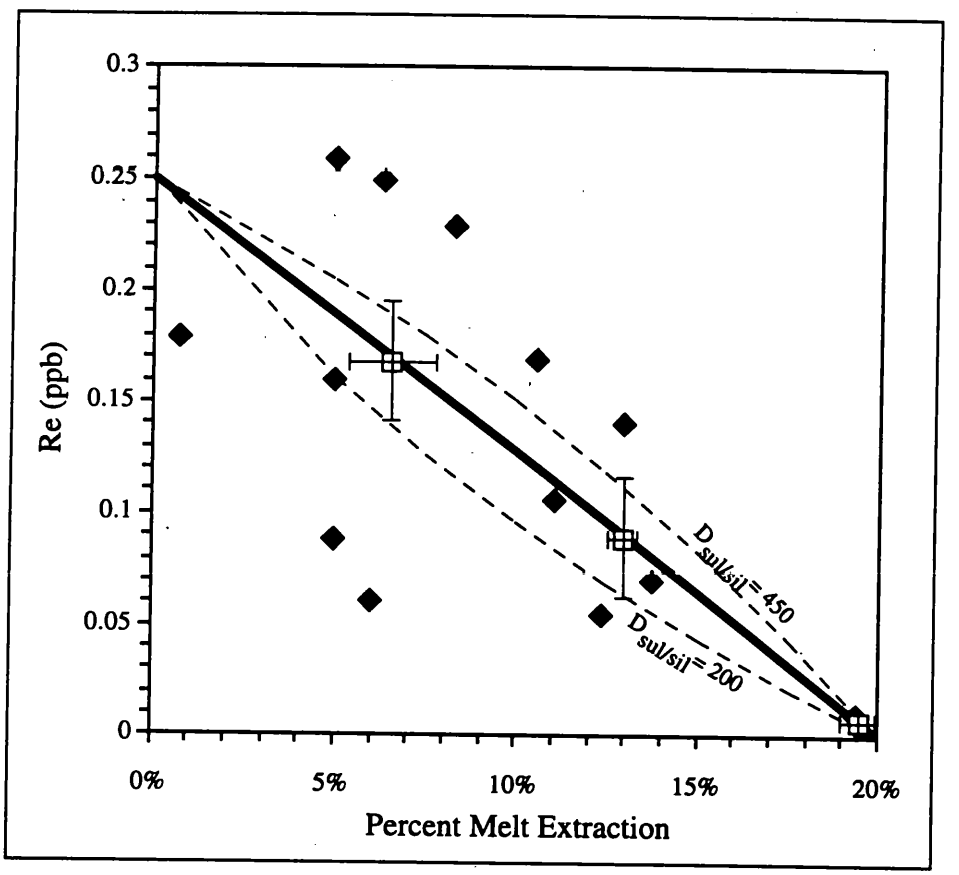


**Figure 2.4** Variation of Re with the proportion of melt extracted from spinel lherzolites collected from intraplate alkali basalts in the Western United States, Central America, Alaska and Australia (Morgan, 1986). Solid symbols represent individual xenoliths, open symbols refer to the mean values of xenoliths grouped according to their Ca/Si values, with error bars representing one standard error of the mean (after Morgan, 1986). The proportion of melt extracted was calculated using the xenolith Mg contents, assuming $[Mg]_{pyrolite}$= 22.6% and $[Mg]_{melt}$= 6.15% (Ringwood, 1977). Also shown are the trends expected for the extraction of a melt containing 1000 ppm S, formed by the non-modal melting of fertile mantle containing 0.25 ppb Re and 200 ppm S. The solid line assumed $D_{sul/sil}$ = 325, whilst the dashed lines assumed $D_{sul/sil}$ = 200 or 450.

Because the concentration of Re decreases linearly with increasing F, right up to the exhaustion of the element at ~20% melting, the behaviour of Re during melting cannot be accounted for using simple batch or fractional melting models, in which the residual

concentration of a moderately incompatible element should decrease as a curvilinear function of the degree of melting and only tend to zero at the limit of 100% melting. The linear trend may, however, be explained by a process involving non-modal melting, in which the partitioning of Re between the mantle residue and silicate liquid is dominated by a single phase which enters the melt in greater proportions than are present in the original peridotite. As this phase is removed from the source the concentration of Re in the residue falls, approaching zero when the phase is entirely consumed.

Whilst the clinopyroxene content of the mantle may be removed by the correct degrees of partial melting, the partitioning experiments of Watson *et al.* (1984) indicate that Re is insufficiently compatible in the mineral for it to affect the bulk distribution of the element during melt extraction. A second, and considerably more likely phase to control the behaviour of Re during mantle melting, however, is the base-metal sulphide. When plotted

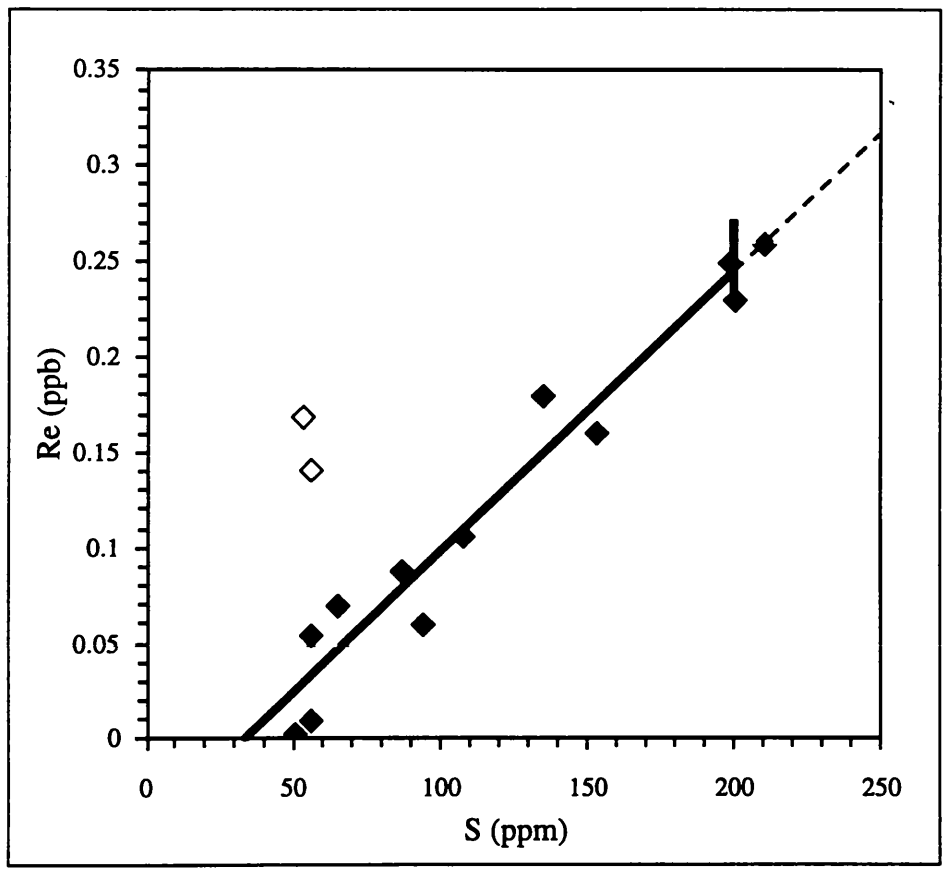


**Figure 2.5** Variation of Re as a function of S content in the xenoliths described by Morgan (1986), The line shown ($r^2$ = 0.95) is regressed through filled data points only, passing through the Re abundance of the undepleted mantle, as estimated from Re-Os isotope systematics (bar at 0.25 ± 0.02 ppb Re; Allègre & Luck, 1980), at ~ 200 ppm S.

as a function of whole-rock S abundances, the Re concentrations of the xenolith suite described by Morgan (1986) define an excellent linear correlation (Figure 2.5), confirming that the two elements follow each other into the melt.

If the range of sulphur contents observed in the xenolith suite was created by the extraction of variable amounts of a sulphur-saturated melt from an undepleted mantle source, then the sulphur should be consumed after approximately 20% melting (assuming $[S]_{melt} \approx$ 1000 ppm (Wendlandt, 1982) and $[S]_{mantle} \approx 200$ ppm (Morgan, 1986)), as required for the disappearance of Re from the xenolith suite. Using the estimated concentration of Re in the undepleted mantle (0.26 ppb; Morgan, 1986) and the non-modal batch melting equations of Shaw (1970), the linear decrease in Re with increasing melting may be successfully modelled using a $D^{Re}_{sul/sil}$ value of ~325 (Figure 2.4). Although the observed variation in the Re content of the xenoliths during mantle melting is consistent with the predominantly chalcophile behaviour predicted by the thermochemical calculations, Re appears to behave more like a moderately chalcophile element, such as Cu ($D_{sul/sil} \approx 245$; Rajamani & Naldrett, 1979), than the highly chalcophile PGE ($D_{sul/sil} \approx 10^3$ -$10^5$).

Although the relatively low value of $D_{sul/sil}$ calculated for Re is unexpected, it may be accounted for by the relatively high activity of rhenium oxide at mantle solidus temperatures, as determined during the thermochemical calculations. In their model for the solubility of metals in silicate liquids, Borisov & Kadik (1990) proposed that metals dissolved as oxide species during melting. The high activity of $ReO_2$ would, therefore, enable greater quantities of Re to dissolve in the melt, lowering its partition coefficient relative to those of the PGE, whose oxides are far less stable under the same conditions.

### *Melt Transport and Crystal Segregation*

The behaviour of Re during magma transport and crystallisation is very poorly constrained. Evidence from mafic layers in mantle peridotites suggests that the element may behave compatibly during fractionation, increasing in abundance with increasing MgO in the layers (Reisberg *et al.*, 1991). Conversely, the Re abundances of a suite of komatiite flows are inversely correlated with both MgO and NiO (Walker *et al.*, 1988) and the Re contents of chromites from the Stillwater complex have been shown to be consistently low relative to typical Re concentrations in mantle melts (Hertogen *et al.*, 1980; Martin, 1989). These

observations suggest that the incompatibility exhibited by Re during melting may also operate during crystallisation and that it does not partition appreciably into either olivine or spinel.

Although S abundances were not presented in each of the mentioned studies, much of the observed behaviour of Re may be accounted for by the presence or absence of a sulphide phase. In the simplest case, the incompatible behaviour of Re in the massive chromites of the Stillwater complex may be explained by the absence of base-metal sulphides in the rocks (Martin, 1990). However, the incompatibility of Re in the chrome-spinel phase is contrary to the predictions of the thermochemical calculations, suggesting that either the activity coefficient for Re in the melt phase is lower than that in the solid oxide, or that $\gamma_{ReO_2}$ is considerably greater than that estimated using the calculated value of $\gamma_{RuO_2}$.

To explain the apparently compatible behaviour in the mafic layers of the Ronda massif requires the comparison of these layers (in which the sulphide component has not been investigated in detail) with those occurring within the peridotites of the N.E. Pyrenean massif, which have been the subject of numerous studies by Jean-Pierre Lorand (e.g. Lorand, 1989a-d, 1991). Both sets of mafic layers are believed to be the products of crystal segregation from melts *en route* to the surface and are strongly enriched in S relative to average mantle peridotites (200 - 1300 ppm *vs.* $\leq$ 200 ppm; Suen & Frey, 1987; Lorand, 1989a; Morgan, 1986).

In the mafic layers of the N.E. Pyrenean massifs, Lorand (1989a) observed that the S and Cu abundances were strongly correlated and were highest in the thinnest veins and vein margins. These observations were explained by the more rapid diffusion of heat outward from these layers, leading to greater degrees of S-saturation and the creation of higher S and chalcophile element abundances. Because the vein margins and thinner veins are composed of the earliest phases to crystallise from the melt, they are also characterised by higher modal proportions of orthopyroxene and more mafic compositions. The coincidence of sulphur saturation and early silicate mineral segregation from the mafic melts may therefore account for the correlation of Cu and S with MgO, in spite of the supposed incompatibility of the former elements. If the similarity between $D^{Cu}_{sul/sil}$ and $D^{Re}_{sul/sil}$ observed during melting is unchanged during crystal fractionation, then the correlation between Re and MgO observed

in the Ronda mafic layers may arise from a similar process of simultaneous S-saturation and mineral segregation.

In the komatiite flows analysed by Walker *et al.* (1988), Re exhibits no correlation with S, suggesting that either the behaviour of Re may be controlled by a phase other than Fe-Ni sulphides under crustal conditions or that the sulphur abundances of the komatiites have been altered since the flows were emplaced. The observation of considerable S mobility during low-grade metamorphism of other ultramafic rocks (Gelinas *et al.*, 1982) and the relatively low S abundances of these flows may suggest the latter to be true and that any correlation or lack of correlation between Re and S in these samples may not be significant.

In summary, the observed behaviour of Re during processes in the mantle and mantle melts appears to agree with the conclusions of the thermochemical calculations. Under mantle conditions, the partitioning of Re is probably controlled almost entirely by the presence of a base-metal sulphide phase, although the comparatively high stability of its oxide enables it to dissolve in the silicate melt relatively easily, leading to a silicate-sulphide partition coefficient that is more like that of Cu than those of the highly chalcophile PGE. Contrary to the conclusions of the thermochemical calculations, in the absence of a base metal-sulphide phase, Re does not appear to partition appreciably into crystallising oxide phases. Although this disagreement is not fully understood, it may be explained by either a lower activity coefficient for Re in the melt phase than in the solid oxide, or $\gamma_{ReO_2}$ being considerably greater than, rather than equal to $\gamma_{RuO_2}$, as assumed in the calculations.

### 2.5.2 Behaviour of the PGE During Mantle Melting and Crystal Segregation

Naldrett *et al.* (1979) observed that, when plotted in order of descending melting point (i.e. Os, Ir, Ru, Rh, Pt, Pd), the chondrite-normalised abundances of the PGE present in magmatic sulphides frequently define smooth curves, analogous to REE profiles. Although the smooth variation in the behaviour of the REE may be accounted for by the continuous variation in the chemistry of the elements, resulting from the contraction in the elements' ionic radii across the the periodic table, the order in which the PGE are plotted on chondrite-normalised diagrams is not directly related to their positions in the periodic table, or their ionic radii, but is derived from observations of their abundances in a number of magmatic settings. Such diagrams are conventionally used to illustrate the fractionation of the PGE in

magmatic rocks and are commonly divided into the Ir-group of PGE (IPGE: Os, Ir and Ru), on the left of the plots, and the Pd-group of PGE (PPGE; Rh, Pt and Pd), on the right.

### *Mantle Melting*

Figure 2.6 shows that the chondrite-normalised PGE profiles of residues after melting are usually relatively flat and differ little from the profiles of undepleted mantle material. The PGE abundances in most mantle peridotites range between 0.7 and 1% of those in chondrites and do not correlate with their lithophile element compositions (Chou *et al.*, 1983; Morgan, 1986; Lorand, 1989c). Such decoupling of the PGE from the lithophile elements may be adequately explained by strong partitioning of the PGE into the BMS phase, as predicted by both the thermochemical calculations and partitioning experiments.

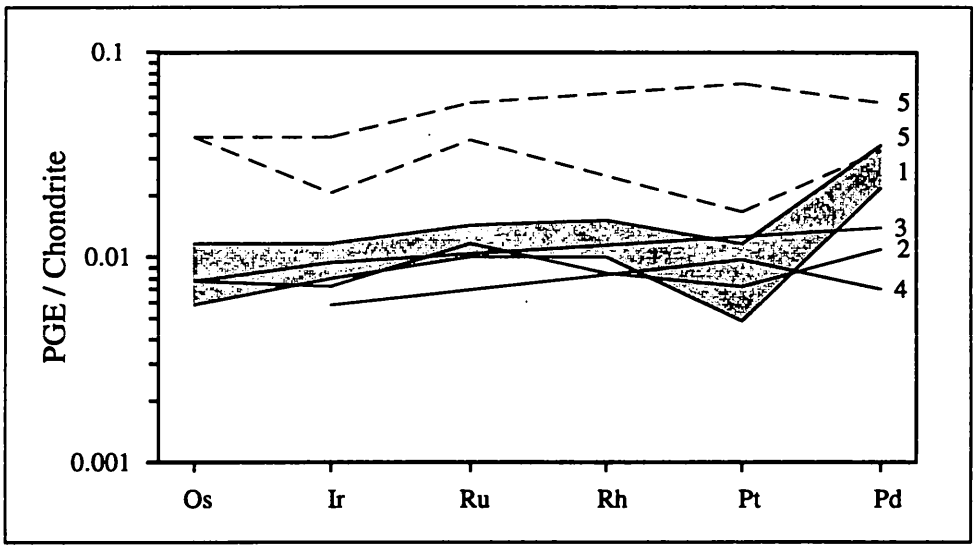


**Figure 2.6** Chondrite-normalised plot of PGE abundances in harzburgite and lherzolite whole-rocks and spinel mineral separates from ophiolitic harzburgites. 1 = orogenic peridotites from the N.E. Pyrenean massifs (Lorand, 1989c), 2 = harzburgite, Bay of Islands ophiolite complex (Edwards, 1990), 3 = harzburgite, Troodos ophiolite (Barnes *et al.*, 1985), 4 = harzburgite, Thetford Mines ophiolite (Oshin & Crocket, 1982), 5 (dashed) = spinels from harzburgites of the Vourinos ophiolitic complex, Greece (Cocherie *et al.*, 1989). Normalisation performed using the values compiled by Naldrett & Duke (1980) for a C1 chondrite.

With increasing degrees of partial melting, the PGE may concentrate in the remaining sulphide phase until either it is exhausted at high degrees of melting or the concentrations of the PGE exceed their solubilities. On the final consumption of the BMS phase, the bulk distribution coefficients of the elements would be considerably reduced, resulting in less compatible behaviour and significantly higher concentrations in the melt. Such a model was proposed by Hamlyn & Keays (1986) to account for the high PGE abundances in second

stage melts. Evidence for this change in behaviour is also shown by the significantly different PGE concentrations in oceanic basalts (e.g. FAMOUS MORB glasses with ≤ 1.5 ppb Pd; Hertogen *et al.*, 1980; Peach *et al.*, 1990), which result from low to moderate degrees of melting, relative to those in komatiitic melts, produced by more than 25 - 30% melting and containing ~9 ppb Pd (Barnes *et al.*, 1985).

From the flat PGE profiles of most mantle peridotites, it may appear that the elements are all similarly compatible in the mantle residue. Although this may be true, calculations to model the fractionation of highly chalcophile from moderately chalcophile elements (e.g. Pd vs. Cu) during the segregation of massive sulphide deposits suggest that the true contrast in the partition coefficients of the two elements will only be observed if the ratio of the mass of silicate melt to the mass of sulphide liquid with which it is in effective equilibrium, R, is more than an order of magnitude greater than the sulphide-silicate partition coefficient of the more compatible of the two elements (Keays & Campbell, 1981; Campbell *et al.*, 1983). Likewise, if R is very small (≤10% of the partition coefficient of the less compatible element), the ratio of the two elements may remain unfractionated, such that their ratio in the silicate melt is the same as that in the coexisting sulphide.

If this argument is applied to the PGE during mantle melting, for which D values are in the range $10^3$ - $10^4$, then no fractionation should be observed for R < 100 - 1000 and values of R > $10^5$ would be required for the true differences in $D_{sul/sil}$ to be observed. In contrast, the considerably lower values of $D^{Cu}_{sul/sil}$ (~250), and probably $D^{Re}_{sul/sil}$ (325), would mean that fractionation of Cu from the PGE may be observed for values of R ≥ 25. For the extraction of 10% melt from a peridotite containing 0.05 wt% BMS, a value of R ≈ 200 may be calculated. Consequently, during partial melting, the different chalcophile elements present in the mantle may be expected to display contrasting behaviours. The highly chalcophile elements, including the PGE, should exhibit little or no fractionation from each other (despite minor variations in $D^{PGE}_{sul/sil}$), but may be fractionated from the moderately chalcophile elements, such as Cu and Re.

In Figure 2.7, the Cu/Pd and Pd/Rh ratios of mantle peridotite samples collected from the Baldissero and Balmuccia massifs in the Western Italian Alps are plotted against their "Primitiveness Index" (defined as $(SiO_2+Al_2O_3+CaO+FeO)/(FeO+MgO)$ and provide a rough estimate of the clinopyroxene content; Garuti *et al.*, 1984). Although both plots

exhibit considerable scatter, with increasing major element depletion the Cu/Pd ratio is progressively reduced, whilst there is little appreciable change in Pd/Rh.

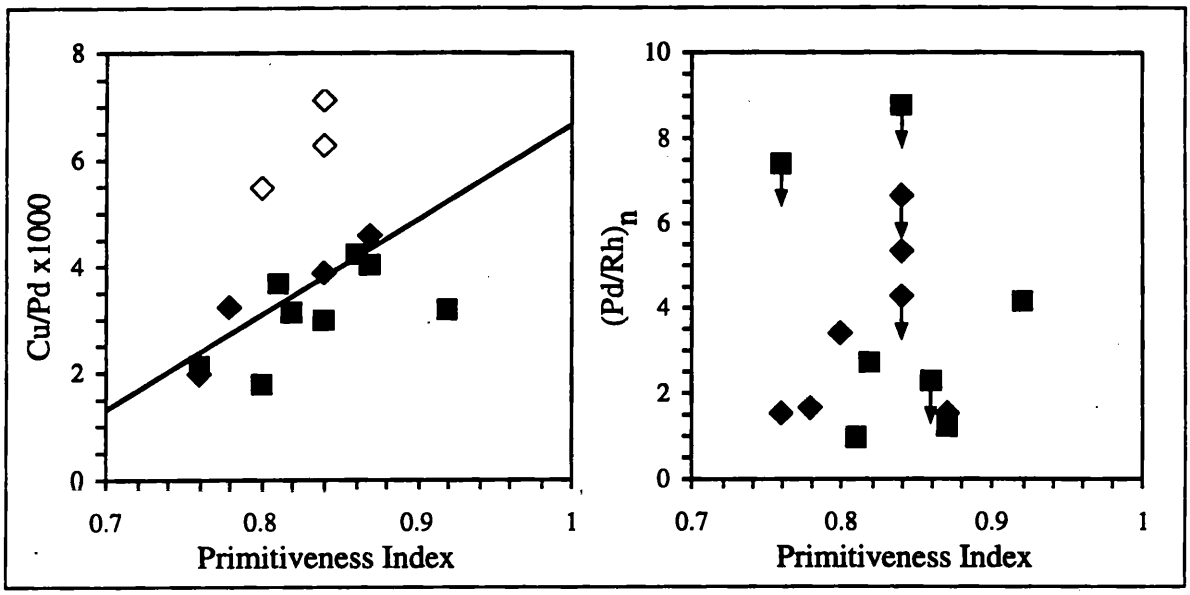


**Figure 2.7** Fractionation of the chalcophile elements as a function of melt depletion in the massive peridotites of the Baldissero (■) and Balmuccia (◆) peridotite massifs. Pd/Rh ratios normalised to the C1 chondrite values compiled by Naldrett & Duke (1980). Symbols with arrows indicate maximum values, owing to Rh concentrations below detection. Data from Garuti *et al.* (1984). "Primitiveness Index" calculated as (SiO2+Al2O3+CaO+FeO) / (FeO+MgO). Line shown in plot of Cu/Pd ($R^2 \approx 0.5$) is regressed through only the filled data points: open symbols, samples containing anomalously high Cu and S concentrations.

The suggestion that either some or all of the PGE are hosted by the mantle spinel phase may be tested by the analyses of the PGE abundances in spinel mineral separates from ophiolitic harzburgites (Cocherie *et al.*, 1989; Figure 2.6). These appear to define flat chondrite-normalised profiles whose concentrations exceed those expected in the whole rock. Leaching experiments by Oshin & Crocket (1982), using HF + $H_2SO_4$, demonstrated that the PGE may be wholly stripped from such spinels, but may be only partially removed from cumulate chromites. Taken together, the flat PGE profiles and the easy removal of the PGE from harzburgitic spinels imply that either a) the PGE were exsolved from spinel during cooling (and migrated to the grain boundaries at discrete Pt-group minerals) and that the spinel did not fractionate the PGE under mantle conditions, or b) that the PGE were located in the intergranular component during melting and that their determined abundances in the spinel separates reflect contamination by the intergranular component on the grain boundaries. In view of the contrasting solubilities of the PGE in spinel predicted from the thermochemical calculations and the observed differences in the experimentally determined partition coefficients of Capobianco and co-workers, the former interpretation appears

unlikely. Consequently it is inferred that partitioning into spinels does not strongly influence the behaviour of the PGE in the mantle.

In conclusion, although the flat PGE profiles in both fertile and depleted mantle peridotites do not prove that the behaviour of the PGE is controlled by the mantle BMS phase during partial melting (as predicted from the thermochemical calculations), they are consistent with such a model. The absence of fractionation in the PGE profiles of mantle residues (yet decreasing Pd/Cu ratios with increasing degrees of melt depletion) may indicate that the moderately chalcophile elements are able to equilibrate between the BMS phase and silicate melt during mantle melting, but that the amount of silicate melt with which the highly chalcophile PGE can equilibrate is insufficient for any differences arising from variations in their compatibility to be expressed.

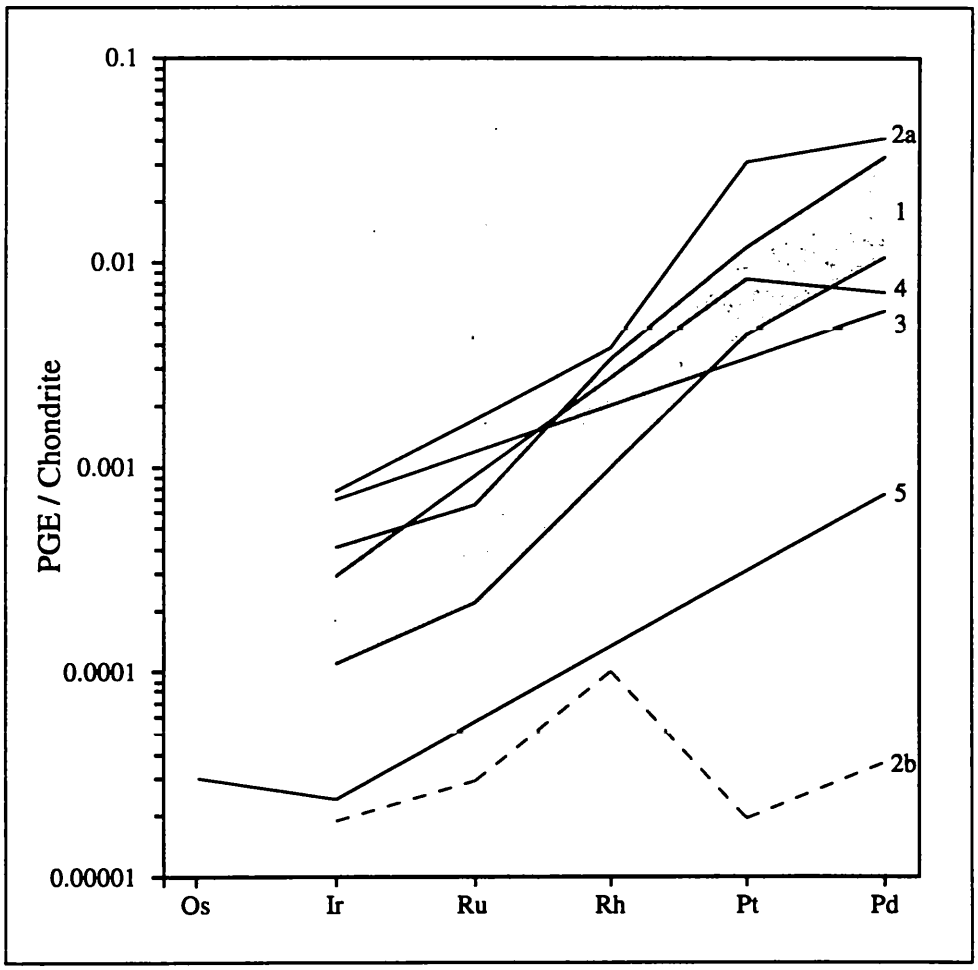


**Figure 2.8** Chondrite-normalised plot of PGE abundances in mantle-derived melts. 1 = continental tholeiitic basalts, Greenough & Owen (1992); 2 = ocean island basalts, Reunion hot spot trace (2a, maximum values, 2b, minimum values, as dictated by detection limits of analyses), Greenough & Fryer (1990); 3 = ocean island basalt, Hawaii, Crocket & Kabir (1988); 4 = MORB, FAMOUS area, Peach *et al.* (1990); 5 = MORB, FAMOUS area, Hertogen *et al.* (1980). Normalisation performed using the values compiled by Naldrett & Duke (1980) for a C1 chondrite.

### *Melt Transport and Crystal Segregation*

Although the flat chondrite-normalised profiles of residual mantle peridotites suggest that primitive melts should also contain unfractionated PGE profiles, such profiles are rarely observed. Most mantle-derived melts exhibit variably fractionated PGE patterns, with chondrite-normalised abundances increasing from Os or Ir to Pd (Figure 2.8).

To account for the fractionated PGE profiles of erupted melts, it has been frequently proposed that Os, Ir and Ru are removed during transport by the precipitation of discrete Pt-group minerals associated with the fractionation of high-temperature magmatic phases (e.g. Agiorgitis & Wolf, 1978; Barnes *et al.*, 1988; Greenough & Fryer, 1990). The products of such fractionation are represented by the olivine and spinel cumulates which are commonly located close to the base of ophiolite complexes and frequently contain either laurite, (Ru, Os, Ir)$S_2$, or Os-Ir alloy grains (Prichard *et al.*, 1981; Stockman & Hlava, 1984; Tarkian *et al.*, 1991). The presence of such Pt-group minerals in the cumulates produces negative gradients on the whole-rock chondrite-normalised plots (Figure 2.9) which complement the positive gradients observed in the erupted melts.

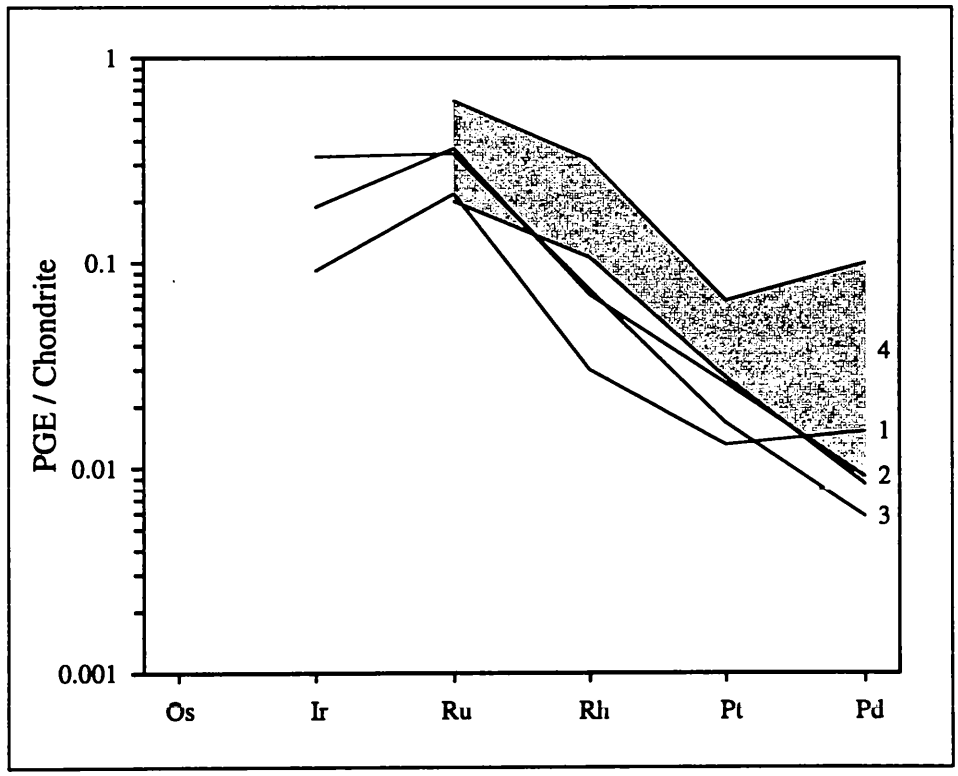


**Figure 2.9** Chondrite-normalised plot of PGE abundances in ophiolitic chromitites. 1 = Samail ophiolite, Oman; 2 = Josephine ophiolite, Oregon; 3 = Tiebaghi and Massif du Sud ophiolites, New Caledonia (lines 1-3 represent average values; Page *et al.*, 1982); 4 = Bou-Azzer ophiolite complex, Morocco (Fischer *et al.*, 1988). Normalising values taken from the compilation of Naldrett & Duke (1980) for a C1 chondrite.

The proposal that the melt is only fractionated during relatively near-surface processes, however, is inconsistent with the PGE compositions of anhydrous pyroxenite layers present in the peridotites of the N.E. Pyrenean massifs (Lorand, 1989a), which are interpreted as high pressure (15 - 20 kbar) crystal segregates from tholeiitic melts *en route* to the surface (Conquéré, 1977). Compared to their peridotite hosts, these layers are strongly enriched in both sulphur and the PPGE, with positively sloping PGE profiles (Figure 2.10). Whilst the sulphide inclusions demonstrate that the melts were probably sulphur saturated at the time of their emplacement in the peridotites, the PGE profiles suggest that they were either depleted in the IPGE prior to emplacement, or that the PPGE may have been preferentially removed from silicate melts by the segregation of the BMS phase. Because a repository for Os, Ir or Ru close to the source of such mantle melts has to be found, the cause of the observed fractionation remains unresolved.

To conclude, the behaviour of the PGE during melt transport and crystal segregation appears to be relatively complex, with both the formation of discrete Pt-group element minerals and the partitioning of the elements into base-metal sulphide phases controlling the abundances of the elements in magmas and crystal segregates. Despite the apparent absence of fractionation of the PGE during melting, the chondrite normalised PGE abundances of sulphides exsolved from magmas relatively close to their source suggest that either a phase enriched in Os, Ir and Ru has been removed from the melts prior to their emplacement or that the PGE may be significantly fractionated by partitioning between silicate and sulphide liquid phases.

### 2.5.3 Interaction of Peridotites with Mafic Melts

Analyses of the peridotites adjacent to the mafic layers in the N.E. Pyrenean massifs show pronounced variations in their chalcophile element abundances, which may be attributed to the interaction of the peridotite with the mafic melt (Lorand, 1989c). The extent to which the chalcophile element compositions of the peridotites were altered by this interaction appears to depend upon the nature of the magma from which the mafic layers segregated, the timing of S saturation and the peridotite temperature at the time of equilibration.

The peridotites adjacent to anhydrous pyroxenite layers exhibit a strong enrichment in both Cu + S and Pt + Pd, relative to massive peridotites sampled more than 0.5 m from the veins (Figure 2.10), although the enrichments in the two element pairs are apparently independent. In contrast, the wall-rock peridotites to amphibole-bearing mafic layers lack any overall enrichment in S, but are relatively depleted in Cu. Although these peridotites exhibit similar Ru, Ir and Pd abundances to those sampled at a distance from the veining, their Os, Rh and Pt contents are consistently low, falling below the detection limits of the analytical technique.

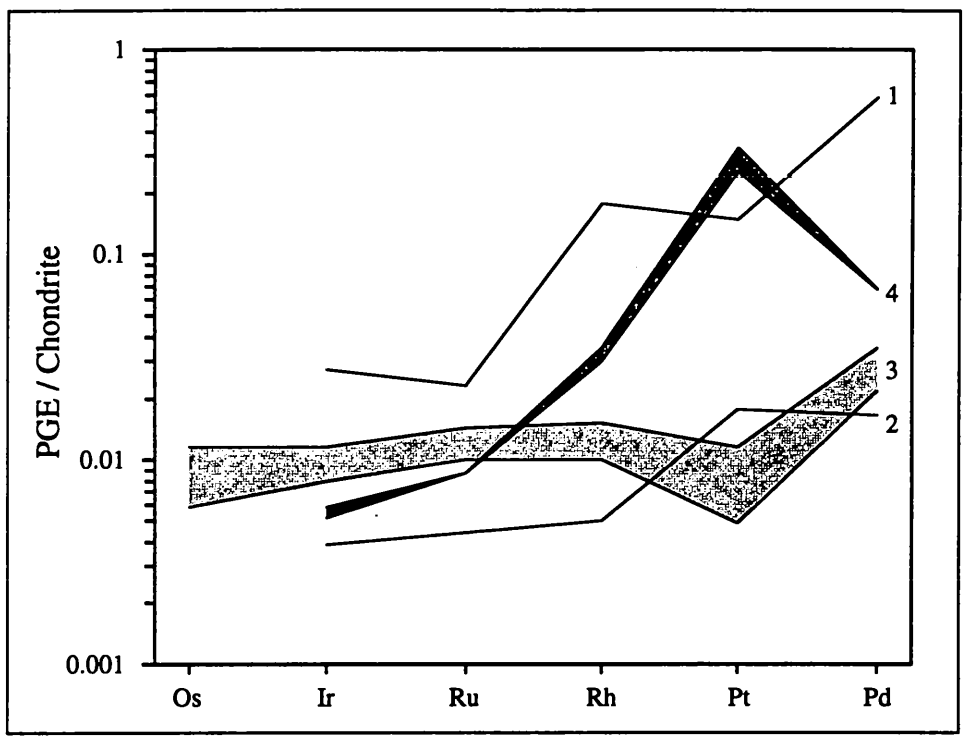


**Figure 2.10** Chondrite-normalised plot of the PGE abundances of mafic layers and adjacent peridotites in the N. E. Pyrenean massifs (Lorand 1989a, 1989c). 1 = spinel websterite layer, Prades; 2 = spinel websterite layer, Bestiac; 3 = range of PGE contents in peridotite away from veining; 4 = wall-rock peridotites to websterites. Normalisation values taken from the compilation of Naldrett & Duke (1980) for a C1 chondrite.

Lorand (1989c) accounted for the contrast in the behaviour of the chalcophile elements during peridotite-pyroxenite interactions by the infiltration of an exotic sulphide component into the wall-rocks to the anhydrous pyroxenites, but not into those adjacent to the amphibole-bearing layers. The difference was thought to result from the exsolution of the BMS phase at relatively high temperatures (T > MSS solidus) from the anhydrous pyroxenites, but at lower temperatures from the amphibole-bearing layers (T < MSS solidus). The liquid sulphide formed in the former would have been sufficiently mobile to migrate away from the mafic layers, carrying the PGE and Cu into the peridotite wall-rocks.

The solid sulphides in the latter would have been immobile, hence the loss of Cu, Os and Pt may be attributed to the direct equilibration of the sulphide component of the peridotites with a percolating melt characterised by low Cu, Os and Pt concentrations.

The effects of peridotite-melt interactions on the Re-Os isotope systematics of the CML and percolating melts should depend on factors similar to those which determine the behaviour of the other chalcophile elements. Partial or total equilibration of the two elements between the peridotite and magmas may occur, resulting in Os isotopic exchange and changes in the abundances of the two elements, depending on the chemistry of the melts. The abundances of the PGE and Cu in the peridotites adjacent to the melts which experienced early S saturation suggest that, whilst the Os abundances of the mantle peridotites may be unaffected by interaction with such melts, the Re abundances may be increased, producing elevated Re/Os ratios in the wall-rock peridotites and an evolution towards more radiogenic Os isotopic ratios. Similarly, interaction between mantle peridotites and the alkali basalts parental to the amphibole-bearing pyroxenites may result in the removal of both Re and Os from the peridotites, leading to thorough disturbance of their Re-Os isotope systematics and contamination of the melt by Os derived from the mantle lithosphere through which it passed.

## 2.6 Conclusions

By combining the behaviour of the PGE and Re predicted from the thermochemical calculations with the results of the experimental studies and observations of the abundances of the PGE, Cu and Re in mantle peridotites and mafic melts, it is possible to suggest how the Re Os isotope systematics of mantle peridotites may be affected by a number of different processes, including the extraction of partial melts, interaction with magmatic or volatile-rich fluids and alteration of the peridotites either *en route* or subsequent to emplacement in the upper crust.

### *Melt Extraction*

The behaviour of Re and Os during mantle melting appears to be primarily controlled by the partitioning of the elements between the BMS phase of the mantle, where the elements exist as dissolved sulphide species, and the silicate liquid, in which the metals may be present as oxide species. Because the activity of $OsS_2$ during partial melting is considerably

greater than that of $OsO_2$, Os partitions predominantly into the mantle BMS phase and remains in the mantle following melt segregation, providing sufficient BMS is left in the residue.

In contrast to Os and the other PGE, the activities of both $ReS_2$ and $ReO_2$ are relatively high, leading to greater solubility of Re in the silicate melt, but predominantly chalcophile behaviour in the solid peridotite. During mantle melting, therefore, the depletion of Re in the residual peridotite, but negligible reduction in its Os content, leads to a decrease in the Re/Os ratio of the residue. In view of the linear decrease in Re as a function of F, the Re/Os ratio of the residue would be expected to exhibit a linear correlation with its moderately incompatible element abundances.

No evidence was found for significant solubility of either Re or Os in the spinel, olivine or clinopyroxene phases which constitute mantle peridotites, despite the apparent correlation of Os abundances with the fractionation of such minerals in mafic and ultramafic melts and experimental data demonstrating the potential solubility of chemically similar Ru in mantle spinel phases.

***Interactions Between Mantle Residues and Magmatic or Volatile-Rich Fluids***

Analyses of peridotite wall-rocks to pyroxenite layers indicate that interaction of mantle residues with mafic melts may either deplete the residue in both elements (S-undersaturated alkali basalts) or enrich it in Re relative to Os, elevating its Re/Os ratio (S-saturated, tholeiitic melts), depending on the composition of the melt and its S-saturation state.

Thermochemical calculations of the stabilities of potential volatile species of Re and Os suggest that the transport of the elements in hydrous fluids with low halide contents should be negligible under mantle conditions. However, the elements may be mobilised under amphibolite-facies metamorphism in the crust, when either the oxygen fugacity or halide concentration of the fluid may be higher.

***Effects of Alteration***

Under conditions of low $f_{S_2}$ and $f_{O_2}$, e.g. during the serpentinisation of mantle peridotites, the loss of sulphur and decreased activity of $OsS_2$ may lead to the exsolution of

the element from the base-metal sulphides as an alloy phase. Because osmium and osmiridium alloys are chemically inert, however, alteration of the mantle peridotite by serpentinisation should result in negligible mobility of the element.

The behaviour of Re during serpentinisation is harder to predict than that of Os. Provided some of the BMS phase remains, the thermochemical calculations predict that the element should remain in solid solution, however, if the sulphide phase is entirely removed, Re may form an alloy phase on account of the instability of $ReS_2$ relative to its constituent elements at the low sulphur fugacities. However, metallic Re has never been observed in mantle-derived rocks.

# Chapter 3

# Analytical Techniques for the Determination of Rhenium and Osmium

## 3.1 Introduction

The methods used to separate and analyse Os from silicate samples are strongly dictated by the element's physical and chemical properties. Firstly, under oxidising conditions Os forms a volatile tetroxide ($OsO_4$, b.p. 130 °C). Unless the sample can be contained in a closed system, it is therefore necessary to maintain reducing conditions during all stages of the preparation procedure. Consequently, for the determination of Os, conventional sample dissolution procedures (which normally employ nitric or perchloric acid in open beakers) must be either modified to prevent oxidation of the Os or avoided in favour of alternative techniques of sample decomposition.

Secondly, the high ionisation potential of Os (8.7 eV) precludes its determination by conventional positive thermal ionisation mass spectrometry (P-TIMS). To overcome this obstacle, a number of methods have been developed for the analysis of Os, in which ionisation is achieved by either bombarding the sample with high energy ions (e.g. secondary ion mass spectrometry, SIMS, Luck & Allègre, 1983, or accelerator mass-spectrometry, AMS, Wilson *et al.*, 1991); photo-ionising the volatilised metal using a pulsed laser (e.g. resonance ionisation mass-spectrometry, RIMS, Walker & Fasset, 1986) or introducing the sample into a plasma, in which the high temperature and electrically excited environment result in high ionisation efficiencies (inductively coupled mass spectrometry, ICP-MS, Russ *et al.*, 1987). More recently, the problem of ionisation has been by-passed by the formation and analysis of negative osmium oxide ions (e.g. $OsO_3^-$), using negative thermal ionisation mass-spectrometry, N-TIMS (Völkening *et al.*, 1991).

In many ways, the limitations on the methods used for the preparation of samples for the determination of Re are fewer than those for Os. Despite the formation of a relatively volatile

oxide ($Re_2O_7$, b.p. 270 °C), significant loss of Re does not occur during the acid attack of silicate samples, enabling conventional HF + $HNO_3$ digestions to be used. Unfortunately, like Os, Re is difficult to ionise efficiently by P-TIMS (the metal is both refractory and possesses a high ionisation potential, for which reason Re wire is widely used as filaments for P-TIMS analyses). Consequently, for its final analysis, it requires similar techniques to those used for Os.

A further consideration in the determination of Re and Os is their low concentrations in most geological samples, requiring techniques in which the analytical blanks are low, yet which separate the elements from the largest feasible mass of sample.

In this study both ICP-MS and N-TIMS techniques were developed for the determination of the Re and Os contents and Os isotopic composition of a suite of ultramafic rocks. The poorer sensitivity of the ICP-MS technique required Os to be separated from a greater mass of sample than was needed for analyses by N-TIMS. However, this was balanced by the need for less extensive purification of the sample Os prior to analysis by the ICP-MS technique, owing to its greater tolerance of non-spectroscopic interferences. The marked difference between the requirements of the two instruments demanded that distinctly different procedures were developed for the preparation of samples for analysis by each technique. In view of these differences, the two analytical techniques for the determination of Os, and their associated preparation schemes, will be discussed separately.

Although attempts were made to analyse Re abundances by ICP-MS, the sensitivity of the instrument was insufficient for accurate determination of the element at the low levels encountered in ultramafic samples. Consequently, all Re analyses were performed by N-TIMS.

### 3.1.1 Choice of Reference Isotope

Although $^{186}Os$ was used as the reference isotope in most early work on the Re-Os isotope system (as well as many more recent studies), for a number of reasons $^{188}Os$ has started to be used recently, when discussing either Re/Os ratios or Os isotopic compositions. Firstly, the higher isotopic abundance of $^{188}Os$ (~13.3%; Nier, 1937) permits more accurate determination of the Os isotopic ratio than $^{186}Os$ (~1.6%; *ibid.*), owing to the order of

magnitude greater intensity of the ion beams. Secondly, $^{186}Os$ is the daughter isotope of a long-lived radioactive isotope of platinum ($^{190}Pt$, $t_{1/2} \approx 600$ Ga; Heath, 1975) and, as a result, may be enriched relative to the other Os isotopes in Pt-rich samples. Finally, most Os isotope analyses are fractionation-corrected using a constant $^{192}Os/^{188}Os$ ratio, making $^{188}Os$ a more natural choice for the reference isotope in the description of the determined radiogenic isotope ratio. Whilst many authors now determine the $^{187}Os/^{186}Os$ ratio by measuring the $^{187}Os/^{188}Os$ ratio then dividing by a constant factor ($^{186}Os/^{188}Os = 0.12035$; Luck & Allègre, 1983) to obtain the desired values, in view of the potential variation of the $^{186}Os/^{188}Os$ ratio in some samples it seems more sensible to use the $^{187}Os/^{188}Os$ directly. Consequently, all Os isotope ratios described in this study will be quoted as the $^{187}Os/^{188}Os$ ratio.

## 3.2 Previous Studies of the Re-Os Isotope System Using ICP-MS

The potential of ICP-MS analysis in the study of the Re-Os isotope system in geological samples has previously been demonstrated by studies of the Sudbury and Rankin Inlet nickel ore deposits by Dickin *et al.* (1992) and Hulbert & Grégoire (1993), respectively. In these studies, the technique was used to analyse mineralised mafic and ultramafic bodies, in which Re and Os were present at concentrations in the range 50 – 1000 ppb. Using a sample introduction technique similar to that used in this study (Section 3.5), Hulbert & Grégoire (1993) demonstrated that, under standard instrumental conditions, relative precisions of up to 0.3% were possible on individual $^{187}Os/^{186}Os$ ratio determinations.

## 3.3 Sample Preparation for Analysis by ICP-MS

The methods developed for the preparation of samples for Os analysis by ICP-MS were governed by the need for both an improvement in the instrument sensitivity and the extraction of Os from large quantities of sample. The procedure, outlined in the flow diagram of Figure 3.1, used a nickel sulphide (NiS) fire-assay fusion technique for the initial separation of Os from the sample's silicate matrix, followed by the purification of Os by double distillation to produce a solution containing the element as its tetroxide, in which form it was analysed. Analysis of Os as its tetroxide has been shown to produce significant improvements in the sensitivity of both ICP-MS and ICP-AES determinations (Mallet *et al.*, 1979; Summerhays *et al.*, 1983; Grégoire, 1990).

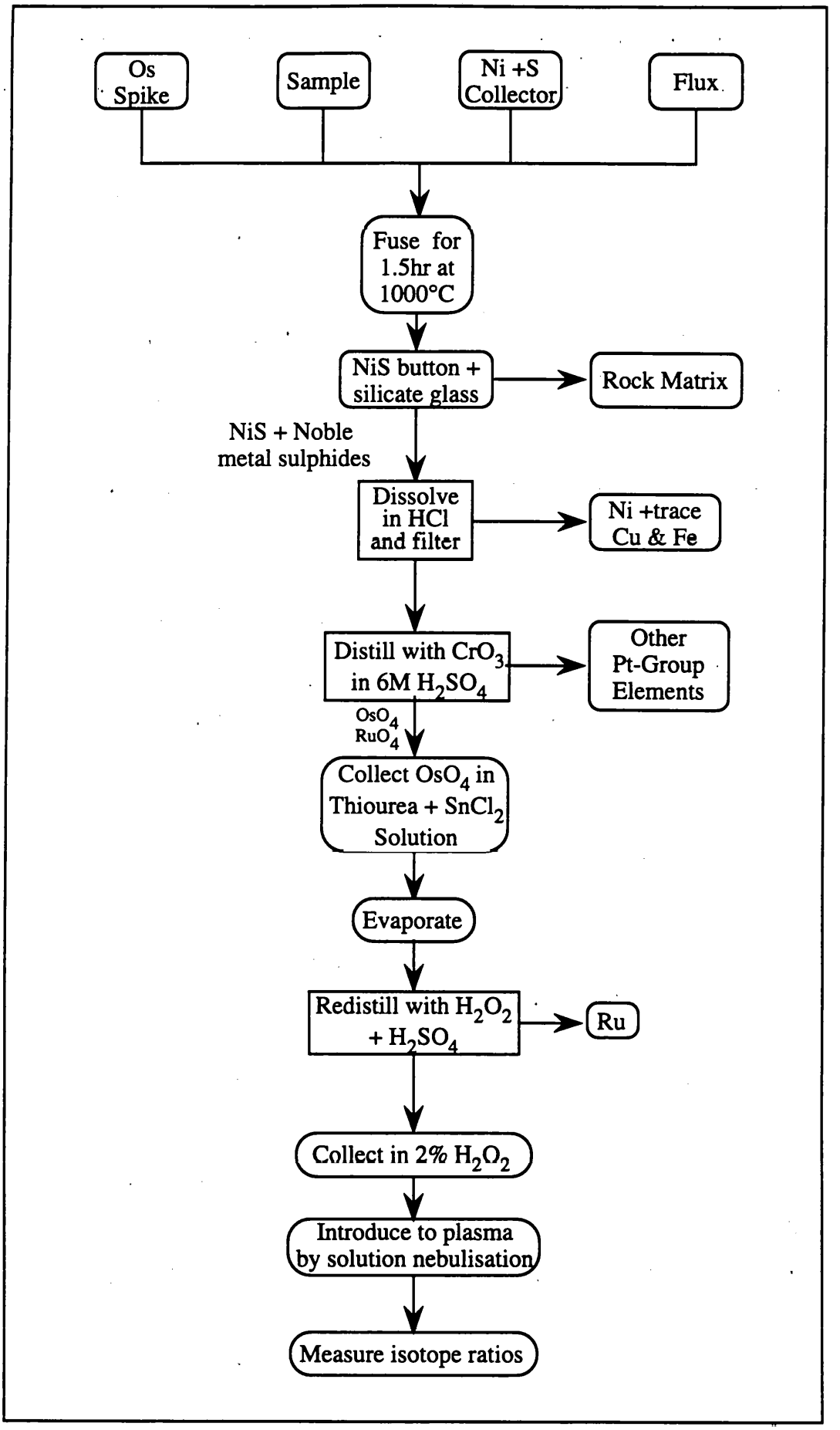


**Figure 3.1** Flow diagram for the separation and purification of Os for analysis by ICP-MS, indicating the processes and products at each stage of the preparation scheme.

Initial work on the development of the preparation procedures was carried out during a two month visit to the Analytical Section of the Geological Survey of Canada (GSC), Ottawa, under the supervision of D. C. Grégoire. For the remainder of the project samples were prepared at the Open University and transported to the NERC ICP-MS facility (then at Royal Holloway and Bedford New College (RHBNC), Egham) for analysis.

## 3.4 Nickel Sulphide Fire-Assay Fusions

Fire-assay, using NiS as the collector, is a well established technique for the concentration of precious metals and gold from large amounts of sample material. The powdered sample is fused with a mixture of sodium carbonate, sodium tetraborate, nickel (as either the metal, oxide or carbonate) and sulphur. During the fusion, the nickel and sulphur react to form an immiscible liquid sulphide phase which scavenges the noble metals from the borosilicate melt. Because of its significantly greater density, the sulphide liquid sinks to the bottom of the crucible, physically separating the noble metals from the rock matrix. The original techniques, introduced by Robért *et al.* (1971) and Hoffmann *et al.* (1978), employed approximately 10 g nickel for the extraction of the Pt-group elements from a 25 g rock sample. More recently, however, studies have shown that the mass of Ni may be greatly reduced, without affecting the recovery of the PGE (Lodders, 1988; Asif & Parry, 1989, 1990; Martin, 1990). By using less Ni, the contribution of the metal to the fusion blank may be reduced (commercial sources of Ni potentially contain substantial amounts of the noble metals; Hoffmann *et al.*, 1978) as well as the contribution from the acid used for the dissolution of the NiS bead. During this study, therefore, a fusion technique based on that described by Asif & Parry (1989) was used, producing NiS buttons with masses of approximately 1 g.

### 3.4.1 NiS Fusion Procedure

The sample was weighed accurately into a pre-cleaned glass beaker and a depression made in the centre of the powder into which a $^{190}Os$ spike solution was pipetted and the sample re-weighed. The sample powder was then gently agitated to cover the hole and the beaker placed under a heat lamp at a low setting to dry the spike solution onto the sample. Care was taken that no spike seeped through the sample to the sides or base of the beaker.

Spiking the sample before mixing it with the flux avoided any reaction of the acidic spike solution with the carbonate of the flux, which may cause spattering of the spike onto the crucible walls, potentially resulting in poor spike-sample equilibration during fusion.

A flux of sodium tetraborate and sodium carbonate (both anhydrous), in a ratio of 5:2 by weight, was measured into a paper bag and intimately mixed. The proportion of flux to sample was approximately 7:4 by weight (20 g sample for 25 g $Na_2B_4O_7$ and 10 g $Na_2CO_3$). To prevent excessive corrosion of the crucible during the fusion of small samples and blanks, up to 10 g of powdered quartz was also added to the assay charge. The quartz powder was prepared from hand picked, optically clear crystals, using similar techniques to those employed for the preparation of samples (Appendix A). All the flux reagents were analytical grade and were obtained from BDH Chemicals, Poole, Dorset, U.K.

The reagents for the NiS collector were mixed separately. Carbonyl refined nickel (Inco Metals Co. Ltd.) and sulphur (sublimed, laboratory grade) were combined to give a Ni/S ratio of ~0.7, and approximately 1.7 g were added to each bag containing flux. Care was required in the use of powdered nickel metal owing to its highly carcinogenic nature.

Following the combination and homogenisation of the flux and collector, the sample was added to the bag, which was then sealed and the contents thoroughly mixed. After the transfer of the sample, the empty beaker was re-weighed to determine the mass of sample used. The bag containing the assay charge was then placed directly into a fireclay crucible (Beecroft and Partners, Rotherham, U.K.) ready for fusion. By combining sample, flux and collector in a bag which could be placed directly into the crucible, an homogeneous mixture was produced and any sample loss during transfer was avoided.

The sample was fused for 2 hours at 1000 °C in a pre-heated muffle furnace (Carbolite, Sheffield, U.K.). Although the furnace had the capacity for the simultaneous processing of six crucibles, only four were treated at any time. The greater space between the samples eased handling during the fusion procedure. After 45 minutes the crucibles were briefly removed with tongs and mixed using a swirling motion. This was repeated every 30 minutes to aid the coalescence of the nickel sulphide beads and to increase the interaction of the two fluid phases. When the fusion was complete, the crucible contents were poured into separate conical stainless steel moulds. Once cool the NiS bead could be separated easily from the

glassy boro-silicate slag.

Although incomplete collection of some or all of the precious metals by the NiS fusion technique has been chronicled by a number of authors, with losses of Os estimated at between 0 and 5% (Palmer & Watterson, 1971; Shazali *et al.*, 1987; Hoffman *et al.*, 1978), tracer experiments have shown that the recovery of the noble metals during NiS fire assay is primarily dictated by the quality of the sulphide-borate phase separation (Lodders, 1988). The conical moulds used in this study encouraged this separation by rapidly collecting the denser nickel sulphide phase into their basal points during pouring, then promoting fragmentation of the glass to release any smaller beads.

For most peridotite samples, a single NiS bead of 1.2 - 1.4 g was formed, suggesting that the fusion melt was sufficiently fluid for the efficient separation of the two phases. For samples with higher silica contents, however, the melts were more viscous and the separation of the sulphide phase from the glass was occasionally incomplete.

### 3.4.2 Dissolution of NiS Button

The NiS fusion beads were hand crushed in a percussion mortar into sub-millimeter grains then ground in a ball mill (Glen Creston, Stanmore, U.K.), using a 2 ml agate vial. Before crushing and after each sample, the mortar and ball mill vial were cleaned by processing a sample of crushed quartz and rinsing with methanol. Because isotope dilution was employed to determine Os concentrations, the slight loss of sample ($\leq 2\%$) arising from smearing of the NiS onto the walls of the crushing vial and losses during transfer between the mortar, ball mill vial and beaker used for the dissolution should not have adversely affected the results.

The NiS matrix of the powdered bead was dissolved in 11M HCl (BDH Aristar or Fisons Primar grade) in a glass beaker, covered by a watchglass. Approximately 25 ml of acid were used per gram of bead. At 60 - 80 °C, the NiS matrix of most beads dissolved in approximately an hour, releasing $H_2S$ and leaving an acid-insoluble residue consisting of nickel sulphide with minor amounts of Cr and sulphides of Co, Sb and As, as well as the trace quantities of precious metal sulphides desired (Shazali *et al.*, 1987). Although prolonged contact of the insoluble residue with the hydrochloric acid solution (following the

cessation of hydrogen sulphide evolution) has been shown to result in significant losses of the PGE into solution (5 - 15% Pt and Pd; Kuznetsov *et al.*, 1974), the loss of the PGE into solution appears to be negligible, provided the atmosphere over the acid remains saturated with $H_2S$ (Shazali *et al.*, 1987; Robért *et al.*, 1971).

Experiments with uncrushed NiS beads required more than 12 hours for complete dissolution, during which the rate of $H_2S$ production by the reaction was insufficient to maintain its saturation in the vapour over the acid. Undersaturation of $H_2S$ in the vapour led to the formation of elemental sulphur and the possible loss of the PGE into solution. Dissolution of the beads in less concentrated, teflon distilled hydrochloric acid (6M TD HCl) was also tried in an attempt to limit the reagent blanks. However, the beads required several hours to react fully with the dilute acid, even at moderate temperatures, leading to similar problems to those encountered with the dissolution of whole beads.

After cooling slightly, the residue was vacuum filtered using a 0.47 μm polycarbonate filter and washed with reverse-osmosis (RO) purified water. The filter membrane was then stored prior to further chemistry.

### 3.4.3 Behaviour of Rhenium and Osmium During NiS Fire Assay

In order to investigate the distribution of the elements within the fire assay charge, experiments were carried out with irradiated Re and Os standards, using beta-autoradiography to detect their location in the fusion products. Mysen and Seitz (1975) described how beta-autoradiography may be used in experimental petrology to study the distribution of trace elements in experimental charges. Their technique involved the addition of a small quantity of an artificially radioactive isotope of the element of interest to an experimental charge prior to fusion. After quenching of the charge, the distribution of the element was determined by measuring the ß-activity of the various phases present in the sample. ß-autoradiography has also been shown to be a powerful tool for the location of minor phase inclusions, for example rare mineral grains predominantly composed of the rare-earth elements or precious metals, using neutron activation induced ß-activity in thin sections (Potts *et al.*, 1984; Potts & Prichard, 1986).

Both Re and Os possess isotopes which undergo (n, γ) reactions on irradiation with thermal neutrons to produce ß-emitting isotopes with suitable half lives for study by this

technique (Table 3.1). Some of the ß particles emitted by these isotopes, however, possess relatively high particle energies. Although these high energies improve the sensitivity of the technique, by deeper penetration into the photographic emulsion, they also produce more diffuse tracks leading to poorer resolution. In addition to the determination of the relative abundances of each element in the two fire assay phases, *in situ* ß-autoradiography of the fire assay charges allowed any discrete Os- or Re-bearing minerals formed during the fusion process to be recognised.

***Procedure***

Solutions containing 50 µg Os and 5 µg Re were dried down on separate filter papers which were then irradiated for approximately 7 hours in the "Consort" reactor at the Imperial College Reactor Centre near Ascot, using thermal and epithermal neutron fluxes of $1.25 \times 10^{12}$ and $4 \times 10^{10}$ $ncm^{-2}s^{-1}$, respectively. After two days 'cooling' the filter papers were fused using the procedure of Section 3.4.1, adding 5 g silica to simulate the sample silicate matrix. The fire assay charges were allowed to solidify in the crucibles to prevent the break-up of the boro-silicate slag. Once cold the fused samples were vacuum impregnated with epoxy resin and sectioned with a circular saw to expose the NiS beads *in situ*. The four halves were then oven dried overnight before being placed on a sheet of X-ray film (Fuji RX-100) and sealed in a light-proof box. Autoradiographs were recorded one and three weeks after irradiation, lasting 12 and 39 days respectively. The results are shown in Plates 3.1 and 3.2.

***Sampling Depth***

In order to interpret the autoradiographs it was necessary to estimate the depth from which the radiation was sampled. The penetration of electrons in a thick absorber is dictated by the energy of the electrons and the density of the absorber, but is not strongly dependent on the elemental composition of the stopping material. A "practical range" of monoenergetic electrons, $R_p$ (cm), may be calculated using an equation similar to Equation 3.1 (which is written for aluminium).

$$R_p = 5.37 \times 10^{-4} \frac{E}{\rho}\left(1 - \frac{0.9815}{1 + 0.003123E}\right) \qquad \textbf{(Eqn. 3.1)}$$

where E is the energy of the incoming electron (keV) and ρ is the material density ($gcm^{-3}$)

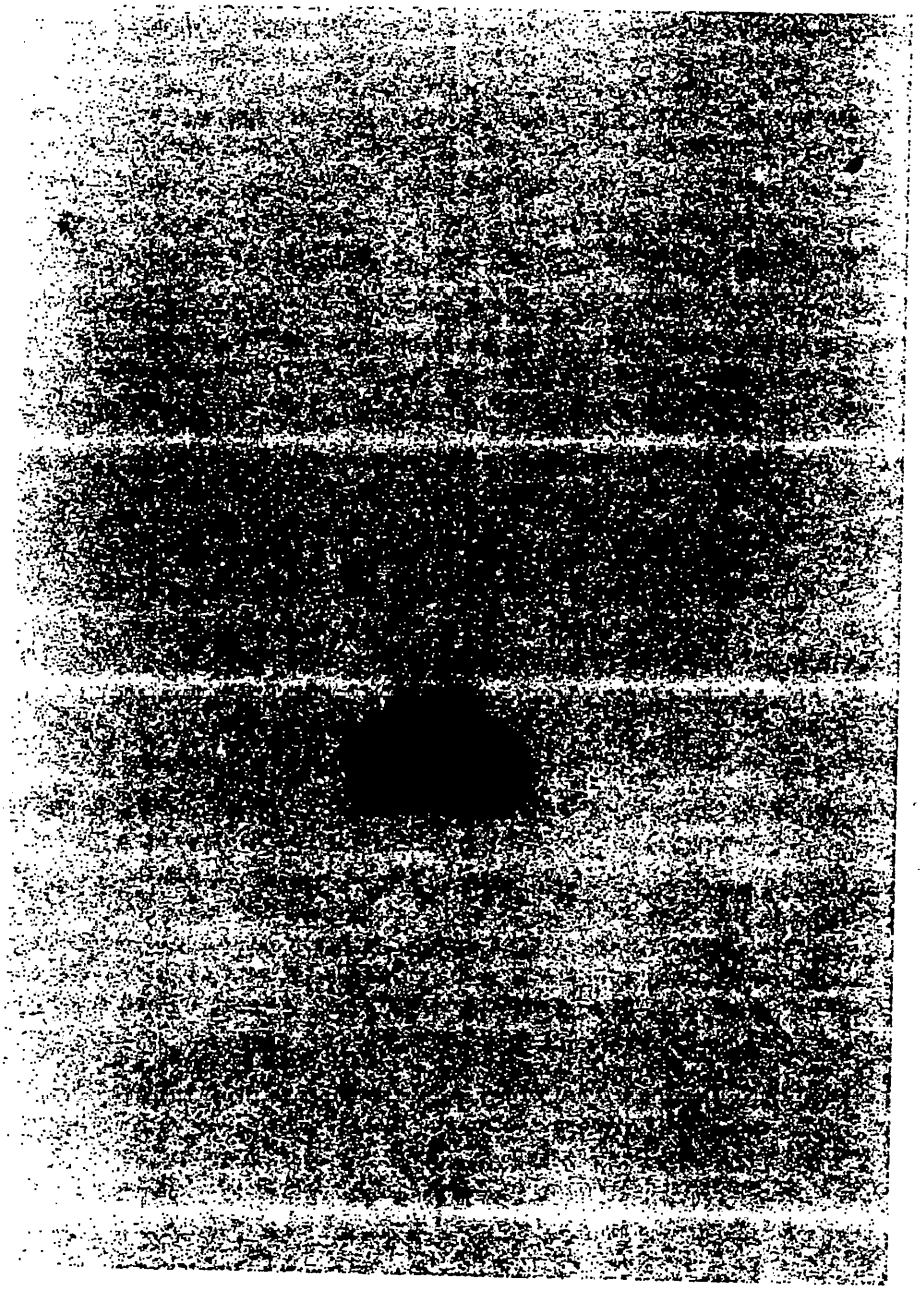

**Plate 3.1** ß-autoradiograph of the NiS fire assay charge containing a $^{191}Os$ radiotracer. 5½ week exposure. 3 weeks after irradiation. For experimental details, see text.

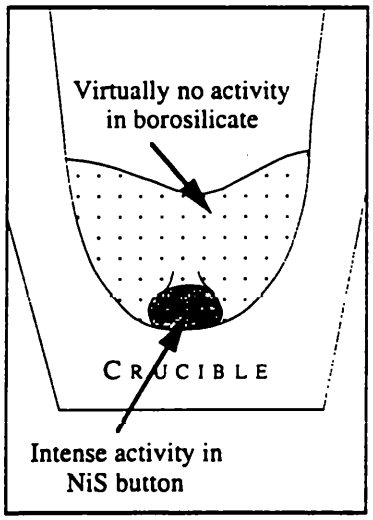

**Plate 3.2** ß-autoradiograph of the NiS fire assay charge containing a $^{186}Re$ radiotracer. 5½ weeks exposure, 3 weeks after irradiation. For experimental details, see text.

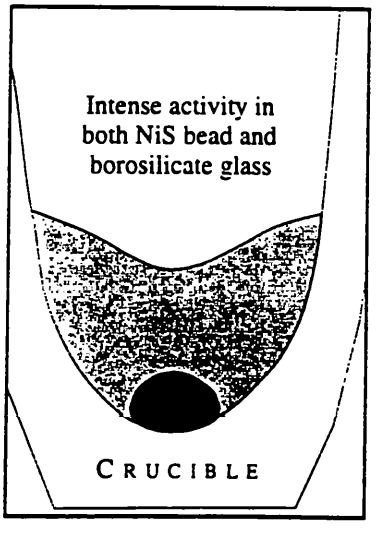

(Kobetich & Katz, 1968). Equation 3.1 predicts the maximum penetration depth of monoenergetic electrons. ß-particles, however, are emitted with a continuum of energies, with the peak intensity occurring at approximately one third of the maximum particle energy. In practice, therefore, the depth of origin of the majority of the detected radiation will be less than the value calculated from this equation, using the ß-particle energies listed in Table 3.1.

| Element | ß-Emitting Isotope | Half-life | Maximum energy of emitted particles, $ß_{MAX}$, (keV) and relative intensity | Sampling Depth (mm) NiS | Glass |
|---|---|---|---|---|---|
| Os | $^{191}Os$† | 15.3 days | 143 (100%) | 0.045 | 0.1 |
| | $^{193}Os$ | 30.2 hours | 1132 (67%) | | |
| Re | $^{186}Re$† | 90.6 hours | 1070 (73%)<br>930 (23%) | 0.81 | 1.8 |
| | $^{188}Re$ | 16.7 hours | 2118 (79%)<br>1962 (20%) | | |

†Principle ß-emitter in autoradiographs.

**Table 3.1.** Data for ß-emitting irradiation products of Re and Os. Particle energies and relative intensities from Wilson (1966).

For the NiS bead ($\rho \approx 5.5$ gcm$^{-3}$) and borosilicate glass ($\rho \approx 2.5$ gcm$^{-3}$), the maximum sampling depths, assuming particle energies of ~ $ß_{MAX}$, are only 0.05 mm and 0.1 mm for $^{191}Os$ or 0.8 mm and ~2 mm for $^{186}Re$, respectively. However, the majority of the ß-radiation, with an energy around 1/3 $ß_{MAX}$, will originate from a considerably shallower depth below the surface of the sample, owing to its lower energy. Thus, for $^{191}Os$ the sampling depth will be lower by a factor of ~7 (0.007 and 0.015 mm in the two phases), whilst for $^{186}Re$ it will be less by a factor of ~4 (0.2 and 0.4 mm).

In the light of these calculations, the autoradiograph should record the distribution of the irradiated elements in only those parts of the fire assay charge immediately adjacent to the film. Owing to the significant difference in the densities of the two phases, however, the activity recorded by the autoradiograph in the glass may originate from twice the depth interval of that recorded in the sulphide phase.

### *Results*

The autoradiograph of the charge containing the Os radiotracer (Plate 3.1) records a high

intensity of radiation in the bead but negligible activity in the glass, demonstrating the efficient collection of the element by the sulphide phase. On account of the low energy of the radiation emitted by $^{191}Os$, the image of the bead displays sharp contacts. However, no internal structure is visible in the bead, suggesting the Os may be distributed homogeneously in the nickel sulphide phase. The apparent 'flaring' above the bead is caused by the presence of a gas bubble formed during cooling, enabling ß-particles from the bead to reach the film from a range of positions on the surface of the bead and from a variety of angles.

The autoradiograph of the Re fusion product (Plate 3.2) shows intense activity in both the sulphide and borosilicate phases. Considering the significantly greater volume of the latter phase (the bead volume is less than 1.5% of the total volume of the charge) and the greater sampling depth of the radiation, it is clear that a considerable proportion of the Re must have remained in the borosilicate glass during the fusion. The high energy of the radiation produced by the decay of $^{186}Re$ unfortunately produces a diffuse exposure both around and within the bead, preventing the determination of the distribution of Re within the sulphide phase.

The poor yield of Re to the NiS bead is consistent with the few studies which have analysed the element in the products of NiS fusions (Lodders, 1988; Martin, 1990). These studies suggest that the partitioning of Re between the sulphide and borosilicate phases is dependent on the sample composition and the oxidation state of the fire assay charge during the fusion: under similar fusion conditions to those used in this study (1025 °C in air), Martin (1990) found that the Re yield for basic and ultrabasic samples is variable and may be as low as 0.05%, however, under an inert nitrogen atmosphere Lodders (1988) found that the element may be quantitatively recovered. Owing to the poor yield of Re to the bead and its high dilution in the slag, neither material could be successfully used for the determination of Re abundances in the silicate samples.

## 3.5 Separation and Clean up of Osmium

The most efficient way to separate Os from the other Pt-group elements utilises the volatility of the element's tetroxide by employing a strong oxidising agent to distil the Os from the decomposed samples and collecting the vapours in solution (Westland & Beamish,

1954; Jones *et al.*, 1971; Walker, 1988; Martin, 1990). For samples prepared for analysis by ICP-MS, two distillations were used: the first to separate the Os from the other noble metals, the second to clean up the solution and convert the Os to its tetroxide ready for analysis.

### 3.5.1 Apparatus

The apparatus for the distillation of Os is shown in Figure 3.2. A 100 ml round bottomed distillation flask was attached to a primary reflux condenser which, in turn, was connected to a smaller secondary condenser followed by a delivery tube through which the distilled vapours were passed into a receiving solution. The condensers were connected to a supply of cold mains water. In view of the reduction of $OsO_4$ by most greases, deionised water or sulphuric acid were used to seal the ground glass cone and socket joints between components of the distillation apparatus, which were held together by steel spring clips. A carrier gas of air was drawn through the apparatus using a water pump, and the flow rate controlled so that several bubbles passed through the receiving solution each second. The presence of a slight negative pressure in the apparatus helped to prevent the loss of $OsO_4$ vapour through any of the joints.

### 3.5.2 Procedure

The distillation apparatus was assembled and the filter membrane bearing the insoluble residue after NiS bead dissolution was placed in the empty flask. A solution of chromium (VI) oxide (0.5 - 1 g) in 6M sulphuric acid was added through one of the flask's side ports which was then sealed and the flask heated using an electric mantle heater. The chromium oxide was added in excess to ensure that oxidising conditions were maintained, despite the reduction of the $CrO_3$ by the filter membrane. During the heating stage, the condensers were cooled by a flow of water, however, once the acid began to boil, the cooling water was turned off. The temperature of the distillation was monitored at the stillhead and lay in range 95 - 105 °C. The $OsO_4$ was trapped in 20 ml of 1% thiourea solution in dilute hydrochloric acid, which was chilled in a ice-water mixture at -8 to -2 °C. Trace tin (II) chloride (Aldrich Chemical Co.) was added to the receiving solution to aid the reduction of the osmium tetroxide.

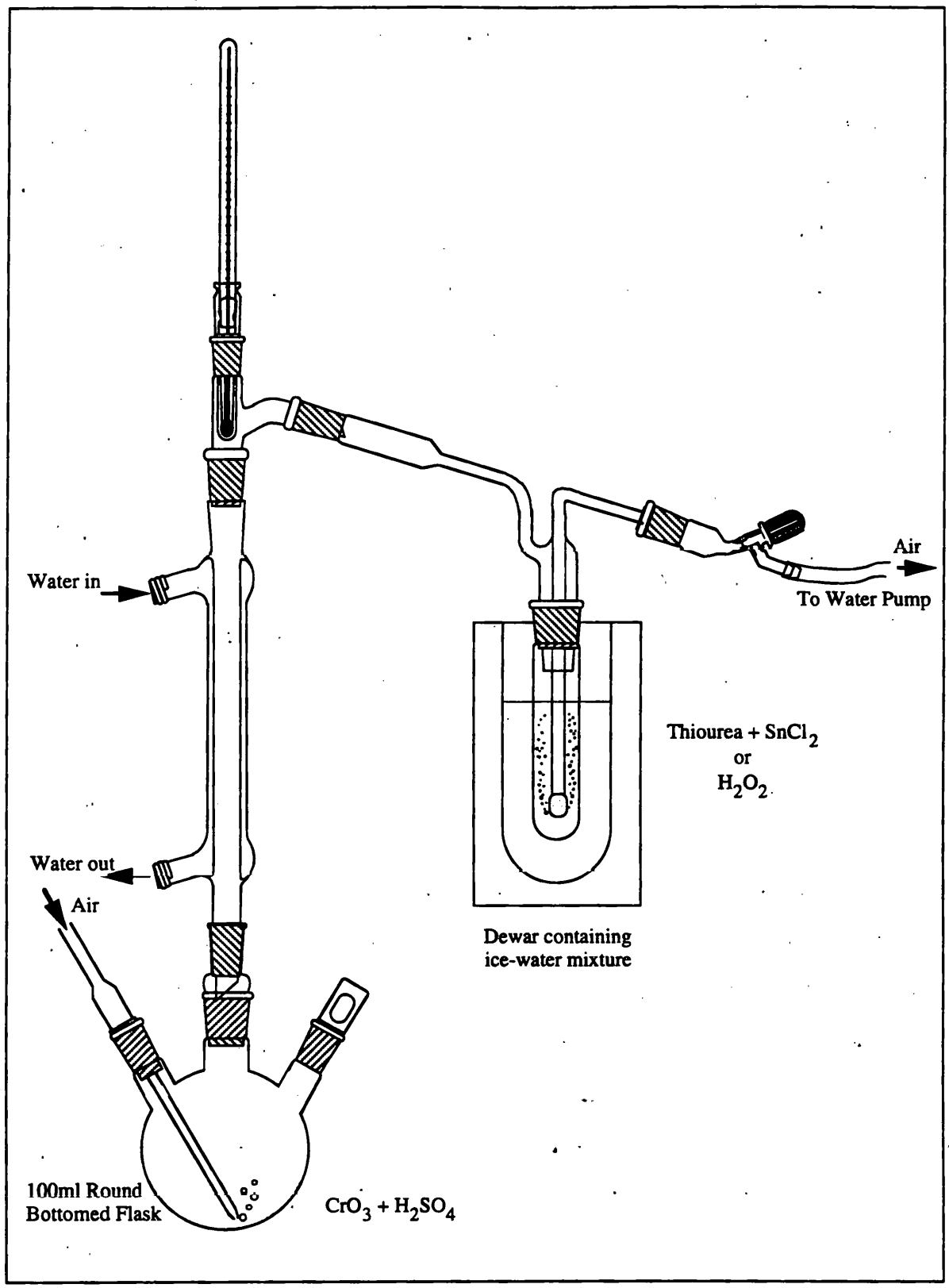


**Figure 3.2** Apparatus used for the oxidative distillation of Os from the insoluble residue of NiS fire assay buttons.

Distillations were carried out for 1 to 1.5 hours, after which the receiving solution was partially evaporated. Heating the solution should stabilise the Os as a thiourea complex (Balcerzak, 1988) in which form it was stored prior to redistillation and analysis.

The second distillation was carried out in similar apparatus to that used for the first, with

the addition of a 50 ml dropping funnel and the omission of condensers. In the second distillation peroxymonosulphuric acid (PMSA) was used as the oxidising agent. This was prepared separately using a 1:1 mixture of concentrated sulphuric acid and 30% hydrogen peroxide and chilled in an ice bath prior to placing it in the dropping funnel.

The sample was poured into the distillation flask through the air inlet port and the inlet tube replaced. Once a slow flow of air was established, the PMSA was slowly added to the sample, which was chilled in an ice bath to prevent rapid heating. When all the PMSA had been added, the solution was gently heated to 90 °C and the Os distilled into 10 ml of chilled 3% hydrogen peroxide for 30 minutes. During heating, the PMSA decomposes to produce oxygen gas, carrying the $OsO_4$ to the receiving solution. Once the decomposition was complete, however, an additional flow of air was necessary for continued transport of the tetroxide vapours. The second distillation served to separate the Os from the thiourea and tin present in the first receiving solution as well as removing any Ru and Re which may have co-distilled with the Os during the first distillation, either as volatiles or as droplets entrained in the air flow.

During the second distillation, the Os was trapped in the receiving solution solely on account to its low temperature. The addition of a small quantity of hydrogen peroxide to the solution ensured that the element remained in the oxidised form. Because the volatile $OsO_4$ may be lost easily from the peroxide solutions, the samples were refrigerated in sealed vials until final analysis, which was performed as soon as possible after the second distillation was carried out. Although experiments on solutions stored for a range of periods prior to their final analysis suggested that there was little loss of sensitivity over periods of up to five days, provided the samples were sealed and refrigerated, after five days the solutions showed a significant decrease in response with time. This loss in sensitivity may result from either the gradual loss of the Os from solution (by the escape of volatile $OsO_4$ from the vial or the plating of Os onto the walls of the vial, for example) or the reduction of the $OsO_4$ to a less volatile species, which would have lowered the efficiency with which the analyte was carried to the plasma.

### 3.5.2 Procedural Blanks

The total Os blanks determined for the fusion and distillation procedures used in the

preparation of samples for analysis by ICP-MS decreased from ~ 1.3 ng during early work at the Geological Survey of Canada to ~ 0.4 ng during later analyses, with $^{187}Os/^{188}Os$ ~ 0.19 ± 3. The decrease in the blank may reflect improvements in the cleanliness of the reagents used to prepare the samples for the later analyses. Although the contributions of individual reagents to the total blank for the procedure were not assessed, the most likely sources of Os contamination may be the Ni metal powder used in the fire assay or the tin chloride added to the receiving solution of the first distillation. The determined procedural blanks are consistent with previous studies which have used the NiS fire assay technique, in which Os contents of ≤ 1 - 3 ng/g were determined in nickel purified by the carbonyl technique (Shazali *et al.*, 1988). Although a blank of 0.4 ng is considerably higher than that possible for acid dissolution techniques, the large quantity of sample used in each analysis meant that the blank represented less than 1% of the total Os present in the peridotite samples.

## 3.6 Osmium Analysis by ICP-MS

Inductively coupled plasma mass spectrometry is a relatively young analytical technique and is capable of analysing most elements in aqueous solution at and below the part per billion level. Most applications of the technique use the intensities of selected isotopes (calibrated against matrix matched standard solutions) to determine elemental concentrations in a sample solution. Because it is capable of measuring the intensities of individual isotopes, however, the technique is also applicable to the measurement of isotope ratios, either for more accurate concentration determinations by isotope dilution or for the measurement of naturally occurring variations in the isotopic composition of samples. With the increasing number of instruments and the high sensitivity of the technique, ICP-MS is now becoming a widely available technique and is finding an increasing number of applications in trace element and isotope analyses in the geological, environmental and life sciences (e.g. Jarvis *et al.*, 1990).

### 3.6.1 The ICP-MS Instrument

An ICP-MS instrument may be divided into three sections: the sample introduction mechanism, the torch assembly and the mass spectrometer (Figure 3.3).

### *Sample Introduction*

To enable rapid desolvation, volatilisation and atomisation of the analyte in the plasma, a sample solution must be introduced as an aerosol of fine droplets or particles. Conventionally, the solution is pumped through a nebuliser into a spray chamber, generating a mist of droplets with a broad distribution of sizes (up to 100 μm). Within the spray chamber the finest of these droplets (<10 μm, about 1-2% by mass of the original sample) are separated out and transported to the torch by a flow of Ar gas (nebuliser gas). The coarser droplets hit the walls of the chamber and are removed from the instrument via a drain.

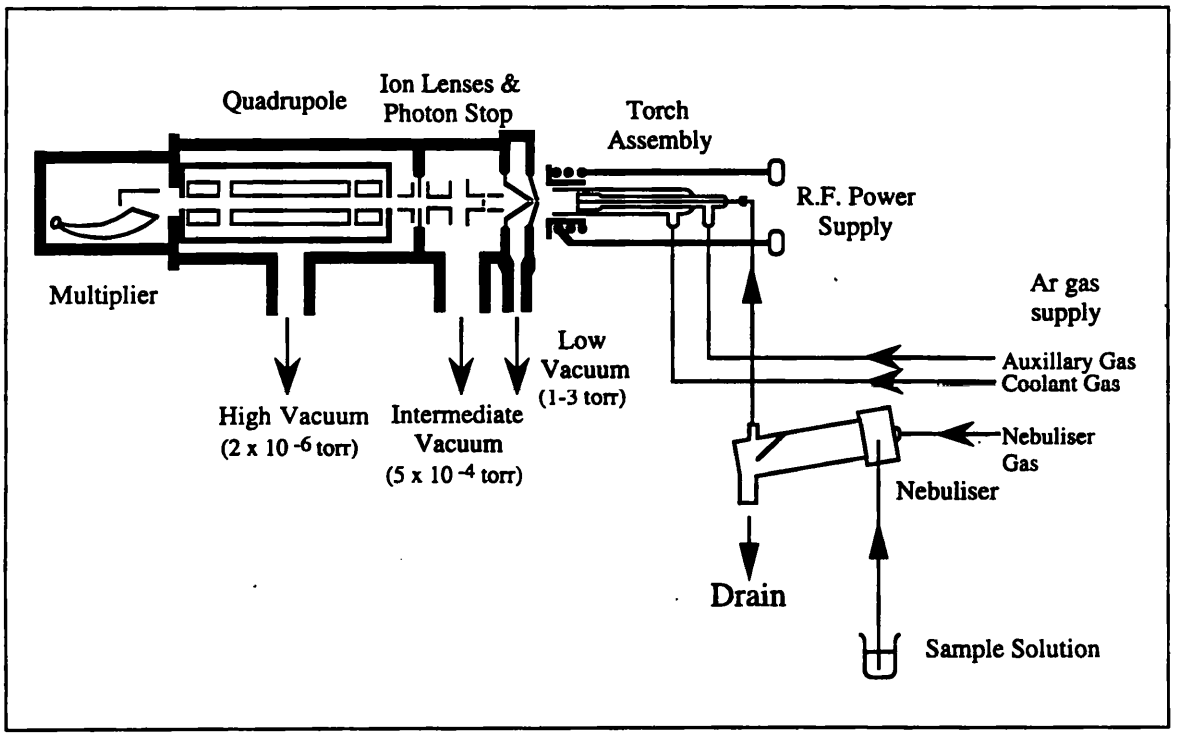


**Figure 3.3** Schematic diagram of ICP-MS, with sample introduction by solution nebulisation (After Gray, 1988).

### *The Torch Assembly*

Ionisation of the sample occurs by its injection into a plasma fireball, formed by the excitation of Ar gas using coupled radio-frequency energy. The plasma is generated by the torch assembly, where it is supported in an envelope of coolant gas, away from the other parts of the instrument, and lifted off the end of the torch by a third, slower flow of Ar gas (auxiliary flow). Surrounding the end of the torch are water-cooled work coils, which

supply the energy for plasma formation.

As the sample enters the plasma, it is almost immediately desolvated, atomised and ionised. The high plasma temperatures ($T_{core}$ > 8000 °C) result in very efficient atomisation of the sample, whilst the ionisation potential of the Ar gas (15.76 eV) buffers the ion spectrum of the sample, it being above the first ionisation potential of most other elements, but below the majority of their second ionisation potentials. Such buffering results in a moderately simple spectrum, in which only singly charged ions of most elements are present.

*Mass Spectrometer*

The ionised sample is normally analysed using a quadrupole mass filter and electron multiplier detector, separating each mass in turn from a cylindrical beam of ions. Because the mass spectrometer requires a high vacuum to operate successfully ($p \leq 10^{-6}$ torr), an interface through which the ions may be extracted from the plasma at atmospheric pressure and a series of vacuum stages at decreasing pressures are required. This interface normally consists of a pair of cones, each with a 0.5 - 1 mm diameter aperture, the design of which is critical to the rapid extraction of ions from the plasma before they can recombine to form molecular ions. The steep pressure gradient through the first aperture propels a jet of gas from the centre of the plasma into the first vacuum stage, where it is intercepted by a second, sharper cone, extracting ions from the core of the expanding mass of gas. The ions are focussed and collimated into a cylindrical beam by a series of lenses in the second vacuum stage before passing through another aperture into the third stage, where the quadrupole mass analyser separates the ions according to their mass/charge ratio. Finally, the ions pass through the exit slits and are counted by an electron multiplier detector.

### 3.6.2 Choice of Introduction Technique

To overcome the inefficient transport of sample solutions to the plasma, a number of alternative sample introduction techniques have been developed for the analysis of Os by ICP-MS. These include the generation of osmium tetroxide vapour directly into the plasma (Bazan, 1987; Russ *et al.*, 1987; Dickin *et al.*, 1988), electrothermal vaporisation (ETV) of the Os into a carrier gas flow (Hirata *et al.*, 1989) and the analysis of osmium tetroxide in solution, using conventional solution nebulisation (Masuda *et al.*, 1986).

The three methods of introduction were reviewed by Grégoire (1990), who concluded that the choice of technique was dependent upon the method of sample preparation, the mass of Os present and the precision required. For samples with high Os concentrations, and where high precision was required, nebulisation of $OsO_4$ in solution offered the best results, with the stable signal enabling long analysis times to be used without any modification of the standard ICP-MS instrument. Because the $OsO_4$ is volatilised from the nebulised solution and carried to the torch in vapour form, the efficiency with which the element may be transported to the plasma is greatly improved over that which can be obtained by nebulising Os in a more reduced state. For samples with low Os concentrations, ETV offered the best sensitivity, requiring only a few millilitres of analyte and producing a short, but intense, signal. The transient nature of this signal, however, results in less precise data. Direct generation of $OsO_4$ vapour into the plasma was found to give a maximum count rate of over an order of magnitude less than that obtained by the nebulisation of $OsO_4$ in solution and produced a noisier signal, leading to poorer precision. However, by on-line separation of Os from any Re or W present in the samples, generation of $OsO_4$ vapour into the plasma does reduce the amount of sample preparation required prior to analysis.

| | VG PlasmaQuad PQ2+ | VG PlasmaQuad STE |
|---|---|---|
| Plasma Conditions | | |
| R.F. Power | 1.30 kW | 1.35 kW |
| Auxiliary Gas Flow Rate | 0.5 L $min^{-1}$ | 1.5 L $min^{-1}$ |
| Nebuliser Gas Flow Rate | 0.75 L $min^{-1}$ | 0.76-0.95† L $min^{-1}$ |
| Cooling Gas Flow Rate | 14 L $min^{-1}$ | 14 L $min^{-1}$ |
| Ion Lens Settings | Optimised for maximum signal using $^{169}Tm$ | Optimised for maximum signal using $^{169}Tm$ |
| Sample Uptake Rate | 0.5 mL $min^{-1}$ | 0.5 mL $min^{-1}$ |
| Measurement Parameters | | |
| Measurement Mode | Scanning | Scanning |
| Mass Range | 182.95 - 196.85 amu | 182.6 - 194.4 amu |
| Channels $amu^{-1}$ | 74 | 80 |
| Dwell Time | 80 µs | 80 µs |
| Number of Sweeps | 400 | 376 |

**Table 3.2** Operating conditions for ICP-MS analyses.
†Nebuliser gas flow rate altered between some analytical sessions.

Despite the low concentrations of Os in the samples analysed in this study, the nebulisation of $OsO_4$ in solution was chosen for its higher precision and the most efficient use of the limited machine time.

### 3.6.3 Mass Spectrometry and On-line Data Processing

Samples were run under the instrumental conditions outlined in Table 3.2. Initially the analyses were performed on a Plasmaquad PQ2+, however, in mid-1992 this was replaced by a Plasmaquad STE (both manufactured by VG Instruments). Because both the instrument and the software used to run it were changed, the plasma conditions and measurement parameters were different for the analyses by the two instruments. The mass spectrometer was operated in a scanning mode, repeatedly sweeping across the mass range shown. Optimisation of the ion lenses was carried out using $^{169}Tm$, which was contained in the daily set-up solution. Each set of data consisted of around four hundred sweeps across the mass range (taking approximately 80 ms each), during which the signal from the electron multiplier was stored in a multichannel analyser (MCA). At the end of each set of sweeps the output of the MCA was integrated using the manufacturer's software and saved on computer disk for off-line processing at the Open University.

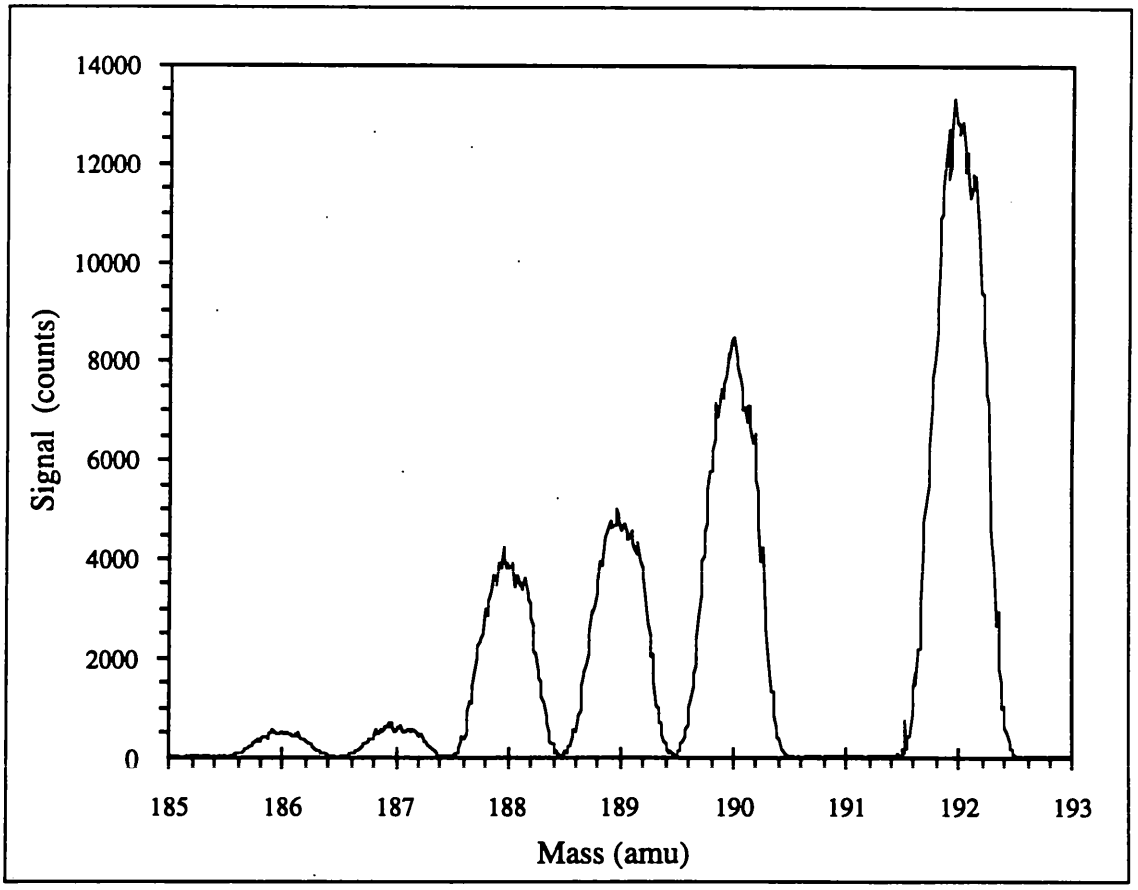


**Figure 3.4** Mass spectrum obtained for an aliquot of the Johnson-Matthey Os solution diluted to 80 $ngml^{-1}$, illustrating the angularity of the peaks and the noise present on the peak tops. Data acquisition time 25 seconds.

The short acquisition time of each set of sweeps allowed up to thirty sets to be collected for each sample before the solution was exhausted, permitting the precision of the analyses to be accurately assessed. The intensity of the instrumental background was determined between each sample by analysing a matrix matched blank solution.

### *Peak Shape and Integration Technique*

Figure 3.4 shows a typical spectrum obtained by ICP-MS using an unspiked standard solution. The peak shapes are roughly triangular (rather than flat-topped, as preferred for TIMS analyses), however, noise superimposed by the plasma source degrades the peak shape considerably. Figure 3.5 shows the peak shapes for the six masses, normalised to their maximum intensities. The plot illustrates that the noise on each peak is related to the signal intensity and that all peaks are of a similar widths.

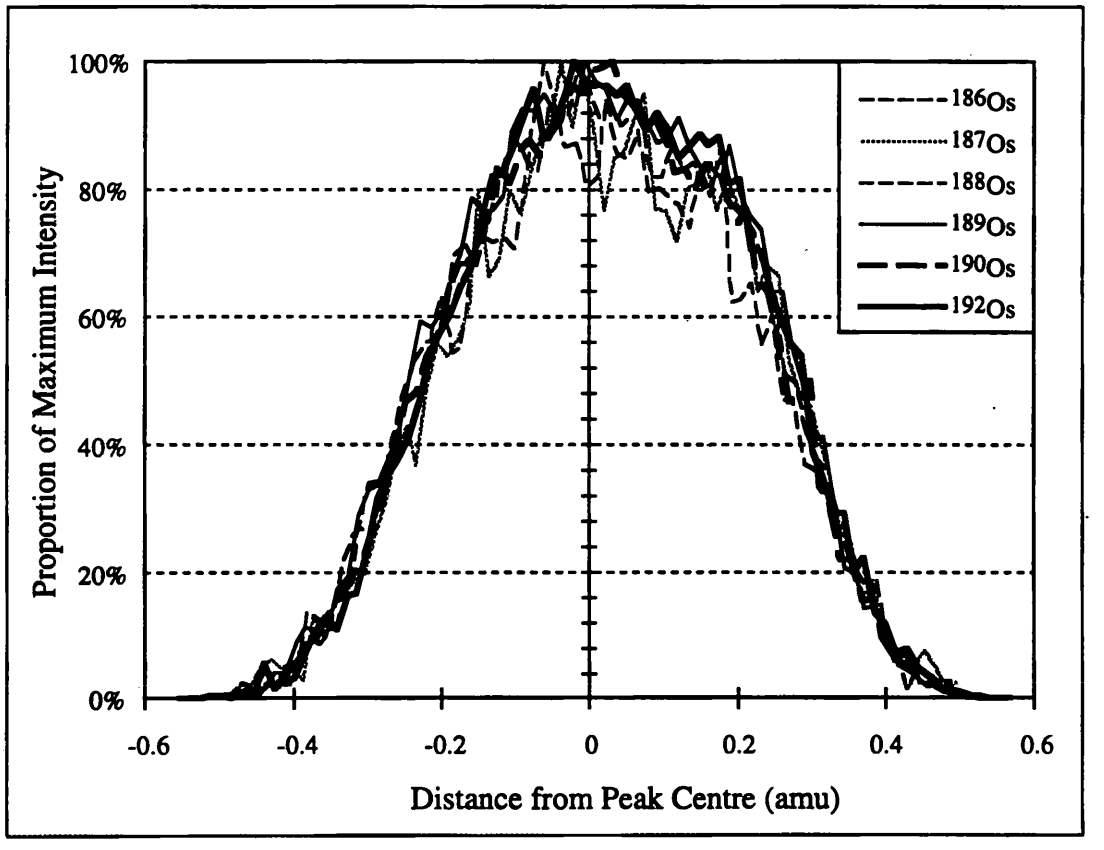


**Figure 3.5** Superimposed peak shapes for the six main Os isotopes of the ICP-MS spectrum shown in Figure 3.4. Beam intensities normalised to the maximum value for each isotope. The noise on each mass appears to be related to the signal intensity, whilst the peak width is similar for all isotopes and ~1 amu.

The sharp peaks and noisy signal of the ICP-MS spectra prevented the peak height from being used as an accurate measurement of signal intensity. To obtain quantitative results,

therefore, the peak was integrated across a fixed mass range either side of its centre. To avoid the incorporation of tails or precursors to adjacent peaks and include the maximum number of counts in the integration, the width of this integration was set at 0.4 mass units either side of the peak's centre. At a distance of 0.6 mass units from the centre of the $^{192}Os$ peak, the signal intensity was less than 0.5‰ of its maximum value and was indistinguishable from the background (Figure 3.5).

### 3.6.4 Off-line Data Processing

The majority of the data processing was performed off-line at the Open University. Throughout the data processing each set of integrated data were treated individually, producing a set of adjusted isotope ratios and Os concentrations for each of the original sets of scans. The data were corrected for a number of factors, including the instrumental background measured prior to the start of sample analysis, interferences from Re and W, mass bias and spiking. The $^{187}Os/^{188}Os$ ratio and Os concentrations were then averaged to produce the final set of values for the sample. The errors quoted on the final values were twice the standard error of the means ($2\sigma_m$) of the individual sets.

#### *Interferences*

Although ICP-MS spectra are relatively simple, with most elements present as singly charged ions, some interferences are still possible. These may be divided into either spectroscopic or non-spectroscopic interferences.

Spectroscopic interferences occur owing to the presence of two ions of nearly identical mass and may be further separated into those arising from either monatomic or polyatomic ion species. Although there are only four possible monatomic ion interferences on Os ($^{186}W^+$, $^{187}Re^+$, $^{190}Pt^+$ and $^{192}Pt^+$), there are a number of possible polyatomic species, arising from the combination of lighter elements (principally the rare-earths) with elements such as H, O, N, Cl or Ar, which may be present in the either the sample solution, atmosphere or Ar plasma gas. Although interference by doubly charged ions is also possible during ICP-MS analysis, involving elements with twice the mass of the analyte, no elements have been discovered with twice the mass of Os, hence such interferences may be disregarded.

Non-spectroscopic interferences are manifested by the suppression or enhancement of the signal by the matrix of the solution. Such interferences may be caused by the presence of a particular element in the sample solution or, more generally, by the presence of large quantities of dissolved solids (> 2000 $\mu g ml^{-1}$). Experiments have shown that non-spectroscopic interferences can introduce mass discrimination into the determination of the isotope ratios of some elements (Grégoire, 1987; Sun *et al.*, 1987). In general, the severity of these non-spectroscopic-induced mass discrimination effects is related to the relative masses of the element to be analysed and the concomitant element. The isotope ratios determined for the lighter elements are more affected than those of the heavier ones, whilst the presence of heavy elements in the analyte solution causes greater mass discrimination than does the presence of light elements, at similar concentrations (Grégoire, 1989).

Any organic compounds present in the sample solution should be thoroughly decomposed by the plasma. Consequently, such compounds should have little affect on the analyses, provided they are present in trace amounts.

Analysis of sample solutions prepared by distillation into hydrogen peroxide solution showed no trace of polyatomic rare earth element species (e.g. oxides or nitrides of the heavy REE or chlorides or argides of the mid-REE) or Pt. However, W was detected in several early sample analyses. This tungsten appeared to originate from the disposable pipette tips employed in the preparation of the peroxide solutions used to collect the $OsO_4$ following the second distillation. Following this discovery, all pipette tips were soaked in 6M HCl followed by concentrated hydrogen peroxide prior to use. Whilst the determination of precise $^{186}Os/^{188}Os$ ratios was not essential for the investigation of the Re-Os isotope systematics of geological samples, owing to the similarity between the values of the $^{187}Os/^{188}Os$ and $^{186}Os/^{188}Os$ ratios in most unradiogenic samples, the accuracy of the $^{186}Os/^{188}Os$ ratio may be used as guide to the quality of the determined $^{187}Os/^{188}Os$ data. Consequently, the interference of $^{186}W$ on $^{186}Os$ was monitored using the intensity of the 184 peak, and a correction applied where necessary.

$^{185}Re$ was routinely measured in the analyses of both samples and standards and used to correct the $^{187}Os$ data for $^{187}Re$ interference. The intensity of the peak at 185 amu, however was rarely significantly greater than the intensity of the instrumental background, as

measured between samples. The correction for $^{187}Re$ on the determined $^{187}Os/^{188}Os$ ratios was therefore negligible for most sample and standard solutions.

Non-spectroscopic interferences should have also been insignificant during the analysis of both samples and standards owing to the simple chemistry of the sample solutions (only H, O and Os present) and the resulting very low level of dissolved solids with high atomic mass in the sample solutions.

### *Memory Effects and Background*

The largest factor which influenced the rate at which samples could be analysed was the time taken to wash the previous sample out of the instrument. The Os appeared to plate onto the walls of the sample uptake apparatus, which therefore required extensive cleaning between samples. The nebuliser and spray chamber were first flushed with 5% HCl to remove any remaining sample solution. Two "slugs" of a solution containing 1% thiourea and 2500 ppm tin (II) chloride in hydrochloric acid were then taken up to reduce and complex any tetroxide which remained on the walls of the apparatus. The uptake apparatus was then flushed with hydrochloric acid once more, to remove traces of the thiourea solution. Although the Os memory was significantly reduced by this procedure, it was necessary to replace all the pump and uptake tubing used to carry the sample to the nebuliser before the signal approached the instrumental background measured at the start of the day. During a day's analysis, however, it was not always possible to remove all of the Os between samples, possibly owing to inefficient cleaning of the torch or a build up of Os on the sampling cone of the interface. Consequently, there was a gradual increase in the background count rate of $^{190}Os$ and $^{192}Os$ over any period of analysis. By sensible choice of the sample running order, however, it was possible to ensure that this memory was never more than a few per mil of the sample's signal above the instrumental background noise, which was estimated from the intensity of the signal at masses 191 and 193.

### *Mass Bias*

Isotope ratios measured using an ICP source deviate from their true values because of bias in the transmission of ions to the detector, the magnitude of which varies as function of the mass of the analyte isotope (Russ & Bazan, 1987). Several different processes are considered to contribute to this bias, including space charge effects in the region of the

sampling and skimmer cones of the interface, the settings of the ion lenses and the transmission of the quadrupole mass filter (Longerich *et al.*, 1987; Russ *et al.*, 1987; Gillson *et al.*, 1988). The deviation of the measured isotope ratio ($R_{meas}$) from its true value ($R_{true}$), as a function of the difference between the two masses ($\Delta m$), follows the relationship

$$R_{true} = R_{meas} (1 + C)^{\Delta m} \qquad \textbf{(Eqn. 3.2)}$$

where C = mass bias factor. Within the limits of the precision of most isotope ratio determinations by ICP-MS, however, Equation 3.2 may be simplified to the linear relation (Russ & Bazan, 1987; Masuda *et al.*, 1986)

$$R_{true} = R_{meas} (1 + \Delta mC) \qquad \textbf{(Eqn. 3.3)}$$

Although the effect of the mass bias during the analysis of Os standard solutions could be corrected by normalising the measured isotope ratios to a constant value of $^{192}Os/^{188}Os$ (3.0827; Luck & Allègre, 1983), the disturbance of the natural Os isotopic ratios in samples containing the $^{190}Os$ spike required an additional monitor of mass bias to be used, in order to correct the data. Initially, an Os standard solution was used as the bias monitor, however, this was found to produce an intense memory effect owing to remobilisation of the standard Os by the sample solutions. The mass bias was therefore corrected using an Ir standard, which was was easily removed from the ICP-MS instrument and, despite possessing masses in a range similar to those of Os, does not exhibit an isobaric overlap with it. The accuracy of Pb isotope ratio determinations, using an internal Tl standard to correct for mass bias (Longerich *et al.*, 1987) has demonstrated that the bias experienced by elements of a similar mass is comparable.

| Date | Measured $^{192}Os/^{188}Os$ Ratio | Measured $^{191}Ir/^{193}Ir$ Ratio | Bias using $^{192}Os/^{188}Os$ ($amu^{-1}$) | Bias using $^{191}Ir/^{193}Ir$ ($amu^{-1}$) |
|---|---|---|---|---|
| 6th May 1992 | 3.239 ± 68 | 0.5765 ± 64 | 1.27 ± 0.55% | 1.54 ± 0.54% |
| 7th May 1992 | 3.220 ± 11 | 0.5812 ± 22 | 1.11 ± 0.91% | 1.15 ± 0.19% |
| 10th March 1993 | 3.424 ± 43 | 0.5609 ± 8 | 2.76 ± 0.35% | 2.85 ± 0.07% |
| Reference Values | 3.0826† | 0.5948‡ | | |

**Table 3.3** Comparison of mass bias values calculated using Os and Ir standards. Errors represent ± two standard errors of the mean ($2\sigma_m$).
†Luck & Allègre, 1983
‡Creaser *et al.*, 1991.

Although the mass bias was only assessed on two occasions during the analyses at the GSC, during each day's analysis at RHBNC three determinations of the $^{191}Ir/^{193}Ir$ ratio were made, enabling any drift in the bias during the day to be corrected. Correction factors calculated for three occasions when both Os and Ir solutions were analysed are shown in Table 3.3. Within experimental error, the differences between the values are not significant, supporting the use of Ir solutions to correct sample Os isotope ratio determinations. When correcting for either W or Re interference, a similar value for the mass bias was assumed for both Os and the interfering element.

## 3.7 Spike and Standard Solutions

A concentrated Os spike was prepared by dissolving Os metal enriched in $^{190}Os$ (obtained from Oak Ridge National Laboratories) in hot aqua regia in a miniaturised version of the apparatus used for the second distillations. Although no carrier gas was used during the dissolution, it was necessary to attach a receiving tube to the flask to allow for expansion of air during heating and the escape of the nitrogen oxides produced from the aqua regia, whilst still retaining the osmium. The flask was gently heated for three days to dissolve the osmium fully. The contents of the flask and receiving solution were then combined and a ~1.6 ppm stock solution made up by diluting the spike with a 3:1 mixture of concentrated HCl and ethanol. The addition of ethanol to the stock solution was intended to reverse the oxidation of the osmium by the aqua regia during dissolution and stabilise it as the reduced hexachlorosmate complex.

The spike was calibrated by isotope dilution using a commercial Os standard solution. Initially the calibration was carried out by simply combining weighed-out aliquots of the two solutions and analysing the mixture using a similar routine to that employed for samples. The results of these analyses, however, showed that the osmium in the spike had been insufficiently reduced by the ethanol added to the spike stock solution: the contrasting chemical forms of the two solutions resulting in preferential transport of the more oxidised Os of the spike solution to the plasma, producing erroneously high $^{190}Os/^{192}Os$ ratios. The spike was later calibrated by N-TIMS, using the Carius tube method documented by Shirey & Walker (1994) to equilibrate the spike and standard solutions (Section 3.10.4). For later

sample preparations by acid digestion for N-TIMS analysis, a second spike was obtained from R. Walker at the University of Maryland (MD), in which the Os was present in a more stable, reduced form.

| Solution | $\frac{^{186}Os}{^{188}Os}$ | $\frac{^{187}Os}{^{188}Os}$ | $\frac{^{189}Os}{^{188}Os}$ | $\frac{^{190}Os}{^{188}Os}$ | $\frac{^{192}Os}{^{188}Os}$ |
|---|---|---|---|---|---|
| **Standards** | | | | | |
| **J-M (ICP-MS)†** | 0.1235[a] ± 36 | 0.1516 ± 31 | 1.220 ± 11 | 1.990 ± 17 | 3.0827 |
| **J-M (N-TIMS)‡** | 0.12001 ± 3 | 0.14921 ± 1 | 1.21991 ±3 | 1.9839 ± 2 | 3.0827 |
| **DTM (N-TIMS)** | 0.12071 ± 14 | 0.17397 ± 25 | 1.2192 ± 8 | 1.9834 ± 22 | 3.0827 |
| **Spikes** | | | | | |
| **OU (ICP-MS)†** | 0.285[a] ± 6 | 0.122 ± 6 | 2.90 ± 5 | 289 ± 7 | 5.00 ± 9 |
| **OU (N-TIMS)‡** | 0.067 ± 5 | 0.103 ± 9 | 2.931 ± 1 | 296.3 ± 1 | 5.034 ± 2 |
| **OU (Oak Ridge)** | 0.063 ± 2 | 0.34 ± 6 | 3.03 ± 10 | 302.9 ± 9.5 | 5.15 ± 17 |
| **MD (N-TIMS)†** | 0.0408 ± 2 | 0.0498 ± 5 | 1.8943 ± 6 | 191.77 ± 6 | 3.741 ± 1 |

**Table 3.4** Summary of isotopic compositions of the standard and spike solutions used during this study. Analyses performed by ICP-MS at RHBNC and N-TIMS at the O.U. Standard isotope ratios normalised to $^{188}Os/^{192}Os = 0.32439$ (Luck & Allègre, 1983). Errors represent $\pm 2\sigma_m$ on individual analyses the J-M standard and spikes and $\pm 2\sigma$ on numerous replicate analyses of the DTM standard.
[a] $^{186}Os/^{188}Os$ ratios affected by W contamination.
† Data for a single analysis of spike.
‡ Data for duplicate analyses.

The isotopic composition of the two spikes are shown in Table 3.4. The ratios between the heavier isotopes of the OU spike determined by ICP-MS are similar to those determined independently using N-TIMS and well within error of the values quoted by the Oak Ridge laboratory. The determined $^{186}Os$ and $^{187}Os$ contents of the spike, however, are significantly different from those quoted by the suppliers. Although the high $^{186}Os/^{188}Os$ ratio may imply that W was present during the analysis of the spike by ICP-MS, the low $^{187}Os/^{188}Os$ ratios determined by both ICP-MS and N-TIMS suggest that the $^{187}Os$ content of the spike is lower than that specified by the suppliers.

Two Os standard solutions of different isotopic composition were employed during the development and testing of the Os analytical procedures (Table 3.4). The less radiogenic standard (J-M) was obtained as a 1000 ppm standard solution directly from Johnson-Matthey and was used predominantly for the spike calibrations and investigation of the instrumental mass bias by ICP-MS. A second, slightly more radiogenic standard, prepared at the Department of Terrestrial Magnetism (DTM) of the Carnegie Institute, Washington

was also used in the study. Because the isotopic composition of this solution was well characterised following repeated analyses at DTM and elsewhere, it was extensively used during the establishment of the N-TIMS technique, to provided a check on the accuracy of the determined isotopic ratios.

## 3.8 Accuracy and Precision of Osmium Analyses by ICP-MS

In view of the difficulties associated with carry-over of Os in the sample introduction system after the analysis of standard solutions and the limited machine time, the accuracy and reproducibility of the Os isotope ratios and elemental concentrations were assessed by the analysis of international reference materials and an internal monitor sample prepared in duplicate during each analytical session.

| Date | $\frac{^{187}Os}{^{188}Os}$ | Os Concentration (ppb) |
|---|---|---|
| Geological Survey Canada | | |
| 10th June 1991 | 0.1301 ± 0.0024 | 4.90 ± 0.02 |
| 20th June 1991 | 0.1420 ± 0.0034 | 4.36 ± 0.10 |
| 20th June 1991 | 0.1343 ± 0.0038 | 4.59 ± 0.06 |
| R.H.B.N.C. | | |
| 6th May 1992 | *0.1396 ± 0.0009* | 2.86 ± 0.01 |
| 6th May 1992 | *0.1428± 0.0020* | 4.62 ± 0.03 |
| 11th June 1992 | 0.1333 ± 0.0028 | 3.59 ± 0.08 |
| 11th June 1992 | 0.1310 ± 0.0013 | 4.87 ± 0.06 |
| 10th Mar 1993† | 0.1335 ± 0.0008 | 4.40 ± 0.02 |
| 10th Mar 1993† | 0.1322 ± 0.0007 | 4.37 ± 0.04 |

**Table 3.5** $^{187}Os/^{188}Os$ ratios and Os concentrations determined for the monitor sample MBR 2 during the period of study. Errors are two standard errors of the mean for both the $^{187}Os/^{188}Os$ ratios and Os concentrations.
†Separate aliquots of sample solution analysed at start an end of an analytical session.

The monitor sample (MBR 2, a spinel lherzolite originating from the Ivrean Zone of the Italian Alps) was chosen from the university's teaching collection and matched the matrix and Os concentrations of the peridotite samples studied later. Powders of MBR 2 were prepared by similar techniques to those used for the preparation of the sample powders (Appendix A), starting with 4.5 kg of rock, crushed to lentil-sized fragments, from which approximately 1.3 kg were separated and powdered. Sieving showed that the grain size of the monitor sample powder after grinding was predominantly less than 125 μm, although

some material remained in the 125 - 250 μm range. Os concentrations and $^{187}Os/^{188}Os$ ratios determined for the monitor sample at both the NERC ICP-MS facility (RHBNC) and at the Geological Survey of Canada, Ottawa are shown in Table 3.5.

The within-run precisions[1] of the determined Os isotope ratios, prior to correction for mass bias and spiking, varied between 5 and 8‰. Although such precisions were acceptable for the range of $^{187}Os/^{188}Os$ ratios anticipated for the sample suite, they are considerably poorer than would be expected from counting statistics alone. During a typical sample analysis approximately $4 \times 10^7$ and $1.3 \times 10^7$ counts were measured for the peaks at masses 192 and 188, leading to a theoretical precision of ~0.3‰ in the determined $^{192}Os/^{188}Os$ ratio. Propagation of errors during the correction of the determined Os isotope ratios for the effects of mass bias and spiking further reduced the precision of the analyses, leading to an overall within-run precision of between 0.5 and 2.1% on the determined sample isotope ratios.

If the $^{187}Os/^{188}Os$ ratios determined by the earliest analyses at RHBNC are excluded from the dataset (owing to suspected cross-contamination during sample preparation), the reproducibility of the Os isotope ratios is reasonably good. The $^{187}Os/^{188}Os$ ratios of duplicate analyses of the monitor sample vary by less than 2%, as do repeated analyses of the same sample solution performed at the start and end of an analytical session. The variation of the $^{187}Os/^{188}Os$ ratios between the later analyses is not significantly different from the instrumental precision.

The agreement between the Os concentrations determined for the monitor sample is not as good as that shown by the $^{187}Os/^{188}Os$ ratios. The range of concentrations (2.86 - 4.87

*[1] During this study three different estimates of precision are discussed: the within-run precision, the repeatability and the reproducibility.*

*Within-run precision refers to the closeness of agreement between the separate values determined for individual sets obtained during the analysis of a single sample or standard. It was calculated as two standard errors ($2\sigma_m$) of the mean ratio determined during the analysis.*

*Repeatability is used to refer to the agreement between analyses of the same sample or standard carried out under similar operating conditions, on the same instrument and over a limited period of time (normally during the same analytical session, i.e. separated by a few hours for ICP-MS analyses or up to several days during the longer N-TIMS sessions). Where quantified, it was calculated as two standard deviations ($2\sigma$) of the distribution of measured ratios.*

*Reproducibility is used to denote the agreement between the results of measurements of the same material over a longer period of time (i.e. between analytical sessions) or under changed operating conditions. It was calculated as two standard deviations ($2\sigma$) of the values determined over the period of interest.*

ppb) greatly exceeds the errors on the individual determinations, which are less than 2% in most cases. Several possible explanations exist for the variation of the concentrations including inhomogeneity of the monitor sample powder or incomplete equilibration of the sample and spike, either because of Os in the sample in a refractory phase (which may be incompletely recovered during the NiS fusion process, leading to the determination of anomalously low Os concentrations), or partial loss of spike when it was dried onto the sample or when the sample was fused (leading to the determination of high Os concentrations).

| Reference Material | Date | $\frac{^{187}Os}{^{188}Os}$ | Os Concentration (ppb) |
|---|---|---|---|
| SARM-7 | 7th May 1992 | 0.1921 ± 0.0006 | 59.2 ± 1.8 |
| | 10th March 1993 | 0.1953 ± 0.0028 | 60.5 ± 0.4 |
| | Reference Value | – | 63.0 ± 6.8 |
| WMS-1 | 7th May 1992 | 0.1770 ± 0.0028 | 121.1 ± 0.6 |
| | Marcantonio *et al.* (1994) | 0.1762 – 0.1780 | 114.4 |
| | Reference Value | – | 119 |

**Table 3.6** $^{187}Os/^{188}Os$ ratios and Os abundances for the reference materials SARM-7 and WMS-1 determined by ICP-MS during this study. Uncertainties represent the errors propagated from within-run $2\sigma_m$ errors on ratios. Reference value for SARM-7 obtained from Steele *et al.* (1975). Reference value for the Os concentration of WMS-1 is the provisional value taken from the certificate of analysis (CANMET report CCRMP 94-5E).

The accuracy of the technique was assessed using the reference materials SARM-7 (a feldspathic pyroxenite pegmatite from the Merensky Reef, South Africa) and WMS-1 (a Ni-Cu-Fe sulphide from the Wellgreen deposit, Canada). Although it would have been preferable to use materials more closely matching the matrix and Os concentration of the peridotite samples to be studied, no such reference materials were sufficiently well-characterised for either Os abundance or isotopic composition at the time the analyses were carried out. To compensate for the relatively high Os concentrations of the reference materials, the mass of material used in the analyses was scaled down so that the mass of Os present in analysis was comparable with that expected in the mantle peridotites. The results are illustrated in Table 3.6.

The Os concentrations in the reference material SARM-7 determined by two replicate analyses are close to the certified value of 63 ppb (Steele *et al.*; 1975) and differ by only ~2%. Although this difference is greater than the $2\sigma_m$ errors on the two analyses, it suggests

that reasonably reproducible and accurate Os concentrations are possible by the technique used. The isotope ratios determined in the reference material exhibit similar precisions and reproducibility to that shown by the analyses of the monitor sample MBR 2.

The Os concentration determined for the reference material WMS-1 is within 2% of the provisional value of 119 ppb (CANMET report CCRMP 94-5E). Because no uncertainty is placed on the reference value, it is not possible to judge whether the minor difference between the determined concentration and the provisional value is significant. The concentration determined by the single analysis of this study, however, is similar to that determined by Marcantonio *et al.* (1994) by a sodium peroxide fusion technique (followed by analysis by N-TIMS), confirming that the accuracy of the determined Os concentration.

In conclusion, the analyses of reference materials and an internal monitor sample demonstrate that, despite precisions on individual $^{187}Os/^{188}Os$ ratio determinations of better than 1% in most cases, the ratios are only reproducible within ~2%. The agreement between the determined $^{187}Os/^{188}Os$ ratio of the reference material WMS-1 and the value obtained by Marcantonio *et al.* (1994) using N-TIMS suggests that, despite corrections for spiking and the relatively high Os blank, the analysis of samples by ICP-MS following NiS fusion preconcentration does not impart a significant error to the determined $^{187}Os/^{188}Os$ ratios.

The Os concentrations determined for both the reference materials analysed by ICP-MS and using NiS fire assay preconcentration show close agreement with their published values, with only a 2% difference between the duplicate analyses of SARM-7. This close agreement suggests that the sample Os may be successfully equilibrated with the $^{190}Os$ spike during the NiS fusion procedure. The spread of concentrations obtained for the repeated analyses of the monitor sample may thus represent sample heterogeneity, rather than the effects of incomplete or variable sample-spike equilibrium.

## 3.9 Sample Preparation for N-TIMS analysis

Preparation of samples for analysis by N-TIMS followed a similar process to that used to prepare samples for analysis by ICP-MS. The sample was decomposed, either by acid dissolution or NiS fusion and the Os separated by distillation under oxidising conditions. Although the acid dissolutions could be spiked for both Os and Re, separate acid

dissolutions were required for the determination of Re in all samples which were prepared for Os analysis using the NiS fusion technique.

Compared to ICP-MS, N-TIMS analysis has an extremely limited tolerance for both organic and inorganic impurities in the sample. Consequently, the thiourea/tin solution used to collect the distilled $OsO_4$ was replaced by high purity hydrobromic acid. After 'fixing' the Os in the hydrobromic acid, the samples were evaporated down to a few microlitres and either loaded directly onto metal filaments ready for analysis or further purified using a single resin bead clean-up technique.

## 3.10 Sample Digestion Techniques for N-TIMS Analysis

### 3.10.1 NiS Fire Assay

Although N-TIMS is sufficiently sensitive to analyse the Os isotopic composition and Os abundances in considerably smaller samples than were prepared for analysis by ICP-MS, many of the peridotites collected from the Eastern Pyrénées were prepared for N-TIMS analysis using the NiS fusion technique described in Section 3.4. In addition to minimising the effects of sample heterogeneity, the use of large sample sizes enabled greater quantities of Os to be separated, resulting in more stable ion beams at low filament currents and the determination of more precise $^{187}Os/^{188}Os$ ratios.

### 3.10.2 Acid Dissolution using HF, HCl and Ethanol

The acid dissolution technique employed was a modified version of that described by Walker (1988). Between 1 and 3 g of sample powder were accurately weighed into a 60 ml screw topped Teflon 'bomb', to which appropriate quantities of the Re and Os spikes were added. The sample was then slurried with 5 - 10 ml of teflon distilled (TD) 6M HCl and ~1 ml ethanol (EtOH). Once the powder was thoroughly wetted, approximately 15 ml of concentrated HF were added and the bomb tightly sealed before being placed in a oven at 110 °C overnight.

During acid dissolution it is essential that the Os is kept in a reduced state and that, where possible, the digestion vessel is sealed during any heating. The presence of ethanol and HCl during the digestion reduces any Os released from the sample as Os(VIII) to the stable hexachlorosmate complex, in which the Os is present as Os(VI). Coating the thread of the

bomb with PTFE tape prior to sealing also limited the loss of Os which may have resulted from the escape of vapour during digestion. Corrosion of the stainless steel interior of the oven, however, suggested that some acid vapours may escape during heating.

Once cool, the sample solution was evaporated under a heat lamp with a supply of filtered air, until it attained a gelatinous consistency. Approximately 20 ml 6M TD HCl were then added to the sample and the sealed vial placed in an ultrasound bath for 30 minutes to redissolve the residue. The bomb was then returned to the oven for a further 8 hours after which the sample was once more evaporated to near dryness and the HF-HCl-EtOH stage repeated. Although this digestion cycle should, in theory, have been repeated until the sample was entirely dissolved, spinels present in the peridotite samples never completely dissolved, despite the repeated acid attack, and the digestion procedure was normally stopped once only these black grains remained in the bomb.

After the final dissolution in HCl, the sample was evaporated to dryness and taken up in 30 ml 6M $H_2SO_4$ (double quartz distilled, Seastar) in an oven overnight, in preparation for the separation of the Os by distillation.

### 3.10.3 HF-$HNO_3$ Acid Dissolution for Re

Although it may have been possible to separate and analyse Re from the products of the NiS fusions, because of the substantial distribution of Re between both the glass and NiS bead, it was decided to use a separate acid dissolution to determine the Re abundances of those samples which were prepared for Os analysis by the fusion technique. Despite the formation of a relatively volatile oxide ($Re_2O_7$, b.p. 270 °C), significant loss of Re does not occur during the digestion of samples under oxidising conditions, hence a more conventional mixed acid attack may be used, involving HF and $HNO_3$.

The HF/$HNO_3$ acid digestion procedure was similar to the one using HCl, HF and ethanol described above. Approximately 1 g of sample powder was weighed into a 60 ml Teflon bomb and the grains wetted with 3 - 4 ml 15M TD $HNO_3$. An appropriate mass of spike was then added, followed by ~10 ml concentrated TD HF. The bomb was then sealed and placed in an oven at 120 °C for approximately 9 hours. Following evaporation to a gelatinous texture under heat lamps, 15 ml 15M TD $HNO_3$ were added to the sample and the bomb returned to the oven overnight. Finally, the samples were evaporated to dryness and

10 ml 6M HCl added to dissolve the residue.

To aid dissolution, the samples were placed in an ultrasound bath for 30 minutes before being returned to the oven. If necessary the stages involving concentrated nitric and hydrochloric acid were repeated until the sample was fully dissolved. However, as with the digestions under reducing conditions with ethanol, the spinels in the samples failed to dissolve fully, despite repeated acid attack.

### 3.10.4 Aqua Regia Attack in Carius Tubes

For the calibration of spikes and the analysis of selected samples, a procedure was used which involved the high temperature attack of the sample powder by aqua regia in thick walled quartz tubes (named after Carius, by whom they were first described in 1860). The technique employed was a modified version of that described by Shirey & Walker (1994), involving the sequential addition of spike, concentrated HCl and concentrated $HNO_3$ (in a 3:1 ratio) to between 1 and 3 g of sample in the thick-walled glass tube. The tube was chilled in a mixture of dry-ice and methanol, freezing each liquid as a distinct layer before the next was added and preventing the sample reacting prematurely with the acid mixture. Once all the reagents were added, the neck of the tube was torched off, sealing in the reagents, and the tube placed in an oven at 240 °C. To protect the oven and other samples from damage in the event of a Carius tube fracturing during heating, each of the Carius tubes was placed in an individual, screw-topped steel jacket whilst in the oven.

Under the highly oxidising conditions and high temperatures in use, the Re and Os appear to be entirely released from refractory Pt-group minerals, sulphides and even the silicate minerals of samples (Shirey & Walker, 1994). During digestion, the Os and Re are both oxidised to their highest valence states. However, owing to the fully enclosed nature of the digestion vessel, no loss of $OsO_4$ should be possible, leading to complete equilibration of Os between the spike and sample.

Following a period of slow cooling after removal from the oven, the tube was chilled in an ice-water mixture prior to opening. Although the $OsO_4$ may be distilled directly from the aqua regia solution, ~20 ml 6M $H_2SO_4$ were added to the sample to elevate the boiling point of the liquid during distillation.

Despite its apparent advantages, the Carius tube technique was established at the Open University only when this project was reaching its conclusion. Consequently, it was employed in the preparation of only a limited number of the peridotite samples.

### 3.10.5 Comparison of Digestion Techniques

***Blanks***

The absolute Os blank calculated for the total fusion technique (700 - 1100 pg) was significantly greater than those of the acid digestion (13 - 42 pg) and Carius tube (11 pg) digestions. The greater quantity of sample used in the former technique (20 g versus 2 - 3 g), however, resulted in the proportional blanks of the two techniques being almost comparable at 0.5 - 2% of the sample Os. The principle sources of contamination in the fusion process were discussed in Section 3.5.2.

The Re blanks determined for the earliest acid digestions, using the HF/HCl/EtOH digestion technique, were exceptionally high (500 - 900 pg). The principal cause of these elevated values was believed to be contamination introduced from the compressed air supply used to dry down the samples after collection of the Re from the resin columns. Subsequently, sample evaporations were carried out under a filtered air supply from an oil-free compressor, yielding Re blanks of ~100 pg. Despite this improvement, all Re analyses were eventually performed using the HF-$HNO_3$ procedure.

The Re blank of the HF/$HNO_3$ digestion procedure was between 8 and 14 pg and was comparable to that of the Carius tube digestions (15 pg). The considerably lower Re blanks for sample preparations without the distillation of Os using $CrO_3$ suggest that the high Re blank may have originated primarily from the $CrO_3$ used in the distillations. Analyses of the Re contents of each of the acids used in the HF/$HNO_3$ procedure suggested that the determined total procedural blank was not dictated by reagent blanks (calculated to be ~1.2 pg for volumes of acid used), and may reflect either Re from the ion-exchange columns or inefficient cleaning of the teflon beakers used during the preparation procedure.

A single Re blank determination was carried out for the extraction of Re from the NiS bead used in the preparation of sample for Os analysis. Re spike was added to the fire assay charge prior to fusion and the Re separated from the distillation pot liquor following a similar

procedure to that used for the samples digested by the HF/HCl/EtOH technique. The high value of this blank (4.8 ng) was consistent with the determination of high Re concentrations in the sodium tetraborate used for NiS fusions by Martin (1991), however, the beam intensity during the blank determination was very poor, confirming that little of the Re present in the assay charge was recovered by the NiS bead, as suggested by the ß-autoradiograph of the fusion mixture.

***Osmium Spike Equilibration***

For samples prepared using the O.U. spike and the HF/HCl/EtOH digestion technique, the incomplete reduction of the Os during the preparation of the $^{190}Os$ spike resulted in the preferential loss of the spike during the first evaporation stage, leading to significant overestimation of the Os concentrations of the samples in these analyses.

The agreement between the Os concentrations determined by ICP-MS (in which the NiS fusion technique was used to decompose the samples) and the preferred values of the reference materials, however, suggested that any loss of the Os spike during the NiS fusion procedure was insignificant. The gentle evaporation of the spike once it was added to the sample and the presence of excess carbon dioxide (produced by the thermal decomposition of the sodium carbonate of the flux), may have helped to retain the spike, despite the high temperatures employed in the fusion process.

## 3.11 Separation and Clean-up of Rhenium and Osmium

Although the distillation procedures used for the separation of Os from either the filter membrane bearing the acid insoluble residue of the NiS fusion or the solution produced by digestion of the sample by the HF/HCl/EtOH technique were essentially similar to those described for the preparation of sample for analysis by ICP-MS, minor changes were made to the distillation apparatus and the Os was distilled only once, replacing the 20 ml thiourea/tin solution used to collect the $OsO_4$ with ~10 ml 9M HBr (double sub-boiling distilled, Seastar). A technique involving double distillation of the Os (in which the Os was first collected in a solution of concentrated NaOH, then in concentrated HBr) was tried, however, the resulting solutions were no cleaner than those prepared by single distillations into concentrated HBr. Consequently, single distillations were used to separate the Os from

the digestion products, which was then cleaned up using a single bead of chelating resin.

Re was separated from the digested samples by anion exchange chromatography, following the technique described by Morgan & Walker (1989). For samples digested by the HF/HCl/EtOH technique, in which both Re and Os were determined, the Re was extracted from the pot liquors remaining after the distillation of Os. For samples digested using the $HF/HNO_3$ technique, however, the Re was separated from the digestion products directly.

### 3.11.1 Osmium Chemistry Following Sample Decomposition

***Alterations to Distillation Apparatus***

Although the apparatus used for the distillation of samples for analysis by N-TIMS was similar to that illustrated in Figure 3.2, some minor modifications were made to accommodate the use of a smaller volume of receiving solution and to prevent the co-distillation of the sulphuric acid. The large Pyrex receiving tube and sintered head on the delivery tube were replaced by a smaller quartz receiving tube and a delivery tube with a tapered and slightly bent end. The redesigned collection apparatus promoted the formation of small bubbles whilst avoiding the dead volume produced in the sintered head. A second water cooled condenser was also added between the stillhead and receiving tube. This was angled backwards towards the distillation flask so that any condensing liquids flowed away from the receiving solution and back into the distillation flask. The flow of air through the apparatus was replaced by a positive pressure of nitrogen gas applied to the inlet tube of the distillation flask. This proved to be considerably more controllable than the earlier air flow, with which the solution in the distillation flask occasionally backed up the air inlet tube during the distillation, owing to fluctuations in the mains water pressure used to drive the water pump.

***Distillation Procedure***

The distillation procedure was similar to that described earlier. For samples prepared by acid digestion the sample was introduced to the distillation flask as the solution in 6M $H_2SO_4$ and 30 ml of teflon distilled water were used to wash any insoluble precipitate remaining in the bomb into the flask, diluting the acid down to ~3M. Because even trace sulphuric acid would interfere with the subsequent chemistry, the flow of water through the

condensers was maintained throughout the distillations to hold back any acid fumes.

Although the $OsO_4$ may react with the HBr during collection, the Os was held in the receiving solution predominantly as a result of the low temperature of the solution. Following the distillation, therefore, the HBr solution was sealed in a 15 ml Teflon vial and placed in an oven overnight to 'fix' the Os as a bromine complex, preventing volatilisation of the Os during the evaporation of the HBr. The sample was then evaporated slowly to dryness under a heat lamp.

***Single Resin Bead Clean-up***

Although the sample may be loaded directly onto a filament ready for analysis at this point, it was found that the intensity and stability of the ion beam produced during analysis were considerably improved by cleaning up the sample using a single bead of Chelex 20 resin (in sodium form). Prior to use, the resin beads were cleaned by first rinsing with methanol to remove any organic impurities, then repeatedly washing with 6M TD HCl. The beads were then converted to the sodium form by equilibrating with a dilute solution of NaOH (Analar, BDH Chemicals) in TD water.

The residue after evaporation of the HBr receiving solution was picked up in 20 µl 0.05M HBr and a single resin bead added. The vial containing the sample and bead was then placed in an ultrasound bath for between 1 and 2 hours to facilitate equilibration of the bead with the sample solution. The Os was recovered from the resin bead by equilibrating it with 5 - 10 µl 9M HBr for approximately an hour.

***Sample Loading***

The sample was loaded from 5 - 10 µl 9M HBr onto outgassed Pt filaments using a 5 µl micropipette and disposable Teflon pipette tips. Prior to use the tips were soaked in 6M TD HCl followed by 9M HBr, then rinsed with TD water and oven dried. The sample was taken up, 0.5 µl at a time, and deposited in the centre of the filament ribbon. An electrical current passed through the filament was used to warm the sample solution and evaporate off the HBr. To avoid the premature evaporation of Os, the filament was kept relatively cool during sample loading, so that each 0.5 µl fraction required up to 10 minutes to dry fully. Although some spreading of the samples along the filament occurred during the loading of samples

which were insufficiently cleaned during the Chelex resin procedure, by loading the samples onto the filaments in small fractions it was normally possible to obtain a load diameter of no more than 1 mm, which produced very stable ion beams during analysis.

After loading, the osmium bromide complex was reduced to osmium metal by heating the filament to ~600 °C in an outgasser under high vacuum ($p < 10^{-6}$ torr) for several hours. Any organic impurities or Br formed by the decomposition of the HBr were also vaporised, improving the ionisation efficiency during analysis.

After removing the filament from the outgasser, approximately 2 µl of a saturated solution of $Ba(NO_3)_2$ were added on top of the loaded sample to form a thin crystalline layer. The $Ba(NO_3)_2$ was produced and purified by the repeated dissolution and reprecipitation of $BaCO_3$ (99.99 Grade, Aldrich) from TD $HNO_3$.

### 3.11.2 Rhenium Chemistry Following Sample Decomposition

***Preparation of Samples for Loading on to Exchange Columns***

To prevent degradation of the resin during extraction of Re from the distillation pot liquor, the excess Cr(VI) was reduced using ~10 ml 30% $H_2O_2$ (Analar, BDH Chemicals). The hydrogen peroxide was added whilst the pot liquor was still warm, in order to speed up the reaction. Once the effervescence had died down, the sample solution was returned to the Teflon bomb originally used in its digestion and placed in an ultrasound bath for 30 minutes to decompose the excess $H_2O_2$. The solutions were then left to stand for a few days to enable any dissolved oxygen to escape before the samples were added to the ion-exchange columns. Insufficient degassing of the solutions or decomposition of the hydrogen peroxide resulted in the formation of bubbles in the resin column, which inhibited the flow of the sample solutions.

The samples digested using the $HF/HNO_3$ dissolution technique were loaded onto the ion-exchange columns as solutions in 1M HCl, formed by dilution of the solutions in 6M TD HCl produced at the end of the dissolution procedure. Because the samples were incompletely dissolved by the acid attack, leaving undissolved spinel grains, the solutions were centrifuged before loading on to the columns. Centrifuging also removed a gelatinous precipitate which formed during the dilution of the samples.

*Column chemistry*

The Re was separated from the sample solutions using the ion exchange procedure described by Morgan & Walker (1989). Before use, the resin (AG1-X8, 100-200 mesh; BioRad) was batch cleaned by washing repeatedly with TD 6M HCl (20 column volumes) and $HNO_3$ (30 column volumes) to remove the pink dye and any Re from the beads. The resin was then equilibrated with several column volumes of 2.5M TD HCl before storing ready for use.

Because any Os remaining in the solution irreversibly sticks to the anionic resin, a fresh resin column was made up for each sample. The resin columns were made up in quartz tubes with an internal diameter of 6 mm and a bowl capacity of 50 ml and containing a permeable frit at the base to retain the resin. A millilitre of resin was slurried in TD water and transferred by pipette to the quartz column, producing a resin column with a height of ~37 mm. The resin was then further cleaned using a bowlful of 4M $HNO_3$. Although more concentrated acid may have been more efficient at removing any remaining Re, trials with 8M $HNO_3$ were found to degrade the anionic resin severely. After cleaning, the resin was washed with TD water and preconditioned with either 1M HCl or 2M $H_2SO_4$ in preparation for sample loading.

Approximately 50 ml of sample solution were loaded on to the columns and allowed to flow through the column under gravity. After washing the samples on to the columns with two 2.5 ml batches of either 1M HCl or 2M $H_2SO_4$, the columns were treated with 10 ml 1M HCl in two batches followed by 2.5 ml 0.8M $HNO_3$ and 4 ml 4M $HNO_3$, all of which were discarded. The Re was recovered from the columns by eluting a further 10 ml 4M $HNO_3$ into a 15 ml Teflon vial and the solution was evaporated to dryness under heat lamps.

For samples prepared by the HF/$HNO_3$ dissolution technique it was often possible to load the dried down solution directly onto filaments for analysis, however the solutions of samples from which the Os had been distilled frequently required further purification, using a scaled down version of the anion-exchange procedure (comprising 50 µl of resin in shrink-fit Teflon tubing). The dried down sample was loaded on to the clean-up column using 1 ml 0.1M $HNO_3$ and the column washed with 6 ml 0.1M $HNO_3$ before eluting the Re in 6 ml 8M $HNO_3$ and evaporated the sample to dryness once more.

### *Anion-Exchange Column Calibration*

The anion exchange columns were calibrated using solutions of 20 and 6 ng Re in 1M HCl, prepared from a 1000 µg/ml standard solution in 5% $HNO_3$ (Aldritch). Individual 1 ml fractions of the 0.8M $HNO_3$ and 4M $HNO_3$ were eluted, evaporated down to a few microlitres then made up to 5 ml with 5% $HNO_3$. Analyses were performed by ICP-MS at the NERC Facility, Royal Holloway and Bedford New College, using a similar acquisition routine to that for Os analyses. The results of the calibration are illustrated in Figure 3.6.

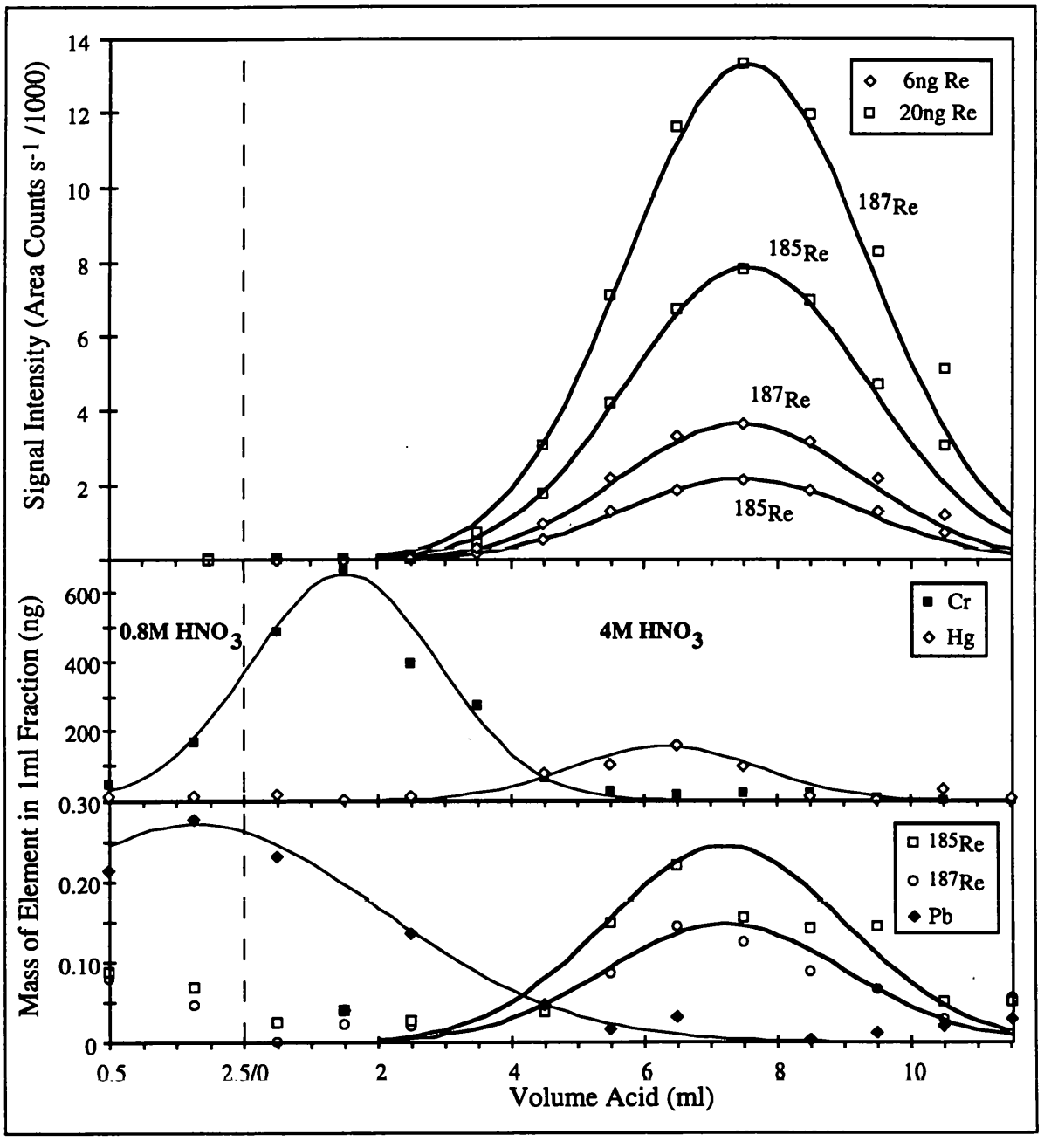


**Figure 3.6** Calibration of anion exchange columns for the separation of Re from acid solutions. 0.8M and 4M $HNO_3$ eluted as 1 ml fractions, evaporated to dryness and made up to 5 ml with 5% $HNO_3$. a) Calibration using standard solutions containing 20 ng and 6 ng Re as $ReO_4^-$ b) & c) Elution peaks for Cr, Hg, Pb and Re separated from a dissolved aliquot of the monitor sample MBR 2. Concentrations calculated using a matrix matched standard solution and recorded as the total mass of the element in the eluted fraction.

To investigate potential contaminants of the separated Re, an aliquot of the monitor sample MBR2 was dissolved using the $HF/HNO_3$ procedure and passed through an anion exchange column. 1 ml fractions were collected from the column, as for the Re standard, and analysed for elements in the mass range 6 - 238 amu. The signal intensities were calibrated using a multi-element standard solution to give elemental concentrations in each fraction. By analysing the solutions produced by the anion exchange of an acid digested peridotite it was possible to duplicate the relative elemental concentrations and sample matrix expected for samples. On account of the low concentrations of the elements present in trace quantities in the peridotite and the wide mass range scanned, however, many elements were barely detectable above the instrumental background.

Included in Figure 3.6 are some of the elemental peaks observed in the Re elution interval of sample MBR 2. Whilst Cr and Pb appear to be eluted in the first few millilitres of 4M $HNO_3$, several heavy metals (including Hg) may co-elute with Re. Although W, Tl and Bi were also present above the background determined from an acid blank, their concentrations were too low for accurate determination. The elution peak of Re in the anion-exchange profile of MBR2 is considerably weaker than that observed for the standard. However, it is in a similar position to that found for the standard, confirming that the column calibration determined for the standard also applied to samples.

***Sample Loading***

The procedure for loading the Re samples was similar to that for Os. The dried down solutions from the anion-exchange columns were picked up in several microlitres of 4M $HNO_3$ and mixed with ~2 µl of a saturated solution of $Ba(NO_3)_2$. After evaporating the combined solutions to dryness under a heat lamp, the samples were picked up in 1 - 2 µl 4M $HNO_3$ and loaded onto Pt filaments using a similar technique to that used for Os samples, although the Re was not reduced to the metal prior to analysis. Because the Re in the sample occasionally appeared to stick to the walls of the beaker in which it was dried down, care was taken after each dry-down to move the acid around the whole of the sample beaker in order to ensure that the sample Re was transferred to the filament.

## 3.12 Spikes and Standards

During the development of N-TIMS at the Open University, an Os solution obtained from DTM was used for the calibration of the Os spike and for the repeated analyses from which the instrumental reproducibility was assessed. Several dilutions were made of the original 56 ppm solution, so that absolute quantities of Os ranging from 50 pg to 100 ng could be loaded from 1 - 2 µl solution by a similar technique to that used for samples. Conversion of the loaded Os to a metal prior to analysis of the standards appeared to have negligible effect on either the way they ran or the determined isotope ratios. Consequently, most standards were not metallised prior to analysis. Two analyses of the J-M standard were also performed for comparison with the results obtained by ICP-MS analysis (Table 3.4).

Although the spike prepared at the Open University was initially used in the preparation of samples by both the NiS fusion and acid dissolution techniques, it appeared to be preferentially lost during the evaporation stages of the acid dissolution procedure, resulting in the determination of unrealistically high Os abundances in a number of samples. For later dissolutions a second spike was obtained from R. Walker at the University of Maryland, in which the Os was present as the stable hexachlorosmate complex.

## 3.13 Analysis of Rhenium and Osmium by N-TIMS

Although it is a decade since Heumann *et al.* (1985) demonstrated that Re could be measured as $ReO_4^-$ thermal ions, it was not until relatively recently that a sensitive and precise N-TIMS technique was developed for Os. The recent advances were marked by the near simultaneous publication of papers by Völkening *et al.* (1991) and Creaser *et al.* (1991), who showed that relative precisions of better than 0.01% could be obtained for loads of only a few nanograms Os.

### 3.13.1 Principles of N-TIMS Analysis

Before it was applied to the analysis of Re and Os, N-TIMS was successfully used to study a broad range of other elements (Heumann *et al.*, 1985). Although only the heavier non-metals form singly charged monatomic anions (e.g. $Cl^-$, $Br^-$, $I^-$, $Se^-$ and $Te^-$), many of the transition metals and non-metals of the second period form more complex polyatomic

anions, involving either oxygen or nitrogen atoms (e.g. $BO_2^-$, $CN^-$, $NO_2^-$, $WO_3^-$, $TcO_4^-$ and $MoO_3^-$).

The formation of thermal ions from a metal filament is described by the Langmuir-Saha equation, which, when modified for negative ions, takes the form

$$\beta = \frac{n_-}{n_- + n_0} = \left(1 + \frac{g_0}{g_-}.\exp\left(\frac{W-EA}{kT}\right)\right)^{-1} \qquad \textbf{(Eqn. 3.4)}$$

where ß is the ion yield, n is the number of atoms or molecules (the subscript denoting the charge on the species), g is a statistical factor, W is the electron work function of the filament material, EA is the electron affinity of the analyte, T is the absolute temperature of the filament and k is the Boltzmann constant (= $1.38 \times 10^{-23}$ J $K^{-1}$).

As can be seen from Equation 3.4, the highest ion yields are obtained for elements with high electron affinities loaded onto filaments made of a material with a low electron work function. Although the electron affinities of the various osmium oxides are unknown, from the occurrence of negative thermal ions of other transition metals Heumann and co-workers at the University of Regensberg predicted the formation of negative osmium oxide ions (Heumann *et al.*, 1985), leading Wachsmann to demonstrate the possibility of producing $OsO_3^-$ and $OsO_4^-$ thermal ions from osmate samples (Wachsmann, 1991).

In order to produce measurable intensities of negative oxide ions of either Os or Re, it was first necessary to reduce the electron work function of the filament material (the work functions of all of the filament materials commonly used in thermal ionisation mass spectrometry being too high for the efficient generation of negative thermal ions, e.g. Re, 5.0 eV; Pt, 5.7 eV; Ta 4.3 eV and W, 4.3 eV). This was done by covering the filament surface with a thin coating of a metal oxide such as BaO, $La_2O_3$, CaO or even NaO (by loading the oxide in the form of either the nitrate or hydroxide) and led to appreciably higher ion yields (Zeininger & Heumann, 1983; Völkening *et al.*, 1991). Tests of various filament materials and metal oxides showed that the optimum ion currents were produced using Pt filaments coated with BaO, loaded as $Ba(NO_3)_2$ (Heumann & Zeininger, 1985).

During these tests, it appears that the performance of Hf metal filaments was not

investigated, despite the low work function of the uncoated metal ($W_{Hf}$ = 3.53 eV) and its relatively high melting point. In tests performed at the Open University, however, no negative osmium oxide ions were observed during the analysis of an Os standard loaded onto a $Ba(NO_3)_2$ coated Hf metal filament, suggesting that BaO is unable to lower the work function of Hf enough to promote the production of negative ions. The absence of Os oxide ions and the observation of a moderately intense $HfO_4^-$ signal (potentially interfering with $^{192}OsO_3^-$) during the analyses meant that the investigation of Hf as a filament material was not pursued. Pt filaments coated with $Ba(NO_3)_2$ were therefore used throughout this study.

During the analysis of Re and Os by N-TIMS, Pt filaments from two different manufacturers were used (H. Cross, New Jersey and Electronic Space Products International (ESPI), California). The blanks for the two filament materials were both reasonably low, although those for the ESPI filaments (0.05 pg Os, 0.1 - 0.25 pg Re) appeared to better than those obtained from Cross (0.16 pg Os). Although no Re blank was measured for the Pt ribbon obtained from Cross, blanks measured by Hauri & Hart (1993) on similar material suggest that this filament material contains considerably more Re than the ESPI Pt, for which blanks as low as 50 fg have been measured (R. A. Creaser, pers. comm.).

### 3.13.2 Machine Conversion

One of the greatest advantages of the N-TIMS technique for the analysis of Re and Os is that the analyses may be carried out using a conventional P-TIMS instrument with only minor modifications. The N-TIMS technique, therefore, benefits from many of the features developed for the determination of precise ratios on small sample loads by P-TIMS, including good peak shapes, counting efficiency and dark noise as well as comprehensive software for routine analysis and data handling.

In order to convert a positive thermal ion mass spectrometer to negative mode the only changes necessary are to reverse the polarities of the magnet and ion-acceleration high voltage power supplies and the phase of the Hall probe used to determine the magnetic field. By adding a variable leak valve to the ion source, however, oxygen gas may be introduced, enhancing the emission of osmium oxide ions from the filament by a factor of ten or more (Walczyk *et al.*, 1991).

The limited modifications required to convert a conventional positive thermal mass spectrometer into one which can analyse either positive or negative ions has prompted several manufacturers to include an optional feature of negative ion analysis in many of their new instruments and to market devices with which existing instruments may be converted to operate in either ionisation mode. These optional features promise to permit the instruments to be switched between the two modes easily, enabling Os isotope ratios to be determined in most radiogenic isotope laboratories. However, care must be taken to avoid the analysis of Re and Os on instruments routinely used for the analysis of Nd, Pb, Th and U isotopes, owing to the use of Re metal filaments for either sample evaporation or ionisation during such analyses. Under these conditions the Re evaporated from the filaments may condense on the cooler surfaces of the ion source, from which it may be remobilised during N-TIMS analysis, creating a significant instrumental blank.

Prior to each analytical session the ion lenses, focusing slits, magazine and all electrical connections within the source chamber were therefore thoroughly cleaned to remove any Re deposits. Initially this was done by simply soaking the individual components in dilute $H_2O_2$ or $HNO_3$, however it was later found that only sand-blasting and soaking in 30% $H_2O_2$ followed by concentrated $HNO_3$ was sufficient to reduce the instrumental Re blank to reasonable levels.

## 3.14 Mass Spectrometry

All analyses by N-TIMS were performed at the Open University using a standard Finnigan-MAT 261 equipped with seven Faraday collectors for static ion collection and a single secondary electron multiplier (SEM) for data collection on smaller beam intensities, using a dynamic peak-hopping routine. Instrumental software was written by D. Wright of the Open University.

### 3.14.1 Data Collection

The mass spectrometer was operated in either a static or dynamic collection mode, depending on the intensity of the signal. For samples prepared by acid dissolution, Os was usually determined using a dynamic, peak-hopping routine, however the greater mass of Os separated using the NiS fusion technique enabled more intense ion beams to be produced,

which could be measured using the Faraday collectors in the static mode. Because the isotopic abundance of both Re isotopes to be measured was relatively high, sufficiently intense beams could be produced for the collection of data using a static routine. Consequently many of the Re analyses were initially performed using the SEM, then repeated on the Faradays. Apart from speeding up the acquisition of data, static collection was less prone to interferences than the multicollector routine (see below).

***Dynamic Routine***

The signal intensity during the acquisition of data using the electron multiplier was limited by the non-linearity of the detector at high count rates, when the dead time correction becomes a significant factor in the calculation of the ion current. An upper limit of ~6 x $10^5$ counts $s^{-1}$ (0.09 pA) was therefore placed on the intensity of the most abundant mass analysed during a dynamic run. In order to obtain the best precision on the $^{187}Os/^{188}Os$ ratio, therefore, most Os samples were run so that the strongest signal intensity (usually $^{190}OsO_3^-$) was close to this limit.

During the analysis of Os using the dynamic data collection routine, all the oxide species from $^{186}OsO_3^-$ (234 amu) to $^{192}OsO_3^-$ (240 amu) were measured, as well as the $^{185}ReO_3^-$ ion, from which the interference of $^{187}OsO_3^-$ by $^{187}ReO_3^-$ could be corrected. Each of the beam intensities of the less abundant isotopes, including $^{187}OsO_3^-$, was measured for twice the time used for the more abundant isotopes ($^{192}OsO_3^-$, $^{190}OsO_3^-$, $^{189}OsO_3^-$ and $^{188}OsO_3^-$), in order to obtain adequate precisions. To accommodate all the major isotopes of Os and a monitor of the Re interference in the collection cycle, it was not possible to include a measurement of the background.

The dynamic routine for the analysis of Re included only three masses, the two Re oxide ions ($^{185}ReO_4^-$ and $^{187}ReO_4^-$ at 249 and 251 amu respectively) and a determination of the background at 249.5 amu. Although Os does form $OsO_4^-$ ions during N-TIMS analysis, their intensity is more than two orders of magnitude less than that of the $OsO_3^-$ ions. Consequently, no correction was applied for the interference of $^{187}OsO_4^-$ on $^{187}ReO_4^-$.

***Static Routine***

When collecting data in the static mode, the Faraday collectors were positioned at similar masses to those used during peak-hopping. Baseline and gain calibrations for the Faraday

collectors were performed before the start of each sample analysis to correct for any variation in the response of the different collectors.

### 3.14.2 Running conditions

***Filament Temperature***

Equation 3.4 predicts that the ion currents of $ReO_4^-$ and $OsO_3^-$ ions should increase continuously with increasing filament temperature for any given sample. During analysis, however, it was found the $OsO_3^-$ signal intensity reached a maximum at filament temperatures in the range 850 - 900 °C, after which it rolled over and started to decrease with increasing filament temperature. If the temperature were then decreased, however, the signal intensity returned to its higher value, indicating that the drop in ion current is not merely a result of the more rapid depletion of the sample. Similar behaviour was noted by Völkening *et al.* (1991) for $OsO_3^-$, who attributed the decrease in ion current to secondary effects including the increasing emission of electrons from the filament and the shorter adsorbtion times of the molecules to be analysed on the filament surface at higher temperatures.

Analysis of Re samples was performed at similar or slightly lower filament temperatures to those used for Os. In order to obtain the maximum beam intensities for Re, the $ReO_4^-$ peak was usually found and focussed at low filament temperatures, following which the temperature was rapidly raised to that used for the analyses and the ratios measured immediately.

***Oxygen Pressure***

During the analysis of Re and Os, high purity oxygen was slowly bled into the source chamber via a variable leak valve. Whilst the oxygen was delivered to a point close to the sample filament, its pressure during analysis was determined close to the turbomolecular pump, which was located below the source. Although the measured pressures may have been significantly less than those occurring close to the sample, they enabled the oxygen pressure to be monitored and reproduced between samples.

The presence of oxygen in the source has two effects. Firstly it increases the ionisation efficiency by stimulating the production of oxide ions, particularly for small sample amounts, and secondly it shifts upwards the temperature range at which the optimum ion

currents are produced (Walczyk *et al.*, 1991). In their description of the analytical methods used in their study, Hauri & Hart (1993) suggested that the presence of oxygen also enhances the oxide speciation of Re and Os to $ReO_4^-$ and $OsO_3^-$, however such effects were not observed in this study and have not been documented elsewhere.

The oxygen pressures used for the analysis of Re and Os were in the range 2 - 4 x $10^{-8}$ torr and 5 - 10 x $10^{-8}$ torr respectively. By increasing the oxygen pressure in the source the beam intensity was decreased, however the rate with which the beam decayed was also reduced.

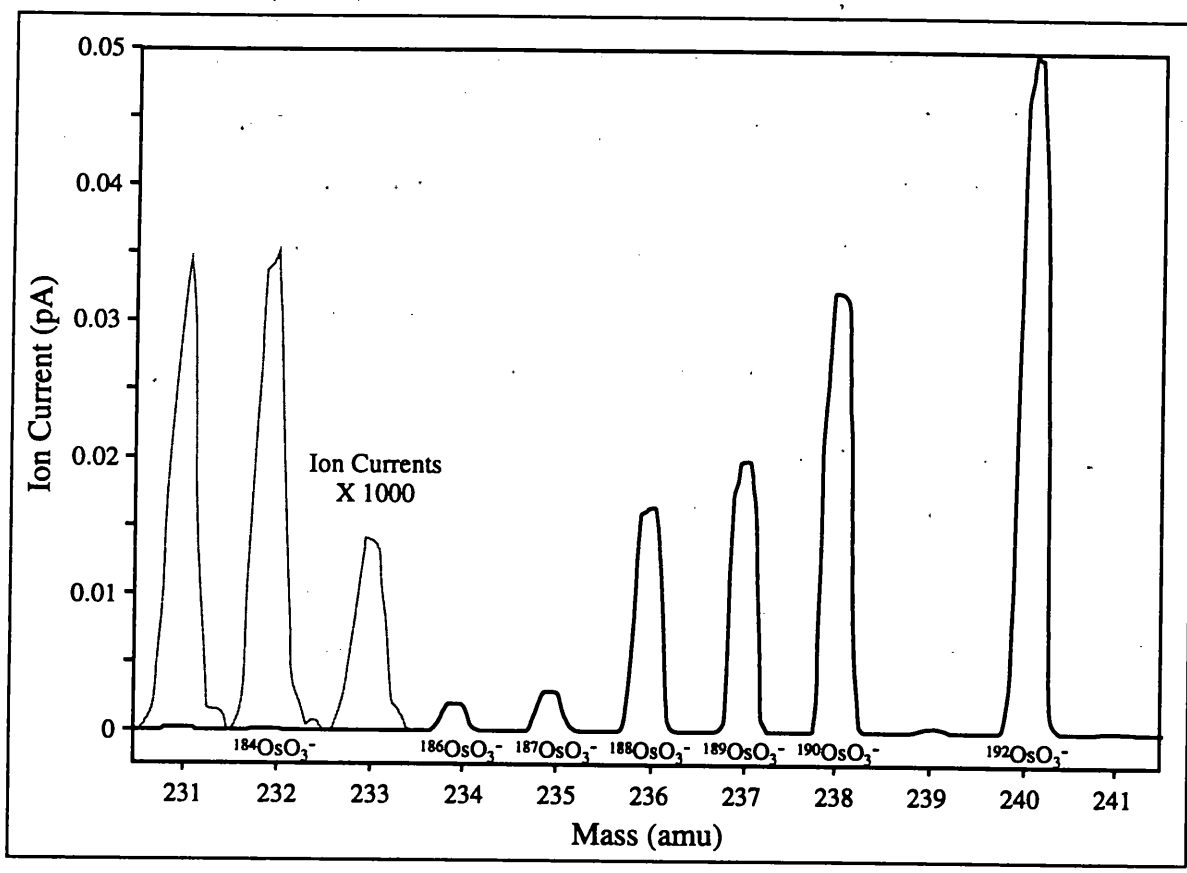


**Figure 3.7** Mass spectrum measured using the electron multiplier on 5 ng Os standard on a Cross Pt filament. Interference peaks at masses 231 - 233 shown on an expanded scale (full scale is 5 x $10^{-5}$ pA). Os spectrum labelled according to main oxide ion species (in which all three oxygens are $^{16}O$). Interference peaks at masses 231 - 233 are a combination of $^{198}PtO_2^-$ (with $^{17}O$ and $^{18}O$ replacing one or more of the $^{16}O$), $^{184}OsO_3^-$ and possibly $WO_3^-$, PtCl or $^{185}ReO_3^-$. The uncorrected $^{187}Os/^{188}Os$ ratio of the standard, however is within error of the correct value, suggesting that $^{185}ReO_3^-$ does not form the majority of the peak at mass 233. Compared to the spectra produced by ICP-MS analysis, the mass spectra determined by N-TIMS exhibit superior peak resolution and relatively flat-topped peaks (also shown in Figure 3.8).

### *Peak Shape*

Figures 3.7 and 3.8 shows a typical spectrum for the analysis of Os by N-TIMS and an enlargement of an individual peak. The most notable features of the spectrum are the flat

peak tops, resulting from the relatively small spread of energies of ions emitted from the filament source, and the resolution of adjacent peaks following collimation of the ion beam by the exit slits. In contrast to the triangular peaks produced during analysis by ICP-MS, using a quadrupole mass analyser and plasma source, the flat-topped peaks produced during N-TIMS analysis enable the intensity of the ion beam to be determined by measuring the ion current at a fixed mass close to the centre of the peak. The determination of ion beam intensities by measuring at a fixed mass enables the majority of the machine time to be spent at the maximum beam intensity at each mass, decreasing the contribution of signal noise to the measured intensities as well as increasing the total number of ions measured.

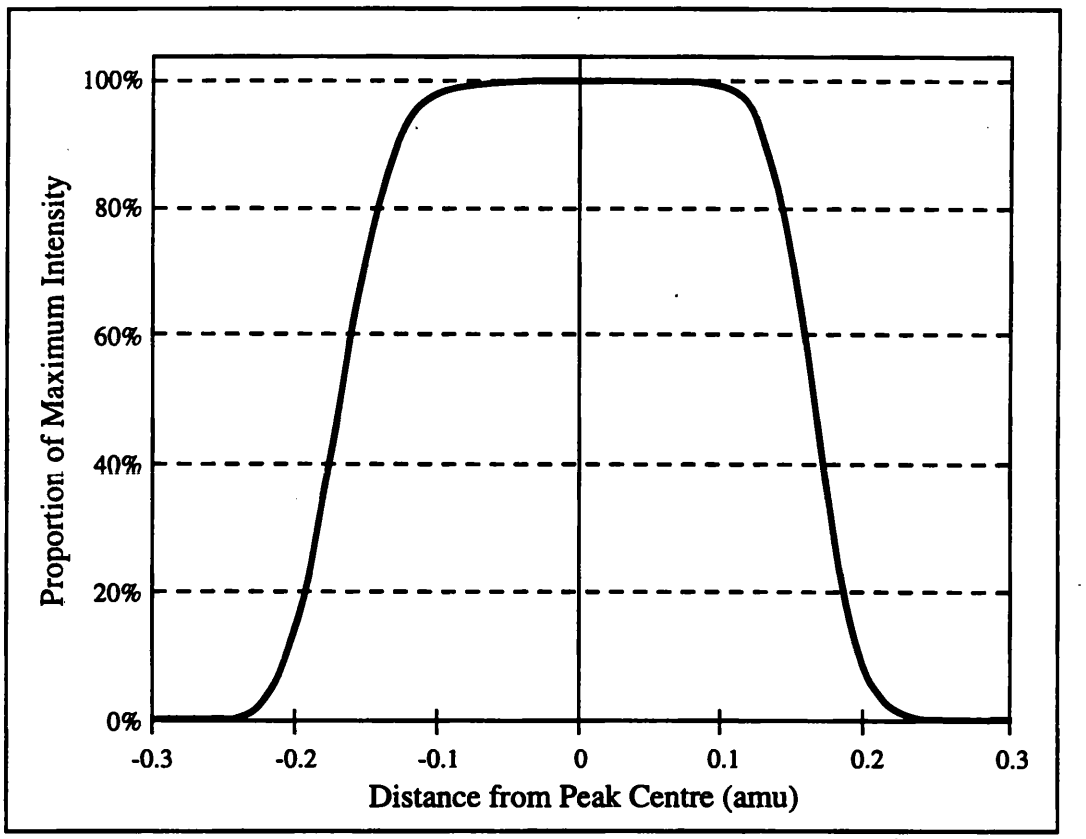


**Figure 3.8** Shape of $^{192}OsO_3^-$ peak produced during N-TIMS analysis of a standard, illustrating the flat top, steep sides and low noise characteristic of peaks produced during TIMS analysis. Beam intensity 1.7 pA, measured using static collection on the Faraday collectors.

### 3.14.3 Data Handling

The raw intensity data were manipulated using instrumental software adapted from routines for the determination of Nd isotopic ratios from the measurement of neodymium oxide positive ions (Wasserburg *et al.*, 1981). The oxide ion data were first corrected to metallic ratios assuming $^{17}O/^{16}O = 0.0003708$ and $^{18}O/^{16}O = 0.002085$ (Nier, 1950). The

Os isotope ratios were then corrected internally for mass dependent isotope fractionation, assuming an exponential law, and normalised to $^{192}Os/^{188}Os = 3.08271$ (Luck & Allègre, 1983), with simultaneous correction for fractionation and the contribution of the spike to each isotope for spiked samples.

Because Re possesses only two stable isotopes it was impossible to use an internal correction to compensate for the fractionation of the Re isotope ratios of spiked samples. Although it would have been possible to apply an external correction for fractionation (by analysing a Re standard under similar conditions to those used for the sample analyses), the significantly lower temperature at which standards ran made it in difficult to match the running conditions of the samples and standards. On account of the large mass of the Re oxide ions, however, the degree of fractionation experienced by the element should be small small (<1‰ $amu^{-1}$), hence, for well-spiked samples, the effects of fractionation on the determined Re abundances should be minimal, enabling the uncorrected ratios to be used without significant loss of accuracy.

### 3.14.4 Interferences

During the analysis of Re and Os by N-TIMS a number of other molecular and elemental anions were observed, both in the mass region in which Re and Os were analysed and at lower masses. The ion species observed included $WO_3^-$, $PtO_2^-$, $PtO_3^-$, $BaCl_3^-$, $BO_2^-$, $Cl^-$, $Br^-$ and $I^-$. Although the halide and borates ions do not interfere directly with the analysis of Re or Os, high ion currents of these species may decrease the ionisation efficiency of both $ReO_4^-$ and $OsO_3^-$, leading to poorer beam intensities and greater signal noise. Interferences from molecular ions formed by the combination of either W, Pt or Ba with oxygen, chlorine or bromine, on the other hand, have the potential to interfere directly with the analysis of Re and Os, as shown in Table 3.7.

Of the species shown in Table 3.7, only $WO_3^-$ (possibly derived from W contamination acquired up from the pipette tips) and $PtO_2^-$ (from the Pt filament) were positively identified during the analysis of samples. The presence of the $WO_3^-$ molecular ion during the analysis of Os introduces an interference on $^{186}OsO_3^-$. Although this may be corrected by monitoring $^{183}WO_3^-$ or $^{184}WO_3^-$ at 231 and 232 amu respectively, on account of the limited number of

masses that could be measured simultaneously and the low importance placed on this ratio in most samples, any W interference was not corrected. Because no peaks were observed in the mass range 242 - 244, $PtO_3^-$ was assumed to be absent from the sample spectra and no correction for interference by $^{190}PtO_3^-$ and $^{192}PtO_3^-$ was applied to the intensities of the $^{190}OsO_3^-$ and $^{192}OsO_3^-$ peaks.

| Mass | Os Oxides | Re Oxides | W or Ir Oxides | Pt Oxides | PtCl | BaOBr | $BaCl_3$ |
|---|---|---|---|---|---|---|---|
| **229** | | | $\underline{WO_3}$ | 1541 ppm | 25.12% | 1.27% | |
| **230** | | | 26.11% | 7.27% | 25.61% | 3.33% | |
| **231** | $\underline{OsO_3}$ | | 14.23% | 56 ppm | 27.14% | 5.16% | |
| **232** | 199 ppm | $\underline{ReO_3}$ | 30.62% | 288 ppm | 8.19% | 8.93% | |
| **233** | | 37.13% | 1203 ppm | | 11.59% | 40.13% | |
| **234** | **1.59%** | 424 ppm | 28.58% | | | 5.56% | |
| **235** | **1.59%** | 62.37% | 328 ppm | | 1.74% | 35.35% | 461 ppm |
| **236** | **13.21%** | 712 ppm | 1712 ppm | | | 245 ppm | |
| **237** | **16.01%** | 3743 ppm | | $\underline{PtO_3}$ | | 707 ppm | 882 ppm |
| **238** | **26.30%** | | $\underline{IrO_3}$ | 99 ppm | | | |
| **239** | 1261 ppm | | 37.03% | | | | 1.11% |
| **240** | **40.86%** | | 423 ppm | 0.78% | | | 2.87% |
| **241** | 468 ppm | | 62.47% | | | | 4.44% |
| **242** | 2451 ppm | | 713 ppm | 32.67% | | | 7.64% |
| **243** | | | 3749 ppm | 33.59% | | | 34.79% |
| **244** | | | | 25.35% | | | 5.57% |
| **245** | | | | 2307 ppm | | | 31.00% |
| **246** | | | | 7.30% | | | 1.59% |
| **247** | $\underline{OsO_4}$ | | | 87 ppm | | | 9.68% |
| **248** | 198 ppm | $\underline{\mathbf{ReO_4}}$ | | 433 ppm | | | 1597 ppm |
| **249** | | **37.04%** | | | | | 1.02% |
| **250** | 1.58% | 564 ppm | | | | | |
| **251** | 1.59% | **62.30%** | | | | | |
| **252** | 13.19% | 948 ppm | | | | | |
| **253** | 15.98% | 4982 ppm | | | | | |
| **254** | 26.27% | | | | | | |

**Table 3.7** Calculated relative abundances of potential and observed negative ion species in the mass range 229 - 254 amu. Shown in bold are the principal masses measured for $ReO_4^-$ and $OsO_3^-$. Species abundances were calculated using isotope compositions taken from Barnes *et al.* (1991) and the oxygen isotope composition of Nier (1950). Molecular ions present as less than 10 ppm of the total ion species are not shown.

An intense beam of $BaCl_3^-$ ions was observed in the spectrum of an Os standard in which the standard solution (in HCl) was mixed with the $Ba(NO_3)_2$ solution prior to loading, depositing the Ba on the filament surface as $BaCl_2$. Because most samples were metallised from solution in HBr prior to the addition of the $Ba(NO_3)_2$ and the Os standard solutions

and $Ba(NO_3)_2$ were subsequently loaded separately, interference by $BaCl_3^-$ was not observed in any of the sample or later standard analyses.

During the measurement of Os isotope ratios at low beam intensities on the electron multiplier, a low intensity beam (~ 5 - 10 x $10^{-6}$ pA) was frequently observed at mass 233 (where $^{185}ReO_3^-$ was monitored in order to correct for interference of $^{187}ReO_3^-$ on $^{187}OsO_3^-$). This beam was usually less than 0.5% of the intensity of the $^{187}OsO_3^-$ peak, however, during poor runs its relative magnitude increased.

For Os standards its was found that changes in the intensity of this peak were not matched by substantial changes in the intensities of any of the peaks at which Os oxide ions were measured (including mass 235, $^{187}OsO_3^-$), indicating that the peak was not primarily due to the presence of either $ReO_3^-$ or most of the other molecular ion species listed in Table 3.7 (which should all affect significantly one or more of the determined Os isotope ratios). However, when samples were analysed at low and high beam intensities it was found that the uncorrected $^{187}Os/^{188}Os$ ratios were often different, with significantly lower ratios determined at high beam intensities. Although the ratios between the ion beams measured at masses 233 and 236 also decreased substantially with the increase in the Os oxide ion beam intensities, the magnitude of the decrease in the $^{187}Os/^{188}Os$ ratios was less than that expected if the peak at mass 233 was wholly the result of $^{185}ReO_3^-$, suggesting the presence of another ion species.

From Table 3.7 it is apparent that the molecular ion species $PtCl^-$ may represent a possible source of the peak at mass 233. $PtCl^-$ is a simple dimer composed of elements present in abundance in the source during the analysis of both samples and standards and possesses a low 233/235 ratio (~0.15), consistent with the limited change in the intensity of the peak at mass 235 with changes in intensity of that at 233 amu. In most cases the $^{190}Pt^{16}O_2^-$, $^{190}Pt^{16}O^{17}O^-$ and $^{190}Pt^{16}O^{18}O^-$ ions dominate the mass range 230 - 232 amu, hence $PtCl^-$ may be recognisable only at masses 233 and 235. During the analyses of a blank Pt filament, coated with $Ba(NO_3)_2$, however, the peaks at both 233 and 235 amu were very small, implying that if $PtCl^-$ were present, then its intensity was small or insignificant. It was not possible to prove conclusively whether or not the presence of $PtCl^-$ accounted for the

interference at mass 233, and the origin of this peak, therefore remains unresolved.

In view of the uncertainty surrounding the origin of the interference at mass 233, the correction for Re interference using the measured $^{185}ReO_3^-/^{188}OsO_3^-$ ratios was believed to be inappropriate in many cases. Consequently, unless the peak at 233 was proven to be predominantly $^{185}ReO_3^-$ (by the correlation of the uncorrected 235/236 ratio with the 233/236 ratio determined for the individual sets of data), no correction was applied for the interference of $^{187}Re$ on $^{187}Os$. For samples analysed at low ion beam intensities, therefore minor amounts of $^{187}Re$ interference ($\leq 0.2\%$ of the total $^{187}Os$ intensity) may have gone uncorrected, resulting in an overestimation of the $^{187}Os/^{188}Os$ ratios. However without understanding the origin of the peak at mass 233 better, it was impossible to separate the Re interference from that due to ions of another species, in order to apply the relevant correction.

During this study, virtually no interferences were observed in the mass range used for the determination of Re isotope ratios in samples and standards (249 - 251). Peaks observed in the mass range 252 - 256 at high filament currents, however suggested that $OsO_4^-$ molecular ions were present. Although $^{187}OsO_4^-$ may potentially interfere with $^{187}ReO_4^-$, the low isotopic abundance of $^{187}Os$ and large difference in the relative intensities of the $OsO_4^-$ and $ReO_4^-$ ion beams meant that any correction for Os interference on Re would have been insignificant, relative to the within-run precision of the Re isotope ratio determinations.

## 3.15 Accuracy and Reproducibility of N-TIMS Analyses

### 3.15.1 Osmium Standard Solutions

To investigate the within-run precision of individual Os isotope ratio determinations by N-TIMS and their long-term reproducibility over the period that the technique was used for sample analyses, several Os standards were analysed during each analytical session. The standards were run under the same instrumental conditions as samples. However, the acquired data were (understandably) not corrected for the presence of the $^{190}Os$ spike. The full set of fractionation and oxide corrected Os isotope ratios for the standards are presented in Table 3.8 and illustrated in Figure 3.9. The data are separated into those obtained during static runs, using the Faraday cups, and those from dynamic runs on the electron multiplier.

| Sample Mass | Collector | Date | No. of Analyses | $\frac{^{190}Os}{^{192}Os}$ | $\frac{^{189}Os}{^{192}Os}$ | $\frac{^{187}Os}{^{188}Os}$ | $\frac{^{186}Os}{^{192}Os}$ |
|---|---|---|---|---|---|---|---|
| 23 ng | F | 25-Mar-93 | 270 | 0.64358±1 | 0.39571±1 | 0.17406±1 | 0.038917±5 |
| 23 ng | F | 25-Mar-93 | 240 | 0.64371±1 | 0.39572±1 | 0.17398±1 | 0.039009±42 |
| 23 ng | F | 27-Mar-93 | 230 | 0.64378±7 | 0.39568±3 | 0.17383±15* | 0.039438±27 |
| 23 ng | F | 28-Mar-93 | 270 | 0.64362±2 | 0.39576±1 | 0.17390±2 | 0.039061±7 |
| 23 ng | F | 29-Mar-93 | 110 | 0.64355±2 | 0.39576±2 | 0.17385±4 | 0.039063±13 |
| 23 ng | F | 29-Mar-93 | 150 | 0.64361±2 | 0.39578±2 | 0.17389±2 | 0.038998±8 |
| 1.1 ng | F | 30-Mar-93 | 150 | 0.64385±5 | 0.39586±5 | 0.17359±11 | 0.040851±80‡ |
| 23 ng | F | 30-Mar-93 | 100 | 0.64361±2 | 0.39578±2 | 0.17389±2 | 0.038998±8 |
| 23 ng | M | 2-Apr-93 | 100 | 0.64359±1 | 0.39577±1 | 0.17406±1 | 0.039111±6 |
| 56 ng | F | 29-Jun-93 | 150 | 0.64337±2 | 0.39573±2 | 0.17392±6 | 0.038969±8 |
| 250 ng | M | 2-Jul-93 | 250 | 0.64302±6 | 0.39528±4 | 0.14922±4†* | 0.038983±12 |
| 23 ng | M | 4-Jul-93 | 220 | 0.64403±9 | 0.39584±6 | 0.17357±6 | 0.038774±19 |
| 250 ng | F | 4-Jul-93 | 270 | 0.64354±1 | 0.39574±1 | 0.14922±1† | 0.038929±3 |
| 5 ng | M | 5-Jul-93 | 250 | 0.64252±7 | 0.39512±5 | 0.17399±5 | 0.039017±13 |
| 250 ng | F | 6-Jul-93 | 270 | 0.64360±1 | 0.39575±1 | 0.14923±1† | 0.038937±4 |
| 56 ng | F | 6-Jul-93 | 270 | 0.64368±2 | 0.39548±2 | 0.17401±2* | 0.039141±20 |
| 56 ng | F | 6-Jul-93 | 270 | 0.64352±1 | 0.39570±1 | 0.17397±2 | 0.039047±11 |
| 56 ng | M | 31-Oct-93 | 245 | 0.64371±21 | 0.39592±16 | 0.17387±14 | 0.038930±37 |
| 5.8 ng | M | 2-Feb-94 | 100 | 0.64373±35 | 0.39570±17 | 0.17421±13 | 0.039053±152 |
| 4.5 ng | M | 3-Feb-94 | 190 | 0.64264±16 | 0.39531±9 | 0.10996±4† | 0.038999±22 |
| 0.56 ng | M | 6-Feb-94 | 180 | 0.64268±21 | 0.39517±14 | 0.17430±10 | 0.039084±35 |
| 11.5 ng | M | 7-Feb-94 | 100 | 0.64317±21 | 0.39542±12 | 0.17388±9 | 0.038950±30 |
| 11.5 ng | M | 16-Jun-94 | 50 | 0.64340±17 | 0.39560±14 | 0.17407±10 | 0.039110±31 |
| 11.5 ng | M | 16-Jun-94 | 50 | 0.64340±17 | 0.39560±14 | 0.17407±10 | 0.039110±31 |
| 11.5 ng | M | 18-Jun-94 | 150 | 0.64330±12 | 0.39543±8 | 0.17403±8 | 0.040268± 2‡ |
| 11.5 ng | M | 20-Jun-94 | 250 | 0.64328±31 | 0.39545±17 | †† | 0.039007±17 |
| 0.54 ng | M | 20-Jun-94 | 80 | 0.64334±18 | 0.39545±13 | 0.17380±11 | 0.039389±30 |
| 0.54 ng | M | 22-Jun-94 | 80 | 0.64339±14 | 0.39546±10 | 0.17389±9 | 0.039217±28 |
| 0.54 ng | F | 22-Jun-94 | 110 | 0.64370±4 | 0.39562±3 | 0.17369±7 | 0.038973±19 |
| 5 ng | M | 23-Jun-94 | 110 | 0.64317±17 | 0.39542±12 | 0.17399±10 | 0.039050±25 |
| 5 ng | M | 23-Jun-94 | 110 | 0.64321±2 | 0.39543±10 | 0.17397±9 | 0.040116±39‡ |
| 5 ng | M | 24-Jun-94 | 130 | 0.64329±9 | 0.39546±8 | 0.17394±6 | 0.039043±16 |
| 5 ng | M | 24-Jun-94 | 50 | 0.64289±18 | 0.39551±13 | 0.17395±11 | 0.039214±38 |
| 125 pg | M | 25-Jun-94 | 60 | 0.64342±16 | 0.39548±13 | 0.17397±10 | 0.039086±29 |
| 125 pg | M | 27-Jun-94 | 80 | 0.64456±15 | 0.39553±12 | 0.17429±9 | 0.039889±51‡ |
| 125 pg | M | 28-Jun-94 | 100 | 0.64334±14 | 0.39538±12 | 0.17397±10 | 0.039992±59‡ |
| 125 pg | M | 28-Jun-94 | 40 | 0.64353±30 | 0.39572±17 | 0.17394±16 | 0.039311±62 |
| 125 pg | M | 29-Jun-94 | 80 | 0.64358±13 | 0.39562±13 | 0.17399±10 | 0.039140±28 |
| 125 pg | M | 29-Jun-94 | 260 | 0.64326±10 | 0.39539±9 | 0.17393±7 | 0.039347±22 |
| 0.5 ng | M | 30-Jun-94 | 160 | 0.64282±15 | 0.39523±7 | 0.17411±7 | 0.040105±40‡ |
| 50 pg | M | 2-Jul-94 | 140 | 0.64828±31[a] | 0.39550±13 | 0.17381±11 | 0.039406±37 |
| 11.5 ng | F | 6-Jul-94 | 160 | 0.64358±2 | 0.39573±1 | 0.17396±2 | 0.038961±7 |
| **Mean (±2σ)** | | | | **0.64343±76** | **0.39557±39** | **0.17395±30** | **0.03908±30** |
| **Mean of Faraday Data (±2σ)** | | | | **0.64362±23** | **0.39572±17** | **0.17389±25** | **0.03903±26** |
| **Mean of Multiplier Data (±2σ)** | | | | **0.64332±86** | **0.39549±38** | **0.17398±31** | **0.03911±31** |

**Table 3.8.** Replicate analyses of Os standard solutions over period of study. Errors on individual analyses are ± two standard errors of the mean ($2\sigma_m$) and are therefore dependent on the number of ratios determined in each run. Mean ratios (after the rejection of outliers) are shown for both the whole dataset and for the data collected using the faraday cups (F) and electron multiplier (M).

‡ $^{186}Os/^{192}Os$ ratios rejected due to significant W interference.

[a] Outlying $^{190}Os/^{192}Os$ ratio rejected.

* $^{187}Os/^{188}Os$ ratios corrected for Re interference.

† Less radiogenic Os standard solution analysed, $^{187}Os/^{188}Os$ ratio not included in mean.

†† Standard solution contaminated with less radiogenic standard.

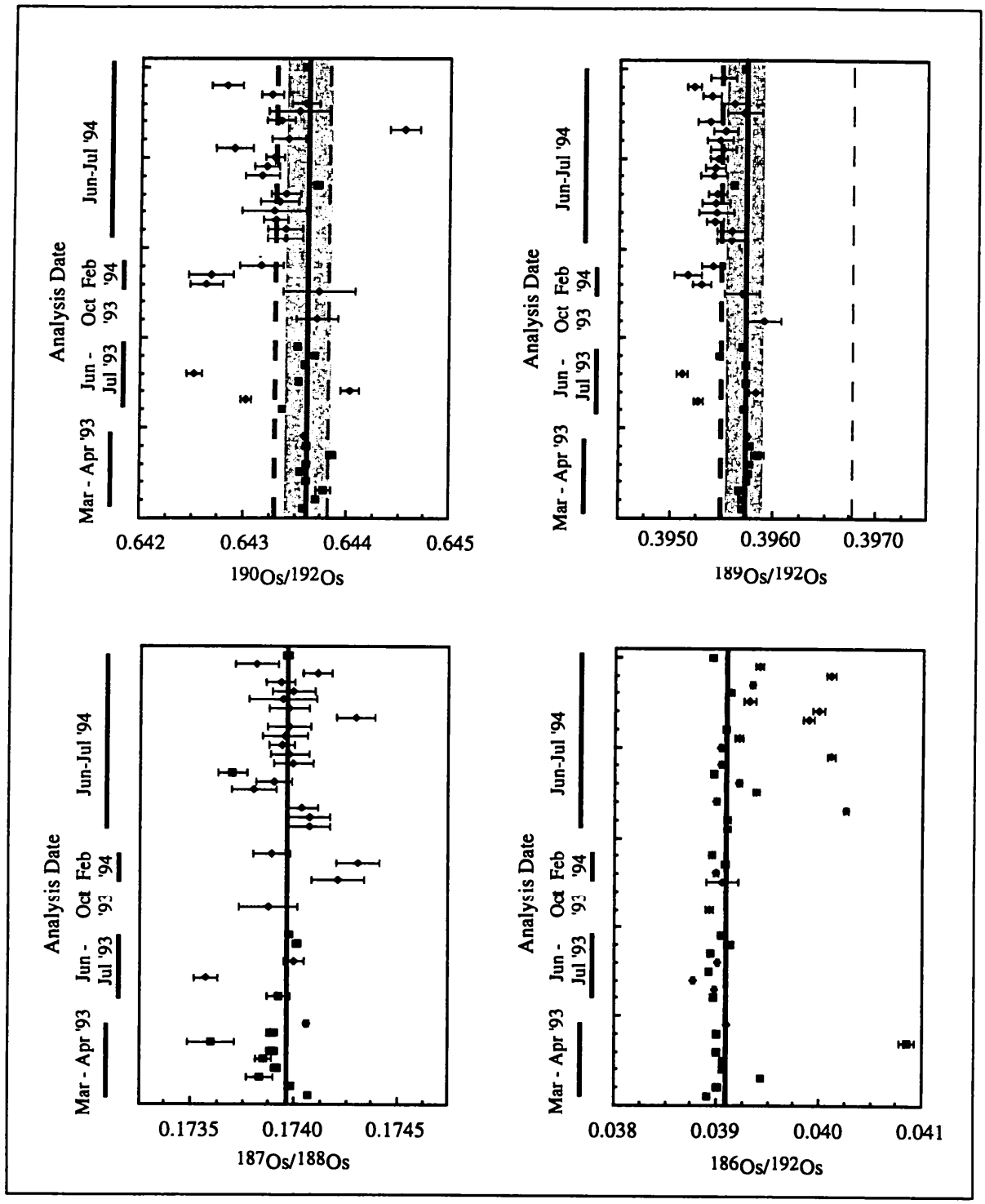


**Figure 3.9** Os isotope ratios determined for Os standards over the period of the study. Error bars on individual analyses represent ±2 standard errors of the mean ($2\sigma_m$). The average value of each ratio is indicated by the thick solid line, whilst the shaded region represents $2\sigma$ of the analyses. For $^{189}Os/^{192}Os$ the averages of the data collected using the electron multiplier and Faraday cups are presented separately. Thinner dashed lines represent the values of $^{189}Os/^{192}Os$ and $^{190}Os/^{192}Os$ reported by Luck & Allègre (1983). The mean $^{186}Os/^{192}Os$ ratio of this study is coincident with that of Luck & Allègre (1983).

The data obtained during static runs of the standard exhibited both better within-run precision and better long-term reproducibility than those obtained during dynamic runs. For each method of collection, the relative precisions of the determined isotope ratios was best for the $^{190}Os/^{192}Os$ ratios and worst for the $^{186}Os/^{192}Os$ ratios, consistent with the

decreasing relative abundance of the isotopes used in the ratio. As a consequence a range of precisions exists for each of the two methods of analysis.

For sample loads of between 50 pg and 250 ng, average within-run precisions ($2\sigma_m$) for the ratios determined during static runs varied between 0.04‰ and 0.4‰, whilst those of dynamic runs lay in the range 0.25‰ - 0.88‰. The better precision of the static runs reflects the more intense ion beams present during these analyses. Despite these excellent within-run precisions, however, the overall precision of the analyses is limited by the reproducibility of the determinations ($2\sigma$), which varied between < 0.4‰ and ~7‰ (static runs) and between 1.3‰ and 8‰ (dynamic runs) for the $^{190}Os/^{192}Os$ and $^{186}Os/^{192}Os$ ratios respectively. The poor reproducibility of the $^{186}Os/^{192}Os$ ratios may reflect the presence of variable, but minor, amounts of W contamination and contrasts with the < 2‰ $2\sigma$ variation of the determined $^{187}Os/^{188}Os$ ratios.

Whilst there is no significant difference between the mean $^{187}Os/^{188}Os$ and $^{186}Os/^{192}Os$ ratios obtained by the two methods of collection, the small difference between the mean $^{190}Os/^{192}Os$ and $^{189}Os/^{192}Os$ ratios determined by the two methods is statistically significant, with higher ratios obtained during static runs. The bias of the ratios determined during static analyses towards marginally higher values (< 0.5‰) resulted in minor differences in the concentrations calculated during sample analysis, leading to a slight bias in the calculated concentration according to the method used to collect the data.

Because no absolute determination is available for the relative abundances of Os isotopes, the accuracy of Os isotope ratio determinations are conventionally assessed by comparison with the ratios determined by Luck & Allègre (1983), using a similar value of $^{188}Os/^{192}Os$ to correct for fractionation. Whilst the $^{190}Os/^{192}Os$ and $^{186}Os/^{192}Os$ ratios of the standards determined during this study do not differ significantly from those of Luck & Allègre, the $^{189}Os/^{192}Os$ ratios determined during both static and dynamic runs are significantly lower than their reported values. If other published values of the non-radiogenic Os isotope ratios (Table 3.9) are compared to the values determined by Luck & Allègre (1983), it is apparent that their $^{189}Os/^{192}Os$ ratio is relatively high and that the value of this ratio may lie closer to 0.3955, with which the data of this study are consistent.

In conclusion, the replicate analyses of the Os standard solutions demonstrate that, after

correction for fractionation and oxide interferences, analysis by N-TIMS may produce very accurate and reproducible Os isotope ratios for a range of sample loads, with the $^{187}Os/^{188}Os$ ratio reproducible within 2‰ (2σ).

| Authors | Method | $\frac{^{190}Os}{^{192}Os}$ | $\frac{^{189}Os}{^{192}Os}$ | $\frac{^{186}Os}{^{192}Os}$ |
|---|---|---|---|---|
| **Luck & Allègre (1983)** | **SIMS** | **0.6438 ± 3** | **0.3968 ± 1** | **0.03907 ± 2** |
| Nier (1937) | P-TIMS | 0.6439 | 0.3927 | 0.03878 |
| Masuda *et al.* (1986) | ICP-MS | 0.6422 ± 7 | 0.3998 ± 6 | 0.0388 ± 1 |
| Russ & Bazan (1987) | ICP-MS | 0.6443 ± 7 | 0.3955 ± 5 | 0.03842 ± 14 |
| Dickin *et al.* (1988) | ICP-MS | 0.6445 ± 19 | 0.3960 ± 17 | n.d. |
| Creaser *et al.* (1991) | N-TIMS | 0.6438 ± 5 | 0.3950 ± 4 | 0.03918 ± 44 |
| Hauri & Hart (1993) | N-TIMS | 0.6436 ± 8 | 0.3956 ± 3 | n.d. |
| This Study | N-TIMS | 0.6434 ± 7† | 0.3956 ± 4† | 0.03908 ± 3 |

**Table 3.9** Compilation of non-radiogenic Os isotope ratios determined in previous studies. Methods: SIMS, secondary ionisation mass spectrometry; P-TIMS, positive thermal ionisation mass spectrometry; ICP-MS, inductively coupled plasma mass spectrometry; N-TIMS, negative thermal ionisation mass spectrometry. Errors are 2σ on the averages. Ratios corrected for fractionation and mass bias using $^{188}Os/^{192}Os = 0.32439$.

† Average of standard data obtained for both dynamic and static runs.

### 3.15.2 Osmium Samples

The $^{187}Os/^{188}Os$ ratios and Os concentrations determined by replicate analyses of eight of the peridotite samples and the reference material WPR-1 are shown in Table 3.10.

At least two separate aliquots of the sample powders were prepared for analysis for each of the replicates. The first of these was prepared using the NiS fusion technique and the resin-cleaned solution in HBr split prior to loading. The two splits were analysed during two different analytical sessions approximately three months apart during the development of the technique, in order to assess the repeatability of the isotope ratio determinations. A second aliquot of each replicate sample was later prepared (using either NiS fusion or acid digestion) and analysed as part of the main period of sample analysis. Although samples prepared using the 'volatile' Os spike are included in Table 3.10, the low $^{190}Os/^{192}Os$ ratios determined for these samples indicated that much of the $^{190}Os$ spike had been lost during sample preparation. Consequently, Os concentrations are not presented for these analyses.

Although all the data for the first set of replicates were collected using the dynamic routine, several of the analyses of the second aliquots of the sample powders were repeated by re-analysing the samples using static data collection on more intense ion beams.

| Sample Number | Preparation Technique | Analysis Date | $\frac{^{190}Os}{^{192}Os}$ | Os Conc. (ppb) | $\frac{^{187}Os}{^{188}Os}$ |
|---|---|---|---|---|---|
| 92-FR3 | fusion | June '94 - Far.[b] | 1.91848±3 | 5.4617±1 | 0.12601±1 |
| | | June '94 - Mult.[b] | 1.9256±7 | 5.4300±32 | 0.12607±8 |
| | acid dig. | June '94 - Far.[a,b] | 0.65677±12 | – | 0.12716±5 |
| | | June '94 - Mult.[a,b] | 0.65680±3 | – | 0.12673±5 |
| 92-LH3 | fusion | Mar '93 - split 1 | 1.8714±21 | 6.4995±40 | 0.12765±54 |
| | | July '93 - split 2 | 1.9002±11 | 6.3515±34 | † |
| | fusion | June '94 - Far.[b] | 1.5419±3 | 7.5135±26 | 0.12357±6 |
| | | June '94 - Mult.[b] | 1.54030±3 | 7.5273±3 | 0.12199±3 |
| | Carius tube | July '94 | 1.6025±4 | 3.8427±16 | 0.12281±11 |
| 92-LH14 | fusion | Mar '93 - split 1 | 1.6137±31 | 8.1358±6 | 0.13377±38 |
| | fusion | July '93 - split 2 | 1.6606±4 | 7.7612±2 | 0.12916±13 |
| | fusion | June '94 - Far.[b] | 1.3450±6 | 4.2788±36 | 0.13094±26 |
| | | June '94 - Mult.[b] | 1.3450±2 | 4.2774±13 | 0.12954±12 |
| 92-LH17 | fusion | Apr. '93 | 5.5102±26 | 6.3208±12 | 0.12741±66 |
| | acid dig. | June '94[a] | 0.6938±3 | – | 0.12815±16 |
| Bo73 | fusion | Apr. '93 - split 1 | 3.5772±16 | 2.9096±12 | 0.12698±86 |
| | fusion | July '93 - split 2 | 3.6149±36 | 2.8975±20 | † |
| | acid dig. | June '94 - split 1 | 0.8314±2 | 2.2271±24 | 0.12586±8 |
| | acid dig. | June '94 - split 2 | 0.8308±1 | 2.2339±36 | 0.12601±12 |
| Rp68 | fusion | Apr. '93 - split 1 | 2.7132±112 | 4.1711±86 | 0.12420±77 |
| | fusion | July '93 - split 2 | 2.7703±9 | 4.0499±8 | 0.12103±7 |
| | acid dig. | June '94 | 1.2644±7 | 0.7815±8 | 0.12205±16 |
| | acid dig. | July '94[a] | 0.6961±5 | – | 0.12418±34 |
| Ta7 | fusion | Apr. '93 - split 1 | 7.7388±12 | 0.9720±2 | 0.12478±13 |
| | fusion | July '93 - split 2 | 8.0089±52 | 0.9547±17 | † |
| | Carius tube | July '94 | 1.2638±7 | 0.7538±8 | 0.12480±90‡ |
| Ta19 | fusion | Apr. '93 - split 1 | 1.8174±13 | 5.5465±11 | 0.11932±9 |
| | fusion | July '94 - split 2 | 1.8142±8 | 5.5640±22 | 0.12052±26 |
| | acid dig. | June '94 - split 1 | 1.6022±11 | 0.3978±26 | † |
| | acid dig. | June '94 - split 2 | 1.5917±5 | 0.4023±3 | 0.11943±13 |
| WPR1 | fusion | June '94 | 0.8300±1 | 17.32±11 | 0.14479±6 |
| | fusion | June '94 | 0.77272±2 | 22.897±4 | 0.14475±3 |

**Table 3.10** $^{190}Os/^{192}Os$ ratios and blank corrected $^{187}Os/^{188}Os$ ratios and Os concentrations of replicate Os analyses by acid digestion, NiS fusion and Carius tube sample preparation methods. All data collected by dynamic analyses on the electron multiplier, unless stated otherwise. Errors on ratios and concentrations are based on $2\sigma_m$ of individual analyses.

† Considerable Re interference present on low intensity beams.

‡ Re corrected data.

[a] Volatile Os spike 'lost' during sample preparation.

[b] Data collected on the same filament in both static mode, using the Faraday cups (Far.) and dynamic mode using the electron multipliers (Mult.).

### *Repeatability of $^{190}Os/^{192}Os$ Ratios*

The $^{190}Os/^{192}Os$ ratios obtained using both the static and dynamic collection routines on the same split of the replicate samples differ by up to 1‰, consistent with the systematic bias of this ratio towards higher values during static analysis of the samples. For the degrees of spiking present in these analyses, the difference in the determined $^{190}Os/^{192}Os$ ratios, however, leads to relative differences in the calculated Os concentration of less than 5‰.

The separate splits of the replicates, analysed during different sessions but using the same collection routine, yielded $^{190}Os/^{192}Os$ ratios which differed by more than the analytical uncertainty of each ratio. The ratios determined in the later of the two analytical sessions are consistently higher than those determined earlier and lead to a difference of up to 5% in the Os concentrations calculated from each of the sessions. The difference between the determined ratios may reflect either higher loading or instrumental blanks or the presence of $PtO_3^-$ interference during the earlier analyses, when the sample loading techniques were still being developed and the metallised samples were often quite 'dirty'. The $^{190}Os/^{192}Os$ ratios determined for separate HBr splits of samples prepared for analysis during the last of the three sessions, however differ by only 1 - 7‰, leading to concentrations whose difference is less than 1%. These later values may reflect more accurately the repeatability of the analyses.

### *Reproducibility of Osmium Concentrations*

Table 3.10 shows that the differences between the Os concentrations determined for separate preparations of the same sample are significantly greater than either the analytical uncertainties (based on the errors on the individual determinations) or the instrumental repeatability. The variation may be separated into two types: the differences between concentrations determined on separate splits of the sample powders prepared by the NiS fusion technique, and the disparity of the concentrations of samples prepared by NiS with those of the same samples prepared by acid dissolution or aqua regia attack.

The potential causes of variation in the determined Os concentrations of samples were mentioned in Section 3.8 in relation to the NiS fusion technique. They include inhomogeneity of the sample powders, the incomplete recovery of Os present in refractory

phases and the loss of spike during the preparation process. Similar arguments may also apply to the determination of concentrations in samples prepared by acid dissolution or aqua regia attack, in which the acid may fail to dissolve insoluble accessory phases or some of the spike may be lost during the digestion process.

The concentrations of the two reference materials analysed by ICP-MS demonstrate that sample-spike equilibrium may be achieved successfully during the preparation of samples using the NiS fusion technique, producing reproducible and accurate concentrations. In view of these results, it is unlikely that the differences between the Os concentrations determined by N-TIMS reflect a failure of the sample to equilibrate with the spike during the fusion process. The relative differences between the concentrations determined by N-TIMS are similar to those found for the replicate analyses of the monitor sample by ICP-MS and may also reflect sample heterogeneity. However, it is notable that the duplicate preparations of the reference material WPR-1 (an altered peridotite of the Wellgreen deposit) yield significantly different concentrations, both of which are substantially higher than the provisional value of 13 ppb (CANMET Report in preparation). If the variation in the determined Os concentrations reflects sample heterogeneity then it appears that even the large masses of material used in preparation of samples by the NiS fusion technique may be insufficient to yield reproducible concentration determinations.

Three of the peridotite xenoliths were analysed following sample preparation by both NiS fusion and acid digestion techniques. Although the ~30% difference between the two concentrations determined for one of the samples (Bo73) is comparable to that between duplicate analyses of samples prepared by NiS, the Os concentrations determined in the aliquots of Rp68 and Ta19 prepared by acid digestion are a factor of 5 - 10 lower than those determined in the aliquots prepared by NiS fusion. This substantial difference may reflect a failure to dissolve resistant Os-bearing phases within the sample by acid digestion under reducing conditions. (The principal Os-bearing minerals (laurite, (Ru, Os, Ir)$S_2$; native Os metal; iridosmine alloys, Ir,Os) being insoluble in most mineral acids, including aqua regia (Gowing & Potts, 1991)). The occurrence of Os in discrete accessory phases may be consistent with the low sulphur contents of these two samples, suggesting that the Fe-Ni sulphide phases originally present in these rocks have been removed, either during transport

to the surface or due to alteration following the eruption of their host basalts.

In conclusion, the Os concentrations determined by N-TIMS analysis of samples demonstrate that, despite within-run precisions of better than 1‰ on the calculated Os concentrations, the reproducibility of the Os concentrations may be up to 1%, as shown by the variation of the determined $^{190}Os/^{192}Os$ ratio between splits of the same sample preparation. Analyses of samples prepared in duplicate using the NiS fusion technique differ by up to 25%. Given the agreement between the Os concentrations determined for the two reference materials by ICP-MS and their published values, however, these differences are interpreted as a reflection of heterogeneity in the duplicated samples rather than the failure of the $^{190}Os$ spike to equilibrate with the sample Os. As such they should not be taken as a measure of the reproducibility of the technique. The low Os concentrations determined for some of the replicates prepared by acid dissolution suggest that the Os may be present in acid resistant phases in some of the peridotite xenolith samples.

***Reproducibility of $^{187}Os/^{188}Os$ ratios***

The $^{187}Os/^{188}Os$ ratios of the replicates are also shown in Table 3.10. Although the ratios determined for each of the replicates show reasonable agreement, the variation is once more greater than the $2\sigma_m$ errors on the individual determinations. Because of the uncertainty surrounding the peak at mass 233, the majority of the data were not corrected for interference of $^{187}ReO_3^-$ on the $^{187}OsO_3^-$ signal. Consequently, much of the variation in the $^{187}Os/^{188}Os$ ratios may result from minor amounts of uncorrected Re interference, particularly in the earlier analyses. The lower ratios determined in the later analytical sessions are consistent with the greater efforts made to remove Re from the source of the mass spectrometer prior to analysis. If the earliest analyses are discarded, the $^{187}Os/^{188}Os$ ratios of the majority of the replicates appear to be reproducible within ~ 1%.

### 3.15.3 Re Samples

The reproducibility of the Re concentration determinations was assessed by the duplicate analysis of one of the Pyrenean peridotite samples (92-FT6), using two separate aliquots of the original sample powder. After correcting for the blank contribution to each analysis, the determined concentrations of the duplicate analyses were 353 ppt and 354 ppt. The excellent

agreement between the two concentrations determined for the sample indicates that the technique used for the Re analyses may be reasonably reproducible. However, further duplicate analyses would be required in order to test this reproducibility more fully.

Because no reference materials were available with sufficiently low, certified Re concentrations, the accuracy of the Re concentration determinations could not be tested. The similarity between range of determined Re concentrations and that found previously for mantle peridotites (Section 5.2.2), however, does show that the determined concentrations may be realistic.

## 3.16 Analysis of Other Pt-group Elements by N-TIMS

In addition to the investigation of the speciation of the Re and Os oxides produced during N-TIMS analysis, the negative ions produced by Ru, Ir and Pt were also investigated during this study, using solutions of Ru and Ir loaded onto Pt filaments, and coated with $Ba(NO_3)_2$ in a similar way to Re samples, and blank filaments coated with only $Ba(NO_3)_2$ (for the investigation of Pt).

Intense ion beams of Ru, Ir and Pt were observed at similar temperatures to those used for the analysis of Re and Os. The dominant oxide ions produced were $RuO_3^-$, $IrO_2^-$ and $PtO^-$, although minor quantities of other oxides were also observed, including $RuO_4^-$ (1.6‰ $RuO_3^-$), $RuO_2^-$ (0.7‰ $RuO_3^-$), $IrO_3^-$ (~1% $IrO_2^-$) and $PtO_2^-$. The negative oxide ion species formed by the noble metals appear to define a systematic trend in accordance with the electronic structure of the elements, with the number of oxygen atoms present in the ion decreasing from four in $^{185}ReO_4^-$ (Re: $[Xe]4f^{14}5d^56s^2$) to one in $PtO^-$ (Pt: $[Xe]4f^{14}5d^96s^1$).

The systematic variation of the oxide species has two important consequences. Firstly, it is possible to predict that not only should both Rh and Pd form negative ion oxide species, but that they will present predominantly as $RhO_2^-$ and $PdO^-$ ions. Secondly, the sixteen mass unit separation of the oxide ions formed by each of the elements within same period (i.e. (Tc), Ru, Rh and Pd or Re, Os, Ir and Pt) and the approximately ninety mass unit separation of the two periods should enable analysis of each element without isobaric interference from it neighbours (a feature critical to the determination of accurate $^{187}Os/^{188}Os$ ratios by the technique). These observations led Creaser *et al.* (1991) to suggest that the concentrations of

all the Pt-group elements may be determined by N-TIMS, using isotope dilution and a single sample preparation. Although this may require a combination of filament materials (e.g. Ta or Re for the analysis of Pt) and the use of an isotopic spike composed of a long-lived radionuclide to analyse monoisotopic Rh, the high sensitivity of the N-TIMS technique has the potential to investigate the behaviour of the Pt-group elements in basaltic rocks, where their low abundances have hitherto hampered progress (Jackson *et al.*, 1990).

Preliminary work at the Open University showed that, although $PtO_2^-$ ions (in particular $^{190}Pt^{16}O^{17}O^-$ and $^{192}Pt^{16}O^{17}O^-$) do not interfere with the the measurement of $IrO_2^-$ ion intensities, the Pt filament material (Cross) contained appreciable quantities of Ir. Determination of ultra-trace concentrations of the Pt-group elements in rock samples by N-TIMS analysis, therefore, may require either higher purity Pt metal for the filaments, or the use of an alternative filament material. The low Ir contents determined in filaments made from a batch of high purity Ni (Goodfellows, 99.999%) suggested that this may represent a suitable material for future work in this field, either untreated or coated with a layer of $V_2O_5$, following the procedure of Walczyk *et al.* (1994)).

## 3.17 Comparison of ICP-MS and N-TIMS Analysis

The analysis of Os by ICP-MS and N-TIMS may be compared on a number of criteria such as the precision of individual isotope ratio determinations and their reproducibility, the time required to prepare and analyse samples and the ease with which the analyses may be carried out.

### 3.17.1 Precision and Instrumental Noise in ICP-MS Analyses

Direct comparison of the precision of individual analyses and the reproducibility of isotope ratio determinations by the N-TIMS technique show that they are more than an order of magnitude better than those determined by ICP-MS, as demonstrated by the results obtained for the J-M standard (Table 3.4). The poorer precision of isotope ratio determinations by ICP-MS may be attributed to the combination of a scanning quadrupole mass analyser with an unstable plasma ion source, or noise from the sample introduction system or ion extraction processes. A number of studies have been carried out into the

sources of noise during ICP-MS analysis (Houk & Thompson, 1988; Crain *et al.*, 1989; Furata *et al.*, 1989). These suggested that the noise may be of two main types: white noise associated with the discrete nature of the sample aerosol and noise at particular frequencies arising from sources such as pulsation of the peristaltic pump, residual ripple of the power supply to the work coils and acoustic noise resulting from turbulence of air entrained close to the torch mouth.

By using a 'bonnet' over the torch (extending its outer wall to beyond the aperture of the sampling cone and shielding the plasma from the surrounding atmosphere), Ince *et al.* (1993) showed that the acoustic noise from the plasma may be eliminated and the white noise and noise from the peristaltic pump may be reduced to extremely low levels. Despite these improvements, however, the determined ratios did not approach the levels expected from counting statistics, possibly on account of poor ion distribution in the plasma (Gray *et al.*, 1994). Although methods of improving the distribution of ions within the plasma and sampling interface are an area of active research (Gray *et al.*, 1994), it is unlikely that the precision of isotope ratio determinations by ICP-MS using a scanning mass analyser will ever approach the level currently obtainable by TIMS.

An alternative approach to the limitation of signal noise on the analytical precision of isotopic ratio determinations by ICP-MS is to replace the quadrupole with a magnetic sector mass analyser and to measure simultaneously the intensities of all the ion beams of interest (Walder & Freedman, 1992; Walder *et al.*, 1993). The merging of a plasma source with a magnetic sector mass analyser combines the precision of TIMS measurements with the ionising capabilities of ICP-MS, enabling precise isotope ratio determinations to be performed on elements with high work functions (e.g. Re, Os and Hf). Analyses of a Hf standard have demonstrated that, with internal correction for mass fractionation, the $^{176}Hf/^{177}Hf$ ratio may be determined both accurately and precisely, with within-run precisions of better than 0.08 ‰ ($\pm 2\sigma_m$). (Walder *et al.*, 1993). Unpublished data by the same group suggests that similar precision may be obtainable for Os isotope ratios, with relative errors on the $^{189}Os/^{188}Os$ ratio of ~ 0.1‰ (A. J. Walder, pers. comm.).

Despite the significantly better instrumental reproducibility of the Os isotope ratios determined by N-TIMS relative to those obtained using an unmodified ICP-MS instrument,

the overall precision of the sample $^{187}Os/^{188}Os$ ratios determined by the two techniques during this study appears to similar (~1%). The uncharacteristically poor precision of the N-TIMS analyses is primarily on account of the inability to correct for minor Re interference which may have been present in the spectra. The potential precision of the N-TIMS technique, therefore, has yet to be realised at the Open University, and requires that the interference at mass 233 is eliminated so that $^{185}ReO_3^-$ may be monitored more accurately.

### 3.17.2 Preparation Time and Ease of Analysis

The time required to prepare the samples for analysis by the two techniques is reasonably similar. For sample preparation by NiS, both techniques require a similar time for sample decomposition and distillation, however the redistillation of samples for analysis by ICP-MS and the time required for the cleaning of the distillation apparatus between samples considerably lengthened the preparation time. Although acid digestion of the sample powders, with its repeated evaporation and dissolution stages, required considerably longer than either the NiS fusion technique or the single digestion in the Carius tube, the ability to process several samples simultaneously resulted in the efficient use of time and an equivalent rate of sample throughput.

Once the samples were loaded onto filaments ready for analysis by N-TIMS, they could be stored easily for a considerable time prior to analysis: several samples produced excellent ion beams despite preparation more than six months prior to final analysis. Thus, a large number of samples could be prepared before each session of N-TIMS analyses. Although such experiments were not performed for the long-term stability of Os in the thiourea/tin solutions, the requirement that the second distillation was performed within a few days of final analysis restricted the number of samples which could be prepared for each ICP-MS session.

Analysis of individual samples by ICP-MS lasted approximately an hour, including cleaning of the sample introduction system between analyses. The time require for analysis by N-TIMS varied according to the collection mode: using static data collection, analyses were completed within approximately two to three hours; however, dynamic runs required up to five hours. Because the N-TIMS analyses were carried out 'in house' at the Open

University the negotiation of machine time was relatively easy and, once the mass spectrometer had been converted to the analysis of negative ions, they could be performed continuously. In contrast, pressure from a large number of users for time at the NERC ICP-MS facility meant that only limited machine time was available for analyses by this technique and, as a visitor, analyses were restricted to normal working hours. Thus, despite the longer periods required for each analysis by N-TIMS, the number of samples which could be analysed within each day was considerably greater than was possible by ICP-MS. Additionally, the greater quantity of machine time available for N-TIMS work enabled the technique to be investigated more thoroughly, prior to the analysis of geologically significant samples

### 3.17.3 Choice of Technique

For the interpretation of Os isotope data on geological samples the precision of the determined isotope ratios dominates in the choice of technique used for sample analysis. Whilst the data presented in this chapter have been concerned primarily with the results obtained using two particular instruments, and as such may not reflect the optimum capabilities of either of the techniques, the considerably better precision of N-TIMS analyses meant that it was chosen for the subsequent study of the Re-Os isotope systematics of mantle material. In addition to the better precision possible by the technique, N-TIMS analysis was also favoured for this study on account of the greater amount of analytical time available and the greater ease of analysis arising from both instrumental software tailored to the determination of Re and Os isotope ratios and the greater number of samples which could be prepared prior to each analytical session.

Whilst N-TIMS appears to be the better technique for the precise analysis of un-mineralised geological samples, the increasing availability of ICP-MS instruments and the successful studies of Dickin *et al.* (1992) and Hulbert & Grégoire (1993) suggest that ICP-MS may represent a more practical and convenient method of investigating the Re-Os isotopic system in a variety of mineralised geological environments, in which a wide range of both Re/Os and $^{187}Os/^{188}Os$ ratios may be expected and less precise data may be acceptable.

# Chapter 4

# Geochemical Systematics of the Eastern Pyrenean Peridotite Massifs and Massif Central Ultramafic Xenoliths

## 4.1 Introduction

Studies of the major element abundances in peridotites from both orogenic massifs and basalt-borne ultramafic xenoliths demonstrate that the continental mantle lithosphere (CML) displays considerable heterogeneity on both local and regional scales. From the range of peridotite compositions found in orogenic massifs and xenolith suites (extending from refractory harzburgites and clinopyroxene-poor lherzolites to fertile lherzolites) and density considerations (e.g. Jordan, 1988), the CML has been interpreted as buoyant refractory peridotite, produced by the extraction of melt from the underlying mantle (e.g. Dickey, 1970; Ringwood, 1975). Following its stabilisation, interaction of the depleted mantle lithosphere with mantle-derived melts may alter the composition of the CML, producing both mineralogical and isotopic variations (Lloyd & Bailey, 1975; Menzies & Hawkesworth, 1987). Consequently, the heterogeneity of the CML may reflect the influence of three independent processes: heterogeneity of the mantle protolith prior to melt extraction, the processes of melt extraction and modification of the CML since its separation from the convecting mantle.

Before discussing the Re-Os isotope systematics of the continental mantle lithosphere underlying central and south-western France, it is necessary to assess the role that each of these processes may have played in the formation of the CML in the two regions. This chapter discusses the chemical composition of the peridotites, utilising elemental data for both whole-rocks and mineral separates. Using data for the Pyrenean ultramafic massifs, two possible models are proposed for the range of peridotite compositions: depletion of a fertile mantle source by the extraction of partial melts and refertilisation of refractory mantle

by the incorporation of basaltic melts. In view of the frequent serpentinisation of orogenic peridotite massifs, the effects of low temperature alteration processes on the whole-rock major and trace element compositions of the Eastern Pyrenean massifs are also included in the discussion.

Although it is not possible to discuss in detail the composition of the mantle protolith or the processes which may have been responsible for the range of major element compositions observed in the Massif Central xenolith (owing to the low number of samples for which comprehensive elemental data are available), using the available elemental and isotopic data it is possible to constrain some of the lithospheric processes which have affected the xenolith source regions, prior to the application of the Re-Os isotope system.

To facilitate direct comparison of the Os isotope systematics of the peridotites and their elemental compositions in Chapter 5, the discussion focuses on the compositions of the samples used in the isotopic study. The arguments, however, are also supported by reference data from previous studies of the mantle in the two regions.

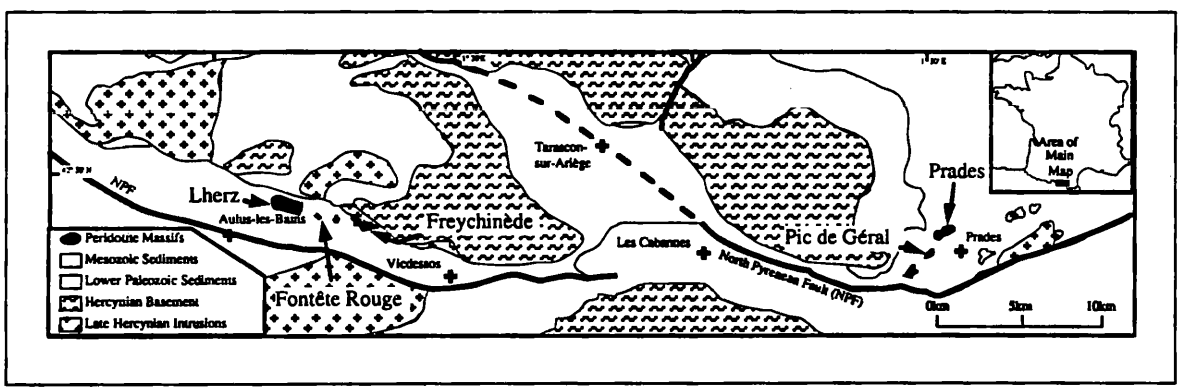


**Figure 4.1** Geological sketch map of the N.E. Pyrénées, illustrating the location of the peridotite massifs, the exposed Hercynian basement (granulites and amphibolites) and Paleozoic sediments (graphite schists and metacarbonates) and metamorphosed Mesozoic sediments (limestones and clays) situated along the North Pyrenean Fault Zone.

## 4.2 Eastern Pyrenean Massifs

### 4.2.1 Geological Setting

The Pyrenean orogenic ultramafic massifs comprise over 40 peridotite bodies which crop out along the narrow North Pyrenean Metamorphic Zone (NPMZ) on the Franco-Spanish Border (Figure 4.1) and range in size from a few metres to over a kilometre. The NPMZ is

characterised by high T, low P metacarbonates of Jurassic to Early Cretaceous age, metamorphosed during the Late Cretaceous to Miocene transcurrent movements of Iberia relative to Europe. Although the peridotite bodies occur in groups along over 350 km of the NPF, more than half are located within the Ariège Department in the Eastern Pyrénées. Over the last decade these massifs have been the subject of a number of intensive studies, producing detailed accounts of their field relations, petrology, geochemistry and geochronology (Conquéré 1971, 1977, 1978; Loubet & Allègre, 1982; Conquéré & Fabriès, 1984; Bodinier *et al.*, 1987a, 1987b, 1988, 1990; Fabriès *et al.*, 1989, 1991; Mukasa *et al.*, 1991; Downes *et al.*, 1991; Choukroune, 1992). These accounts suggest that the peridotite massifs have undergone a complex pre-emplacement history involving partial melting, magma transport, lithospheric contamination and plastic deformation below thinned continental crust.

The contacts between the ultramafic bodies and the surrounding carbonates are characterised by highly brecciated zones, composed of carbonate and peridotite fragments ranging in size from a few millimetres to several decimetres. Although this brecciation is most pronounced in the metacarbonates, it may extend several tens of meters into the ultramafic bodies (e.g. Lherz, Figure 4.2). The disruption of the layering, however, decreases away from the margins, leaving the cores of the massifs unaffected. Some of the carbonate fragments appear to have been affected by the first phase of Alpine deformation (Minnigh *et al.*, 1980). Although sedimentary (Lacroix, 1894; Choukroune, 1973) and tectonic (Lacroix, 1901) processes have been suggested to account for the zones of brecciation surrounding the massifs, an origin by explosive decomposition of the metacarbonates (Ravier, 1959; Avé Lallemant, 1967; Minnigh *et al.*, 1980) may best account for the observed features of the breccia. Such an origin implies that the peridotites were still hot when emplaced into the crust. Hot emplacement is supported by the occurrence of sapphirine and kornerupine-bearing rocks around the margins of the ultramafic bodies, from which Monchoux (1970) determined that the peridotites were emplaced at 800 to 900 °C and 6 to 9 kbar pressure. No other evidence for a regional pressure in excess of 1 kbar exists in the surrounding rocks, however, suggesting that Monchoux may have over-estimated the depth of emplacement. In the silica-deficient, Mg-metasomatic environment which was

present adjacent to the lherzolites at the time of emplacement, these minerals may have formed at considerably lower pressures (Vielzeuf & Kornprobst, 1984).

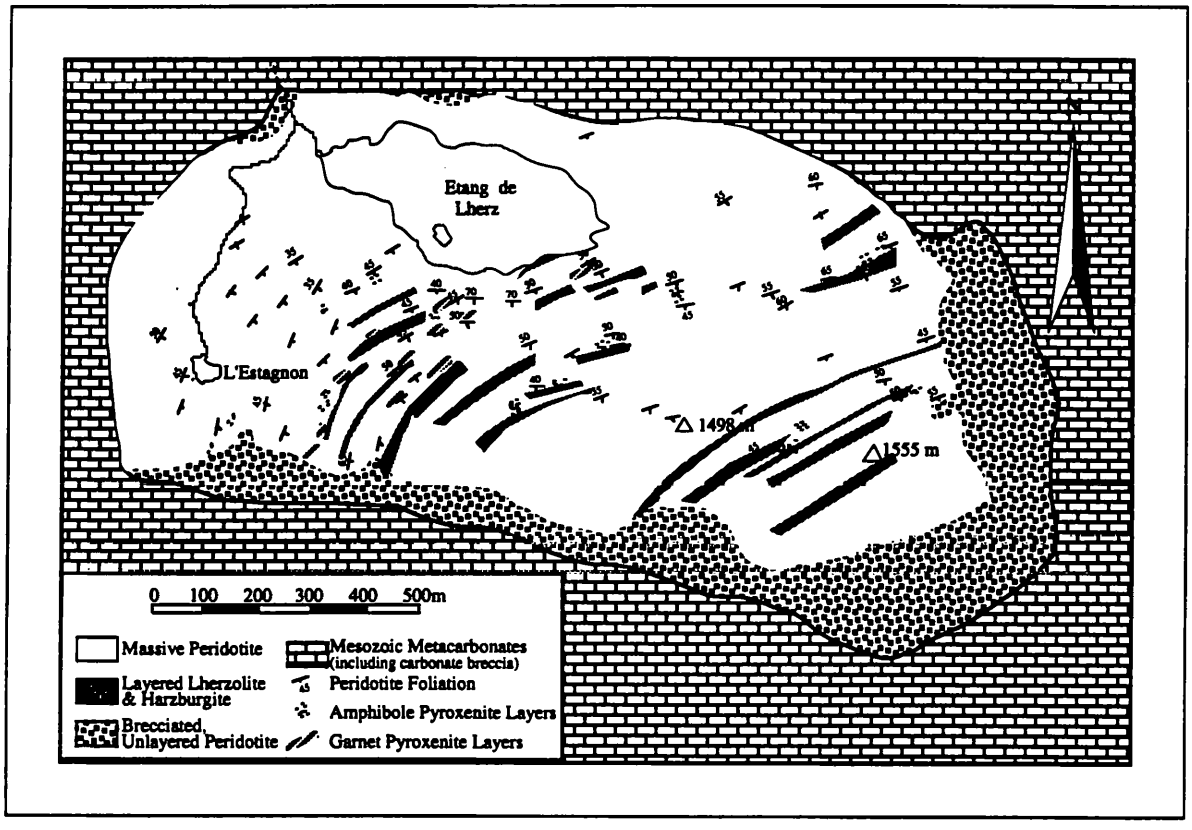


**Figure 4.2** Lithological sketch map of the Lherz area, illustrating the brecciation along the contacts of the massif with the metacarbonate country rocks and the foliation of the peridotites within the massif (after Conquéré, 1977).

From field evidence alone it is impossible to estimate the vertical extent of the majority of the massifs. The rare cliff exposures, however, suggest that the smaller bodies probably thin with depth, forming tectonic slices within the metacarbonates of the fault-zone.

Several authors have tried to account for the emplacement of the lherzolite massifs (in addition to lenses of granulite facies lower crustal rocks) into the Cretaceous carbonates of the NPMZ (Vielzeuf & Kornprobst, 1984; Kornprobst & Vielzeuf, 1984; Nicolas, 1985; Fortané *et al.*, 1986). Because they were concerned with massifs located in widely separated parts of the metamorphic zone, however, the conclusions of these studies are often contradictory in their proposed timing and mechanisms. The preferred model is that proposed by Kornprobst & Vielzeuf (1984), which, although it is based on data from the better exposed massifs of the Ariège district, is sufficiently general that it can be adapted

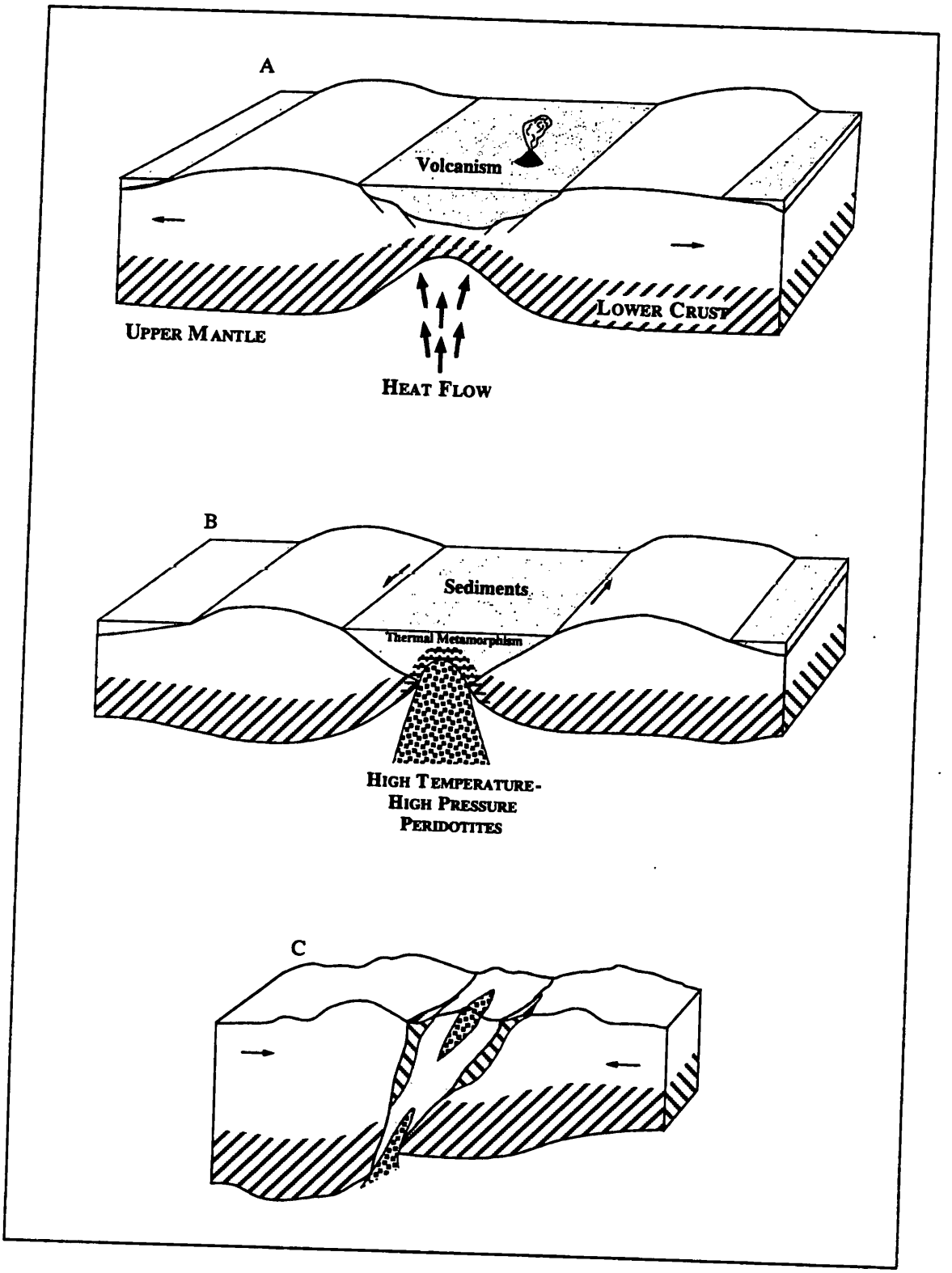


**Figure 4.3** Schematic model for the emplacement of the lherzolites and granulites in the North Pyrenean Metamorphic Zone in the Eastern Pyrénées. A) lower Cretaceous; B) Albian; C) upper Cretaceous, upper Eocene. (After Vielzeuf & Kornprobst, 1984)

to explain the occurrence of lherzolite bodies along the whole of the NPF. This model suggests that tectonic slices of ultramafic and granulite-facies rocks were emplaced into the upper crust during alternating periods of extension and compression along the transform zone separating Iberia from Europe. Early ascent of the lherzolites into the deepest parts of

the crust may have been associated with thermal upwelling during initial rifting (Figure 4.3a). Continued rifting, which may have split the continental crust, enabled the mantle to ascend to relatively shallow depths, leading to contact metamorphism of the carbonate sediments (Figure 4.3b). Finally, the lherzolites, wedged in the sediments, were squeezed up towards the surface during an episode of compression in the transform zone (Figure 4.3c). This episode of compression was also responsible for the elevation of lower crustal rocks to the surface within the NPMZ. Significant crustal thinning is consistent with the rapid deposition of 3000 m of turbidites during the Upper Albian and the presence of alkaline magmatism in the region, dated at 100-90 Ma (Montigny *et al.*, 1982, 1986). Subsequent compression of the fault zone elevated the lower crustal and mantle rocks to the surface as tectonic slices in fault bounded blocks of the carbonate sediments.

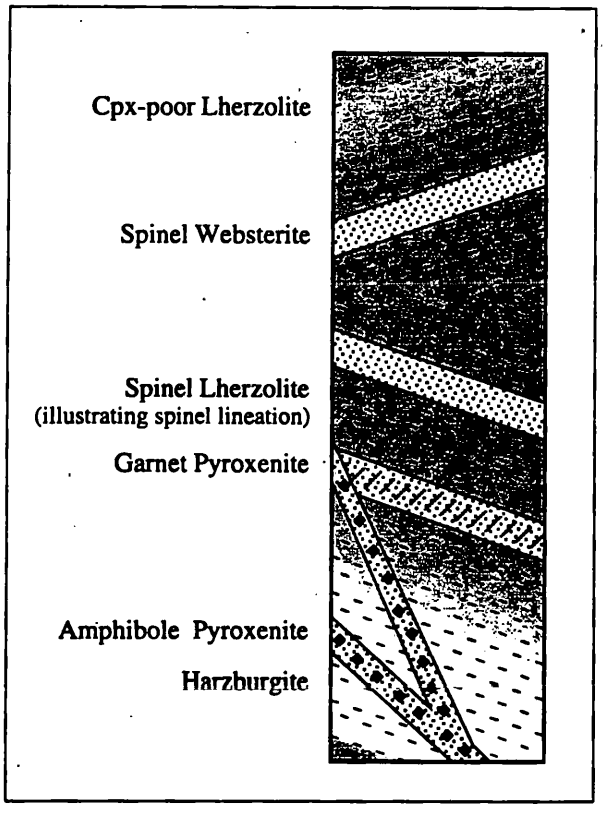


**Figure 4.4** Schematic section illustrating the compositional banding and mafic layers within the N. E. Pyrenean peridotites. The anhydrous pyroxenite layers lie parallel to the compositional banding and the lineation of the spinel grains within the peridotites and define tight to isoclinal folds. The amphibole-bearing pyroxenites, however cross the layering at relatively high angles. Symmetrically zoned garnet pyroxenite layers are found in only the Lherz and Freychinède massifs and are characterised by websterite margins grading into garnet clinopyroxenite or garnet websterite in the core.

### 4.2.2 Petrology

The peridotites of the massifs are composed predominantly of spinel lherzolites, in which a layering is defined by the intercalation of bands of harzburgite, clinopyroxene-poor lherzolite (up to several meters thick) and veins of spinel websterite (3-20 cm). The isoclinal folding observed in the anhydrous pyroxenites, with axial planes parallel to the peridotite

spinel lineations, may imply that these veins were introduced into a hot, plastically deforming mantle diapir, prior to its accretion onto the base of the lithosphere (Fabriès *et al.*, 1991). Rare garnet pyroxenite layers (0.3-1 m thick) are also present in some of the bodies (e.g. Lherz and Freychinède), commonly parallel to the layering, but also cross-cutting it at high angles (Conquéré, 1978; Bodinier *et al.*, 1987b). In addition to these anhydrous pyroxenites, the peridotites of Lherz and Freychinède are cross-cut by a later generation of amphibole-bearing pyroxenite dykes up to 30 cm thick and thin phlogopite-bearing hornblendite veins (Lacroix, 1917; Conquéré, 1971; Bodinier *et al.*, 1987a). The amphiboles present in the hydrous veins are Ti-rich, with compositions ranging from Ti-pargasite to kaersutite, depending on the Ti content. Figure 4.4 shows a schematic section of the various lithologies, illustrating the cross-cutting relationships.

Unlike the much larger Ronda ultramafic massif, no metamorphic zonation is observed in the peridotites of the Eastern Pyrénées and spinel is the only aluminous phase present, placing them in the spinel lherzolite facies. The presence of Mg-rich garnet in the anhydrous pyroxenite layers of Lherz and Freychinède places these massifs in the ariegite sub-facies defined by Obata (1980). Evidence for the presence of garnet in the mantle source of the Pyrenean lherzolites may be preserved in the form of coarse-grained protogranular textures with clusters of orthopyroxene, clinopyroxene and spinel (Plate 4.1). These clusters are interpreted to have been derived from garnet, either by the reaction of the mineral in the solid state (Smith, 1977) or by crystallisation from melt pockets produced on the sites of garnets (Nicolas *et al.*, 1987). The opx-cpx-sp clusters may record an evolution towards lower pressures for the Eastern Pyrenean peridotites.

Away from the brecciation present on the margins of the bodies and along internal faults, the peridotite massifs are moderately fresh, with large internal areas free from alteration. The textures of the peridotites record at least two stages of deformation and recrystallisation (Conquéré & Fabriès, 1984). The first major episode of deformation ($D_1$) was followed by recrystallisation ($R_1$), producing the coarse-grained protogranular texture still observable in some of the peridotites (Plate 4.2). Temperature and pressure estimates for the $D_1$-$R_1$ event range from 900 - 950 °C and 12 - 16 kbar (Sautter & Fabriès; 1990).

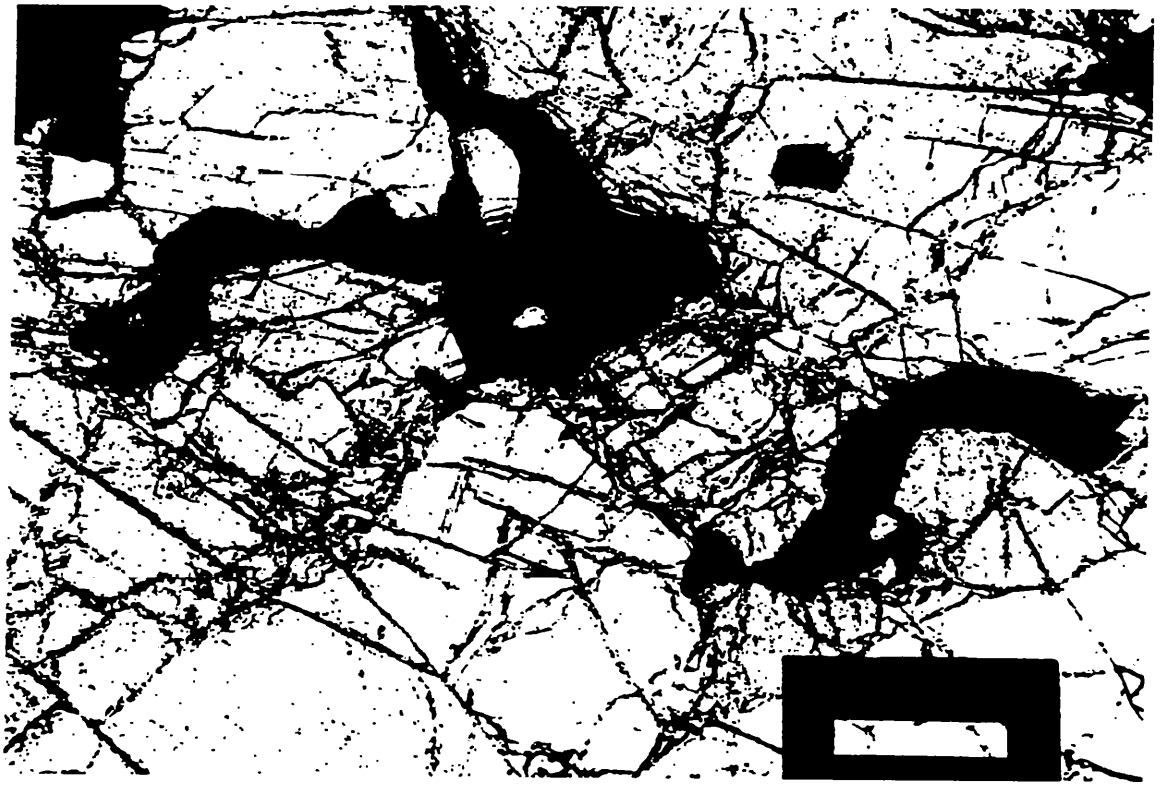

**Plate 4.1** Photomicrographs illustrating coarse-grained orthopyroxene-clinopyroxene-spinel cluster in a protogranular spinel lherzolite from Fontête Rouge. Above, photograph under plane polarised light: below, the same cluster under cross-polars. Scale bar represents 0.5 mm.

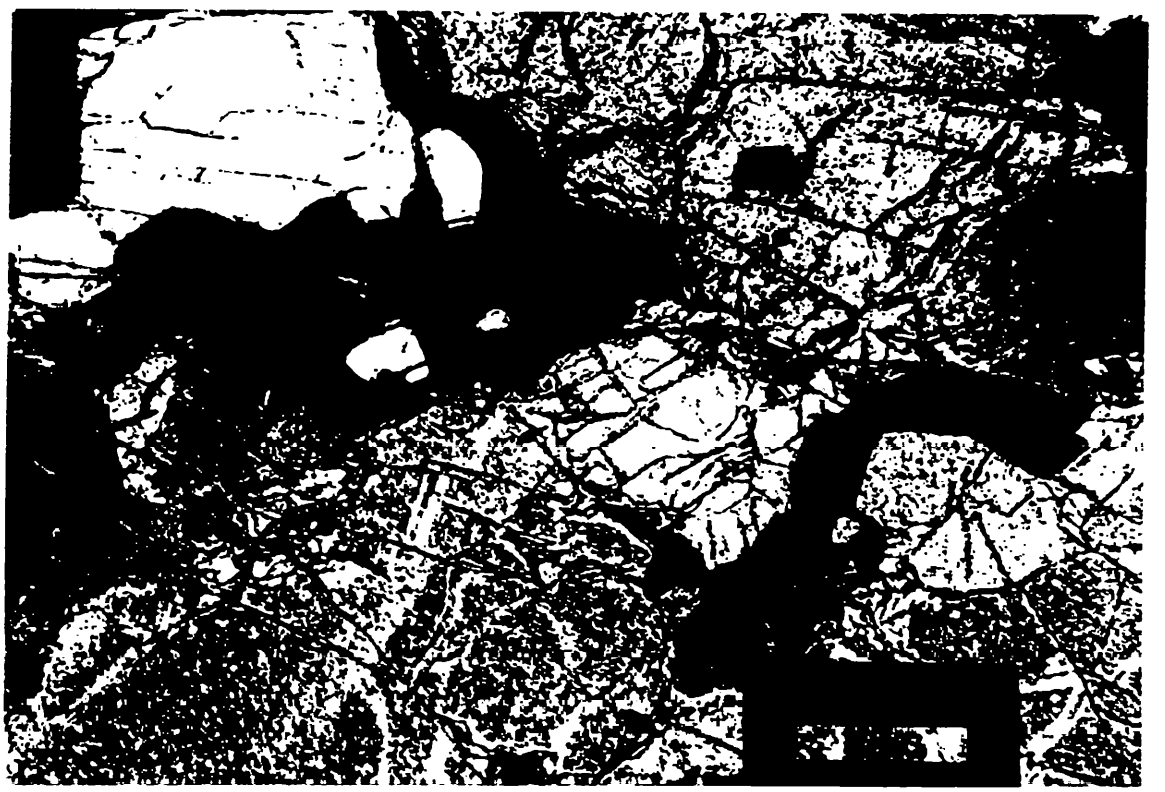

Studies of the anhydrous pyroxenites suggest that the $D_1$-$R_1$ episode was only the last stage of a long history of subsolidus recrystallisations. From the compositions of garnet and orthopyroxene inclusions in a sub-calcic clinopyroxenite of the Freychinède massif, Herzberg (1978a) calculated that the vein may have formed at 1400 - 1500 °C and 30 - 40 kbar. These pressures and temperatures were based on the use of his two-pyroxene thermometer and pyroxene-garnet barometer (Herzberg,1978b) to estimate the conditions at which the inclusions would have totally dissolved, yielding a single-phase clinopyroxenite. Conquéré (1979), however, proposed that the reconstructed compositions of the primary phases in the clinopyroxenite vein used by Herzberg (1978a) did not represent those of stable solidus phases, but were those of crystals segregated in equilibrium with basaltic liquids. He therefore suggested that, although the garnet clinopyroxenite may have initially formed at high temperatures (1400 - 1500 °C), the pressure range was closer to 15 - 20 kbar, as previously suggested (Conquéré, 1977).

The isobaric cooling to 900 - 950 °C following deformation is recorded by both the peridotites of the N.E. Pyrenean massifs and the anhydrous pyroxenite veins contained within them. Such cooling is commonly attributed to the thermal relaxation of asthenospheric diapirs during their accretion into the conductive lithosphere (Nicholas *et al.*, 1987; Witt & Seck, 1987), with the end of cooling corresponding to the attainment of thermal equilibrium with the local lithospheric geotherm. As yet, it has not been possible to date this cooling event accurately, owing to the effects of later metasomatism on the incompatible element isotope compositions of the peridotites.

Whereas the peridotites of several of the massifs may preserve the coarse-grained protogranular texture produced at the end of this episode, the majority of the peridotites collected from the Lherz massif exhibit porphyroclastic textures (Plate 4.3) owing to a second, significantly later episode of deformation and partial recrystallisation ($D_2$-$R_2$). This episode probably occurred at lower temperatures and pressures than the $D_1$-$R_1$ event and was contemporaneous with the introduction of the amphibole-pyroxenites. By applying the olivine-spinel geothermometer of Fabriès (1979) to the fine-grained interstitial spinel formed during the second episode of recrystallisation, Conquéré & Fabriès (1984) estimated that it occurred at 700 - 750 °C. The growth of plagioclase at the expense of garnet in the garnet

**Plate 4.2** Photomicrograph illustrating the protogranular texture of a spinel lherzolite from the N.E. Pyrenean massifs (Fontête Rouge). The grains are commonly large (1 - 2 mm), exhibit virtually no strain and possess curvilinear boundaries. Photograph taken under cross polarised light. Scale bar, 0.5 mm.

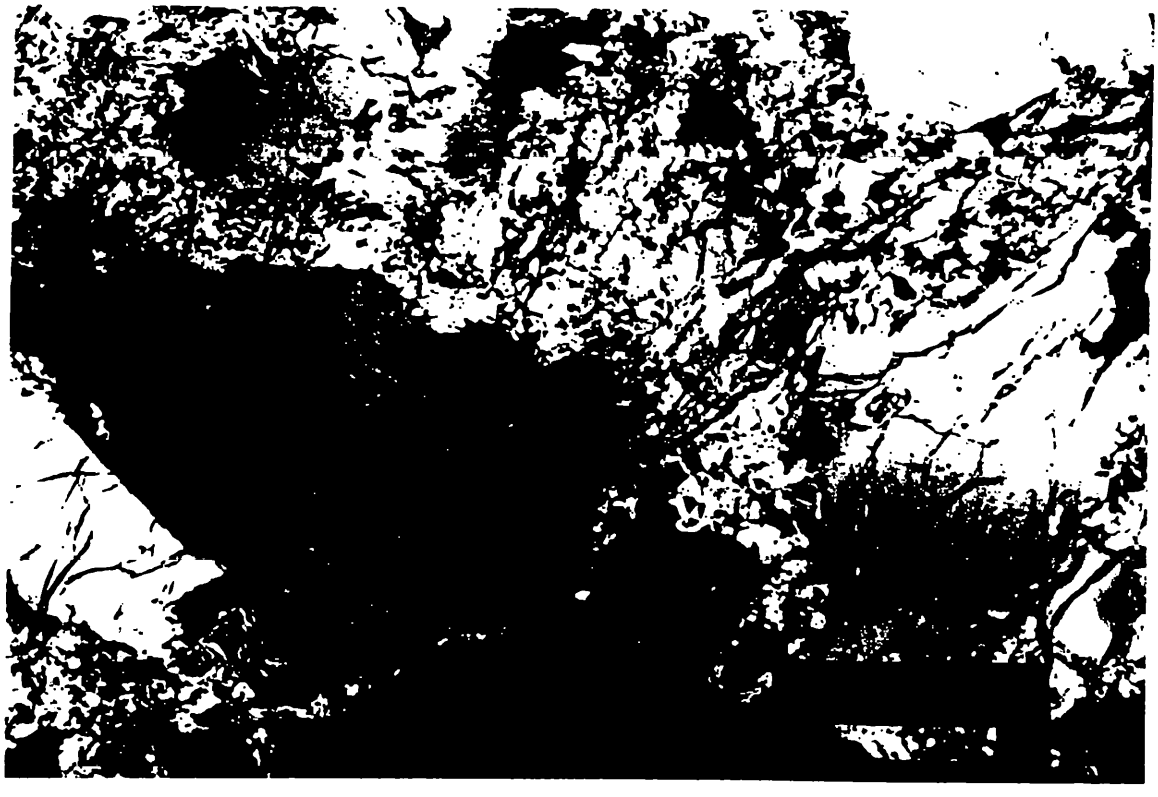

**Plate 4.3** Photomicrograph illustrating the porphyroclastic texture of spinel lherzolite collected from the Lherz massif in the N.E. Pyrénées. The mineral grains possess a range of sizes from ~2 mm to less than 0.1 mm and exhibit variable degrees of strain and ragged boundaries. Photograph taken under cross polarised light. Scale bar, 0.5 mm.

pyroxenites suggests that recrystallisation may have occurred at less than 8 kbar (Conquéré, 1977). The $D_2$-$R_2$ event may have been associated with shearing in the upper mantle, prior to the emplacement of the peridotite body into the base of the crust. Both radiometric ages and geochemical data indicate that the amphibole rich veins represent high pressure crystal segregates of the Cretaceous alkali basalts associated with crustal thinning and extension (Montigny *et al.*, 1986; Bodinier *et al.*, 1987a).

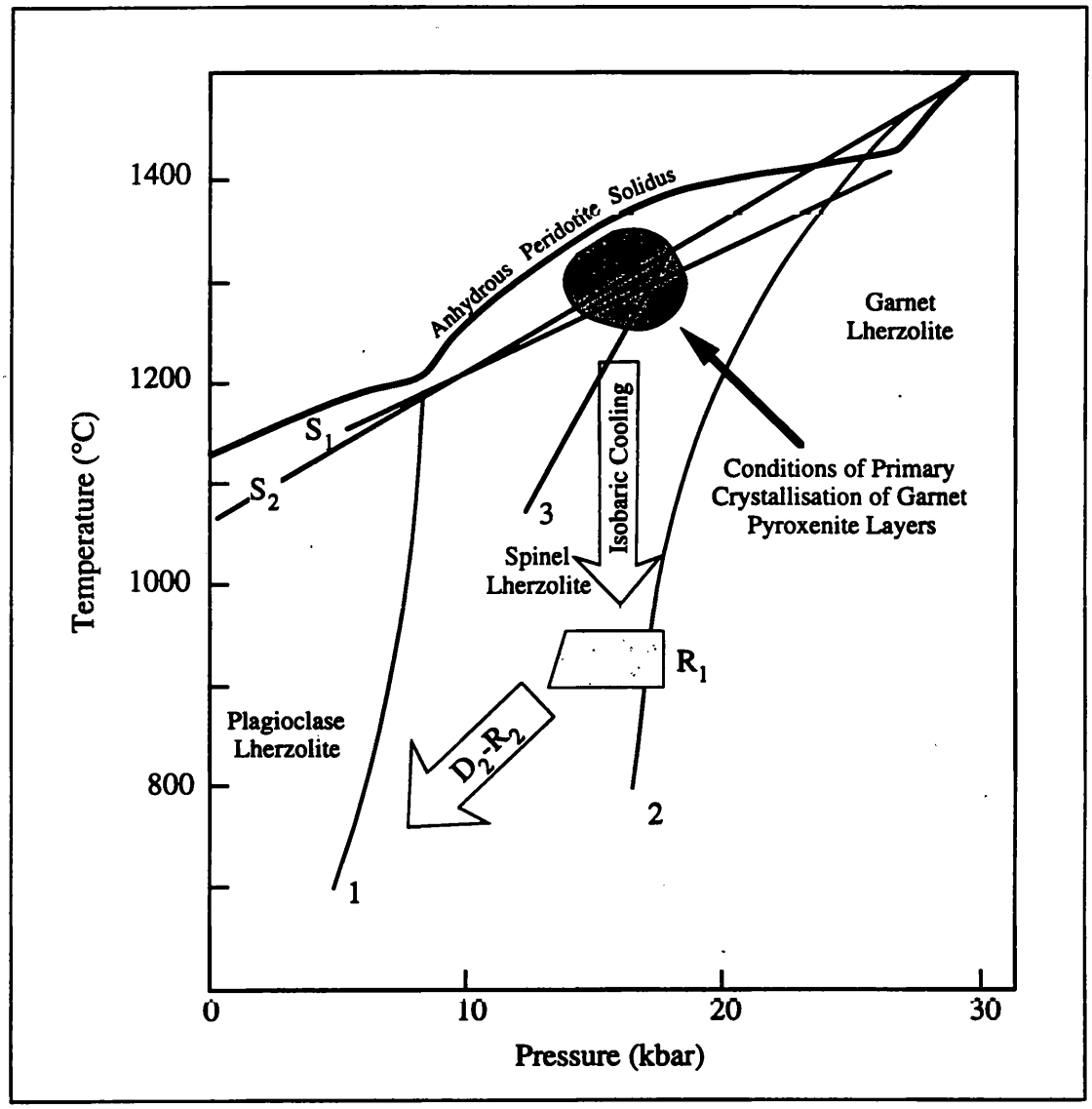


**Figure 4.5** Cooling and recrystallisation path of anhydrous layered pyroxenites using the reconstructed compositions of primary megacrysts from pyroxenites of the Lherz and Freychinède massifs (Sautter & Fabriès, 1990; Fabriès *et al.*, 1991). Shaded quadrilateral $R_1$ = equilibrium conditions of the anhydrous pyroxenites following the earliest recorded recrystallistion event. Thick line = Solidus of fertile anhydrous peridotite (Takahashi, 1986). $S_1$ = solidus for olivine tholeiite composition (Green & Ringwood, 1967); $S_2$ = solidus for B3P1 composition (Ito & Kennedy, 1968); 1 = plagioclase lherzolite-spinel lherzolite transition (Herzberg, 1978); 2 = spinel lherzolite-garnet lherzolite transition (O'Hara *et al.*, 1971); 3 = Opx+Cpx+Sp=Cpx+Gt reaction in olivine tholeiite composition (Green & Ringwood, 1967)

Throughout this sequence of deformation and recrystallisation, the Eastern Pyrenean peridotites appear to have remained at temperatures below the dry peridotite solidus (Figure 4.5). If a partial melting event were responsible for the differentiation of the peridotite bodies, then it must have predated the $R_1$-$D_1$ event and was unrelated to their emplacement either into shallower levels of the continental mantle lithosphere or into the lower crust.

In light of the complex sub-solidus equilibration which has occurred in the Pyrenean peridotite massifs, it is unlikely that textural evidence for melting will be preserved. Detailed discussion of the geochemistry of the peridotites is therefore required in order to constrain the processes involved in the differentiation of the mantle lithosphere below the N.E. Pyrénées.

### 4.2.3 Results of Previous Whole-Rock Geochemical Studies

The whole-rock elemental compositions of the peridotites of the N.E. Pyrenean ultramafic massifs were thoroughly discussed by Bodinier *et al.* (1988). Although they determined the concentrations of a large number of elements in samples originating from most of the massifs in the region, rare-earth element (REE) and selected trace-element data for peridotites from Fontête Rouge were significantly under-represented in their discussions. These peridotites have distinctive protogranular textures and exhibit little evidence of the deformation and metasomatism which affected many of the other massifs. Consequently, their whole-rock elemental compositions may maintain the clearest record of the earliest events in evolution of the massifs.

The principal conclusions of Bodinier *et al.* (1988) were that the peridotites represent residues formed by the extraction of a range of melt fractions from a fertile peridotite source, which have subsequently been affected by variable degrees of both cryptic and modal metasomatism, particularly where the peridotite is adjacent to pyroxenite veins. From the low Tb/Yb ratios and the variation of this ratio with Yb abundances, they showed that garnet was a residual phase during melting in several of the massifs and calculated that the range of peridotite compositions was created by 5 - 10% and 15 - 25% melt extraction, producing the massive lherzolites and clinopyroxene poor lherzolites / harzburgites, respectively.

Bodinier *et al.* also calculated that the melts in equilibrium with the residual peridotites of the Eastern Pyrénées were enriched in LREE and bore strong geochemical similarities to

continental tholeiites erupted in the Pyrénées during the Mesozoic and associated with the opening of the Atlantic (Alibert, 1985). Although isotope data (Alibert, 1985; Hamelin & Allègre, 1988) and the relative timing of partial melting *versus* emplacement of the peridotites in the mantle lithosphere indicate that the peridotites cannot be residues after this magmatic event, they do not preclude the depletion of the peridotites by an earlier phase of tholeiitic magmatism, the surface expression of which has since been removed by erosion.

### 4.2.4 Sample Selection and Analysis

#### *Sample Collection*

In total, sixteen samples were collected from five of the larger peridotite bodies of the Eastern Pyrénées (Lherz, Fontête Rouge, Freychinède, Pic de Géral and Prades; Figure 4.1). To minimise the effects of metasomatism, the massive peridotites were collected at distances greater than 2 m from the nearest visible pyroxenite layers and, where possible, by selecting the most homogeneous specimens. Samples were chosen to exhibit a wide range of depletion, estimated in the field from the modal abundance of clinopyroxene. Although efforts were also made to collect samples showing a minimum of serpentinisation, where the exposure was limited less choice was available and samples exhibiting greater degrees of alteration were also collected (e.g. at Freychinède and Pic de Géral).

#### *Sample Preparation and Whole-rock Analysis*

The methods of sample preparation and whole-rock analysis are described in detail in Appendix A. All powders of the massive peridotites were prepared from at least 2 kg of the material collected in the field. Such sample sizes were believed to be sufficient to obtain representative analyses of both major and trace elements, despite the coarse grain size of the rocks (Potts, 1987). Major and trace elements were analysed by wavelength-dispersive X-ray fluorescence, the precision and accuracy of which were estimated from replicate analyses of internal standards and reference materials with whole-rock elemental compositions which covered the range exhibited by the samples. The rare-earth elements (REE) were determined by isotope-dilution mass-spectrometry, following an adaptation of the method described by Thirlwall (1982). No significant difference was found between the REE profiles measured for leached and unleached whole-rock sample powders. Total sulphur and carbon analyses were performed at the University of Leicester using a Leco spectrophotometer .

*Data Correction*

To correct for variable degrees of serpentinite alteration, reflected by the range of losses on ignition (LOI) for the peridotite samples, the whole-rock elemental data were recalculated as anhydrous compositions. Correction of the data for the effects of alteration improved the correlations between elements. To enable comparisons to be made with previously obtained data for orogenic peridotites (including the Eastern Pyrénées) and collections of spinel lherzolite xenoliths, the iron contents were also recalculated as FeO.

The recalculation of the data assumed that i) serpentinisation was essentially an isochemical process, involving only the addition of water to the system and ii) prior to serpentinisation the peridotites were in a moderately reduced state and contained negligible water, with Fe present predominantly as $Fe^{2+}$. The corrected data are presented in Table 4.1.

### 4.2.5 Whole-Rock Elemental Data

*Major Element Compositions*

The spinel peridotites display distinct variations in their major element composition, reflecting the transition from relatively fertile to clinopyroxene-poor lherzolites and harzburgites. Volatile corrected MgO contents vary from 37.7 wt% to 45.4 wt%, with no apparent difference between the ranges shown by the peridotites from the different massifs. The composition of the most fertile lherzolite sample (92-LH14) is similar to that of the most fertile peridotite analysed from Ronda (R717, Frey *et al.*, 1985) and to estimates of the primitive mantle (Table 4.2).

When plotted on oxide-MgO plots, the major element compositions display several systematic trends, with the CaO, $Al_2O_3$, $TiO_2$ and $Na_2O$ contents correlating inversely with MgO (Figure 4.6) and a well-defined positive correlation of CaO with $Al_2O_3$ (Figure 4.7). Included in Figure 4.6 are the volatile corrected major element compositions of the Eastern Pyrenean peridotites determined by Bodinier *et al.* (1988), using atomic absorption spectrometry. Whilst the variations of CaO, $Na_2O$, $TiO_2$ and $FeO^*$ with MgO coincide with those defined by the peridotites of this study, the trends for $SiO_2$ and $Al_2O_3$ are displaced towards higher silica and lower alumina contents. Although there is no significant difference between the compositions obtained for the reference material UB-N, which was

| | 92-FR3 | 92-FR4 | 92-FT5 | 92-FT6 | 92-FT7 | 92-LH11 | 92-LH12 | 92-LH14 |
|---|---|---|---|---|---|---|---|---|
| $SiO_2$ | 45.15 | 45.49 | 43.58 | 44.83 | 44.74 | 46.51 | 43.50 | 45.95 |
| $TiO_2$ | 0.12 | 0.12 | 0.01 | 0.12 | 0.09 | 0.14 | 0.04 | 0.14 |
| $Al_2O_3$ | 4.31 | 3.12 | 0.97 | 3.52 | 3.07 | 3.52 | 1.14 | 3.79 |
| $FeO^*$ | 7.53 | 8.08 | 8.11 | 8.51 | 8.07 | 7.32 | 8.51 | 7.90 |
| MnO | 0.13 | 0.13 | 0.13 | 0.14 | 0.13 | 0.12 | 0.13 | 0.13 |
| MgO | 38.25 | 39.47 | 45.26 | 38.76 | 40.21 | 38.23 | 45.51 | 37.60 |
| CaO | 3.48 | 2.70 | 1.19 | 3.22 | 2.72 | 3.15 | 0.44 | 3.47 |
| $Na_2O$ | 0.31 | 0.24 | 0.05 | 0.22 | 0.25 | 0.29 | 0.02 | 0.31 |
| $K_2O$ | 0.01 | 0.01 | 0.01 | 0.01 | 0.02 | 0.00 | 0.00 | 0.01 |
| $P_2O_5$ | 0.02 | 0.02 | 0.01 | 0.01 | 0.01 | 0.02 | 0.02 | 0.02 |
| LOI | 1.35 | 3.25 | 2.17 | 0.19 | 0.58 | 1.31 | 2.87 | 1.96 |
| S | 290 | 181 | 55 | 229 | 186 | 304 | 7 | n.d. |
| Sr | 15 | 7 | 7 | 3 | 6 | 13 | 1 | 11 |
| Zr | 10 | 10 | 5 | 8 | 8 | 12 | 6 | 11 |
| Sc | 15 | 11 | 11 | 16 | 17 | 15 | 5 | 14 |
| V | 75 | 68 | 33 | 78 | 70 | 80 | 27 | 80 |
| Cr | 2833 | 2369 | 2244 | 2461 | 2616 | 2730 | 2435 | 2628 |
| Co | 92 | 101 | 115 | 103 | 100 | 91 | 121 | 94 |
| Ni | 1989 | 2064 | 2543 | 2084 | 2123 | 2019 | 2551 | 2009 |
| Cu | 28 | 20 | 7 | 30 | 24 | 29 | 11 | 34 |
| Zn | 54 | 45 | 44 | 49 | 48 | 47 | 46 | 48 |

| | 92-LH16 | 92-LH17 | 92-LH18 | 92-LH19 | 92-LH3 | 92-PG1 | 92-PG2 | 92-PR1 |
|---|---|---|---|---|---|---|---|---|
| $SiO_2$ | 45.04 | 44.89 | 45.35 | 45.80 | 44.96 | 45.04 | 44.47 | 44.80 |
| $TiO_2$ | 0.12 | 0.12 | 0.12 | 0.13 | 0.09 | 0.10 | 0.06 | 0.12 |
| $Al_2O_3$ | 3.36 | 3.52 | 3.31 | 3.62 | 2.58 | 3.22 | 2.06 | 3.17 |
| $FeO^*$ | 7.85 | 8.09 | 7.73 | 7.83 | 7.68 | 7.97 | 7.75 | 8.02 |
| MnO | 0.13 | 0.13 | 0.13 | 0.13 | 0.12 | 0.13 | 0.12 | 0.13 |
| MgO | 39.56 | 39.32 | 39.47 | 38.23 | 41.52 | 40.02 | 42.91 | 40.04 |
| CaO | 2.99 | 2.99 | 2.92 | 3.26 | 2.19 | 2.64 | 1.79 | 2.77 |
| $Na_2O$ | 0.24 | 0.24 | 0.26 | 0.29 | 0.18 | 0.23 | 0.12 | 0.23 |
| $K_2O$ | 0.01 | 0.00 | 0.02 | 0.01 | 0.02 | 0.00 | 0.00 | 0.01 |
| $P_2O_5$ | 0.02 | 0.02 | 0.02 | 0.02 | 0.02 | 0.02 | 0.01 | 0.02 |
| LOI | 2.17 | 0.29 | 3.14 | 2.90 | 2.39 | 6.54 | 0.68 | 2.17 |
| S | 149 | 210 | 307 | 365 | 264 | n.d. | 85 | 170 |
| Sr | 9 | 9 | 13 | 13 | 19 | 9 | 5 | 7 |
| Zr | 10 | 10 | 12 | 11 | 9 | 9 | 7 | 10 |
| Sc | 14 | 16 | 15 | 15 | 11 | 15 | 10 | 15 |
| V | 77 | 75 | 68 | 79 | 56 | 63 | 49 | 70 |
| Cr | 2692 | 2549 | 2570 | 2750 | 2234 | 2317 | 2574 | 2571 |
| Co | 99 | 100 | 95 | 95 | 99 | 102 | 105 | 101 |
| Ni | 2147 | 2124 | 2060 | 2027 | 2219 | 2186 | 2327 | 2170 |
| Cu | 28 | 32 | 26 | 29 | 17 | 28 | 17 | 32 |
| Zn | 50 | 50 | 47 | 50 | 44 | 45 | 44 | 45 |

**Table 4.1** Major and trace element compositions of Eastern Pyrenean massive peridotites recalculated to anhydrous values, converting all $Fe_2O_3$ to FeO ($FeO^*$). Major element concentrations and losses on ignition in wt%, sulphur and trace element abundances in ppm. n.d. not determined.

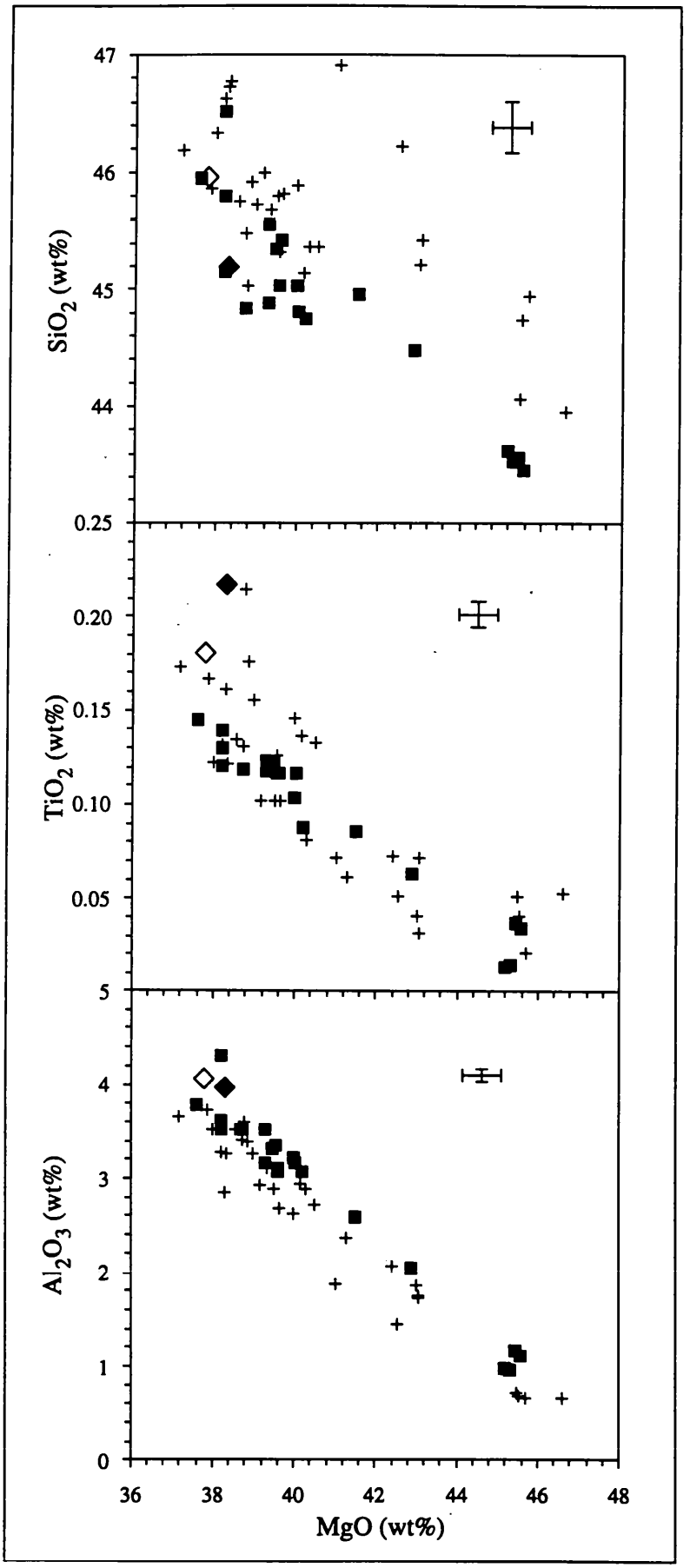


**Figure 4.6 (a)** Variations of whole-rock $SiO_2$, $TiO_2$ and $Al_2O_3$ concentrations as functions of MgO in the peridotites of the Eastern Pyrenean ultramafic massifs. ■ Peridotite analyses (this study); + peridotite analyses (Bodinier *et al.*, 1988); ◆ primitive mantle estimate (Jagoutz *et al.*, 1979); ◇ primitive mantle estimate (Hart & Zindler, 1986). Error bars denote estimated 2σ errors on mid-range values.

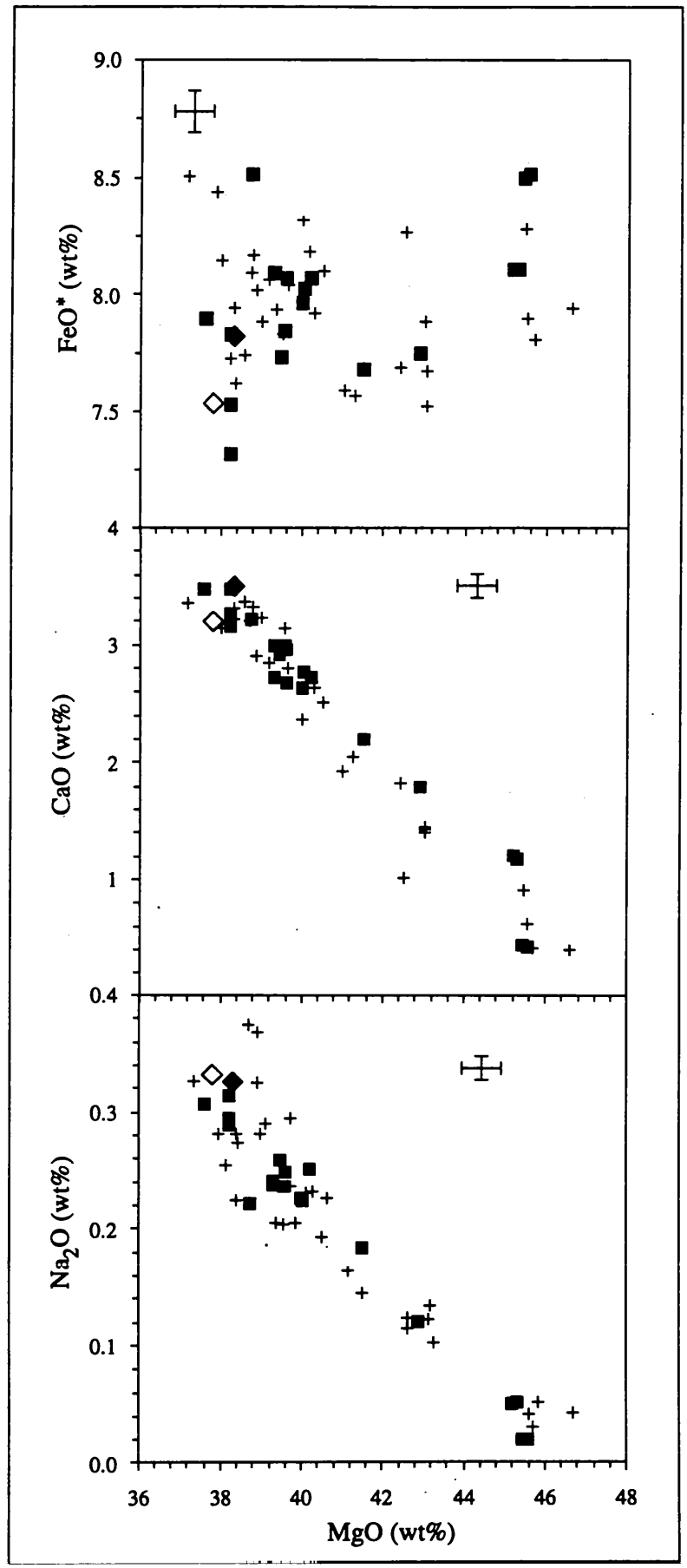


**Figure 4.6 (b)** Variations of whole-rock FeO*, CaO and $Na_2O$ concentrations as functions of MgO in the peridotites of the Eastern Pyrenean ultramafic massifs. Symbols are the same as figure 4.6 (a). Error bars denote estimated $2\sigma$ errors on mid-range values.

| Element | 92-LH14 | R717 | Primitive Mantle (Jagoutz *et al.*, 1979) | Primitive Mantle (Hart & Zindler, 1986) |
|---|---|---|---|---|
| $SiO_2$ | 45.95 | 44.97 | 45.2 | 45.96 |
| $TiO_2$ | 0.14 | 0.17 | 0.22 | 0.18 |
| $Al_2O_3$ | 3.79 | 3.91 | 3.97 | 4.06 |
| FeO* | 7.90 | 8.28 | 7.82 | 7.54 |
| MnO | 0.13 | 0.13 | 0.13 | 0.13 |
| MgO | 37.60 | 37.97 | 38.3 | 37.78 |
| CaO | 3.47 | 3.51 | 3.50 | 3.21 |
| $Na_2O$ | 0.31 | 0.31 | 0.33 | 0.33 |
| $K_2O$ | 0.01 | 0.01 | 0.03 | 0.03 |
| $P_2O_5$ | 0.02 | 0.01 | - | 0.02 |
| Sc | 14 | 15.2 | 17 | 14.8 |
| V | 80 | 73 | 77 | - |
| Cr | 2628 | 2340 | 3140 | 3200 |
| Co | 94 | 102 | 105 | - |
| Ni | 2009 | 1920 | 2110 | 2180 |

**Table 4.2** Comparison of the major element composition of sample 92-LH14 with estimates of undepleted or primitive mantle compositions. R717 from Frey *et al.* (1985).

analysed as part of both this study and that of Bodinier *et al.* (1988), comparison of the two sets of Eastern Pyrenean data with the whole-rock major element compositions of other orogenic peridotites and ultramafic xenoliths (Figure 4.8) shows that the $SiO_2$ and $Al_2O_3$

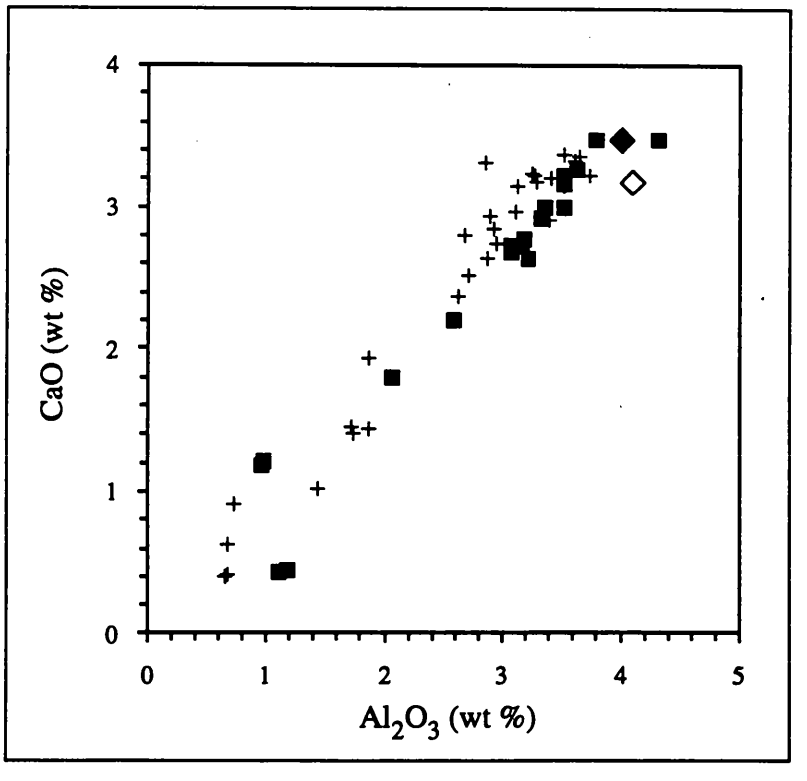


**Figure 4.7** Variation of CaO as a function of $Al_2O_3$ for the peridotites of the Eastern Pyrenean ultramafic massifs, illustrating the well defined positive relationship between the elements and the significant offset of the $Al_2O_3$ concentrations determined by Bodinier *et al.* (1988) in the less depleted peridotites. Symbols are the same as Figure 4.6 (a).

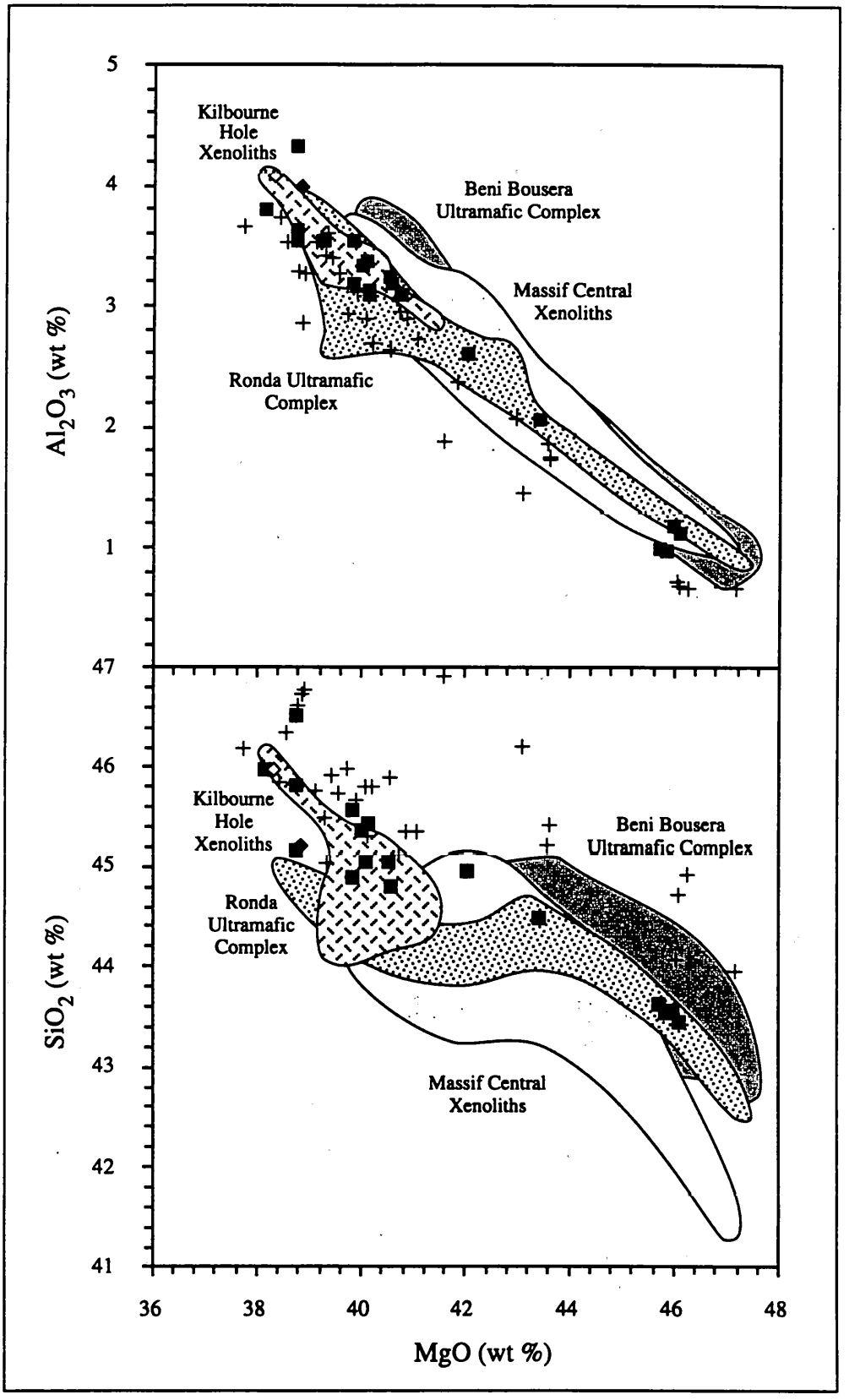


**Figure 4.8** Comparison between the variation of whole-rock $Al_2O_3$ and $SiO_2$ with MgO in the peridotites of the Eastern Pyrenean ultramafic massifs and that shown by other orogenic massifs and collections of spinel lherzolite xenoliths from central France and the Western U.S.A. Data from Basaltic Volcanism Study Project, BVSP, (1981), Frey *et al.* (1985), Downes & Dupuy (1986) and Pearson (1989). Symbols are the same as figure 4.6 (a).

concentrations determined in this study are consistent with those of the other ultramafic sample sets, whereas the data of Bodinier *et al.* (1988) are offset from the trends defined by the literature data. This systematic shift of $SiO_2$ and $Al_2O_3$ concentrations may reflect analytical bias associated with the AAS technique used by Bodinier *et al.* (1988). To maintain consistency, therefore, only data obtained by XRF will be used for comparison in this discussion.

***Transition Metal Trace Elements***

Although both nickel and cobalt behave compatibly in the peridotite samples, exhibiting a positive correlation with MgO (Figure 4.9 (a)), scandium and vanadium abundances are inversely correlated with MgO content, demonstrating their incompatibility in the peridotites. The contrasting behaviour of these elements in the peridotites of the N.E. Pyrénées agree with the range of compatibilities previously observed in (olivine+pyroxene) - melt systems (e.g. Frey *et al.*, 1978).

The variation in Ni and Co contents in the massive peridotites is relatively narrow, with concentrations ranging from 2012 to 2568 ppm and 91 to 122 ppm respectively. The correlations of Ni and Co with MgO are, however reasonably tight for all MgO contents, with less than 100 ppm and 10 ppm (5% and 10% relative) variation in the Ni and Co contents of samples with similar MgO contents. Although the relative ranges of the Sc and V contents of the peridotites are similar, the considerably greater scatter of Sc data results in a poorer correlation with MgO, owing to the proximity of the sample abundances to the instrumental detection limit.

Cr abundances are highly variable, with the least depleted peridotites exhibiting the highest concentrations and increased scatter in samples with high MgO contents. The high variation of Cr content in peridotites of the Ronda ultramafic complex was attributed by Frey *et al.* (1985) to the inhomogeneous distribution of spinel, with the greatest variation occurring in depleted samples, in which the modal abundance of the mineral may be lowest.

The trace element composition of sample 92-LH14 is consistent with the primitive character of this sample indicated by its major element contents. Although estimates of the transition-metal trace element abundances of the primitive mantle show considerable variability (particularly for the compatible elements), the Sc, V, Ni and Co concentrations of 92-LH14 are similar to most of the recent estimates.

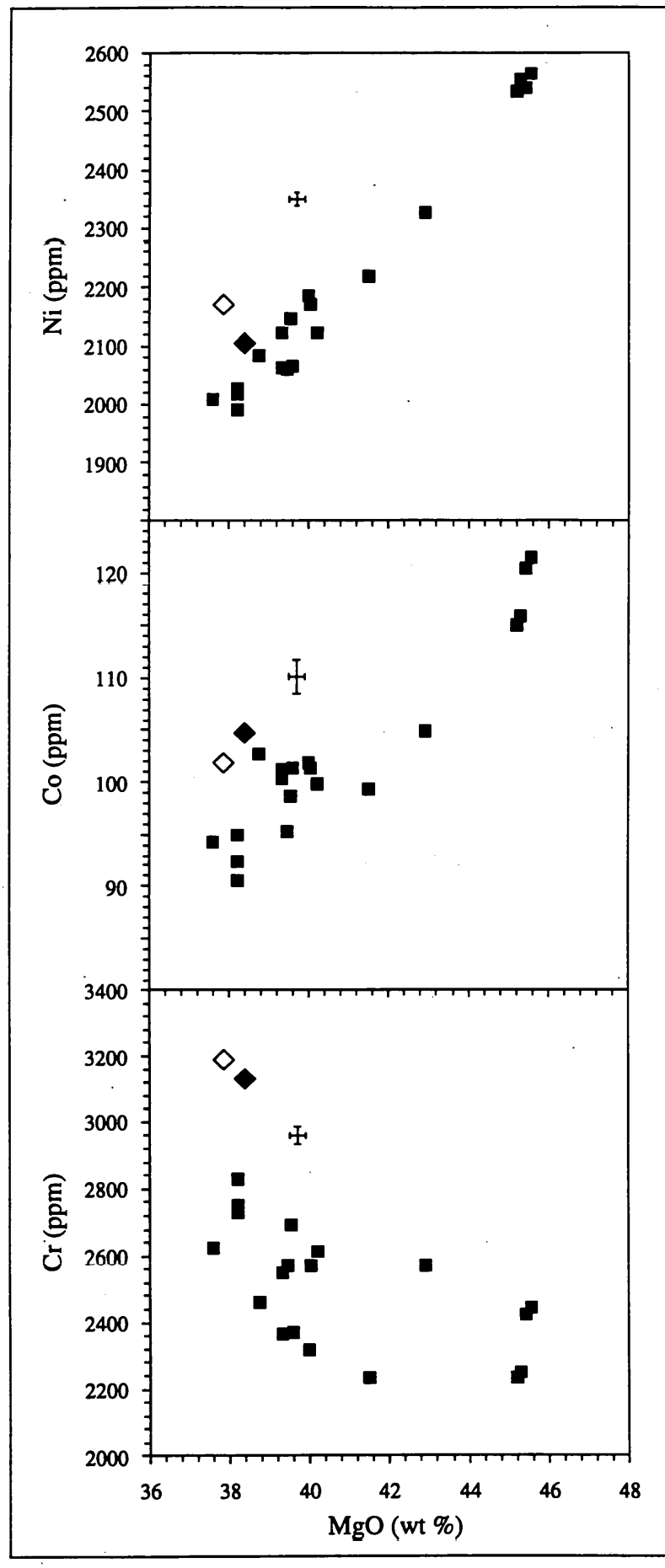


**Figure 4.9** (a) Variation of whole-rock Ni, Co and Cr concentrations in peridotites of the Eastern Pyrenean ultramafic massifs. Symbols are the same as Figure 4.6 (a) Error bars denote estimated 2σ errors on mid-range values.

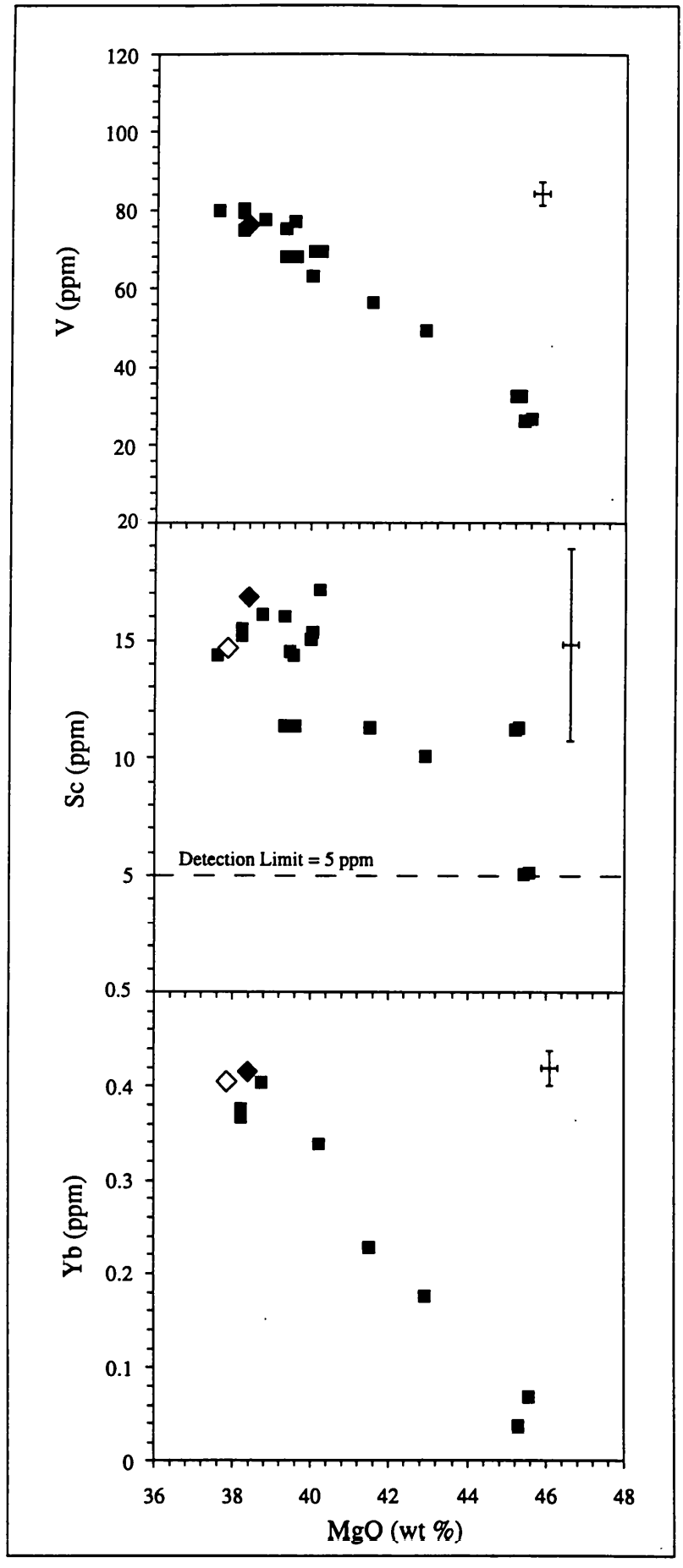


**Figure 4.9 (b)** Variation of whole rock Sc, V and Yb concentrations in peridotites of the Eastern Pyrenean ultramafic massifs. Symbols are the same as Figure 4.6 (a). Error bars denote estimated 2σ errors on mid-range values. Dashed line shows instrumental detection limit for Sc.

***Incompatible elements: Sr and Rare Earth Elements***

The Sr and REE contents of the massive peridotites are negatively correlated with MgO contents (Figure 4.10), confirming the incompatibility of the elements. Whilst the correlations of Sr and LREE abundances with MgO are moderately weak, the correlation of the HREE with MgO are reasonably good, as shown by the Yb - MgO trend of Figure 4.9 (b).

The chondrite normalised whole-rock REE abundances for the massive peridotites are shown in Figure 4.11. The Eastern Pyrenean peridotites display two different types of REE profile. The majority of the peridotites are characterised by LREE depletion ($[Ce/Yb]_N$ = 0.06 - 0.55)† and flat to slightly fractionated HREE ($[Dy/Yb]_N$ ~ 0.79 - 0.93). Similar profiles have been previously reported for both clinopyroxene separates and whole-rocks from the five peridotite bodies (Bodinier *et al.*, 1988; Downes *et al.*, 1991) and for non-metasomatised peridotites from a number of other orogenic peridotite massifs (see review by McDonough & Frey, 1989). The LREE depletion of the two protogranular spinel lherzolites collected from the Fontête Rouge massif ($[Ce/Yb]_N \leq 0.1$) is significantly greater than that shown by the peridotites collected from the other massifs ($[Ce/Yb]_N \geq 0.3$). In addition, the HREE fractionation in these samples is more pronounced than is observed in other lherzolites exhibiting similar degrees of major element depletion.

The second type of REE profile is exhibited by only one sample (92-FT5, a harzburgite from Fontête Rouge) and is characterised by a U-shaped profile produced by pronounced LREE enrichment relative to the MREE and fractionation of the HREE. Similar U-shaped REE profiles have been determined for other refractory peridotites from the Eastern Pyrénées (Bodinier *et al.*, 1988) and are frequently reported in ultramafic xenoliths and ophiolitic harzburgites (Stosch & Seck, 1980; Prinzhofer & Allègre, 1985; Dupuy *et al.*, 1986). Because the REE profile of sample 92-FT5 following repeated leaching in cold HCl is similar to that obtained for the unleached sample (Figure 4.11), its shape is unlikely to reflect a LREE enriched intergranular component.

The REE profiles of the majority of the massive peridotites exhibit variable negative Eu

† "N" subscripts denote chondrite normalised ratios.

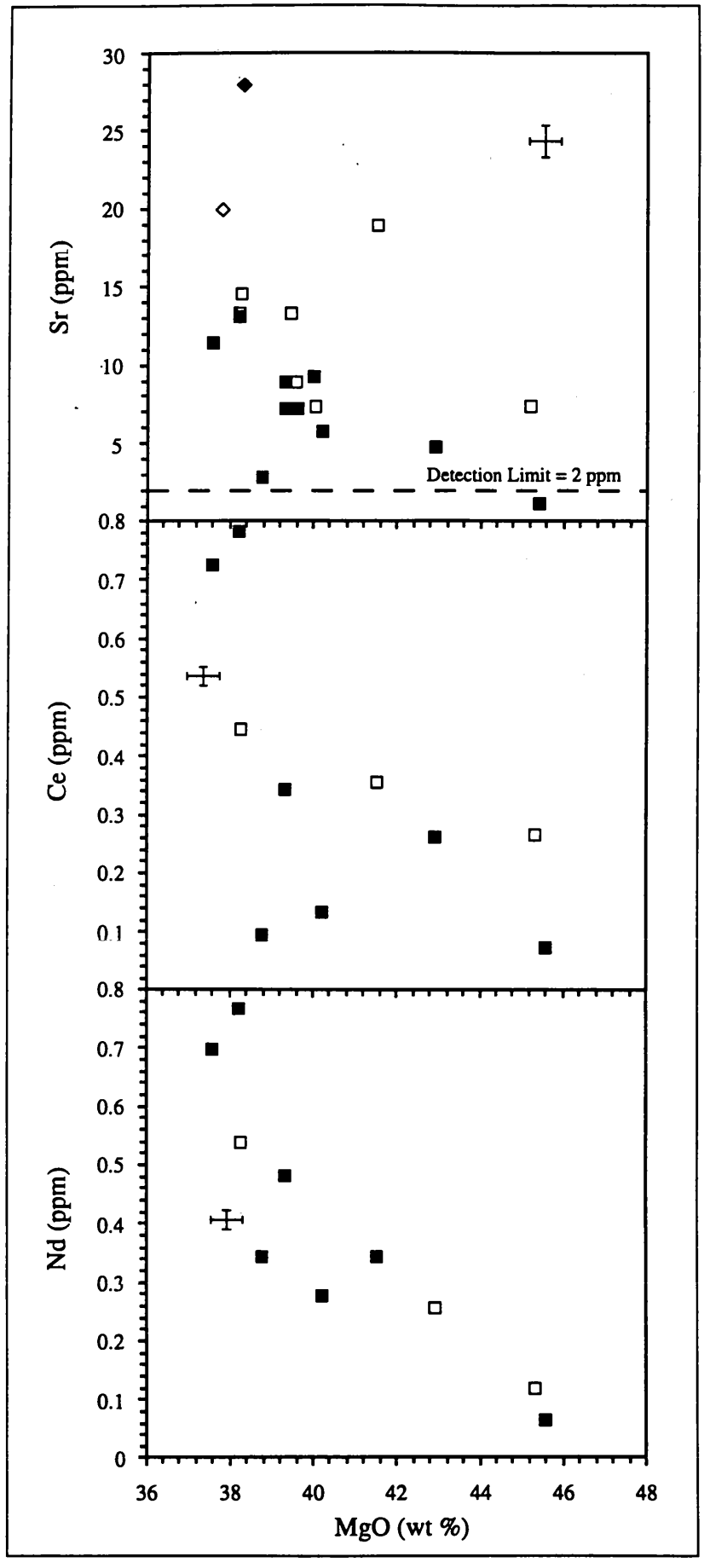


**Figure 4.10** Variations of Sr, Ce and Nd with MgO in the peridotites of the Eastern Pyrenean ultramafic massifs. Symbols are the same as figure 4.6 (a), except open squares indicate high carbon samples (C > 500 ppm) and filled squares, low carbon samples (C ≤ 500 ppm). Error bars denote 2σ errors on mid-range values.

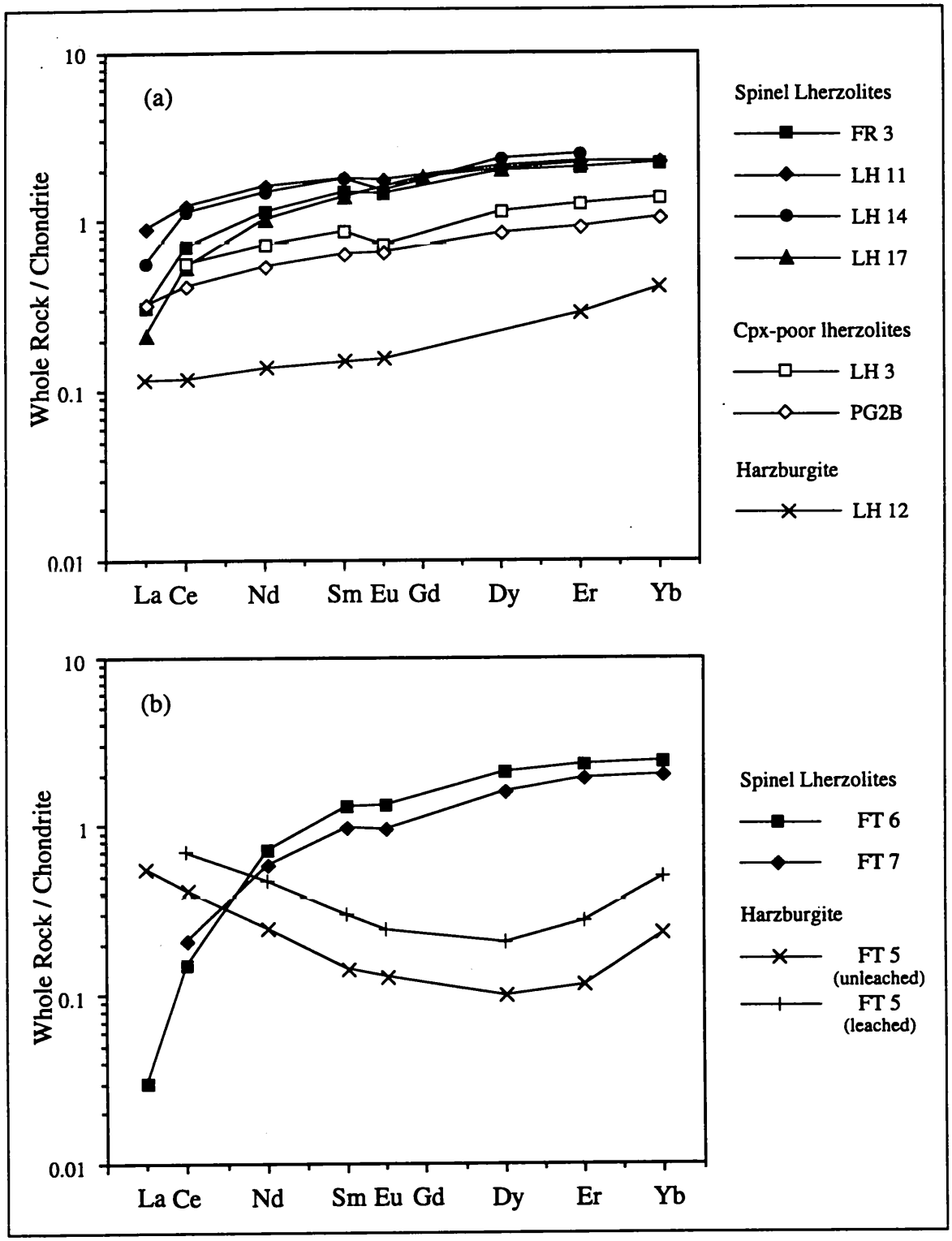


**Figure 4.11** Chondrite normalised REE profiles for peridotites of the Eastern Pyrenean ultramafic massifs. a) Lherz, Freychinède and Pic de Géral, b) Fontête Rouge. Chondrite normalising values from McDonough & Frey (1989).

anomalies ($Eu/Eu^* = 0.6 - 0.96$), which may be accounted for by the overcorrection for Ba interference during REE analysis, particularly in underspiked samples (see Appendix A.3). For duplicate analyses of 92-LH11, which exhibited significant Ba interference and a pronounced negative Eu anomaly ($Eu/Eu^* \sim 0.66$) when first analysed, no anomaly was

observed when the sample was reanalysed following improvements to the ion-exchange procedure which reduced the Ba interference. No Eu anomalies have been observed in previous studies of the REE compositions of the Eastern Pyrenean peridotite massifs (Bodinier *et al.*, 1988; Downes *et al.*, 1991). Consequently the Eu anomalies are regarded as artifacts of the analysis, and as such are not considered geologically significant.

None of the samples have Sr or LREE concentrations similar to estimates of the primitive mantle, however the HREE contents of several samples (e.g. 92-LH14 and 92-LH11) do approach the estimated primitive mantle values of ~2.85 times chondrite (Sun & McDonough, 1989).

### 4.2.6 Effects of Low Temperature Alteration on Peridotite Chemistry

Although the effects of low temperature alteration processes on the composition of orogenic peridotites have not been thoroughly documented, serpentinisation of peridotites appears to be an essentially isochemical process so far as major elements are concerned. In a study of the Lizard ultramafic complex, Green (1964) demonstrated that whole-rock compositions, calculated using unaltered mineral analyses and their modal abundances, were in agreement with bulk chemical analyses recalculated to volatile-free values. Furthermore, Frey *et al.* (1985) and Bodinier *et al.* (1988) noted that samples exhibiting a wide range of serpentinisation defined coherent major and trace element abundance trends, inferring that partial serpentinisation brought about negligible changes to the major element compositions of the ultramafic massifs. Analysis of ground waters in equilibrium with serpentinite, however show significant enrichment in both CaO and $Na_2O$ (White *et al.*, 1963). Thus, although most elements may not be mobile during serpentinisation, subsequent groundwater percolation through the altered rocks may have affected the compositions of the peridotites.

Emplacement of the Eastern Pyrenean massifs into the carbonate rocks of the NPMZ may have resulted in the circulation of hydrothermal fluids through the ultramafic bodies, partially serpentinising the massive peridotites and also introducing carbonate-rich veins. The high Sr contents and significantly LREE-enriched nature of typical limestones (Turekian & Wedepohl, 1961) would suggest that interaction with fluids derived from the surrounding metacarbonates may cause significant enrichment of the peridotites in incompatible trace

elements. Therefore, before the mantle origins of the whole-rock compositions of the Pyrenean ultramafic bodies are addressed, the effects of low-temperature carbonate and serpentine alteration are discussed.

| Sample | Loss on Ignition (%) | C (ppm) | Estimated % Carbonate | Estimated % Serpentine |
|---|---|---|---|---|
| 92-FR3 | 1.35 | 640 | 0.53 | 4.45 |
| 92-FR4 | 3.25 | 384 | 0.32 | 13.3 |
| 92-FT5 | 2.17 | 1400 | 1.17 | 6.9 |
| 92-FT6 | 0.19 | 184 | 0.15 | 0.32 |
| 92-FT7 | 0.58 | 126 | 0.11 | 2.09 |
| 92-LH11 | 1.31 | 301 | 0.25 | 4.8 |
| 92-LH12 | 2.87 | 420 | 0.35 | 11.4 |
| 92-LH14 | 1.96 | † | | *8.25* |
| 92-LH16 | 2.17 | 670 | 0.56 | 7.98 |
| 92-LH17 | 0.29 | 205 | 0.17 | 0.73 |
| 92-LH18 | 3.14 | 945 | 0.79 | 11.5 |
| 92-LH19 | 2.9 | 786 | 0.66 | 10.69 |
| 92-LH3 | 2.39 | 1062 | 0.89 | 8.2 |
| 92-PG1 | 6.54 | 435 | 0.36 | 26.87 |
| 92-PG2 | 0.68 | 203 | 0.17 | 2.48 |
| 92-PR1 | 2.17 | 500 | 0.42 | 8.22 |

**Table 4.3** Carbonate and serpentine contents of samples estimated from total carbon contents and loss on ignition. Carbonate content estimated by assuming all carbon is present in the form of calcite, $CaCO_3$. Serpentinite content estimated from loss on ignition after Reisberg (1988), following correction of the LOI for weight loss owing to the release of $CO_2$ by the decomposition of $CaCO_3$. Serpentine composition taken as $Mg_{2.7}Fe_{0.3}Si_2O_5(OH)_4$.
† C data unavailable.

### *Estimating the Degree of Alteration*

The degree of carbonate alteration and serpentinisation may be independently estimated from the quantity of carbonate minerals and structurally-bound water present in the peridotite samples. If it is assumed that the majority of the carbon present in the peridotites is in the form of carbonates (e.g. magnesite or calcite), then the total carbon content of the peridotite samples may be used to calculate the proportion of carbonate present (Table 4.3). Similarly, the degree of serpentinisation may be estimated from the loss on ignition (LOI) measured for the peridotites during the determination of their whole-rock major element compositions,

with the assumption that serpentine is the only hydrous alteration mineral present in the peridotites and applying a correction to the LOI values for the production of $CO_2$ by the thermal decomposition of any carbonate also present. Although other hydrous alteration products may also occur, their inclusion in the model does not significantly affect the calculated degree of alteration.

Most of the peridotite samples exhibit between 5 and 15% serpentinisation, although sample 92-PG1 is more highly altered, with a calculated serpentine content of ~27%. This value is consistent with the considerable alteration visible in this sample (both in hand specimen and thin section), which was collected on the periphery of the massif, close to the brecciated margin. The carbonate contents of the peridotites range from ~0.1 to 1.2%, but are predominantly less than 0.5%. Although the high carbon contents of samples 92-LH3, 92-LH18 and 92-LH19 probably result from the thin carbonate veinlets observed in the samples, no carbonate alteration was visible in sample 92-FT5 to account for its high total carbon content.

***Effect of Alteration on Peridotite Whole-Rock Compositions***

The effects of alteration on the peridotite whole-rock elemental compositions will be superimposed on pre-existing variations owing to magmatic processes. To investigate the effects of alteration, ratios between elements with similar bulk distribution coefficients were therefore plotted as functions of the degree of alteration. Such ratios should remain unfractionated during magmatic processes, but may be changed by subsequent hydrothermal alteration (due to differing solubilities of the elements in the alteration fluids), enabling the effects of the two processes to be distinguished.

In Figure 4.12 the MgO/Ni, Ca/Sc, Sc/V and Sr/Nd abundance ratios of the N.E. Pyrenean peridotites are plotted as a function of total carbon content and LOI. The elements within each ratio exhibit similar compatibility during melting (McDonough, 1990) and include major, trace and rare-earth elements covering a large range of compatibilities. Ti/Eu* abundance ratios are also plotted as a function of alteration in Figure 4.12. (Eu* is the interpolated value of Eu, using the abundances of Sm and Dy.) In basalts and komatiites the Ti/Eu ratio is nearly constant and chondritic over a range of concentrations covering several orders of magnitude (McDonough & Frey, 1989). Although the Ti/Eu ratios in anhydrous peridotite xenoliths show a wide variation, the average value (7850) is also close to that of

chondrites (7700), suggesting these elements may remain unfractionated during mantle melting. The $(La/Nd)_N$ ratio is also included in Figure 4.12 to determine whether the extent of LREE enrichment relates to alteration processes.

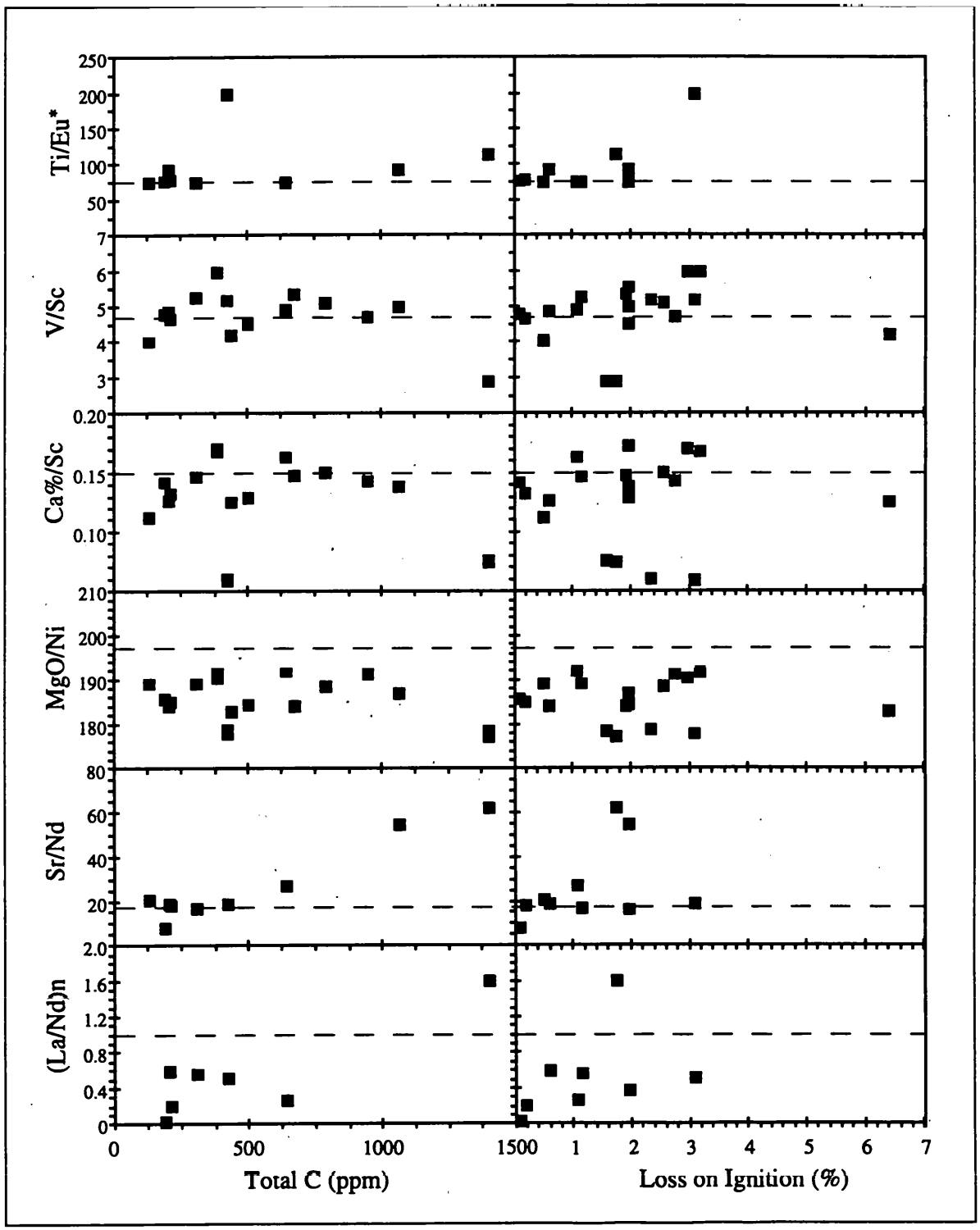


**Figure 4.12** Variation of elemental ratios as functions of the degree of carbonate and serpentinite alteration, indicated by the total carbon content and loss on ignition of the samples, respectively. During magmatic processes the chosen elemental ratios should remain unfractionated, hence should plot close to the primitive mantle values in both residues after melting or refertilised mantle peridotites. Primitive mantle values (dashed lines) are from McDonough (1990).

The absence of elements with similar magmatic behaviour to $SiO_2$, $FeO^*$ and $Na_2O$ prevented the use of similar ratios to investigate the effects of alteration on these elements. However, Figure 4.6 shows that the $FeO^*$ and $Na_2O$ concentrations of samples with both high and low degrees of alteration define similar trends with MgO content, suggesting alteration may have had negligible affect on these elements. When compared to the data for other massifs (Figure 4.8), the $SiO_2$ contents of several relatively undepleted samples appear to be significantly higher than expected from their MgO contents. Although the deviation of the silica contents is not proportional to the estimated degree of hydrous alteration, the anomalous samples do exhibit marginally higher LOI values than samples which fall within the global data set, suggesting that some mobilisation of silica may have occurred during alteration.

Of the elemental ratios plotted in Figure 4.12, only Sr/Nd appears to be related to the degree of alteration, exhibiting a positive correlation with total carbon content for samples containing more than approximately 500 ppm C. This correlation is also reflected in the Sr abundances of the peridotites, which exhibit a poor, but positive correlation with total carbon content. A relationship between the intensity of carbonate veining and the Sr/LREE ratios in peridotites of the small ultramafic body of Pic Couder was also noted by Bodinier *et al.* (1988). Because the Sr/Nd ratios of the peridotites remain close to the primitive mantle value at low total carbon contents, magmatic processes may be the dominant control on Sr abundances in carbonate-poor peridotites. At high total carbon contents, the fractionation of the Sr/Nd ratio and correlation of Sr with C, however, suggest that carbonate alteration may have modified the Sr abundances significantly.

The ratios between compatible (MgO/Ni) and incompatible elements (V/Sc, Ca/Sc and Ti/Eu) all appear to be unaffected by alteration, plotting at similar values which lie close to those estimated for the primitive mantle. No systematic variation is observed with either C or LOI. The calculated MgO/Ni ratios are lower than the primitive mantle ratio of 196, however they are similar to the average value of 190 calculated from over 300 spinel lherzolite xenoliths (McDonough, 1990). Some of the $Ti/Eu^*$ ratios are significantly higher than estimates of the primitive mantle. These samples, however, are the most depleted in major elements, suggesting that the compatibilities of the two elements may in fact differ slightly.

In addition to high Sr/LREE ratios Bodinier *et al.* (1988) noted that the veinlet-rich Pic Couder were also enriched in LREE. There is, however, no obvious relationship between the $(La/Nd)_N$ ratio and the degree of either carbonate or serpentinite alteration of the peridotites analysed in this study. Although the peridotite containing the greatest total carbon (92-FT5) also exhibits strong LREE enrichment, a similar REE profile is found for this sample following repeated leaching in cold HCl, demonstrating that the LREE enrichment cannot be attributed to carbonate alteration and may reflect the effects of processes unrelated to alteration.

In conclusion, the peridotites collected from the Eastern Pyrenean peridotite massifs exhibit variable degrees of alteration due to interaction with fluids derived from the surrounding metacarbonates. Although the abundances of most major and trace elements (covering a range of compatibilities) appear to show no recognisable relationship to either the degree of serpentinisation or carbonate alteration, Sr concentrations appear to be elevated in peridotites with high carbon contents owing to their interaction with carbonate-rich hydrothermal fluids and silica may have been added to several samples during serpentinisation. As a consequence, Sr data for samples with high degrees of carbonate alteration (C > 500 ppm) will be excluded from the discussion of the incompatible element compositions of the peridotites and the samples apparently enriched in silica will also be treated with caution. Although the LREE contents cannot be related directly to the effects of low temperature alteration, to rule out the effects of minor interactions between the peridotites and carbonate-rich fluids, the discussion of the LREE contents of the Eastern Pyrenean peridotites will also be limited to the low C samples.

### 4.2.7 Interpretation of Whole-Rock Major Element Data

When the compositions of the massive peridotites are projected from olivine onto the CS-MS-A plane of the C-M-A-S system (O'Hara, 1968), they define a linear array extending from the enstatite apex towards the projected compositions of basaltic melts (Figure 4.13). This array suggests that the range of major element compositions observed in the Eastern Pyrenean may originate from a two component mixing or unmixing process, such as incomplete or variable extraction of a partial melt from a relatively undepleted mantle source or the re-fertilisation of an homogeneous mantle residue by the addition of variable amounts of a compositionally homogeneous melt (Frey *et al.*, 1985).

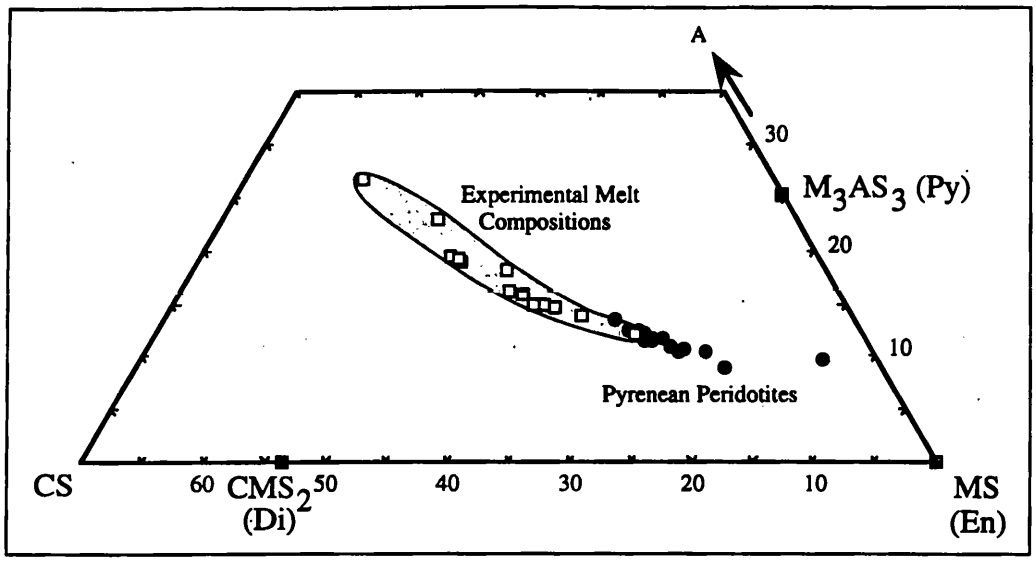


**Figure 4.13** Eastern Pyrenean peridotites plotted in CMAS system (O'Hara, 1968). Projection from forsterite ($M_2S$) into the diopside (Di)-enstatite (En)-pyrope (Py) plane. The straight trajectory of the peridotites projects towards the field of experimental primary melts.

On the basis of the major element compositions alone these two processes cannot be distinguished, however several features of the Eastern Pyrenean peridotite bodies may argue against a process of refertilisation of previously depleted mantle. Firstly, if the variation in the whole-rock compositions of the Eastern Pyrenean bodies were caused by the variable addition of a basaltic melt, then the range of whole-rock major element compositions would not be limited by that of the primitive mantle and could extend to compositions more enriched in basaltic components. Although several of the most fertile massive peridotites of the Eastern Pyrenean massifs approach the estimated primitive mantle compositions, few appear to be more enriched. Secondly, no petrographic evidence is present for the addition of significant quantities of melt to the peridotites of the Eastern Pyrénées. If refertilisation occurred early in the evolution of the massifs, however, it is unlikely that such textures would be preserved during the long history of sub-solidus deformation and crystallisation experienced by the peridotites. Because these arguments are inconclusive, both melting and re-fertilisation models to account for the range compositions exhibited by the Pyrenean peridotites will be discussed.

### 4.2.8 Melt Extraction

Within the context of a partial melting model, the observed range of compositions may have been formed by either a) variable or incomplete extraction of compositionally uniform melts produced by similar degrees of partial melting in all the peridotite bodies, or b) partial

or complete extraction of compositionally heterogeneous melts produced by variable degrees of partial melting of the peridotite massifs. The incomplete removal of a melt of uniform composition suggested in the first model would be expected to produce linear trends between the degree of melt extraction and the concentrations of each element in the residual peridotites. The extraction of melts of variable composition, however, would result in non-linear elemental trends as functions of melt depletion.

Whilst the compositionally uniform melts of the first model would require batch melting of the peridotite source, both batch and fractional melting processes may produce the compositionally variable melts of the second model.

### *Calculating the Percentage Melt Extracted*

The percentage of melt extracted (F) to produce each of the peridotite samples may be estimated using the mass balance equation:

$$C^0 = FC^L + (1\text{-}F)C^R \qquad \textbf{(Eqn. 4.1)}$$

where $C^0$, $C^L$ and $C^R$ are the compositions of the mantle source, the melt and the residual peridotite respectively. Although $C^R$ is provided by the sample analyses, values for both $C^0$ and $C^L$ are unknown and require assumptions to be made.

As noted previously, sample 92-LH14 appears to exhibit minimal depletion in basaltic components. Of the primitive mantle estimates in Table 4.2, its major element composition appears to be most similar to that of Jagoutz *et al.* (1979), however its silica content may be anomalously high in comparison with other lherzolites, both from the Eastern Pyrénées and elsewhere, possibly due to the effects of alteration already discussed. Therefore, although this sample is chosen as the best estimate of the composition of the peridotites prior to melting ($C^0$), for the modelling of the residues following melt extraction, the lower silica value of Jagoutz *et al.* (1979) is used in preference. If any melt has been extracted from 92-LH14, then the calculated values of F would be systematically low. The relative degrees of melting calculated for the peridotites, however, would remain unaffected.

In the absence of data on the composition of the melt ($C^L$), three different approaches were adopted for the calculation of F, using major, trace or REE data for the peridotites and either mineral-melt partition coefficients or bulk distribution coefficients.

**Fe/Mg Ratios in Residual Olivines**

By writing Equation 4.1 independently for MgO and FeO* and solving for F, Frey *et al.* (1985) obtained the expression

$$F = 1 - \frac{(FeO^*)^O - ß(MgO)^O}{(FeO)^R - ß(MgO)^R} \qquad \textbf{(Eqn. 4.2)}$$

in which ß is defined as $(FeO^*/MgO)^L$. If the compositions of the olivines in the residual peridotites are known, then ß may be estimated from the experimentally determined olivine-melt exchange coefficient, $K_D$, defined as

$$K_D = \frac{(FeO/MgO)^{Olivine}}{(FeO/MgO)^L} \qquad \textbf{(Eqn. 4.3)}$$

Roeder & Emslie (1970) found that the parameter $K_D$ has a near constant value of $0.30 \pm 0.01$ in tholeiites at 1 atm. Although this value appears to vary little over a wide range of pressures, it increases slightly with increasing degrees of melting (Hirose & Kushiro, 1993). For up to 30% melting at pressures of 0 - 30 kbar, its value lies in the range $0.300 \pm 0.025$. To estimate the proportion of melt extracted and the effect of ß on the calculated percentage, separate calculations of the degree of melting were performed for the median value of ß = 0.30 and the upper limit of ß = 0.325.

The use of Equation 4.3 to estimate $K_D$ assumes $(FeO/MgO)^L \approx (FeO^*/MgO)^L$, resulting in an overestimate of the amount of melting in proportion to the amount of $Fe^{3+}$ in the melt (Frey *et al.*, 1985). Assuming a melt $Fe^{3+}/Fe^{2+}$ ratio in the range 0 - 0.1 (consistent with melting at oxygen fugacities close to the FMQ buffer; Kilinc *et al.*, 1983), the relative magnitude of this overestimation of F is only ~ 5%, which is acceptable, given the other uncertainties in the model.

Although the compositions of the olivines in the residual peridotites collected for this study have not been determined, Conquéré & Fabriès (1984) stated that "the mg ratio of silicates, especially that of olivines, is closely related to that of the host rocks". Frey *et al.* (1985) also showed that the Mg numbers of olivines from peridotites of the Ronda massif were similar to those determined for the whole-rocks. Consequently, the whole-rock $(FeO^*/MgO)$ ratios of the Eastern Pyrenean peridotite samples were used to approximate

$(FeO/MgO)^{Olivine}$ in the calculation of F. During calculation of F, assuming a batch melting model, the ß value in Equation 4.2 was calculated using the composition of the residual olivine at the end of melting. During fractional melting, however, the composition of olivine in equilibrium with the melt changes and an average value of $(MgO/FeO)^{Olivine}$ was required for the calculation of ß. Because the range of olivine compositions estimated for the Eastern Pyrenean peridotites is relatively limited, the variation in ß during fractional melting would have been small. Therefore, the range of possible degrees of melt extraction caused by fractional melting was bracketed using separate calculations of F, in which ß was estimated from the original and final $(FeO^*/MgO)$ ratios of the peridotites.

| Sample | $FeO^*$ (wt%) | MgO (wt%) | $F_{Fe/Mg}$ (Kd=0.3) $(Fe/Mg) = (Fe/Mg)^R$ | $F_{Fe/Mg}$ (Kd=0.325) $(Fe/Mg) = (Fe/Mg)^R$ | $F_{Fe/Mg}$ (Kd=0.3) $(Fe/Mg) = (Fe/Mg)^0$ | $F_{Fe/Mg}$ (Kd=0.325) $(Fe/Mg) = (Fe/Mg)^0$ |
|---|---|---|---|---|---|---|
| 92-FR3 | 7.53 | 38.25 | 4.5% | 4.9% | 4.3% | 4.6% |
| 92-FR4† | 8.08 | 39.47 | 5.8% | 5.9% | 5.7% | 5.9% |
| 92-FT5† | 8.11 | 45.26 | 23.1% | 23.8% | 21.8% | 22.4% |
| 92-FT6 | 8.51 | 38.76 | 1.2% | 0.9% | 1.0% | 0.8% |
| 92-FT7 | 8.07 | 40.21 | 8.4% | 8.6% | 8.2% | 8.4% |
| 92-LH11 | 7.32 | 38.23 | 5.7% | 6.2% | 5.2% | 5.7% |
| 92-LH12† | 8.51 | 45.51 | 21.8% | 22.3% | 21.1% | 21.5% |
| 92-LH16 | 7.85 | 39.56 | 7.4% | 7.7% | 7.2% | 7.4% |
| 92-LH17 | 8.09 | 39.32 | 5.2% | 5.3% | 5.2% | 5.3% |
| 92-LH18 | 7.73 | 39.47 | 7.7% | 8.1% | 7.4% | 7.7% |
| 92-LH19 | 7.83 | 38.23 | 2.7% | 2.9% | 2.7% | 2.8% |
| 92-LH3 | 7.68 | 41.52 | 14.7% | 15.3% | 13.8% | 14.3% |
| 92-PG1 | 7.97 | 40.02 | 8.3% | 8.5% | 8.1% | 8.3% |
| 92-PG2 | 7.75 | 42.91 | 18.5% | 19.2% | 17.3% | 17.9% |
| 92-PR1 | 8.02 | 40.04 | 8.0% | 8.3% | 7.9% | 8.1% |

**Table 4.4** Proportions of melt extracted calculated from the Fe/Mg ratios of the residues for both batch and fractional melting of peridotite sample 92-LH14 (7.90% $FeO^*$, 37.6% MgO), using ß values calculated from two different values of the olivine-melt exchange coefficients, $K_D$. For each sample two melts were calculated, one using the (FeO/MgO) ratio of the residue, $(FeO/MgO)^R$, the other using the (FeO/MgO) ratio of the source, $(FeO/MgO)^0$. † FeO and MgO concentrations are means of duplicate analyses.

The results of the calculations are presented in Table 4.4, They show that the range of Fe/Mg ratios present in the Eastern Pyrenean peridotite samples is consistent with the extraction of between 1 and 23% melt from a source with a composition similar to that of sample 92-LH14. There is negligible difference between the values of F calculated for the two values of the olivine-melt exchange coefficients. Similar degrees of melt extraction are

determined using values of ß calculated from the (FeO*/MgO) ratios of both the residue and peridotite source (Figure 4.14), leading to the calculation of similar values of F for both batch and fractional melting models and indicating that the degree of melt extraction calculated from the FeO/MgO ratios is largely insensitive to the process of melting.

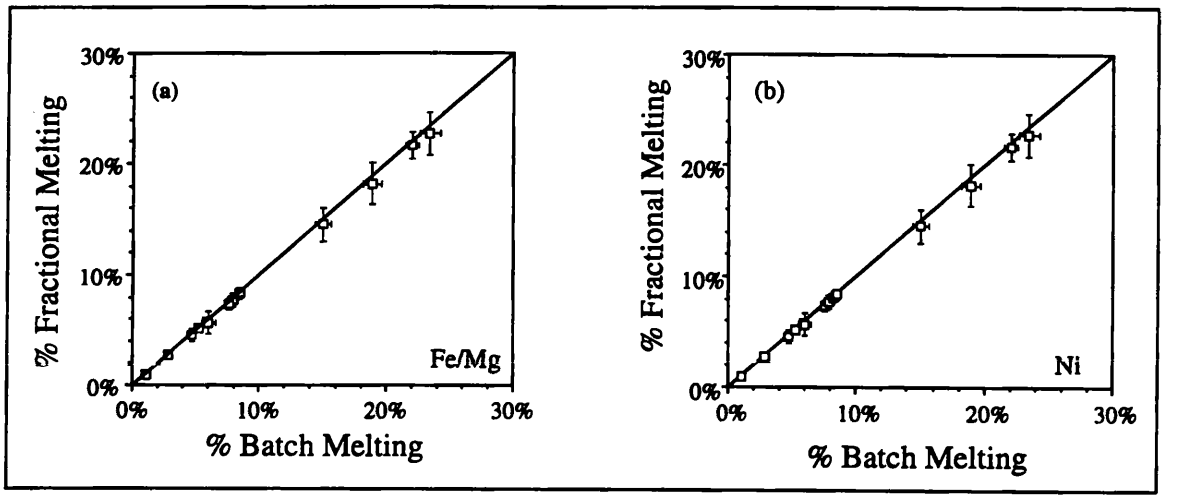


**Figure 4.14** Comparison of degrees of melting, F, calculated for both fractional and batch melting models from a) the whole-rock Fe/Mg ratios and b) the whole-rock Ni contents of the Eastern Pyrenean peridotite massifs. Error bars in (a) represent the variation in F calculated for ß = 0.3 ± 0.025. Error bars in (b) represent the difference between values of F calculated for $D_{Ni}$ = 8 and 20.

## Ni Contents of Residual Peridotites

The variation in the abundances of Ni also may be used to estimate the degree of melt extraction from the massive peridotites of the Eastern Pyrenean massifs. Although the high compatibility of Ni should make the calculated values of F relatively insensitive to the assumed melting process, separate calculations were performed for batch and fractional melting, using Equations 4.4 and 4.5.

$$C^R = \frac{C^0 D^{s/l}}{(D^{s/l}(1-F) + F)} \qquad \textbf{(Eqn. 4.4)}$$

$$C^R = C^0 (1-F)^{(1/D^{s/l}-1)} \qquad \textbf{(Eqn. 4.5)}$$

where $D^{s/l}$ is the bulk distribution coefficient. In olivine-rich rocks, the bulk distribution coefficient of Ni is controlled by the olivine-liquid partition coefficient, $D_{Ni}^{ol/l}$, which is a function of both the temperature of melting and the MgO content of the melt (Hanson & Langmuir, 1978; Hart & Davies, 1978). Two estimates of the quantity of partial melt

extracted were therefore calculated for each sample (Table 4.5), using bulk distribution coefficients which covered the range of published values ($D_{Ni}^{s/l} \approx 8$ - 20; Henderson, 1982).

| Sample | Ni (ppm) | Batch Melting | | Fractional Melting | |
|---|---|---|---|---|---|
| | | $D_{Ni}^{s/l} = 20$ | $D_{Ni}^{s/l} = 8$ | $D_{Ni}^{s/l} = 20$ | $D_{Ni}^{s/l} = 8$ |
| 92-FR3 | 1989 | -1.0% | -1.1% | -0.9% | -0.8% |
| 92-FR4 | 2064 | 2.8% | 3.1% | 2.6% | 2.4% |
| 92-FT5 | 2543 | 22.1% | 24.0% | 25.1% | 22.9% |
| 92-FT6 | 2084 | 3.8% | 4.1% | 3.6% | 3.3% |
| 92-FT7 | 2123 | 5.7% | 6.1% | 5.4% | 5.0% |
| 92-LH11 | 2019 | 0.5% | 0.6% | 0.5% | 0.4% |
| 92-LH12 | 2551 | 22.4% | 24.3% | 25.5% | 23.3% |
| 92-LH16 | 2147 | 7.4% | 6.5% | 6.0% | 5.5% |
| 92-LH17 | 2124 | 6.2% | 5.4% | 5.0% | 4.6% |
| 92-LH18 | 2060 | 2.9% | 2.4% | 2.3% | 2.1% |
| 92-LH19 | 2027 | 1.0% | 0.9% | 0.8% | 0.7% |
| 92-LH3 | 2219 | 10.8% | 9.9% | 9.1% | 8.3% |
| 92-PG1 | 2186 | 9.3% | 8.4% | 7.7% | 7.0% |
| 92-PG2 | 2327 | 15.7% | 15.0% | 13.8% | 12.5% |
| 92-PR1 | 2170 | 8.5% | 7.6% | 7.0% | 6.4% |

**Table 4.5** Proportions of melt extracted calculated from the Ni contents of the residues for both batch and fractional melting, assuming an original Ni concentration similar to that of peridotite sample 92-LH14 (2009 ppm). Separate calculations performed for two estimates of $D_{Ni}^{s/l}$, bracketing the range of possible degrees of melting.

For each sample the degrees of partial melting, calculated using the different values of $D_{Ni}^{s/l}$, exhibit relative differences of between 8 and 10%. For low degrees of melting ($F \leq 10\%$), this variation is small compared with the imprecision introduced through analytical uncertainties, however for the most refractory samples the values of F differ by ~2%. In such cases, an average of the two calculated degrees of melting is used.

Despite the imprecision in the values of F calculated for each sample, there is little difference between the average melt extraction calculated for batch and fractional melting of the peridotite source as expected (Figure 4.14). In general, a batch melting model overestimates the degree of melting, by a maximum of about 1% in the most depleted samples.

## HREE Modelling

The degree of melting may also be estimated by plotting the fractionation of the HREE as a function of the HREE abundances (Figure 4.15), following a similar method to that used by Bodinier *et al.* (1988). In addition to providing evidence for the degree of melting,

fractionation of the HREE can distinguish between garnet-present and garnet-absent melting, owing to the buffering of the HREE by garnet.

On the plot of Dy/Yb ratio against Yb abundances, the peridotite samples overlap with the majority of the data of Bodinier *et al.* (1988) and exhibit a slight decrease in Dy/Yb ratios with decreasing Yb at high Yb concentrations, but a more pronounced decrease in Dy/Yb ratios at lower Yb contents (i.e. high degrees of melting). Several of the least depleted samples, and in particular those from Fontête Rouge, exhibit significantly lower Dy/Yb ratios, which Bodinier *et al.* (1988) interpreted as representing melting in the presence of garnet. The anticipated Dy/Yb-Yb trajectories were therefore calculated for batch and fractional melting of undepleted mantle sources containing variable quantities of garnet (Figure 4.15).

The melting trajectories were calculated using the non-modal melting equations of Shaw (1970), in which the solid-liquid bulk distribution coefficient is given by

$$D = \frac{(D_0 - PF)}{(1-F)} \qquad \textbf{(Eqn. 4.6)}$$

where $D_0$ is the initial value of D and P is the distribution coefficient of the phase assemblage involved in melting. Substituting this into Equations 4.4 and 4.5 and rearranging the terms gives Equations 4.7 and 4.8, which define the compositions of the residues produced by melt extraction, in which the melts are formed by batch or fractional melting, respectively.

$$C_R = \frac{DC_0}{D_0 + F(1-P)} \qquad \textbf{(Eqn. 4.7)}$$

$$C_R = \frac{DC_0}{D_0}\left(1 - \frac{PF}{D_0}\right)^{(1/P-1)} \qquad \textbf{(Eqn. 4.8)}$$

The parameters used in the calculations are shown in Table 4.6. To simplify the model, the proportions of each mineral entering the melt were assumed to remain constant until one of them was exhausted. Melting of a garnet bearing source was modelled using the melting equation of Mysen (1970) (in which the garnet is consumed by 8 - 15% melting). Following the exhaustion of garnet, the garnet-absent melting equation of Baker & Stolper (1994) was employed. At higher degrees of melting (F > 20 - 25%) clinopyroxene should

also be consumed and the products of continued melting were modelled using the less well constrained, clinopyroxene-absent melting equation of Baker & Stolper (1994).

Although the REE composition of sample 92-LH14 was determined, its Yb concentration was considered unreliable, owing to its poor reproducibility and low beam intensities. In the model a source was therefore used with $(Dy)_N = (Yb)_N \approx 2.85$, similar to the estimated composition of the Earth's primitive mantle (McDonough, 1990).

| | D Values | | Initial Modal Composition (%) | | | Melt Proportions (%) | |
|---|---|---|---|---|---|---|---|
| | Dy | Yb | A | B | C | Sp. Lherz.† | Gt. Lherz. |
| **Clinopyroxene** | 0.51 | 0.52 | 17 | 12.5 | 10 | 71 | 41 |
| **Orthopyroxene** | 0.05 | 0.11 | 30 | 22.5 | 20 | 38 | 9 |
| **Olivine** | 0.004 | 0.023 | 50 | 60 | 60 | -22 | -13 |
| **Garnet** | 1.27 | 4.2 | 0 | 5 | 10 | 0 | 63 |
| **Spinel** | 0.0015 | 0.0045 | 3 | 0 | 0 | 13 | 0 |

**Table 4.6** Parameters used for the modelling of HREE abundances during the melting of a fertile lherzolite source. Mineral-melt distribution coefficients from Kelemen *et al.* (1990), with the exception of those for garnet (Set 3, Frey *et al.*, 1978). Melt proportions for garnet-absent and garnet-present melting from Baker & Stolper (1994) and Mysen (1970) respectively. Negative proportions refer to the production of olivine during the melting reaction.
†Once clinopyroxene exhausted, melt proportions altered to fit the equation 1.06 opx + 0.04 sp = 0.1 ol + liq (Baker & Stolper, 1994)

The HREE abundances of the Eastern Pyrenean peridotites match the trajectories calculated for the melting of a fertile lherzolite. The curves show that the low Dy/Yb ratios of some of the less depleted samples are consistent with the melting of a lherzolite source containing between 5 and 10% garnet, whilst others appear to have formed by melting of a garnet-absent source. The degree of melting required to produce the observed HREE profile of each sample was estimated from Figure 4.15 for both batch and fractional melting models. Once more, the degrees of melting calculated assuming fractional melting are lower than those calculated for a batch melting model (Figure 4.16)

In the absence of garnet, the melting trajectories produced by batch and fractional melting processes are virtually indistinguishable, however the two processes produce significantly different trends in garnet bearing sources. Exhaustion of garnet after 10 - 15% batch melting means the HREE are no longer buffered and the garnet signature of the source is lost. At

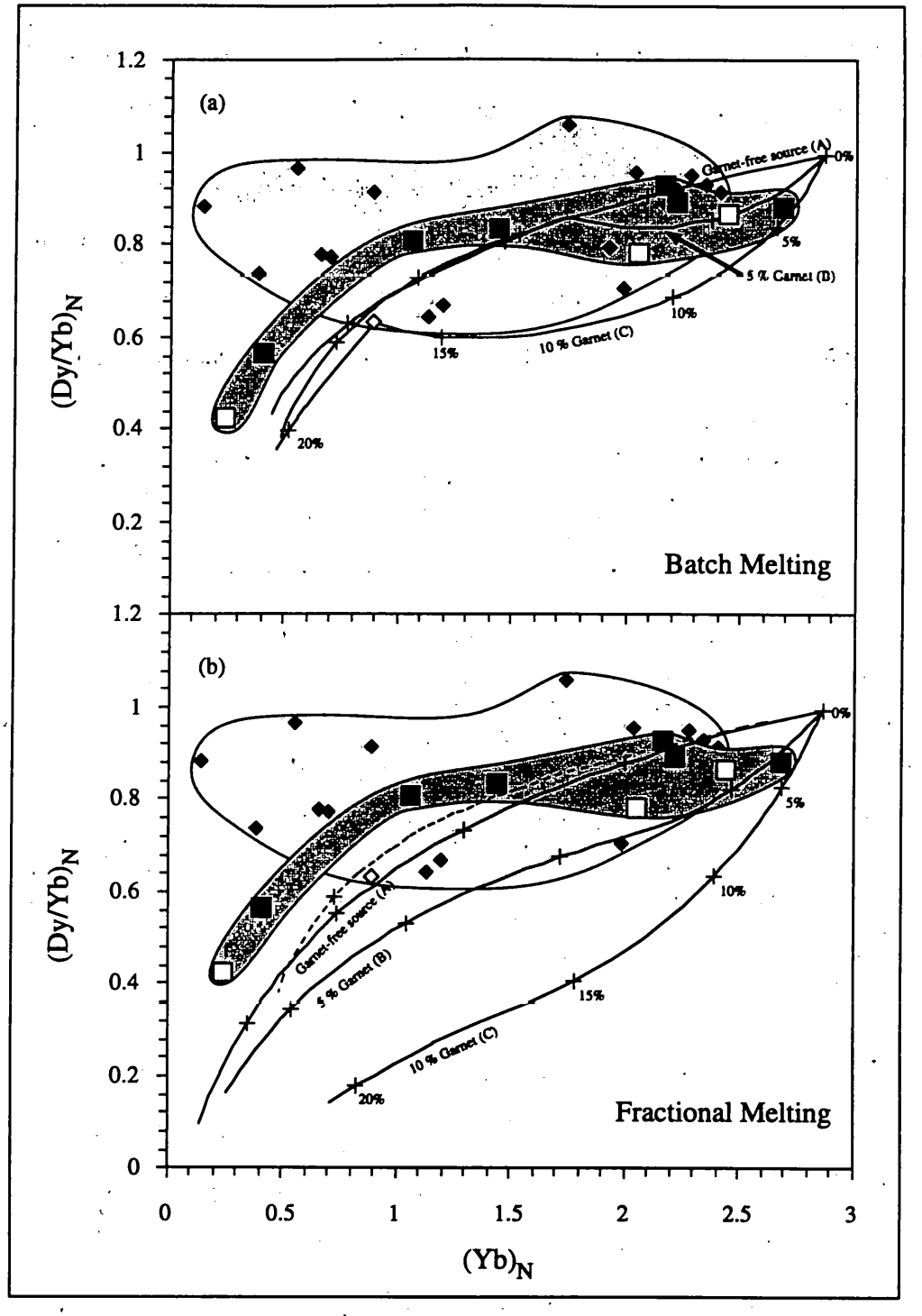


**Figure 4.15** Variation of Dy/Yb ratios with Yb abundances in peridotites of the Eastern Pyrenean ultramafic massifs, superimposed on the calculated variation of Dy/Yb ratios with Yb calculated for up to 25% melting of a peridotite source containing variable quantities of garnet. ■ Lherz, Freychinède and Pic de Géral data (this study); □ Fontête Rouge data (this study); ◆ Lherz, Freychinède and Pic de Géral data (Bodinier *et al.*, 1988); ◇ Fontête Rouge data (Bodinier *et al.*, 1988). Dy/Yb ratios calculated from data of Bodinier *et al.* (1988) using Dy abundances interpolated from Tb and Yb data. Crosses at 5% melting intervals. a) Non-modal batch melting. b) Non-modal fractional melting. Dashed line in (b) is the batch melting trajectory of a garnet-free source.

greater degrees of batch melting the residual peridotites follow similar trajectories to those derived from a garnet-free source. For fractional melting, however the HREE fractionation created in the presence of garnet during the initial stages of melting remains after the mineral

is consumed and HREE fractionation persists in the residue produced by continued melting. None of the more refractory peridotites analysed either in this study or by Bodinier *et al.* (1988) have HREE abundances similar to those predicted for large degrees of fractional melting of a source originally containing garnet, suggesting that either fractional melting only occurred in peridotites in which garnet was absent or that batch rather than fractional melting processes operated to generate the range of observed compositions.

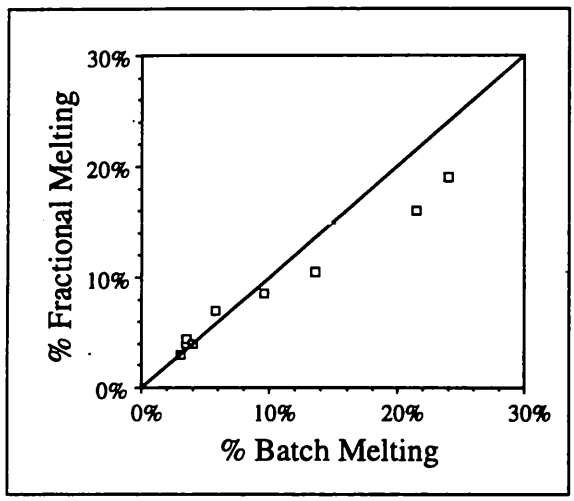


**Figure 4.16** Comparison of degrees of melting, F, estimated for both fractional and batch melting models from the whole-rock HREE composition of peridotites of the Eastern Pyrenean massifs illustrating the greater degrees of melting required by a fractional melting model for the production of similar residual peridotite compositions.

Given the assumptions required in each of the calculations and the widely different chemistries of the elements used, the agreement between results of the three methods is surprisingly good (Figure 4.17). The values of F calculated from the (FeO/MgO) ratios of the residual peridotites are generally higher than those calculated from their Ni contents, with a significant scatter at the lower degrees of melting. The degrees of melting calculated for the HREE abundances of the peridotites using a batch-melting model show considerably better agreement with the F values calculated using Ni than those calculated assuming fractional melting, further favouring this melting process.

The good agreement between the degrees of melting calculated independently from the peridotite Ni and HREE abundances using a batch melting model suggests these methods provide the best means of estimating the degree of melting experienced by the Eastern Pyrenean peridotites. The mean values of F calculated from the Ni abundance data are therefore used in the later discussions of the whole-rock and Re-Os geochemistry of the N.E. Pyrenean massifs.

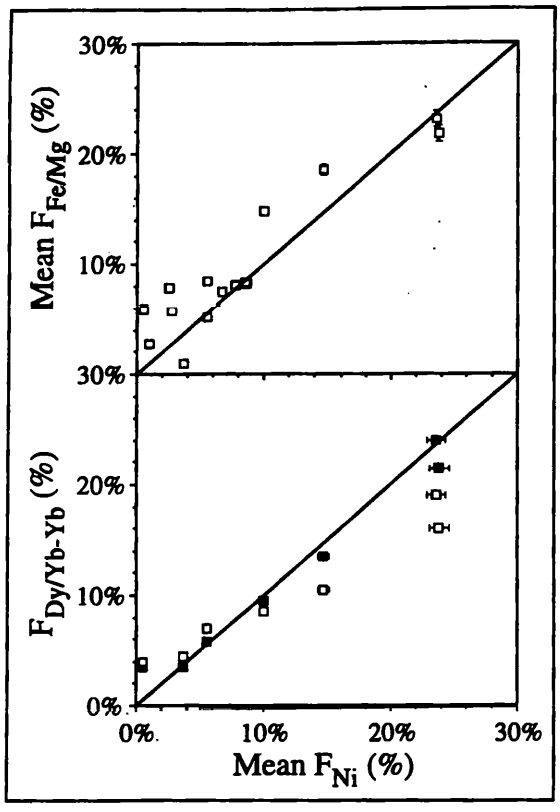


**Figure 4.17** Comparison of proportions of melt extraction calculated from the whole-rock Ni contents with those calculated from a) the whole-rock Fe/Mg ratios and b) the HREE compositions of the peridotites of the Eastern Pyrenean ultramafic massifs. Values of F calculated for both batch (■) and fractional melting (□) are illustrated in (b)

### *Melting Systematics*

### Major Elements

To test the two models of melt extraction the variation of $SiO_2$, $Al_2O_3$, FeO* and CaO were plotted as functions of the calculated degrees of melt extraction (Figure 4.18). As would be anticipated, these plots resemble those against MgO because of the approximate correlation of MgO content with the degree of melting. Included in Figure 4.18 are the compositions of residual peridotites following the extraction of melt from an undepleted peridotite source at pressures of 10 - 30 kbar, calculated using the mass balance equation (Equation 4.1) and the experimentally determined compositions of batch melts produced by Hirose & Kushiro (1993) and Baker & Stolper (1994). Unlike earlier melting studies (e.g. Jacques & Green, 1980; Takahashi & Kushiro, 1983; Takahashi *et al.*, 1993), the use of a diamond aggregate sandwich in these experiments prevented the compositions of the melts from being modified by the overgrowth of minerals during quenching. These melt compositions are therefore viewed as the best estimates of primitive upper-mantle melts.

The compositions of the majority of the Eastern Pyrenean peridotites match the predicted decrease in CaO and $Al_2O_3$ and the nearly constant FeO* contents with increasing degrees of melt extraction calculated for mantle residues with a source similar to 92-LH14. For an

homogeneous source, the degree of scatter of the data about the melting trends would be expected to decrease at smaller F. Although such a decrease is not observed in the plots of Figure 4.18, suggesting that the source was not homogeneous at the time of melting, the increasing relative error in the estimated value of F at low degrees of melting may also account for the scatter. The FeO* contents of several samples lie outside the range of compositions predicted from their estimated degrees of melt extraction and the FeO* contents of the experimental melts, indicating that additional processes may have occurred which altered the iron contents of the peridotites.

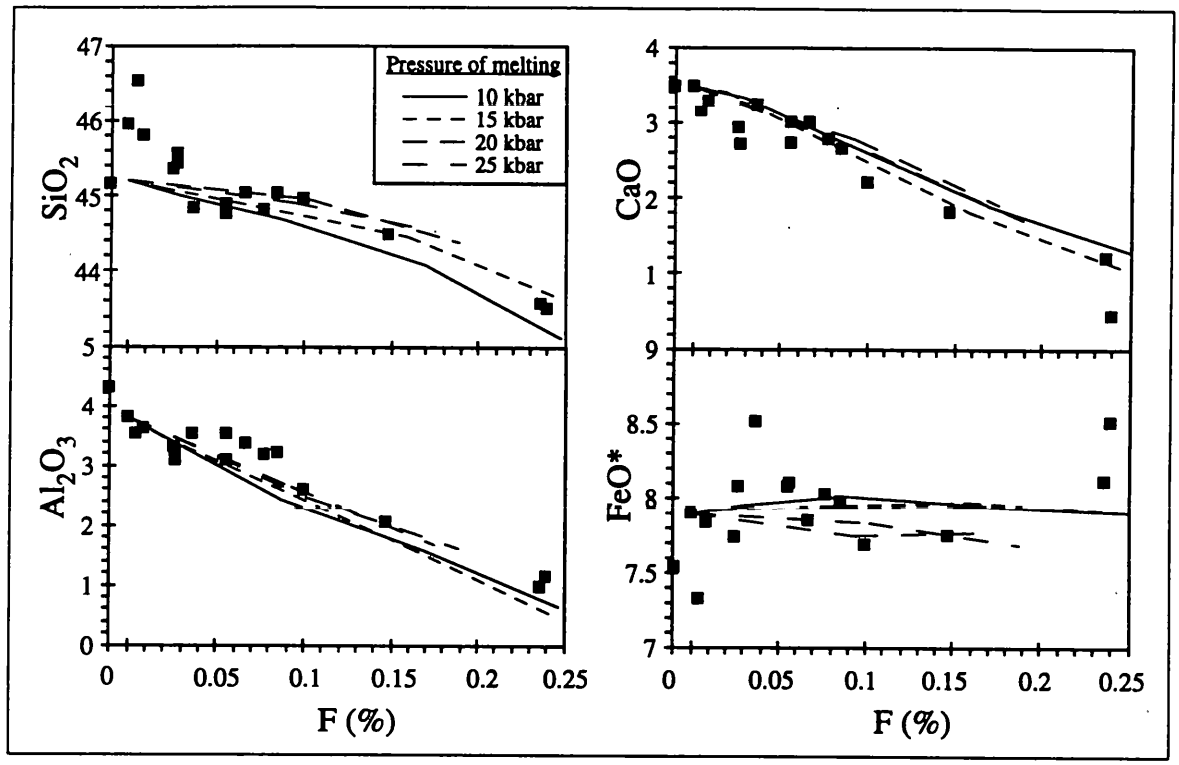


**Figure 4.18** Variation of the the $SiO_2$, $Al_2O_3$, FeO* and CaO contents of the peridotites of the Eastern Pyrenean massifs as functions of the calculated proportions of melt extracted. Shown for comparison are the trajectories of residues following the extraction of basaltic melts at 10 - 25 kbar from a source with a composition similar to sample 92-LH14. Melt Compositions are those determined by Hirose & Kushiro (1993). $SiO_2$ trajectories calculated for a source with a silica content similar to the upper mantle estimate of Jagoutz *et al.* (1979).

The $SiO_2$ - F array defined by the peridotite samples is inconsistent with the melting of a source with the silica content of 92-LH14. As noted previously, 92-LH14 is one of three samples exhibiting significantly elevated $SiO_2$ contents relative to both other peridotites collected from the Eastern Pyrénées and to peridotites from other orogenic massifs. Using the primitive mantle silica concentration proposed by Jagoutz *et al.* (1979), however, the

$SiO_2$ contents of the Eastern Pyrenean peridotites show excellent agreement with the calculated residues after melt extraction and define a curved trajectory of decreasing $SiO_2$ with increasing F. The non-linear decrease in $SiO_2$ as a function of F favours a melting model in which compositionally variable melts, produced by a range of degrees of melting, were extracted from a primitive mantle source. The high silica contents of 92-LH11, 92-LH14 and 92-LH19, however, cannot be explained by melt extraction alone.

The variation of the CaO content of experimental melts with increasing degrees of melting suggests that the CaO content of the peridotites should define a modest S-shaped trajectory as a function of F. Although the determined CaO contents plot close to this trend and may be fitted by a non-linear trend as a function of F (Figure 4.18), they are displaced to lower values than those predicted from the compositions of the experimental melts and exhibit considerable scatter, such that they may also be consistent with a simpler, linear trend. The variation of the peridotite CaO contents as a function of F, therefore, cannot confirm the extraction of compositionally homogeneous melts, as supported by the variation of the $SiO_2$ contents. The observed displacement of the CaO contents of the residual peridotites towards lower values and the variability of the CaO contents of peridotites formed by similar degrees of melting may suggest that some variation existed in the composition of the source prior to melting.

The decreasing $SiO_2$ and increasing $FeO^*$ contents of the experimental melts with increasing pressure are consistent with the observed decrease in the stability field of olivine relative to orthopyroxene and clinopyroxene with melting (O'Hara, 1968; Presnall *et al.*, 1979). As a consequence, the calculated compositions of residues formed by similar degrees of melting at increasing pressures should be progressively higher in silica and lower in iron. Although, in theory, the trends defined by the $SiO_2$ and $FeO^*$ concentrations in the calculated residues may be used to estimate the pressure at which melting occurred for each sample, the predicted correlation of high silica with low iron contents, at similar degrees of melting, is not observed in the data for the Eastern Pyrenean peridotites. Although the lack of correlation may result from either insufficient analytical precision in the whole-rock analyses or minor modification of the $SiO_2$ or $FeO^*$ contents since melting, it is also likely that melting was polybaric (e.g. in an ascending diapir), hence would not be expected to

record melting at a single depth. On the basis of the whole rock major element compositions of the N.E. Pyrenean peridotites, therefore, it is not possible to determine the pressure at which melting occurred.

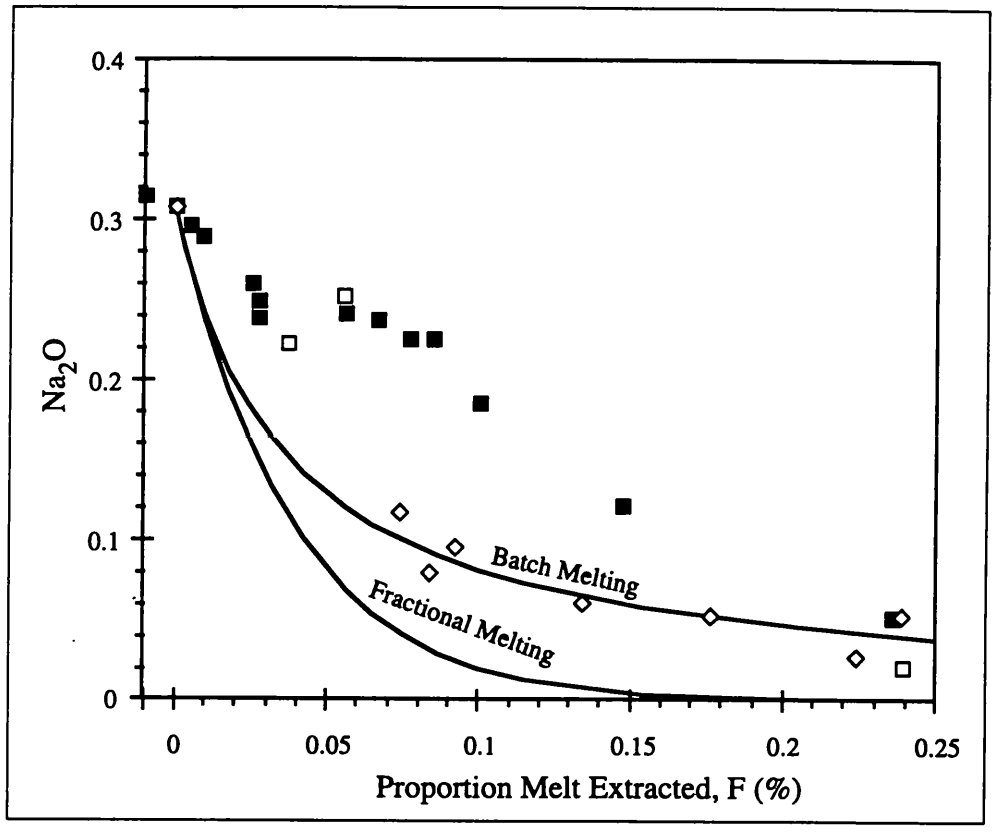


**Figure 4.19** Variation of $Na_2O$ as a function of melt extraction from the peridotites of the Eastern Pyrenean ultramafic massifs. The $Na_2O$ contents of the residues formed by the extraction of partial melts formed by batch and fractional melting of 92-LH14 are also shown, calculated assuming $D_{Na}$ ~ 0.037. ■ Peridotites from Lherz, Freychinède, Prades and Pic de Géral; □ Peridotites from Fontête Rouge; ◇ residues after the removal of the experimental melts of Baker & Stolper (1994).

## Incompatible Elements: The Effects of Metasomatism

During both batch and fractional melting processes, the concentrations of the incompatible elements should become rapidly depleted in the residues, defining highly curved trends as a function of the degree of melting (Elthon *et al.*, 1992). The $Na_2O$ contents of the Eastern Pyrenean peridotites, however, define a linear array extending from ~0.3 wt% at 0% melting to zero at ~25% melting (Figure 4.19), which contrasts strongly with the curved trajectory of the residues formed during the batch melting experiments of Baker & Stolper (1994). Fractional melting of an undepleted source would have produced even greater depletion of the peridotites in $Na_2O$, hence it is also unable to account for the observed linear array.

Similar linear correlations between $Na_2O$ and either the degree of melt extraction or the abundances of MgO or $Al_2O_3$ have been reported for other orogenic massifs (e.g. Ronda, Frey *et al.*, 1985; Reisberg, 1988; Lanzo, Italian western Alps, Bodinier, 1988; Trinity, California, Quick, 1981). Although these linear correlations may be explained by continuous melting of the peridotites and the retention of trapped melt in the residues, the volumes of melt (5 - 10%) that must remain in the residue after melting are physically unrealistic, being unstable under normal mantle conditions and liable to escape along grain boundaries (McKenzie, 1984). Calculations show that basaltic melt fractions greater than ~ 2% should separate rapidly from the peridotite matrix (Ahern & Turcotte, 1979: McKenzie 1985), implying that the presence of 5 - 10% trapped melt is unlikely and that batch melting processes may also be unrealistic beyond a few percent.

Plots of the incompatible trace element abundances as functions of melt extraction display similar arrays to that defined by $Na_2O$ (Figure 4.20). The Sr and LREE abundances in the peridotites of the Lherz, Pic de Géral and Prades massifs define linear trends extending from the compositions of the least depleted sample to almost zero concentration in the most depleted samples at ~25% melt extraction. The peridotites of the Fontête Rouge massif, however, plot below these arrays, close to the trajectories predicted for non-modal melting of the least depleted peridotites.

The linear arrays defined by the incompatible elements as functions of either MgO or the degree of melt extraction are inconsistent with an origin purely by melt depletion of a fertile mantle source and indicate that the peridotites must have interacted with an incompatible element enriched component subsequent to melting. A linear correlation between LREE abundances and whole rock major element depletion is also exhibited by clinopyroxenes separated from the porphyroclastic peridotites of the north-eastern Pyrénées (Downes *et al.*, 1991). Downes *et al.* (1991) accounted for the difference between the pronounced LREE depletion of the protogranular Fontête Rouge peridotites and the less LREE-depleted profiles of the porphyroclastic peridotites of the other massifs by LREE metasomatic alteration of the porphyroclastic lherzolites, as indicated by the presence of accessory Ti-pargasite. Corrected to the time of emplacement into the crust (~100 Ma), they showed that the Sm-Nd isotope systematics of the porphyroclastic peridotites define a linear array on a Nd isochron diagram,

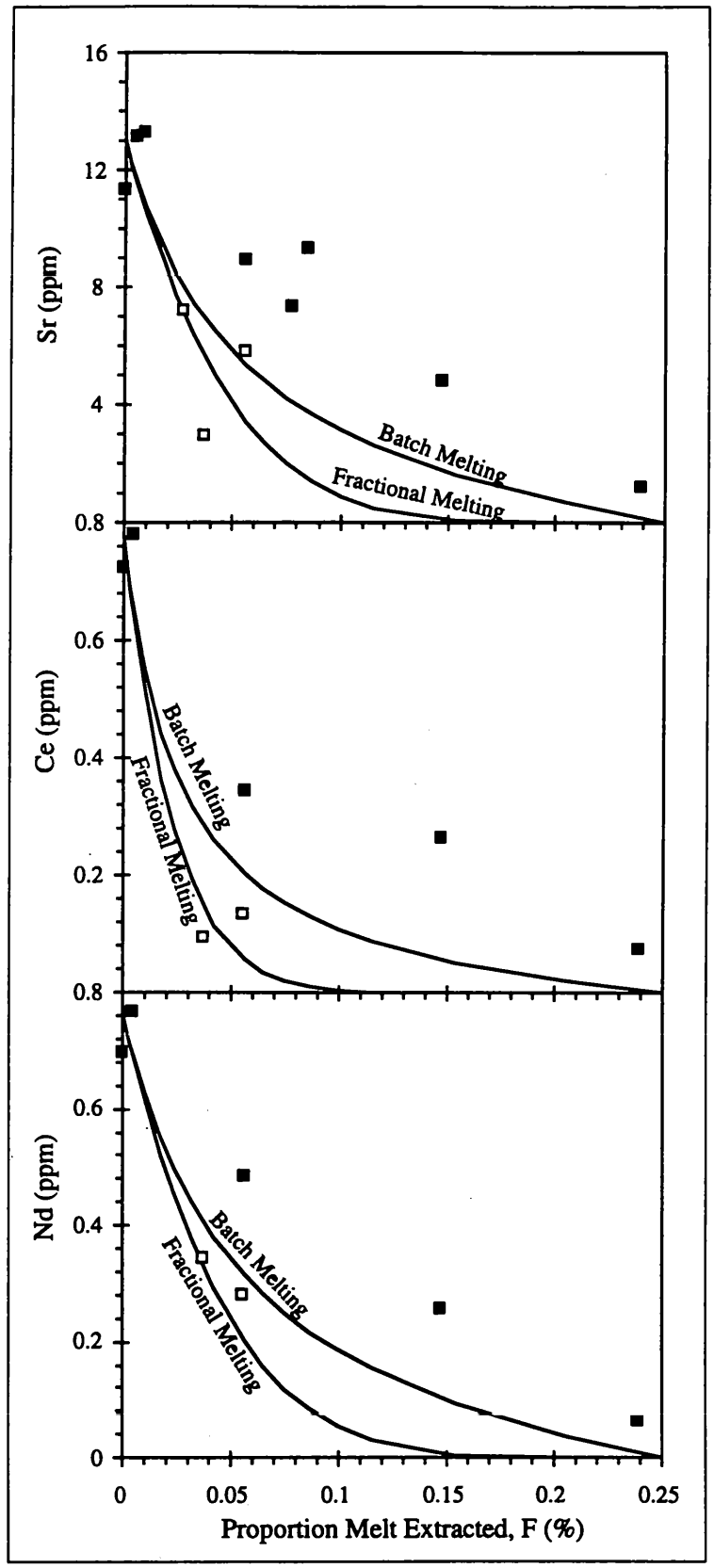


**Figure 4.20** Variation of Sr, Ce and Nd as a function of melt extraction from the peridotites of the Eastern Pyrenean ultramafic massifs. Only those samples with low total carbon contents (C ≤ 500 ppm) are plotted. The majority of the samples (■) form linear arrays extending from almost zero concentration at high degrees of melt extraction to approximately half the concentrations estimated for the undepleted mantle. Samples collected from the Fontête Rouge massif (□) plot below the arrays defined by the incompatible elements of the other massifs, close to the predicted concentrations for residues after non modal melting of a slightly depleted lherzolite source. Melting residues calculated using the melting equation of Baker & Stolper (1984) and the partition coefficients of Kelemen *et al.* (1990). Sr mineral melt partition coefficients assumed to be similar to those of Nd.

extending from the protogranular peridotites of the Fontête Rouge massif towards the field of the Cretaceous alkali basalts. Although this array may be interpreted as the time integrated response to Sm/Nd fractionation, it may also reflect the addition of the metasomatic component responsible for the formation of the Ti-pargasite.

The absence of Ti-pargasite in the protogranular peridotites of the Fontête Rouge massif and the displacement of their incompatible element abundances from the arrays defined by the porphyroclastic peridotites of the other massifs suggests that the incompatible element compositions of these peridotites may not have been affected by metasomatism since the initial melting event. The high $\varepsilon_{Nd}$ of the unmetasomatised Fontête Rouge peridotites may imply that these samples have been isolated from the convective mantle for hundreds of millions of years. Figure 4.20 shows that the incompatible element abundances of these samples would fit with an origin involving either batch or fractional melting of a mildly depleted peridotite source. However, there are insufficient samples from this massif to determine which of the two processes may have operated.

In conclusion, most of the whole-rock elemental data for the peridotites of the north-eastern Pyrenean massifs are consistent with the extraction of a compositionally variable partial melt, formed by a range of degrees of batch melting. Some aberration is observed in the $SiO_2$ and FeO* contents of the peridotites, suggesting these elements may also reflect the effects of undefined alteration processes. The scatter of the data when plotted as functions of the degree of melting suggest that some source variation may have been present prior to melting.

Although the melting depth cannot be estimated from the variation of the major element compositions of the residues, modelling of the fractionation of the HREE ratios during melting (and the absence of Eu anomalies in those samples free from Ba interference during analysis) suggests that melting may have occurred close to the spinel lherzolite - garnet lherzolite transition. The incompatible element compositions of the peridotites require that the majority of the massifs have been affected by metasomatism subsequent to melting. Isotopic evidence suggests that this metasomatism predates emplacement in the crust, however there is insufficient evidence to relate it to any particular event.

### 4.2.9 Mantle Refertilisation

Recently, Elthon (1992) proposed that the chemical trends in abyssal peridotites may result predominantly from a processes of refertilisation rather than fractional partial melting, as had been suggested by various authors (Dick *et al.*, 1984; Dick, 1989; Johnson *et al.*, 1990). Elthon (1992) proposed that the compositions of the abyssal peridotites reflect the effects of a two stage process involving initial fractional melting, depleting the sub-oceanic mantle to a point where clinopyroxene is eliminated, followed by low-pressure refertilisation of the depleted harzburgite by the addition of up to 10% of a strongly depleted $Na_2O$-poor, $TiO_2$-poor, $SiO_2$-rich basaltic melt (Elthon *et al.*, 1992). Subsequent recrystallistion of the melt/residue mixture creates cpx-bearing harzburgites and lherzolites with the observed range of compositions. His rejection of fractional melting as the dominant control on the composition of abyssal peridotites was principally based on the variation of $Na_2O$ with MgO, with significantly greater $Na_2O$ concentrations than expected for realistic degrees of fractional melting of either primitive or depleted upper mantle material, as evident in the Pyrenean peridotite samples.

An analogous model may be presented for the origin of the peridotites of the Eastern Pyrenean ultramafic massifs, in which the elemental trends reflect the variable addition of basaltic melt to a highly depleted mantle residue. In the simplest case the refertilisation process may be considered to be the mixing of two components: a highly depleted harzburgite residue, characterised by the most refractory samples analysed, and the basaltic melts which migrated into the residues, giving rise to the linear arrays observed between MgO and both the compatible and the incompatible element abundances for the majority of the peridotites.

Figure 4.21 shows the major element refertilisation trends calculated for the addition of 0 - 30% of five primitive basaltic melts. Details of the end member compositions are listed in Table 4.7. Basalt compositions were selected from the experimental melts produced in the experiments of Hirose & Kushiro (1993) and cover a range of pressures. A harzburgite with a composition similar to that of the most refractory Eastern Pyrenean peridotites was chosen as the depleted end member.

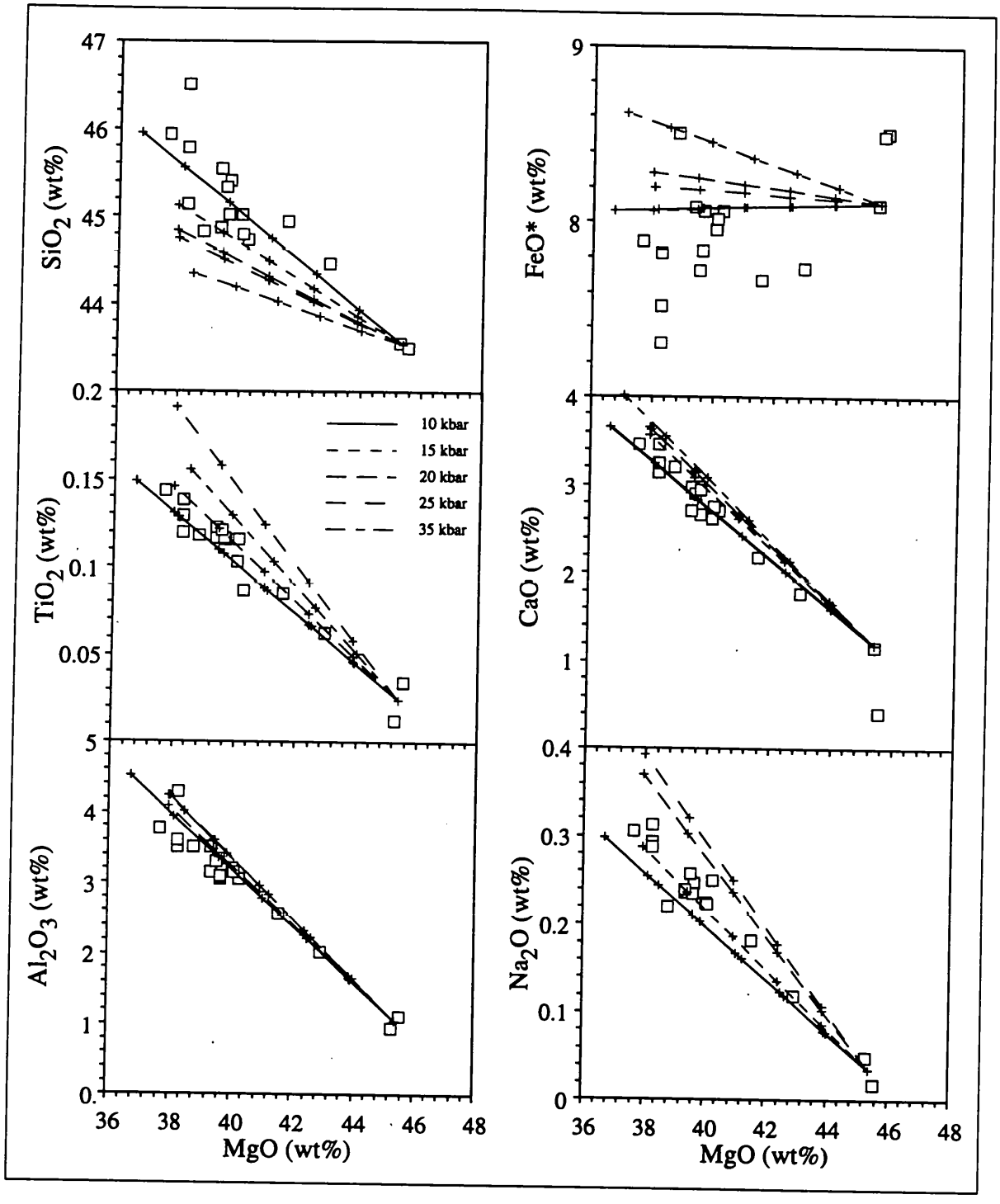


**Figure 4.21** Comparison of refertilisation trends for the addition of up to 30% basaltic melt to a depleted harzburgite mantle composition (crosses placed at 5% intervals). Basaltic melt compositions taken from the experiments of Hirose & Kushiro (1993) for melting at 10 - 30 kbar. Depleted mantle composition (excluding FeO* and CaO) is taken as the mean of samples 92-LH12 and 92-FT5. FeO* and CaO contents of depleted mantle end member taken as those of 92-FT5.

The steep $SiO_2$ - MgO array requires that the refertilising melt was relatively enriched in silica, indicating that it may have originated from relatively shallow depths. The significantly higher $SiO_2$ contents observed in samples 92-LH11, 92-LH14 and 92-LH19 would be consistent with refertilisation by melts originating from shallower depths than those which were added to other peridotites of the massifs. Of the experimental melt compositions

documented by Hirose & Kushiro (1993), only those produced by up to 30% melting at 10 - 15 kbar pressure can reproduce the major element trends observed in the Eastern Pyrenean peridotites. These melts are significantly more enriched in incompatible elements than the 'D' end-member MORB composition used by Elthon (1992) for the refertilisation of oceanic peridotites ($TiO_2$ ~ 0.1 wt%, $Na_2O$ ~ 0.5 wt%).

| | Melts | | | | | Residue |
|---|---|---|---|---|---|---|
| | 10 kbar | 15 kbar | 20 kbar | 25 kbar | 30 kbar | Composition |
| $SiO_2$ | 51.59 | 49.88 | 48.74 | 48.37 | 46.77 | 43.54 |
| $TiO_2$ | 0.44 | 0.45 | 0.51 | 0.69 | 0.55 | 0.025 |
| $Al_2O_3$ | 12.58 | 13.78 | 13.16 | 13.8 | 12.87 | 1.06 |
| FeO* | 7.95 | 7.92 | 8.8 | 8.47 | 9.81 | 8.11 |
| MgO | 16.41 | 15.74 | 15.69 | 15.88 | 17.82 | 45.39 |
| CaO | 9.42 | 10.69 | 11.06 | 10.93 | 10.63 | 1.19 |
| $Na_2O$ | 0.91 | 1.04 | 1.37 | 1.46 | 0.87 | 0.036 |
| F† | 33% | 29% | 22% | 21% | 35% | |

**Table 4.7** Compositions of melts and depleted residue used to model refertilisation trends. Melt compositions taken from Hirose & Kushiro (1993). Composition of depleted residue, excluding CaO and FeO*, obtained from the mean composition of 92-LH12 and 92-FT5. CaO and FeO* contents obtained from 92-FT5 alone, owing to the significant difference between the abundances of these elements in the two samples.
†Degree of melting estimated from $Na_2O$ content of melt by Hirose & Kushiro (1993), assuming total incompatibility of the element in the residue and therefore reflects a maximum value.

The linear arrays defined by the incompatible elements as functions of MgO or F are consistent with a model involving refertilisation of depleted mantle material. Figure 4.20 shows that 10 - 15% fractional melting may easily remove the incompatible elements from the refractory peridotites. Following refertilisation, therefore, the incompatible element compositions of the peridotites will be directly proportional to the quantity of melt added and define linear mixing arrays from the refractory peridotite composition towards the composition of the melt.

In his study of abyssal peridotites, Elthon (1992) demonstrated that the variation of ratios observed in the clinopyroxenes of abyssal peridotites may be produced by the refertilisation of depleted harzburgite by up to 10% depleted basalt melt (with $[Ce]_N = 1.5$, $[Ce/Yb]_N = 0.5$). Figure 4.22 shows that the REE compositions of clinopyroxenes separated from the peridotites of the Eastern Pyrenean massifs lie on the extension of the abyssal peridotite array (Johnson *et al.*, 1990). However, to reproduce the higher $[Ce]_N$ contents of

the Pyrenean peridotites, the basaltic melts responsible for the refertilisation must have been significantly more enriched than the composition assumed by Elthon.

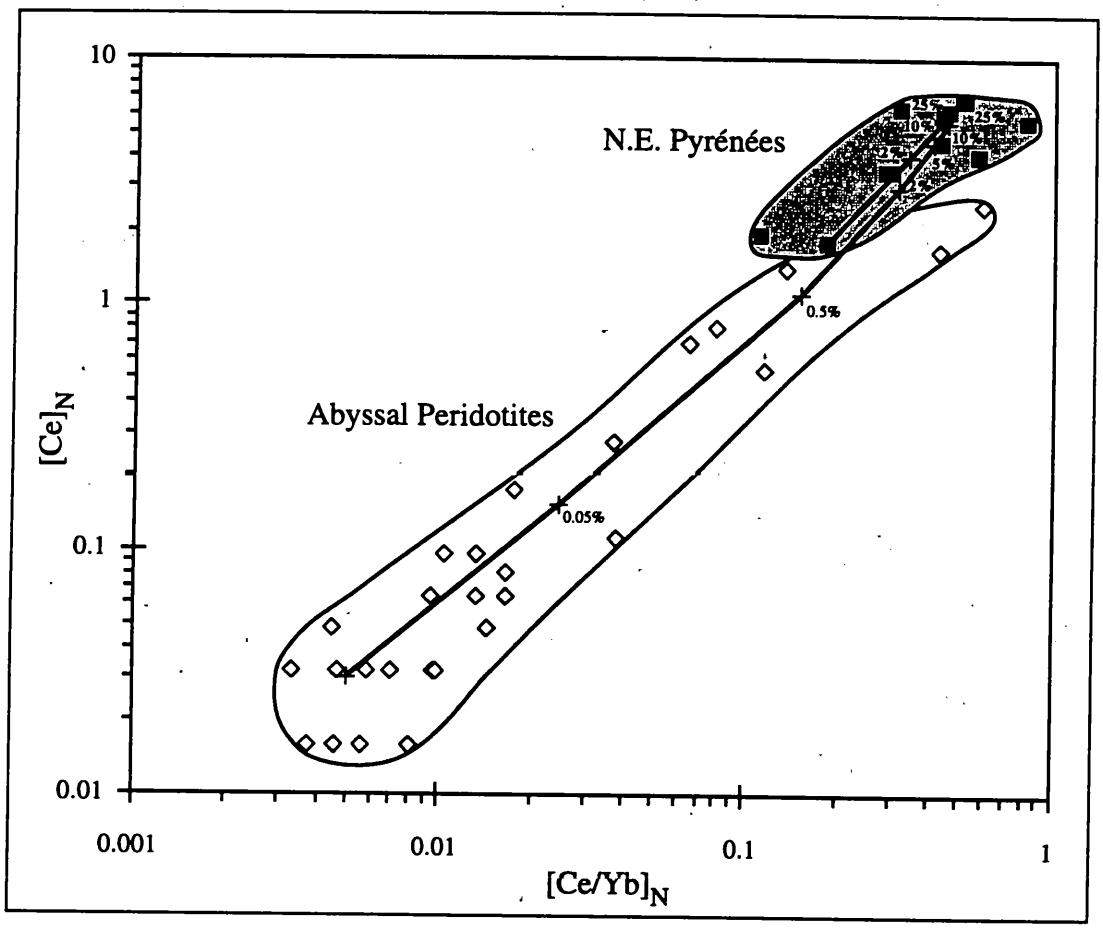


**Figure 4.22** Chondrite normalised Ce abundances and Ce/Yb ratios for clinopyroxenes in abyssal peridotites and peridotites from the Eastern Pyrénées. Solid lines indicate the trends for the addition of up to 25% basaltic melt to depleted mantle. For melt compositions see text. Abyssal peridotite clinopyroxene compositions from Johnson *et al.* (1990). Eastern Pyrenean clinopyroxene data from Downes *et al.* (1991).

Figure 4.22 illustrates the refertilisation trends for two different depleted end members: a harzburgite similar to the most depleted abyssal peridotite of Johnson *et al.* (1990), with 2% clinopyroxene ($[Ce]_N = 0.03$, $[Ce/Yb]_N = 0.005$); and a clinopyroxene-poor lherzolite of Fontête Rouge, with 5% clinopyroxene ($[Ce]_N = 1.76$, $[Ce/Yb]_N = 0.18$; Downes *et al.*, 1991). The refertilising melts were assumed to possess $[Ce]_N \sim 5$ and $[Ce/Yb]_N \sim 0.5$ and to recrystallise as 70% clinopyroxene and 30% (olivine + orthopyroxene + spinel). Despite the significantly different incompatible element compositions of the two depleted end-members, the compositions of the clinopyroxenes of the Eastern Pyrenean peridotites are consistent with the addition of similar quantities of melt to either residue. If the peridotites are assumed to be formed by the refertilisation of a uniformly depleted source, approximately 2% basalt

would be required for the production of clinopyroxene-poor lherzolites, whilst the spinel lherzolites may be produced by the addition of 10 - 25% basaltic melt.

| | 92-FR3 | 92-LH11 | 92-LH14 | 92-LH17 | 92-LH3 | 92-PG2 |
|---|---|---|---|---|---|---|
| $Na_2O$ (wt%) | 0.31 | 0.29 | 0.31 | 0.24 | 0.18 | 0.12 |
| **Proportion melt added** | 30% | 28% | 29% | 22% | 17% | 10% |
| | | | Melt Composition (ppm) | | | |
| **La** | 0.212 | 0.755 | 0.428 | 0.174 | n.d. | 0.626 |
| **Ce** | 1.31 | 2.60 | 2.29 | 1.27 | 1.75 | 1.92 |
| **Nd** | 1.64 | 2.57 | 2.23 | 1.93 | 1.74 | 1.93 |
| **Sm** | 0.713 | 0.927 | 0.878 | 0.885 | 0.687 | 0.750 |
| **Dy** | 1.53 | 1.76 | 1.91 | 2.08 | 1.44 | 1.60 |
| **Er** | 1.04 | 1.20 | 1.31 | 1.45 | 1.01 | 1.09 |
| **Yb** | 1.06 | 1.17 | n.d. | n.d. | 1.02 | 1.12 |

**Table 4.8** Calculated proportions of melt required to reproduce the $Na_2O$ contents of the peridotites of the Eastern Pyrenean ultramafic massifs and REE abundances in refertilising melts. Both the proportions of refertilising melt and the REE composition of the melt were calculated assuming a depleted mantle composition similar to 92-LH12 (0.02 wt%). The $Na_2O$ content of the refertilising melt assumed to be ~1 wt%. REE compositions calculated by mass balance from the proportion of melt added and the REE composition of peridotites.

The REE compositions of the refertilising melts may be estimated from mass balance calculations (Table 4.8), using the REE compositions of the peridotites and melt proportions calculated from the peridotite $Na_2O$ contents. For these calculations the composition of the depleted mantle end-member prior to refertilisation was assumed to be similar to sample 92-LH12, whilst the $Na_2O$ content of the melt was taken as ~1 wt%. The calculated REE compositions of the melts mirror the LREE depletion observed in the peridotites, with $[Ce/Yb]_N$ = 0.32 - 0.58 and $[Ce]_N$ = 2 - 4.1, and resemble the REE profiles of N-type MORB (Figure 4.23). The lower REE abundances calculated for the melt relative to N-MORB would be consistent with an origin involving large degrees of melt extraction from a depleted MORB-mantle source.

Although a refertilisation model can explain the whole-rock elemental compositions of the Eastern Pyrenean peridotites, it is difficult to reconcile the shallow origin of the refertilising melts, implied by the peridotite major element abundances, with the estimated pressures at which the associated pyroxenite layers were emplaced (12 - 15 kbar; Sautter & Fabriès, 1990) and the possibility that these pressures reflect only the last stage of a more

complex history of sub-solidus recrystallisations, possibly starting at considerably higher pressures. The absence of textural evidence for refertilisation in the peridotites of the Eastern Pyrénées requires that the depleted peridotites and refertilising melts were intimately mixed either during or subsequent to refertilisation. Given that such mixing must have predated the introduction of the pyroxenite layers and the shallow origin of the refertilising melts (implied by their low silica contents), refertilisation of the peridotites would have to have taken place at relatively shallow depths, prior to the transportation of the peridotites to deeper parts of the mantle and the emplacement of the anhydrous pyroxenite veins. Although such a sequence of events cannot be dismissed as impossible (e.g. the peridotites may represent ancient subducted oceanic lithosphere, which later became incorporated into the continental mantle lithosphere), it is too complex to be adequately constrained by the available data.

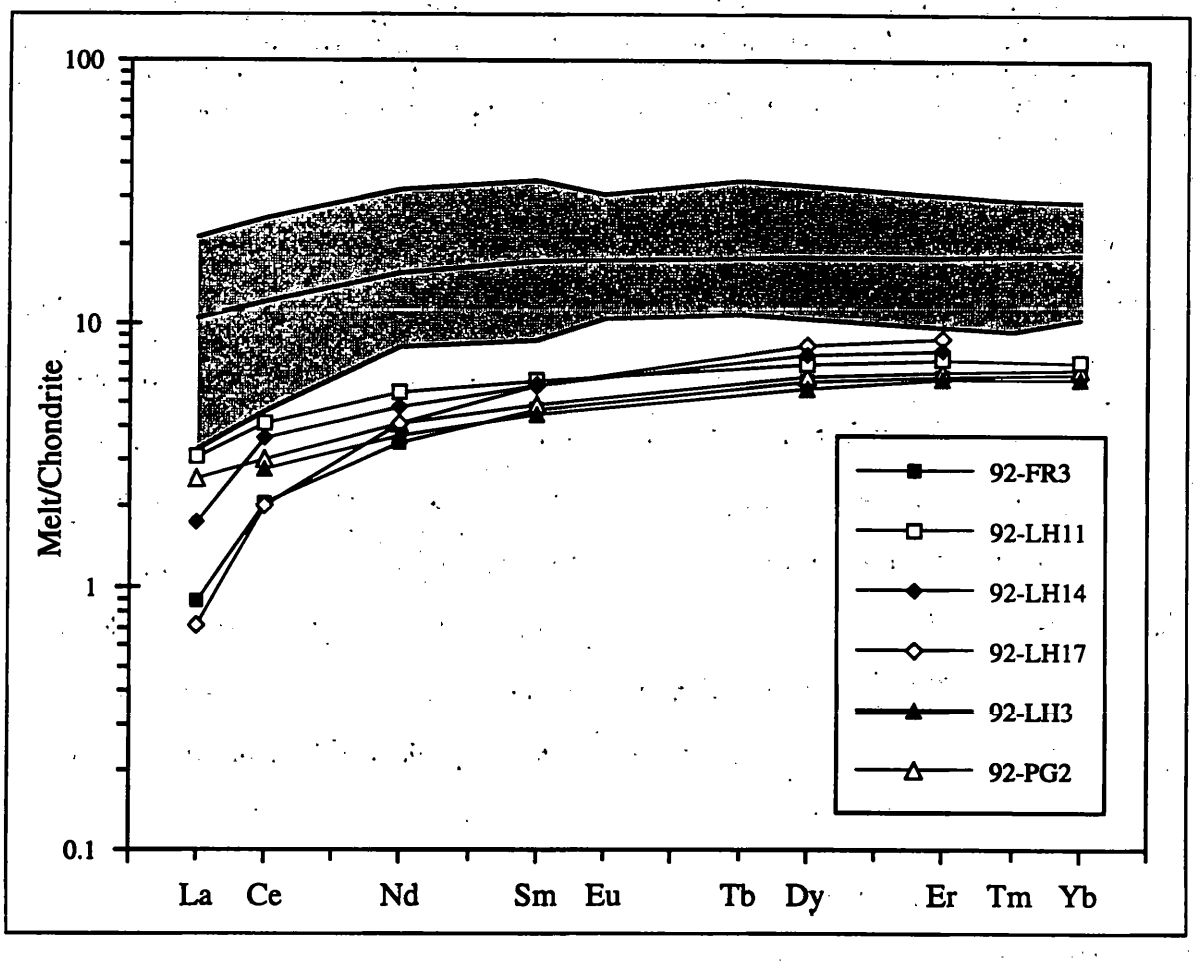


**Figure 4.23** Calculated chondrite normalised REE abundances of refertilising melts calculated by mass balance, assuming a depleted end member composition similar to that of 92-LH12 and calculating the proportion of melt added from the $Na_2O$ contents of the peridotites, assuming ~1 wt% $Na_2O$ in the melt. The shaded field illustrates the range of North Atlantic N-type MORB REE abundances from Schilling *et al.* (1983), whilst the average N-MORB estimate of Sun & McDonough (1989) is shown by the dashed line. Chondrite normalising values taken from McDonough & Frey (1989).

In conclusion, the compositions of the peridotites of the N.E. Pyrenean massifs may be consistent with a similar model to that proposed by Elthon (1992) for the compositions of abyssal peridotites, in which the peridotites represent fertile mantle which underwent extensive melting, producing a refractory harzburgitic residue, followed by refertilisation by a basaltic melt. To produce the range of compositions observed in the Pyrenean massifs, a $Na_2O$-poor, $SiO_2$-rich melt, formed by relatively large degrees of melting at low pressures would be required. In contrast to the model proposed by Elthon (1992), the refertilising melt was derived from a relatively undepleted source, with REE profiles resembling those of N-MORB. If refertilisation processes created the range of whole-rock elemental compositions observed in the N.E. Pyrenean massifs, then a complex history involving considerable vertical transport of the peridotites would also be required

### 4.2.10 Conclusions

The variation in the major and trace element compositions of the peridotites of the Eastern Pyrenean massifs may originate from a process of two component mixing or unmixing, involving either the extraction of melt from an undepleted peridotite source or the refertilisation of depleted mantle material. On the basis of the peridotite whole-rock elemental abundances, however, it is not possible to distinguish between these complementary processes.

The range of whole-rock elemental compositions of the peridotites of the Eastern Pyrenean massifs would be consistent with the extraction of between 0 and approximately 25% basaltic melt, formed by batch melting of a source similar to estimates of the primitive mantle. Although a batch melting model may explain adequately the major and compatible trace element trends of the Eastern Pyrenean peridotites, it is unable to account for the linear correlation between the incompatible element abundances and the degree of melt extraction exhibited by the major element composition of the peridotite samples. These linear arrays suggest that the incompatible element compositions of the the majority of the massive peridotites have been affected by metasomatism subsequent to melting, which may be associated with the presence of Ti-pargasite in the massifs. The absence of this mineral from the peridotites of the Fontête Rouge massif (whose incompatible element compositions plot

off the correlations defined by the other massifs), however, suggests that this massif may not have been affected by the same metasomatic event.

Fractionation of the HREE in the peridotites from the Fontête Rouge massif suggests that approximately 5% garnet may have been present in these peridotites during melting. The HREE compositions of peridotites collected from other massifs in the region, however, show no pronounced fractionation and plot along the trends predicted for the melting of a garnet-free source. From the contrasting HREE profiles of the two sets of massifs it is inferred that the peridotites of the Fontête Rouge massif may have experienced melting at greater depths than those from Lherz, Freychinède, Pic de Géral or Prades. The agreement between the degree of melt extraction calculated from the Ni contents of the peridotites and that estimated from models of the variation of their HREE abundances during melting suggests that batch rather than fractional melting processes may have operated to generate the range of compositions observed in the Pyrenean massifs.

Alternatively, the range of major and trace element compositions of the Eastern Pyrenean peridotite massifs may be reproduced by the refertilisation of depleted mantle peridotite by the addition of a low-$Na_2O$, high-$SiO_2$ basaltic melt. Suitable melts may be produced by large degrees of melting ($\geq$ 30%) at relatively shallow depths (10 - 15 kbar). The calculated REE profile of the refertilising melt resembles that of normal MORB, however its REE concentrations would have been significantly below the range of values measured for erupted melts, consistent with the high values of F required to reproduce the major element trends. The low pressure of melt generation relative to estimates of the pressures of pyroxenite emplacement would require that, following refertilisation, the peridotites were transported to greater mantle depths.

Although interaction with carbonate-rich fluids has modified the Sr abundances of the peridotite whole-rocks, low temperature processes appear to have had little effect on the other major or trace element abundances of the Eastern Pyrenean peridotites. Ratios between elements of similar compatibility during magmatic processes are unrelated to either the degree of serpentinisation (estimated from the loss on ignition) or the amount of carbonate minerals present in the sample (estimated from the total carbon content).

## 4.3 Massif Central Ultramafic Xenoliths

### 4.3.1 Geological Setting

The Massif Central volcanic province covers a large area of uplifted Hercynian crystalline basement (composed primarily of schists, gneisses and granitoid intrusions) and is characterised by lava flows, scoria cones and plugs of undersaturated alkalic basalt (Figure 4.24). Volcanism in the region commenced at ~20 Ma, although the majority of the exposed lavas are between 1 and 4 Ma old. The alkaline volcanic activity is spatially associated with a system of grabens, now infilled by lacustrine sediments (e.g. the Aurillac and Limagne basins), formed during extension of the region since the Oligocene.

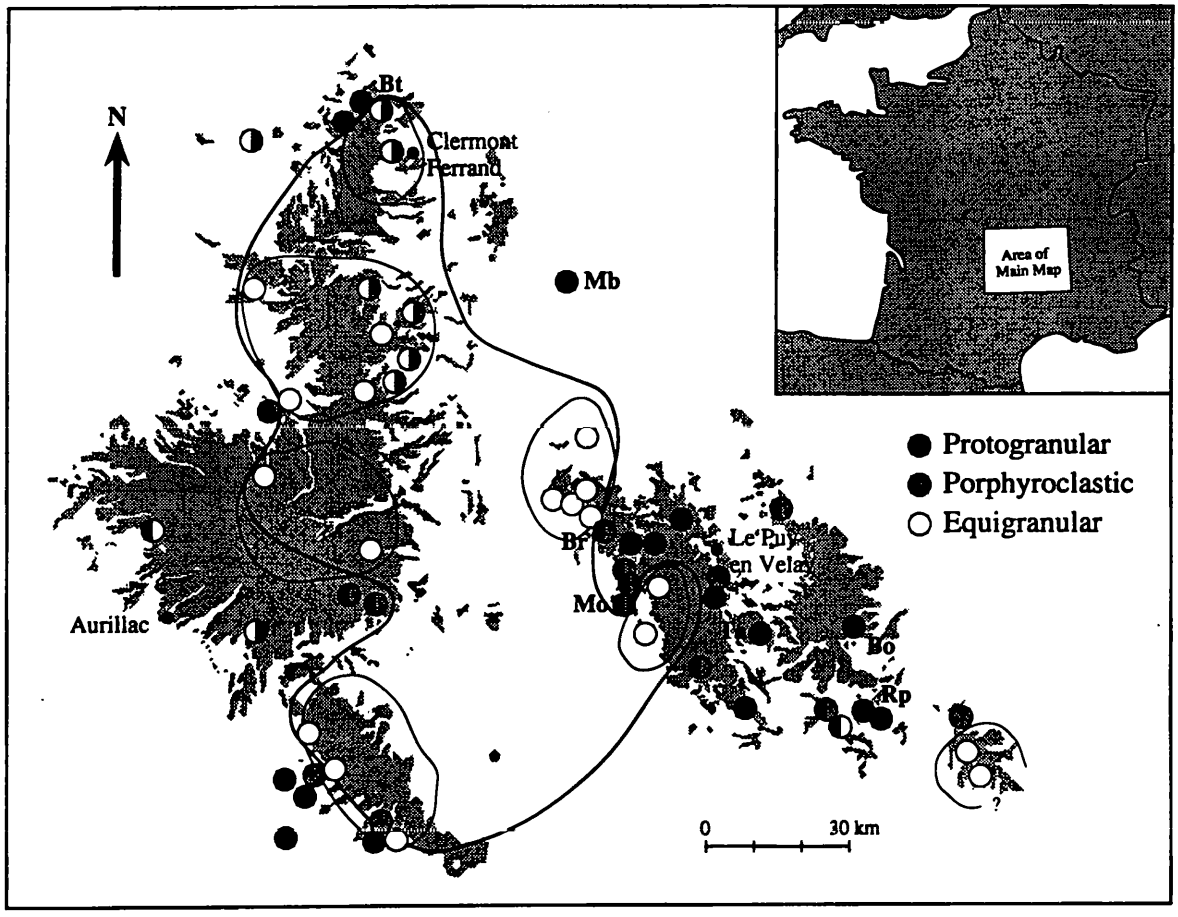


**Figure 4.24** Distribution of sampling locations and principal xenolith textures within the Massif Central volcanic province. Vents in which a mixture of xenolith textural types occur are marked by parti-coloured symbols. Bo, Maar de Borée; Br, Mont Briaçon; Bt, Puy Beaunit; Ms, Monistrol d'Allier; Rp, Ray Pic; Ta, Tarreyres; Z, Zanière. Thick lines, possible outline of mantle diapir. Thinner lines, possible outline of smaller diapirs (after Coisy, 1977). Stippled field, outcrop of Tertiary and Quaternary volcanic rocks.

Although mantle xenoliths may be found in volcanic rocks of all ages, they are particularly abundant in the younger lavas (Coisy & Nicholas, 1978). The host basalts for

these xenoliths possess significantly lower silica contents than other basalts of the province and have compositions which range from basanites to olivine melilitites, containing up to 15% normative nepheline (Brown *et al.*, 1980).

### 4.3.2 Petrology of Mantle Xenoliths

The mantle xenoliths contained in the Massif Central volcanics have been the subject of a number of petrological and textural studies (summarised in the theses of Mercier (1972), Coisy (1977) and Berger (1981)) as well as geochemical and isotopic analysis (Hutchinson *et al.*, 1975; Brown *et al.*, 1980; Downes & Dupuy, 1987; Downes, 1987).

The majority (> 95%) of the mantle xenoliths are Group I spinel lherzolites and harzburgites (following the classification scheme of Frey & Prinz, 1978), but occasional pyroxenite xenoliths occur in some localities. Most of the peridotite xenoliths are anhydrous, although amphibole- or phlogopite-bearing varieties also occur in some of the basalts. Such hydrous mineral-bearing xenoliths are relatively rare and are restricted to particular localities (e.g. Tarreyres, where the many of the xenoliths contain small quantities of a yellow-green amphibole; Hutchinson *et al.*, 1975). Whole-rock elemental analyses of the Massif Central xenoliths have shown that significant chemical differences exist between different xenolith localities, reflecting differences in the average degree of depletion of the xenoliths erupted at each site (Hutchinson *et al.*, 1975).

Considerable work on the textures of the Massif Central mantle xenoliths has given rise to their classification into four principal textural types: protogranular, porphyroclastic, equigranular and secondary recrystallised (Mercier & Nicholas, 1975; Coisy, 1977; Coisy & Nicholas, 1978). The range of textures is thought to reflect increasing degrees of deformation and recrystallistion of the peridotites prior to their extraction by the basaltic melts. Each volcanic vent is normally characterised by xenoliths of a single dominant textural type, with a subordinate quantity of xenoliths "in continuous textural relation with it" (Coisy & Nicholas, 1978). The first two textural types are similar to those described for the Pyrenean massifs (Section 4.2.2) and, together with the equigranular type (in which all the mineral grains have similar sizes and approximately polygonal shapes), are found in a number of localities throughout the Massif Central. The bulk of the fourth textural type

(secondary recrystallised, characterised by "abundant triple junctions and rectilinear grain boundaries"; Downes & Dupuy, 1987) is found at a single locality (Puy Beaunit), situated at the northern extreme of the volcanic province on the faulted margin of the Limagne basin, where they constitute the majority of the mantle-derived inclusions. The observed association of the secondary recrystallised xenoliths with subordinate equigranular xenoliths at this locality suggests that this texture may be formed by the annealing of the equigranular texture following deformation and recrystallisation.

A notable feature of the protogranular xenoliths is the occurrence of orthopyroxene-clinopyroxene-spinel clusters, similar to those observed in the Pyrenean peridotite massifs (Mercier & Nicholas, 1975). These opx-cpx-sp intergrowths have been interpreted as the result of the breakdown of garnet in a garnet peridotite, hence probably record an evolution of the xenolith mantle source towards lower pressures. The textures of the majority of the mineral intergrowths found in the Massif Central xenoliths are reasonably well equilibrated, indicating that the peridotites may have resided in the mantle at sub-solidus temperatures for a considerable time between the breakdown of the garnet and the transport of the xenoliths to the surface (Nicholas *et al.*, 1987).

Systematic mapping of the deformation structures in over 1600 ultramafic xenoliths taken from 70 different volcanic vents (Coisy & Nicholas, 1978) has demonstrated that the textures of the younger Massif Central xenoliths (< 5 Ma) are zoned from the centre to the outside of the volcanic province. In the most central localities, the xenoliths are predominantly equigranular or porphyroclastic, whilst those on the periphery are mostly undeformed, with protogranular textures (Figure 4.24). From the grain size of the olivine neoblasts, Coisy & Nicholas (1978) observed that a group of xenoliths, located in a 1 km wide zone at the limit of the deformed core region, recorded considerably higher stresses (> 700 bar) and strain rates. The zonation of the deformation and the concentration of the strain in a band around a deformed core are consistent with the geophysical data of Perrier & Ruegg (1973), who suggested that an asthenospheric mantle diapir exists below the centre of the Massif Central volcanic province.

By combining the evidence for thermal relaxation implied by the opx-cpx-sp clusters with the geophysical constraints exerted by present-day heat flows and gravimetric and

topographic anomalies, Nicholas *et al.* (1987) proposed a model in which an asthenospheric mantle diapir was introduced into the lithosphere underlying the Massif Central during the early Oligocene. This diapirism was associated with crustal extension in the region and may have caused the onset of volcanism. In their model, a single diapir (~ 80 km) rose initially to ~70 km depth, from which continued ascent to shallower depths (35 - 45 km) occurred by multiple intrusions of smaller diapirs (~10 km). From the textural equilibrium exhibited by the opx-cpx-sp clusters in the rare protogranular xenoliths found within the outline of the proposed diapir it was inferred that a prolonged period of thermal relaxation (~10 Ma) occurred prior to the extraction of the xenoliths by subsequent basanitic magmatism. Although this model accounts for the presence of both highly deformed and texturally equilibrated material within the outline of the mantle diapir, it requires that the exterior of the individual diapirs cooled sufficiently rapidly, following the cessation of shearing, that the deformed olivine microstructure of the porphyroclastic peridotites did not re-equilibrate prior to their extraction by the later magmatism.

In the diapiric model the protogranular xenoliths erupted on the periphery of the volcanic province and outside the zone of deformation may be either unrelated to the asthenospheric diapir or originate from portions of the diapir which have resided in the lithospheric mantle at sub-solidus temperatures for sufficient time that textural re-equilibration has occurred. Thus, the incorporation of the mantle source of the protogranular xenoliths into the continental lithosphere is likely to predate the diapirism which created the source of the deformed xenoliths. A date for this earlier accretion event, however, has not been determined and may have occurred at any time since the initial stabilisation of the continental lithosphere in the region.

In view of the relationship between the textures of the ultramafic xenoliths and their potentially different mantle sources, the geochemistry of the xenoliths will be discussed within a textural framework. By examining the relationship between the texture and the elemental and isotopic compositions of the xenoliths, it is possible to distinguish between the textures that were imposed on the mantle during the Tertiary magmatism and those that are older and relate to earlier events in the sub-continental mantle (Downes & Dupuy, 1987).

### 4.3.3 Sample Selection and Analysis

The xenolith samples used during this study were donated by H. Downes and are a subset of a well-characterised suite of over 75 xenoliths, collected from localities across the width of the plume proposed by Coisy & Nicholas (1987). The chemical and isotopic compositions of the xenolith suite were previously determined as part of an investigation of the relationship between the geochemistry of the mantle xenoliths and their textural type (Downes, 1987; Downes & Dupuy, 1987). Representative samples of each of the textural types were chosen from the set of xenoliths for which both isotopic and geochemical data were available. Details of the preparation and analytical techniques used for the determination of the xenolith compositions may be found in the original works.

| Sample | Ta 7 | Ta 39 | Bo 73 | RP 68 | Ta 19 | Bt 40 |
|---|---|---|---|---|---|---|
| Textural Type | Proto 1A | Proto 1A | Proto 1B | Proto 1B | Porph. | Equi. |
| $SiO_2$ | 44.83 | 44.00 | 43.86 | 44.14 | 43.90 | 44.34 |
| $TiO_2$ | 0.11 | 0.08 | 0.10 | 0.05 | 0.09 | 0.19 |
| $Al_2O_3$ | 3.31 | 2.44 | 3.22 | 1.30 | 1.72 | 3.70 |
| FeO* | 7.66 | 9.31 | 8.00 | 7.98 | 7.89 | 8.37 |
| MnO | 0.12 | 0.18 | 0.12 | 0.12 | 0.12 | 0.13 |
| MgO | 40.52 | 41.22 | 41.84 | 44.58 | 44.73 | 39.59 |
| CaO | 2.88 | 2.22 | 2.31 | 1.31 | 1.03 | 3.13 |
| $K_2O$ | 0.005 | 0.045 | 0.017 | 0.005 | 0.049 | 0.033 |
| S | 5 | 24 | 85 | 2 | 10 | 42 |
| Sc | 15.7 | 13.0 | 13.2 | 12.5 | 8.0 | n.d. |
| V | 75.0 | 57.5 | 65.8 | 48.7 | 39.1 | 87.9 |
| Cr | 3377 | 2943 | 3156 | 2642 | 2160 | 3190 |
| Ni | 2048 | 1961 | 2112 | 2404 | 2346 | 1913 |
| Cu | 11.1 | 13.3 | 8.1 | 11.2 | 12.0 | n.d. |

**Table 4.9** Whole-rock elemental composition of Massif Central xenoliths used in this study. Major elements in wt%, sulphur and trace elements in ppm (n.d., not determined). Original major and trace element abundances obtained from Downes & Dupuy (1987) and H. Downes (pers. comm.). S abundances determined as part of this study. Total iron recalculated as FeO* and data normalised to 100%. Sample localities: Ta, Tarreyres; Ms, Monistrol d'Allier; Bo, Maar de Borée; RP, Cascade de Ray Pic; Bt, Pic Beaunit (Figure 4.24). Textural types: Proto. IA, type IA protogranular; Proto. IB, type IB protogranular; Porph., porphyroclastic; Equi., equigranular.

The portions of the xenoliths used in this study were received as uncrushed sections of the original material, from which sample powders were made following the procedures outlined in Appendix A. Prior to crushing, any visible basaltic material present as rims or veins within the peridotite was removed. In total, six xenoliths were selected from the suite

for investigation using the Re-Os isotope system, however, the total sulphur and carbon contents of all the available samples were analysed by spectrophotometry at the University of Leicester, using the procedure described in Appendix A3.

### 4.3.4 Whole Rock Elemental Data

*Major Elements*

Table 4.9 shows the whole-rock major element compositions of the Massif Central xenoliths used in the Re-Os study. The major element compositions of the samples are also plotted as functions of their MgO contents in Figure 4.25, along with data for other xenoliths

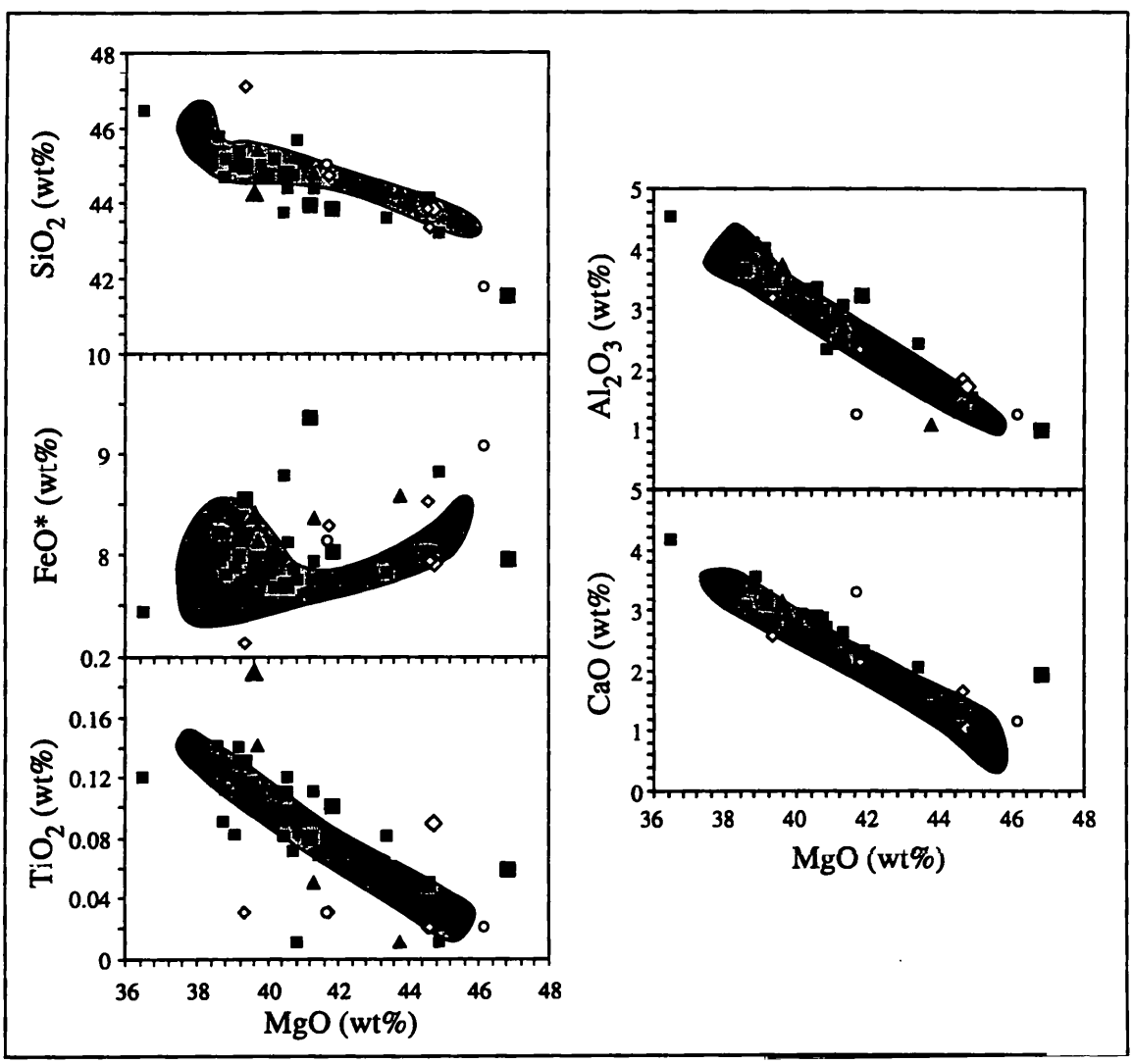


**Figure 4.25** Variation of whole-rock $SiO_2$, $TiO_2$, $Al_2O_3$, FeO* (total iron expressed as FeO) and CaO concentrations as functions of MgO content in mantle xenoliths of the Massif Central. ■ Protogranular xenoliths, ◇ Porphyroclastic xenoliths, ▲ equigranular xenoliths, O secondary recrystallised xenoliths. Enlarged symbols denote xenoliths included in the Os isotope study. Shaded regions show the range of whole-rock compositions observed in the Pyrenean peridotites. Whole rock XRF data from Hutchinson *et al.* (1975) and Downes & Dupuy (1987).

collected in the region (Hutchinson *et al.*, 1975: Downes & Dupuy, 1987) and the compositional fields of the peridotites of the N.E. Pyrenean massifs. To aid comparison with the Pyrenean data, the iron contents of the xenoliths were recalculated such that the total iron was expressed as FeO.

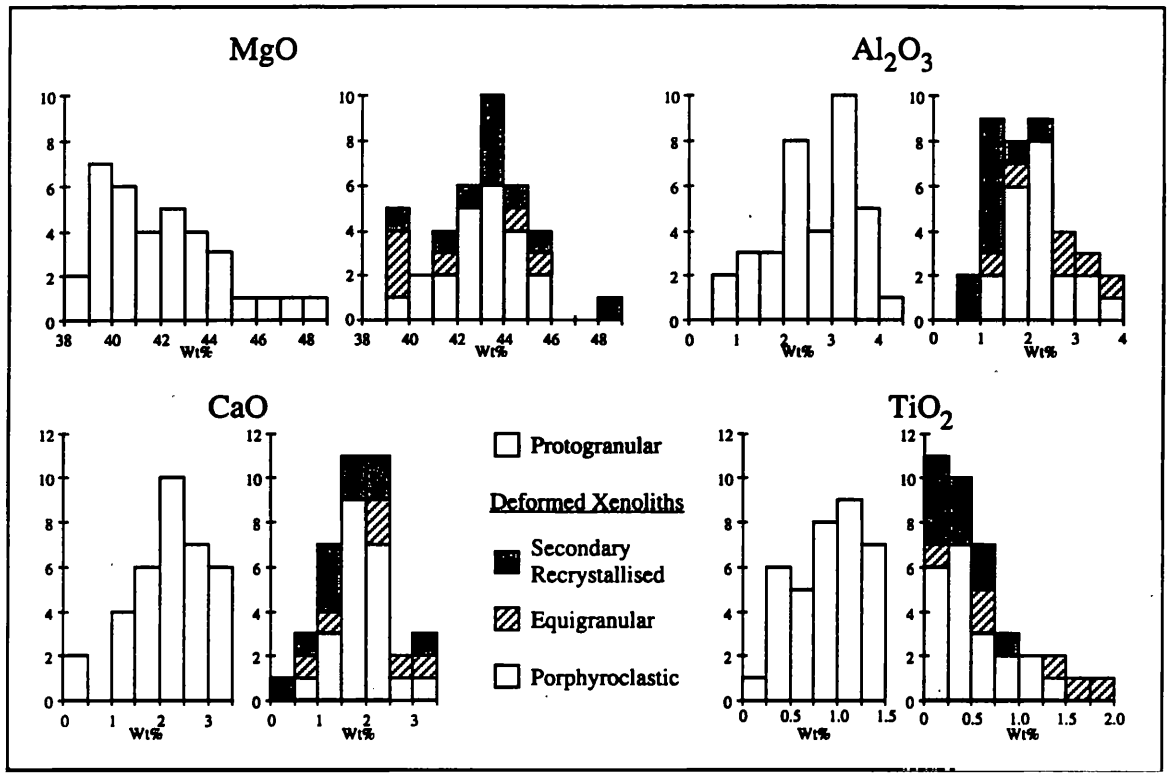


**Figure 4.26** Histograms of whole-rock MgO, $Al_2O_3$, CaO and $TiO_2$ contents of protogranular (left) and deformed (porphyroclastic, equigranular and secondary recrystallised; right) mantle xenoliths from the Massif Central. Data from Downes (1987).

The number of xenoliths of each textural type used in this study was insufficient to enable any conclusions to be drawn concerning the variation of whole-rock major element geochemistry with textural type. Using data obtained for a larger number of samples, however, Downes (1987) observed that protogranular xenoliths tend to have lower MgO contents than those with deformed textures, with a broad peak at ~40 wt% MgO compared to ~43 wt% for porphyroclastic, equigranular and secondary xenoliths (Figure 4.26). On account of the negative correlation of MgO with the 'basaltic' elements, the histograms for the $SiO_2$, $Al_2O_3$, CaO and $TiO_2$ abundances in the deformed xenoliths exhibit peaks at lower concentrations than do those for the protogranular xenolith compositions. Although the differences between the average $SiO_2$, $Al_2O_3$ and CaO contents of the two groups of xenoliths are consistent with the differences in their average MgO content, the $TiO_2$ contents

of the deformed xenoliths are considerably less than would be expected from their MgO contents, plotting off the MgO-$TiO_2$ correlation defined by the protogranular xenoliths (illustrated in Downes, 1987).

The data define similar correlations to those observed for the N.E. Pyrenean massifs, with strong negative correlations between MgO and the 'basaltic' elements $SiO_2$, $Al_2O_3$, CaO and $TiO_2$, although the xenolith data do exhibit greater scatter about the inferred trends.

### *Transition Metal Trace Elements*

The transition metal trace element compositions of the Massif Central xenoliths show similar trends to those of the N.E. Pyrenean massifs (Figure 4.27). Both Sc and V are inversely correlated with the MgO contents of the xenoliths, whilst the Ni content increases with increasing MgO. From the small number of samples for which trace element data were available, no significant difference between the whole-rock Sc, V and Ni contents of the different textural types is discernible.

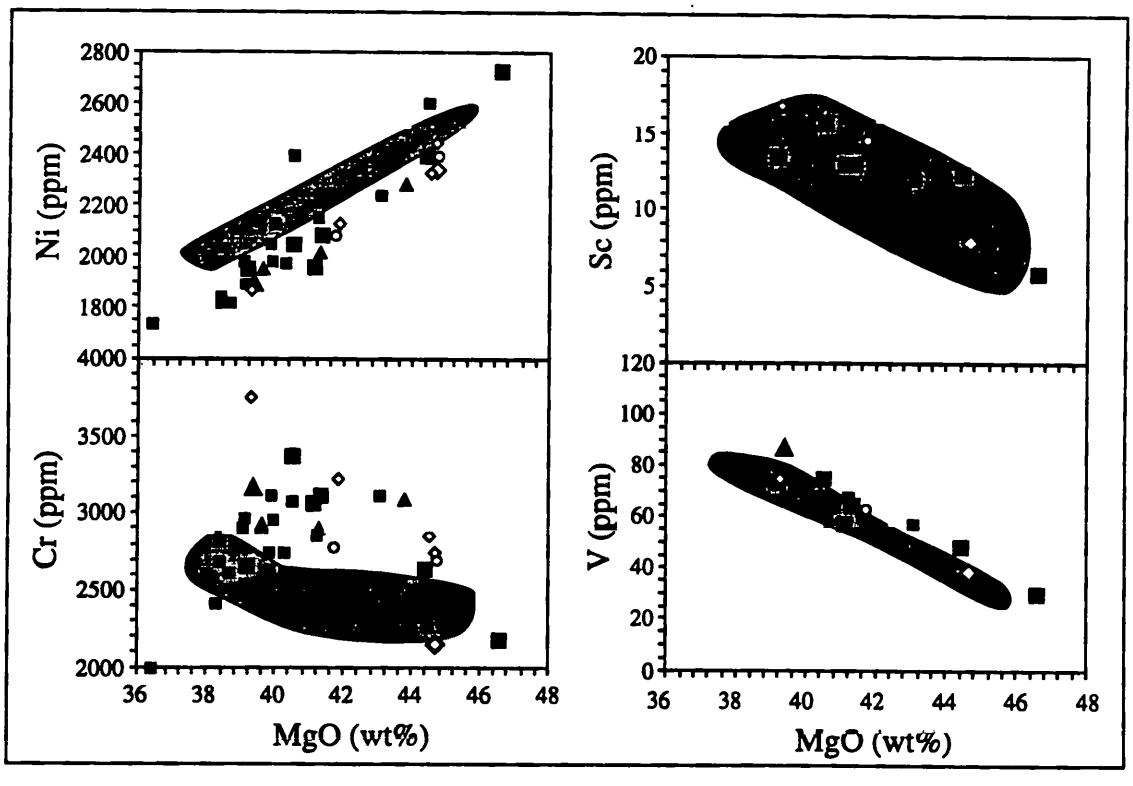


**Figure 4.27** Variation of whole-rock Ni, Cr, Sc and V concentrations as functions of MgO content in mantle xenoliths of the Massif Central. Xenolith symbols as in Figure 4.25. Whole rock XRF data from Hutchinson *et al.* (1975) and Downes & Dupuy (1987).

The whole-rock Cr content of the xenoliths displays no clear pattern. Despite an overall decrease in Cr abundances with increasing MgO content, several samples with low MgO also possess relatively low Cr, thus defining an apparent peak in Cr abundances at ~40 wt% MgO. Once again, no difference is apparent between the compositions of the different textural types.

### *Incompatible Elements: Sr, Th and Rare Earth Elements*

The Sr and REE contents of clinopyroxene separates and some whole-rocks of the Massif Central xenolith suite used in this study were documented by Downes & Dupuy (1987). Using the classification scheme of Menzies (1983), the determined REE profiles may be used to sub-divide the xenoliths into two chemical types: type IA, containing clinopyroxenes which possess flat or LREE depleted profiles, and type IB, in which the clinopyroxenes are incompatible element and LREE enriched.

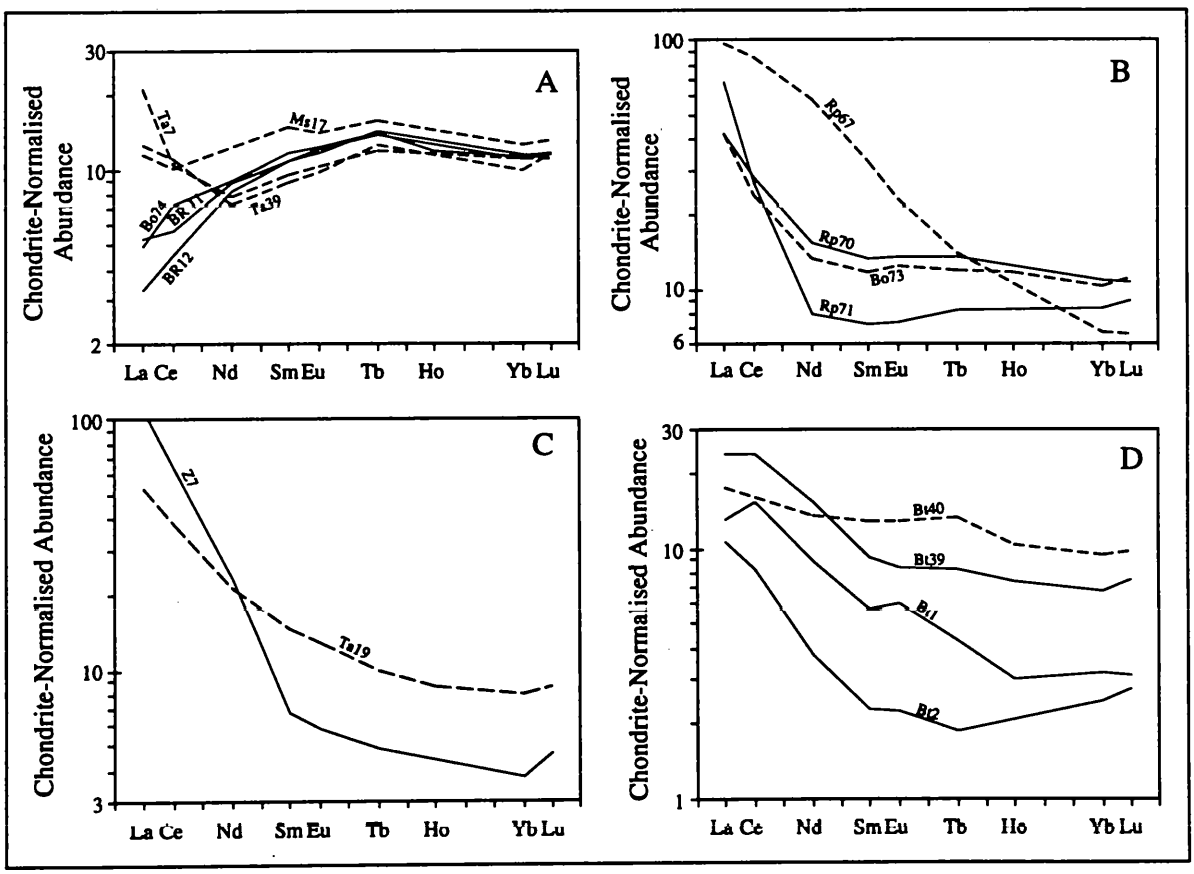


**Figure 4.28** Chondrite-normalised REE profiles of clinopyroxene separates from Massif Central mantle xenoliths, grouped according to textural type. A) Type IA protogranular xenoliths, B) Type IB protogranular xenoliths, C) Porphyroclastic xenoliths and D) Equigranular (Bt40 and Bt39) and secondary recrystallised xenoliths (Bt1 and Bt2). Dashed lines denote xenoliths included in the Os isotope study. REE data from Downes & Dupuy (1987). Chondrite normalising values from McDonough & Frey (1989).

Of the four textural types of xenoliths described in the volcanics of the Massif Central, only the protogranular type includes examples whose REE profiles are those of type IA material. These xenoliths were the most widespread type found during the study of Downes & Dupuy (1987). They possess upwardly convex REE profiles, in which the incompatible element depletion ranges from a pronounced downturn in all LREE through to flatter profiles with high Sm/Nd ratios, but elevated La and Ce abundances (Figure 4.28). The LREE depleted profiles are similar to those observed in the majority of the peridotites collected from the N.E. Pyrenean massifs and resemble the REE composition of the MORB-mantle source. The Sm/Nd ratios of the clinopyroxenes separated from the type IA protogranular xenoliths correlate with their whole-rock MgO and $Al_2O_3$ contents, suggesting that the observed LREE depletion may be the product of melt extraction.

Incompatible element enrichment was observed in the peridotite xenoliths of all four textural types. The enrichment of incompatible elements in the type IB protogranular and porphyroclastic xenoliths is demonstrated by both their high La/Yb ratios and upwardly concave REE profiles and their elevated Sr and Th abundances. Whilst the determined Sr and Th abundances in the type IA protogranular xenoliths of the collection did not exceed 75 ppm and 0.6 ppm, respectively, the Sr abundances of type IB protogranular and porphyroclastic xenoliths were typically in the range 100 - 400 ppm and were accompanied by Th abundances of over 1 ppm.

The REE patterns of the two secondary recrystallised xenoliths analysed by Downes & Dupuy (1987) resemble those of the type IB protogranular xenoliths, with upwardly convex profiles and steep negative gradients, however their REE abundances are appreciably lower than other type IB xenoliths from the region which exhibit similar degrees of major element depletion. Although the REE profiles of the two equigranular xenoliths included in the study by Downes & Dupuy also exhibited LREE enrichment, the similarity between their HREE abundances and those of the type IB protogranular xenoliths (but considerably less pronounced incompatible element enrichment in the equigranular xenoliths) may indicate that the equigranular and secondary recrystallised xenoliths originated from compositionally different mantle regions from those which formed the source of the type IB protogranular xenoliths, and are not simply the products of variable degrees of annealing.

No clear relationship is apparent between the Sm/Nd ratios determined in the clinopyroxenes of the type IB xenoliths and indices of major element depletion (e.g. whole rock MgO, $Al_2O_3$ or CaO abundances), suggesting that the LREE enrichment post-dates the differentiation which created the range of major element compositions.

### 4.3.5 Nd-Sr Isotopic Systematics of Massif Central Xenoliths

Figure 4.29 illustrates the Nd and Sr isotopic compositions of the Massif Central ultramafic xenolith suite as variations in their $\varepsilon_{Sr}$ and $\varepsilon_{Nd}$ values, calculated using data obtained by Downes & Dupuy (1987). The xenolith isotopic compositions are plotted relative to the fields defined by the local Tertiary alkali basalts and nephelinites, granulite-facies lower crustal xenoliths and the MORB mantle array. The mantle xenolith suite exhibits a large range of isotopic compositions, in which the compositional variation appears to be related to variations in the xenolith textures.

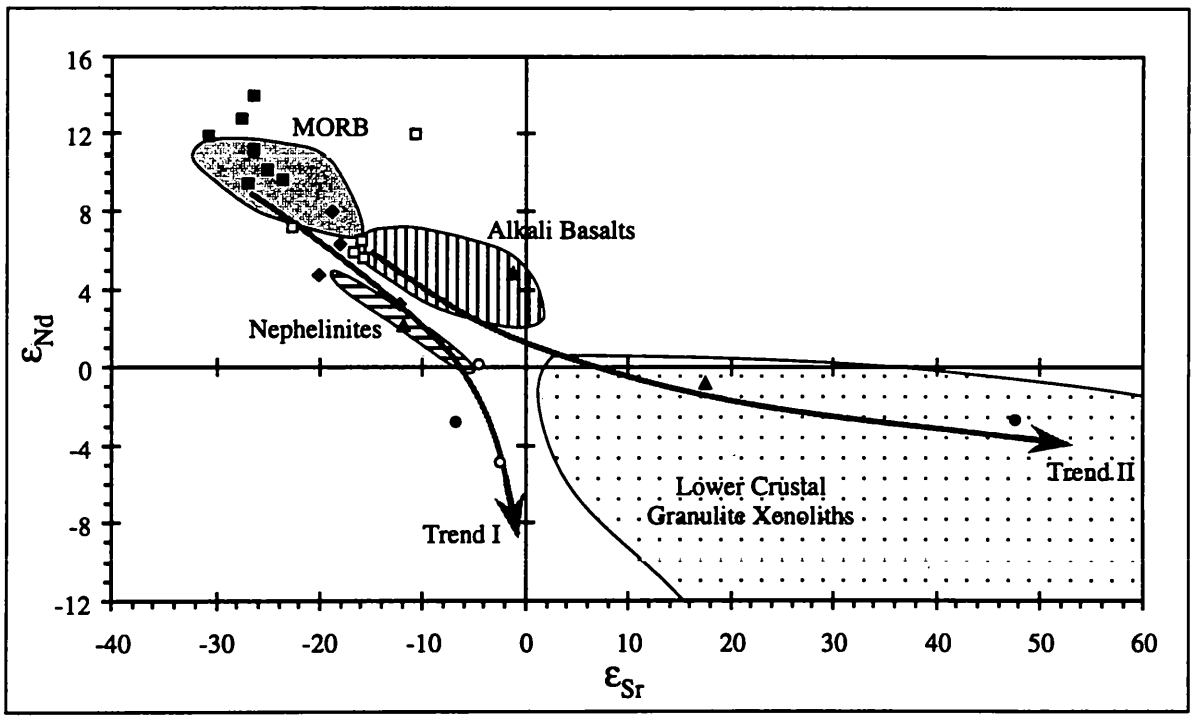


**Figure 4.29** $\varepsilon_{Sr}$ - $\varepsilon_{Nd}$ isotope variations in separated and leached clinopyroxenes from the Massif Central (Downes & Dupuy, 1987). ■, type IA protogranular xenoliths; □, type IB protogranular xenoliths; ◆, porphyroclastic xenoliths; ▲, equigranular xenoliths; ○, secondary recrystallised xenoliths; ●, pyroxenites. Fields of MORB (Ito *et al.*, 1987), local alkali basalts (Chauvel & Jahn, 1984; Downes, 1984), nephelinites (Alibert *et al.*, 1983; Downes, 1984) and lower crustal granulite xenoliths (Downes & Leyreloup, 1986) are also shown.

***Protogranular Xenoliths (IA & IB)***

The isotopic compositions of the type IA protogranular xenoliths show considerable variation, with $\varepsilon_{Nd}$ ranging from less than +9.5 to ~+14. A broad negative correlation exists between their $^{143}Nd/^{144}Nd$ and $^{87}Sr/^{86}Sr$ ratios, which overlaps the field of MORB mantle. The high $^{143}Nd/^{144}Nd$ ratios of the type IA xenoliths suggest that the observed LREE depletion and elevated Sm/Nd ratios may be an ancient feature of the mantle lithosphere in the region. Calculated depleted mantle model ages ($T_{DM}$) for these xenoliths range from 200 to 1600 Ma, using the depleted mantle evolution model of Ben Othman *et al.* (1984b).

The isotopic composition of the type IB protogranular xenoliths plot at significantly lower values of $\varepsilon_{Nd}$ and higher values of $\varepsilon_{Sr}$ than the type IA xenoliths and lie close to the field of the local alkali basalts. The low Sm/Nd ratios, but positive $\varepsilon_{Nd}$ of these xenoliths imply that their mantle source cannot have been derived from a chondritic mantle source by a single stage process, but may be consistent with an origin by the LREE enrichment of previously depleted mantle material.

***Porphyroclastic Xenoliths***

The Sr and Nd isotope compositions of the porphyroclastic xenoliths also plot at lower $\varepsilon_{Nd}$ and higher $\varepsilon_{Sr}$ values than the MORB mantle array. Although the porphyroclastic xenoliths with the most radiogenic Nd isotope compositions overlap with the field of the type IB protogranular xenoliths, the isotopic compositions of the porphyroclastic xenoliths extend to lower values of $\varepsilon_{Nd}$, overlapping the field of the local nephelinites. Despite the low $\varepsilon_{Nd}$ values determined in the porphyroclastic xenoliths, they yield younger depleted mantle model ages than the type IB protogranular xenoliths ($T_{DM} \approx 190$ - 260 Ma vs. 175 - 340 Ma), owing to their lower Sm/Nd ratios. On a plot of $\varepsilon_{Nd}$ as a function of Sm/Nd ratio (Figure 4.30), the porphyroclastic xenoliths and type IB protogranular xenoliths define a linear array emanating from the type IA protogranular xenoliths towards a less radiogenic component, with a low Sm/Nd ratio, similar to the local alkali basalts.

The only porphyroclastic xenolith in which the Os isotopic composition was determined (Ta19) possesses the most radiogenic Nd isotope ratio of the three analysed by Downes & Dupuy (1987), with $\varepsilon_{Nd} \approx +6.4$ and a depleted mantle model age of 216 Ma.

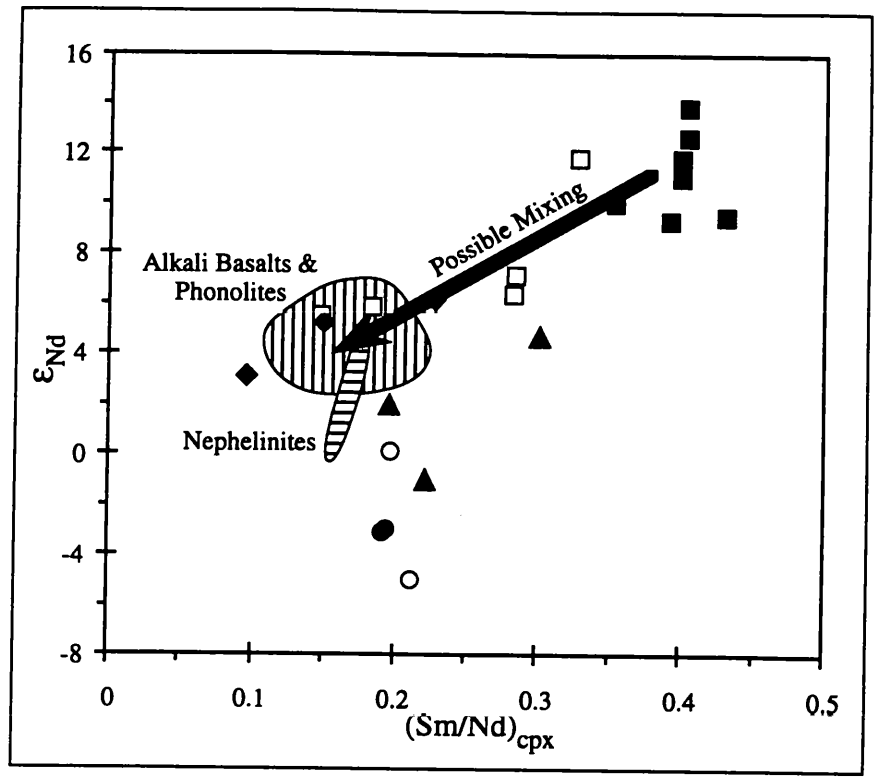


**Figure 4.30** $\varepsilon_{Nd}$ vs. Sm/Nd ratio in clinopyroxenes separated from the Massif Central mantle xenoliths. A possible mixing trend is shown between type IA protogranular xenoliths and a component compositionally similar to the local alkali basalts. Xenolith symbols as in Figure 4.29. Fields of local basalts and nephelinites plotted using data from Alibert *et al.* (1983), Chauvel & Jahn (1984) and Downes (1983, 1984).

### *Equigranular and Secondary Recrystallised Xenoliths*

The equigranular and secondary recrystallised xenoliths have $\varepsilon_{Nd}$ values which are generally lower than those of the local alkali basalts and $\varepsilon_{Sr}$ values similar to those of their basalt hosts. A single equigranular xenolith, however, plots with a positive value of $\varepsilon_{Sr}$ and negative $\varepsilon_{Nd}$, resembling the lower crustal xenoliths found in the Massif Central. Although only a total of five of the xenoliths of this type were analysed by Downes & Dupuy (1987), when the data for two pyroxenites, also from Puy Beaunit, are added to the data set, they clearly define two trends emanating from the end of the mantle array possessing the least radiogenic Nd isotope compositions and extending towards the two enriched mantle end members (EMI and EMII) of Zindler & Hart (1986).

The depleted mantle model ages calculated for these xenoliths are significantly older than those of the other type IB xenoliths from the Massif Central, with $T_{DM} \approx 500$ - 1200 Ma. However, because all of the xenoliths of these textural types were collected from the same locality (Puy Beaunit), it is unclear whether their distinctive isotope systematics are a characteristic of their textural type or merely reflect locally anomalous mantle material.

### 4.3.6 Interpretation of the Elemental and Isotopic Data for the Massif Central Xenoliths

The whole-rock major and trace element abundances of the Massif Central xenoliths exhibit similar trends to those of the peridotites of the N.E. Pyrenean massifs. Consequently, the range of observed xenolith compositions may have been created by similar processes of either melt depletion or refertilisation to those already proposed for the peridotite massifs (Sections 4.2.8 and 4.2.9). In contrast to the Pyrenean peridotite bodies, however, few of the whole-rock elemental compositions of the Massif Central xenoliths approach that estimated for the primitive mantle. One xenolith sample (analysed by Hutchinson *et al.* (1975)) does appear to be similar to, or more fertile than, primitive mantle material, however, its low MgO and high CaO and $Al_2O_3$ contents are anomalous and may also represent the effects of melt-infiltration during transport.

Within the context of the melting model proposed for the Pyrenean samples, the absence of xenoliths with near-primitive compositions may suggest that the mantle lithosphere underlying the Massif Central has, on average, experienced greater degrees of melting than that which underlies the Pyrénées. However, given that the Sm/Nd ratios determined for the type IA xenoliths are all higher than the mean value estimated for the depleted mantle ($0.3556 \pm 0.0023$; Zindler & Hart, 1986), it is also possible that the lithospheric source of the xenoliths may have been derived from a depleted rather than a primitive mantle source. Conversely, if the variation in whole-rock geochemistry is the result of refertilisation of highly depleted residual mantle, then the less "primitive" composition of the most fertile xenolith may suggest that the degree of refertilisation would have been less than that observed in the mantle underlying the Pyrénées.

Given the limited number of samples for which comprehensive elemental data were available and the complications added by the compositional variation with textural type, a thorough discussion of the cause of the major-element variations in the Massif Central mantle xenoliths is difficult and beyond the scope of this study.

Assuming the textures of the porphyroclastic and equigranular xenoliths reflect deformation within the mantle diapir underlying the Massif Central, the observed connection between xenolith textures and major element depletion would imply that processes within the

diapir are responsible for the compositional differences between the protogranular and deformed mantle xenoliths. Downes (1987) suggested that the incompatible element enrichment of the deformed xenoliths may have been accompanied by the introduction of volatiles, which would have lowered the solidus of the mantle material. Coupled with adiabatic decompression associated with the rise of the diapir, this lower solidus temperature may have resulted in small amounts of partial melting within the source of the deformed xenoliths. In addition, if melting was coincident with deformation, it is probable that less melt would have been retained in the deforming matrix of the porphyroclastic and equigranular peridotites, resulting in the greater depletion observed in the deformed xenoliths derived from a source within the diapir.

The widespread occurrence of unmetasomatised, type IA protogranular xenoliths outside the core of the proposed mantle diapir suggests that the majority of the lithosphere underlying the Massif Central may be characterised by depleted mantle material. Within and around the central core of the diapir, however, the elemental and isotopic compositions of ultramafic xenoliths demonstrate that the lithosphere has been enriched in incompatible elements. Although the type IB protogranular and porphyroclastic xenoliths plot close to the enrichment trend defined by the equigranular and secondary recrystallised xenoliths towards the EMI component, the scatter of the equigranular and secondary recrystallised xenolith compositions away from the linear array defined by the type IB protogranular and porphyroclastic xenoliths in Figure 4.30 implies that the $\varepsilon_{Sr}$ - $\varepsilon_{Nd}$ trend cannot be explained by a single simple mixing process.

Downes & Dupuy (1987) suggested that the Nd and Sr isotopic compositions of the Massif Central mantle xenoliths were consistent with an origin involving two separate enrichment events, which possibly affected different regions of the lithospheric mantle.

The earlier enrichment event is recorded by only the equigranular and secondary recrystallised xenoliths and is characterised by moderate incompatible element enrichment and low or negative values of $\varepsilon_{Nd}$. The low $\varepsilon_{Nd}$ values and high $T_{DM}$ ages of the xenoliths which define the two enrichment trends observed in Figure 4.29 are consistent with either ancient enrichment of the mantle lithosphere or interaction of mantle with an ancient component. The overlap between trend II of Figure 4.29 and the isotopic compositions of

local lower crustal meta-igneous xenoliths suggests that the trend toward a component with positive $\varepsilon_{Sr}$ (EMII) may have been generated by the interaction of the mantle lithosphere with continental sediment or fragments of old subcontinental lithosphere subducted during the Hercynian orogeny. The low $\varepsilon_{Sr}$ values which characterise trend I of Figure 4.29 suggest that this trend reflects enrichment by a component with low time-averaged Rb/Sr and Sm/Nd ratios. Such enrichment has been previously interpreted as the result of metasomatism of mantle material by $CO_2$-rich fluids (Menzies, 1983; Zindler & Hart, 1986). In view of the similarity between the maximum $T_{DM}$ model age determined for these xenoliths (1170 Ma) and the model ages of local lower crustal xenoliths (1200 - 1400 Ma; Downes & Leyreloup, 1986), the ultramafic xenoliths may represent mantle originally enriched during the Proterozoic.

The resemblance between the isotopic compositions of the local alkaline magmas and those of the equigranular and secondary recrystallised xenoliths suggests that the magmas may have been derived from an enriched mantle source similar to that found in the core of the diapir.

The second enrichment event in the continental mantle lithosphere underlying the Massif Central is exhibited by the porphyroclastic xenoliths from the periphery of the diapir and the type IB protogranular xenoliths from outside the zone of deformation. Although these xenoliths exhibit values of $\varepsilon_{Sr}$ and $\varepsilon_{Nd}$ less than those which characterise the mantle array, they are generally more radiogenic than the deformed xenoliths from within the diapir. Downes & Dupuy (1987) proposed that the type IB protogranular xenoliths represent depleted mantle material metasomatised by fluids derived from the enriched source represented by the equigranular and secondary recrystallised xenoliths. The two different sets of deformed xenoliths (equigranular/secondary recrystallised, and porphyroclastic/Type IB protogranular), however, probably originated from chemically distinct regions of the mantle, as suggested by the less pronounced LREE-enrichment noted in the clinopyroxenes separated from the former xenoliths, in the core of the diapir.

From the available isotopic data, it is not possible to date accurately either the initial depletion of the lithosphere underlying the Massif Central, or the timing of the second

enrichment event. Although model ages were calculated for the extraction of the type IA xenoliths from a depleted mantle ($T_{DM}$) source, the small difference between the $\varepsilon_{Nd}$ values of the xenoliths and that of the depleted mantle protolith used in the modelling, coupled with the wide range of $\varepsilon_{Nd}$ values which actually characterise the depleted mantle array, mean that such calculated ages are probably unrealistic. Likewise, because the Nd isotope compositions of the type IB xenoliths result from the two-component mixing of depleted mantle material and an enriched mantle end-member, the $T_{DM}$ model ages calculated for the porphyroclastic and type IB protogranular xenoliths do not reflect the date of enrichment.

In conclusion, the lithospheric mantle underlying the Massif Central appears to be composed of at least three different components, distinguished by their chemical and isotopic compositions:

1) The majority of the lithosphere is composed of LREE depleted peridotite which is similar to MORB mantle, but may have experienced additional major and trace element depletion prior to its incorporation. The age of this mantle component has not been determined, but probably predates the two proposed enrichment events.

2) There is clear evidence that parts of the Massif Central lithosphere have experienced an ancient enrichment in incompatible elements. Comparisons with the isotopic compositions of lower crustal granulites which crop out in the region or have been transported as xenoliths in the Tertiary/Quaternary volcanism suggest that this enrichment may be associated with events occurring during the Mid-Proterozoic. Whilst this enriched mantle component may reside predominantly at depths below the zone of xenolith extraction, where it provided a source for the alkaline magmatism, some portions may have become incorporated into the mantle diapir, elevating them sufficiently that they became entrained in the magmas *en route* to the surface. The evidence for ancient enrichment in the equigranular and secondary recrystallised xenoliths suggests that, where sampled by the volcanism, the core of the proposed diapir is composed of lithospheric rather than asthenospheric mantle material.

3) Parts of the mantle lithosphere on the periphery of the diapir and away from its deformation have interacted with fluids derived from the ancient enriched mantle source, similar to alkaline magmas erupted in the region.

## 4.4 Summary of the CML underlying the N.E. Pyrénées and Massif Central

In this chapter the processes that may have affected the continental mantle lithosphere underlying central and south-western France have been discussed, using elemental and isotopic data for both whole-rocks and clinopyroxene mineral separates. The different modes of occurrence and contrasting enrichment histories displayed by the peridotite samples from the two regions, however, meant that the discussion focussed on different mantle processes occurring within the lithosphere of the two regions.

Whole-rock elemental data for the two sample suites demonstrate that the mantle peridotites sampled from both regions display similar trends in their major element compositions. The co-variation of the major elements are consistent with a process of two component mixing or unmixing, involving either the extraction of melt from a relatively fertile source or the refertilisation of depleted mantle material. These processes were discussed in detail for the peridotites collected from the N.E. Pyrénées, for which numerous samples exhibiting limited incompatible element enrichment were available. Two separate models were proposed to account for the observed major element trends, involving either the extraction of up to 25% basaltic melt (formed by batch melting of a primitive mantle source, either in the presence or absence of garnet) or the refertilisation of a depleted mantle residue by the addition of a basaltic melt formed at relatively low pressures. The low pressures required for the generation of suitable refertilising melts would imply that the lithospheric mantle underlying the N.E. Pyrénées was uplifted then returned to greater mantle depths prior to the introduction of garnet-bearing pyroxenite veins. On account of the smaller number of xenolith samples for which comprehensive elemental data were available and the frequent enrichment of the xenoliths in incompatible elements, the possible origins of the major elemental variations within the lithosphere underlying the Massif Central were not discussed in detail.

By sampling a greater volume of the lithospheric mantle, the alkali basalts of the Massif Central volcanic province contain xenoliths which have experienced a wider range of processes than are observed within the N.E. Pyrenean massifs. Although the majority of the mantle xenoliths collected from the Massif Central are incompatible element depleted,

xenoliths exhibiting LREE and incompatible element enrichment are moderately common. REE and isotopic data for these enriched xenoliths suggest that the enrichment may originate from at least two separate events during the evolution of the lithosphere. One of these enrichments may be related to an episode of crust formation in the Proterozoic, implying that parts of the lithosphere in the region may have an ancient origin. Although the original depletion of the mantle lithosphere may be shown to pre-date the incompatible element enrichment, in view of the similarity between the $\varepsilon_{Sr}$ - $\varepsilon_{Nd}$ isotopic compositions of the LREE depleted peridotites of the two regions and those of the MORB mantle, it is not possible to determine accurately the age of this depletion and so determine the time at which the continental lithosphere may have separated from the convecting mantle.

In contrast to the Rb-Sr and Sm-Nd isotope systems, the Re-Os isotope compositions of the mantle lithosphere may be comparatively resistant to metasomatic disturbance. This resistance should enable the Re-Os isotope system to investigate the partial melting history of the two regions better. In particular, it may be possible to use the Re-Os isotope system to investigate whether the three different components identified in the lithosphere underlying the Massif Central separated from the convecting mantle at a similar time or whether their contrasting elemental and Sr-Nd isotope compositions originate from the sequential addition of material to the lithospheric mantle. Although the Re-Os isotope system cannot differentiate between the partial melting and refertilisation models for the differentiation of the mantle in the two regions, it may be used to determine the date at which the differentiation may have taken place.

# Chapter 5

# Re-Os Isotopic Study of the French Continental Mantle Lithosphere

## 5.1 Introduction

In Chapter 4 it was shown that the continental mantle lithosphere underlying central and south-west France has experienced a complex history, involving melt depletion (possibly followed by refertilisation), several phases of deformation and recrystallistion and variable degrees of metasomatism associated with the passage of mantle-derived melts. Previous isotopic studies of the N.E. Pyrenean massifs and Massif Central ultramafic xenoliths (e.g. Downes & Dupuy, 1987; Hamelin & Allègre, 1988; Downes *et al.*, 1991a; Mukasa *et al.*, 1991) have shown that, because of this complex history, the Rb-Sr, Sm-Nd and U-Pb isotope systematics of the mantle lithosphere in the region are highly heterogeneous and reflect mantle melt interactions which may have occurred over a considerable period of time (probably several hundreds of millions of years). As a consequence of these interactions, and the isotopic perturbations associated with them, it is has not been possible to study the earliest events in the evolution of the French continental mantle lithosphere using the determined Sr, Nd or Pb isotope compositions.

Because Os is compatible during partial melting of the mantle, the Os contents of most magmatic fluids are low and metasomatism of the mantle lithosphere should have had negligible impact on its $^{187}Os/^{188}Os$ ratios. The Re-Os isotope system, therefore, offers a method by which the timing and processes involved in the formation of the French continental mantle lithosphere may be investigated, which should be free from the influence of the alteration processes which have obscured the results of previous studies using other isotope systems.

Despite considerable recent work on the geochemistry of Re and Os under mantle conditions, there remains considerable uncertainty regarding the factors which influence their behaviour during magmatic processes. In this chapter, Re and Os abundance data and Os

isotope ratios are therefore presented for the peridotites of the N.E. Pyrenean massifs and ultramafic xenoliths of the Massif Central with the dual objectives of:

a) comparing the behaviour of Re and Os in the French continental mantle lithosphere with the results of the thermochemical calculations, experimentally-derived partition coefficients and observed behaviour of the elements in other mantle rocks discussed in Chapter 2.

b) investigating the origin and timing of the differentiation of the continental mantle lithosphere underlying central and south-western France, in order to contribute to existing models for the early evolution of the regional lithosphere. On a small-scale, the Re-Os isotope systematics of the Massif Central xenoliths may determine whether the textural differences reflect variations in the age of their mantle sources, as suggested by their Nd isotope compositions. On a larger scale, the investigation of the Re-Os isotope system in the continental mantle lithosphere enables events within the mantle to be linked to those occurring in the crust, from which a whole-lithosphere model may be derived.

Although the S contents and the chalcophile trace element compositions of the peridotites used in this study were presented in an earlier chapter (Tables 4.2 and 4.9), they were excluded from the discussion of the geochemical evolution of the mantle lithosphere which followed, owing to the decoupling of the sulphide and silicate systems during the metasomatism or refertilisation of the mantle lithosphere. On account of the strong chalcophile affinities displayed by both Re and Os, however, the behaviour of sulphur and the chalcophile trace elements are central to the discussion of the factors affecting the Re-Os isotope system in the mantle. Consequently, in this chapter, the whole-rock chalcophile abundances of the peridotite samples are discussed in parallel with their Re-Os isotope systematics, enabling the behaviour of Re and Os in the collected samples to be linked to earlier studies of mantle sulphide phases (Lorand, 1989b-d, 1990, 1991).

## 5.2 Results of Analyses

The whole-rock chalcophile element compositions of the peridotites included in this study and the methods used in their preparation and analysis are described in Chapter 4 and Appendix A. Only a subset of the peridotites described in Chapter 4 were analysed for Re

and Os. The samples from the N. E. Pyrenean massifs were selected to encompass the full range of major element compositions shown by the collected peridotites, but to include, where possible, only those which exhibited low degrees of serpentinisation. The xenoliths from the Massif Central were selected to include representatives of each of the main textural types described by Mercier & Nicholas (1975) as well as samples belonging to both the type IA (LREE-depleted) and type IB (LREE-enriched) sub-groups. The methods employed in their preparation and analysis for both Re and Os were discussed thoroughly in Chapter 3.

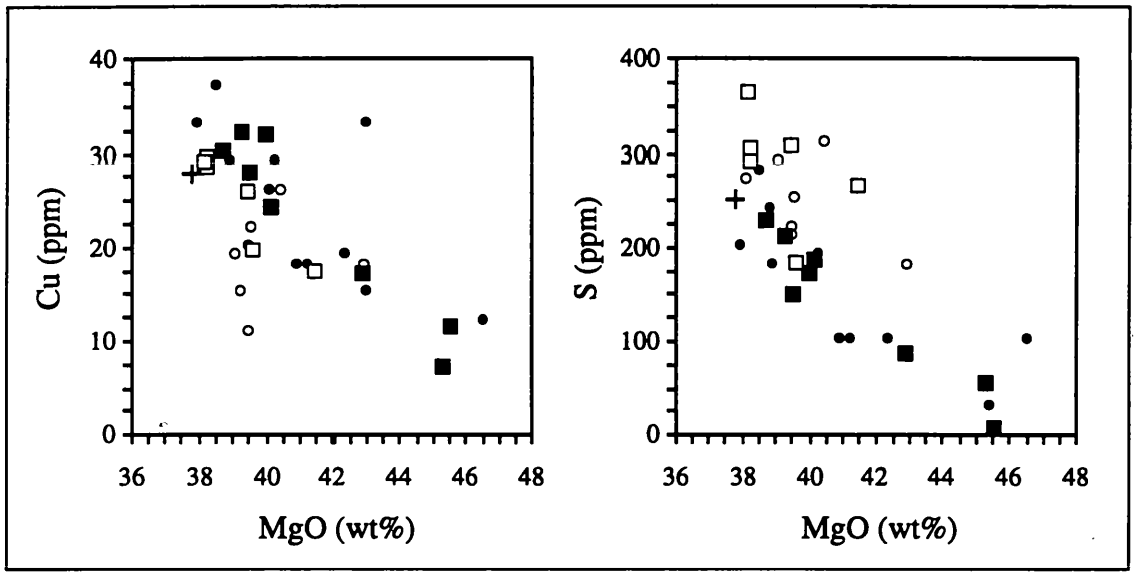


**Figure 5.1** Cu and S abundances of peridotites collected from the N.E. Pyrenean massifs plotted as a function of MgO. ■ "normal" peridotites (this study); □ "low Cu/S" peridotites (this study); ● "normal" peridotites (Lorand, 1989c); ○ "low Cu/S" peridotites (Lorand, 1989c); +, estimated composition of the primitive mantle (S, Sun, 1990; Cu, Sun, 1982; MgO, Hart & Zindler, 1986). For a discussion of the classification by Cu/S ratios, see text and Figure 5.2.

### 5.2.1 Chalcophile Trace Elements and Sulphur

The sulphur abundances of the Pyrenean peridotites range from 7 ppm to 365 ppm and decrease with increasing MgO content (Figure 5.1). Similar positive correlations between S and major element depletion have been observed in other peridotite massifs (Garuti *et al.*, 1984; Lorand *et al.*, 1993), where they were interpreted as the result of the progressive loss of the mantle sulphide phase by increasing degrees of partial melting. The sulphur contents of the Massif Central xenoliths are considerably lower than those of the Pyrenean peridotites, with values lying between the detection limit of the instrument (~10 ppm) and ~90 ppm. These low S abundances are similar to those observed by Lorand (1990) in

ultramafic xenoliths collected from the same region. Lorand suggested that the depletion in S relative to the values observed in orogenic massifs may have been caused by the oxyhydration of the sulphide phase following eruption, during which the sulphur was removed as soluble sulphate ions and the base-metal sulphide (BMS) phase was converted to low temperature oxide and hydroxide minerals.

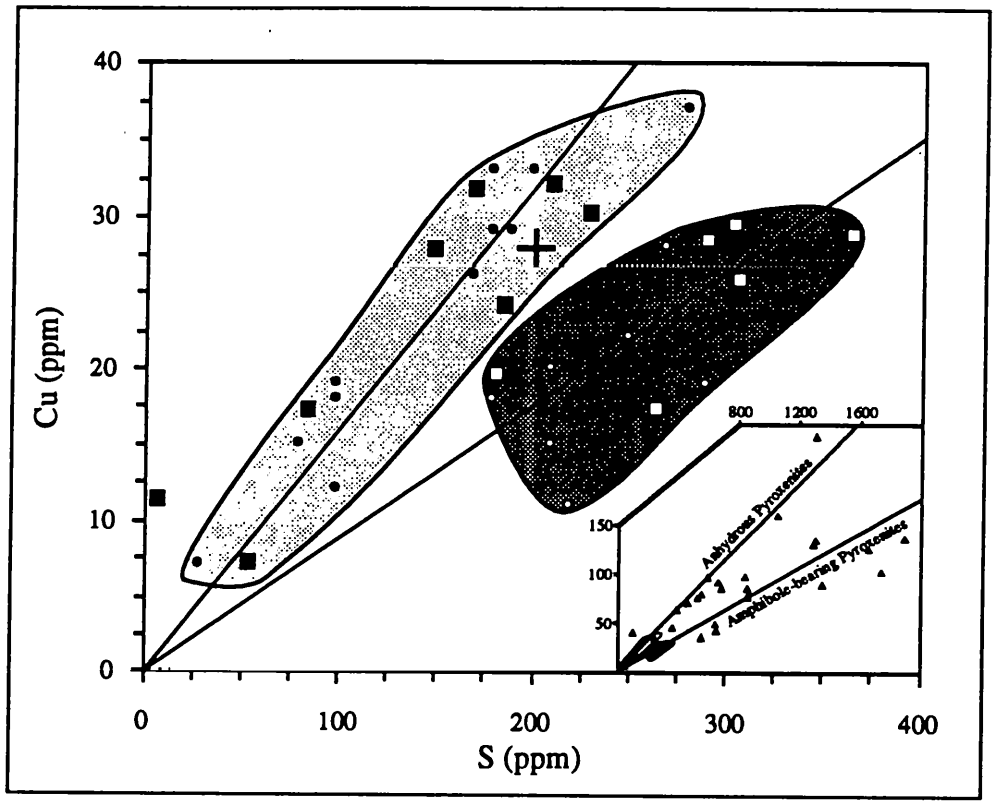


**Figure 5.2** Cu *versus* S plot for peridotites collected from the N.E. Pyrenean massifs, illustrating their division on the basis of their Cu/S ratios. Symbols as in Figure 5.1. Inset, Cu *versus* S plot for pyroxenite layers present in the massifs. △, anhydrous pyroxenites (Lorand, 1989a); ▲, amphibole-bearing pyroxenites (Lorand, 1989d). The two lines shown in each diagram are regressed through the two sets of pyroxenite data and are forced through the origin.

Of the chalcophile elements analysed in the peridotites of the N.E. Pyrénées, only Cu displays a positive correlation with S (Figure 5.2), although the trend exhibits considerable scatter. The range of Cu and S contents resemble those previously determined by Lorand (1989c) for the Pyrenean massifs. In Figure 5.2, most of the samples lie along a trend passing through both the estimated composition of the undepleted mantle and the origin. Several of the data are located off this line, however, with low Cu/S ratios similar to those of the amphibole-bearing pyroxenite layers occurring in the massifs. When plotted as a function of MgO, the S contents of these low Cu/S peridotites are elevated above the MgO - S trend

defined by the rest of the data (Figure 5.1). The plot of Cu *versus* MgO for the peridotites, shows that these samples are not displaced from the overall negative correlation between these elements, suggesting that the low Cu/S ratios of the anomalous peridotites probably arises from the addition of S.

The Cu contents in the Massif Central ultramafic xenoliths are consistently lower than those observed in the peridotites of the N.E. Pyrenean massifs. Whilst these lower abundances may be the result of different magmatic processes occurring within the two regions, the determination of low Cu contents in the altered sulphide inclusions analysed by Lorand (1990) suggests that the element may have also been mobilised during the post-eruption alteration process.

Although both Ni and Co are highly compatible in the base-metal sulphide phase, in mantle rocks they also partition strongly into olivine. Consequently, the abundances of these elements in peridotites are controlled by the olivine phase, rather than the mantle sulphides, leading to compatible behaviour during magmatic processes and the positive correlation of Ni with MgO observed in Figure 4.9.

### 5.2.2 Re and Os Abundances and Os Isotopic Compositions

***Data Selection***

The Re and Os concentrations and Os isotopic compositions determined for the peridotites collected from the N.E. Pyrenean massifs and ultramafic xenoliths from the Massif Central are presented in Tables 5.1 and 5.2. Although repeat analyses were performed for several of the samples (data presented in Table 3.10), only a selection of the data are presented in the tables. These data were mostly collected towards the end of the study, when the blanks were lowest and the analyses exhibited the best precision.

Where the sample was analysed for Os using both static and dynamic data collection routines on the same filament, only the former set of data are presented. Because these data were normally collected using ion beams of greater intensity, the determined $^{187}Os/^{188}Os$ ratios were less affected by the interference observed during some dynamic runs at low beam intensities. Although the large masses of material collected from the massifs of the N.E. Pyrénées enabled the NiS fusion technique to be used routinely in their sample preparation,

the limited size of many of the Massif Central xenoliths required the use of acid dissolution. As noted in Chapter 3, the Os concentrations of xenoliths prepared using the latter technique were consistently lower than those prepared by NiS fusion, suggesting that many of the xenolith Os concentrations presented in Table 5.2 underestimate the total Os content.

| Sample Number | Mg# | Os Conc. (ppb) | Re Conc. (ppt) | $\frac{^{187}Re}{^{188}Os}$ | $\frac{^{187}Os}{^{188}Os}$ |
|---|---|---|---|---|---|
| 92-FR3 | 90.06 | 5.46 | | | 0.12601 ± 1 |
| 92-FT5 | 90.88 | 4.74 | 65.2 | 0.0649 ± 1 | 0.11931 ± 5 |
| | 90.88 | | | | 0.12009 ± 28‡ |
| 92-FT6 | 89.03 | 5.82 | 353.1[a] | 0.2865 ± 2 | 0.12801 ± 2 |
| | | | 354.1[a] | | |
| 92-FT7 | 89.88 | | 267 | | |
| 92-LH12 | 90.51 | 5.92 | 157 | 0.1254 ± 25 | 0.11408 ± 3 |
| 92-LH14 | 89.46 | 4.28 | 437.2 | 0.4819 ± 2 | 0.13094 ± 13 |
| 92-LH17 | 89.65 | 6.32 | | | 0.12741 ± 33 |
| 92-LH18 | 90.10 | 4.15 | | | 0.12541 ± 2 |
| 92-LH3 | 90.60 | 7.53 | 293 | 0.1837 ± 20 | 0.12199 ± 1 |
| 92-PG2† | 90.80 | 5.06 | 149 | 0.1391 ± 28 | 0.12110 ± 20 |
| 92-PR1 | 89.89 | 4.42 | | | 0.12570 ± 3 |

**Table 5.1** $^{187}Os/^{188}Os$ ratios and Re and Os concentrations in peridotites collected from the N. E. Pyrenean massifs. Precision of all Os concentration determinations was better than 0.6‰. Precision of Re abundances depended upon the precision of the blank correction, varying between >0.1% and 2%. Except where indicated, the data were acquired using the static collection routine and multiple Faraday collectors.
‡ $^{187}Os/^{188}Os$ ratio not blank-corrected.
† Data obtained using electron multiplier and dynamic collection routine.
[a] Separate splits of the same sample powder.

Whilst Re concentration data are presented for approximately half of the Pyrenean samples analysed for Os, only two of the Massif Central xenoliths were successfully analysed for Re, owing to the presence of excessive quantities of impurities following digestion. Because Re could not be recovered from the NiS fusion products, the Re concentrations of the peridotites prepared for Os analysis by the fusion technique were determined separately, using a second split of the sample powder.

### *N.E. Pyrenean Massifs*

The $^{187}Os/^{188}Os$ ratios determined for the peridotites of N.E. Pyrenean massifs range from 0.1141 to 0.1309, with Os concentrations between 4.15 and 7.53 ppb. Re concentrations in the peridotites vary from 65 to 440 ppt. Although no relationship is apparent between the Os abundances of the samples and either their $^{187}Os/^{188}Os$ ratios or Re

contents, the $^{187}Os/^{188}Os$ and $^{187}Re/^{188}Os$ ratios are positively correlated, forming a trend on an isochron plot (Figure 5.3). If all the analyses are included in the regression, then the data define an errorchron (MSWD = 8.4), with an apparent age of 2420 ± 680 Ma and an initial $^{187}Os/^{188}Os$ ratio of ~0.114. However, if sample 92-LH12 is excluded from the regression, then the correlation is greatly improved and the data yield an isochron (MSWD = 1.93) which gives an age of 1.96 ± 0.45 Ga and an initial $^{187}Os/^{188}Os$ ratio of 0.1167 ± 0.0014 ($\gamma_{Os_i}$ = 2.8 ± 3.1).

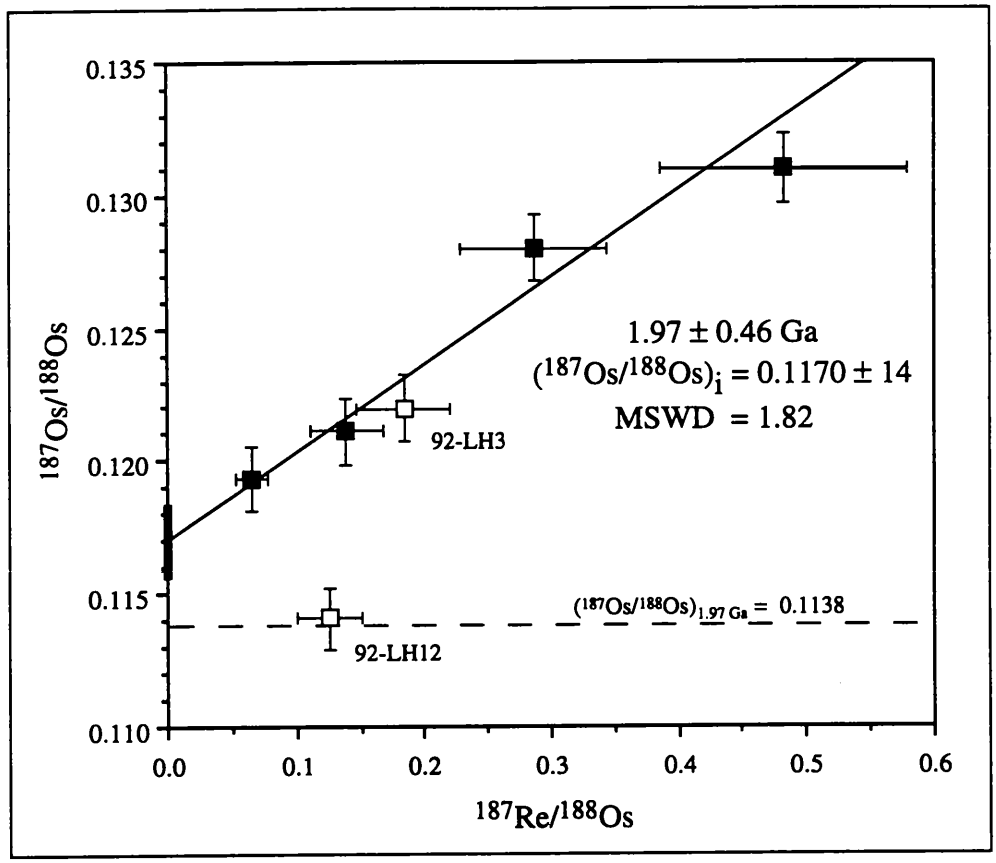


**Figure 5.3** $^{187}Os/^{188}Os$ *versus* $^{187}Re/^{188}Os$ for the peridotites collected from the N.E. Pyrenean massifs. Error bars on points represent uncertainties in values, as judged from the reproducibility of the $^{187}Os/^{188}Os$ and Re/Os ratios ($2\sigma$ = 1% and 20%, respectively; Section 3.15.2). Samples 92-LH3 and 92-LH12 are excluded from the regression on account of the unusual chalcophile abundances of the former and anomalously unradiogenic $^{187}Os/^{188}Os$ ratio of the latter. If the regression is interpreted as an isochron, it yields an age of 1.97 ± 0.46 Ga and an initial $^{187}Os/^{188}Os$ ratio of 0.1170 ± 0.0014 (shown by bar on $^{187}Os/^{188}Os$ axis). In this calculation the data were weighted according to the reciprocal of the squares of their estimated errors. Dashed line shows the $^{187}Os/^{188}Os$ ratio of the bulk Earth at 1.97 Ga, calculated from the mantle evolution curve of Luck & Allègre (1991). Filled squares, "normal" peridotite samples; open squares, anomalous samples.

In both the isochron plot shown in Figure 5.3 and the plot of $^{187}Os/^{188}Os$ as a function of whole-rock $Al_2O_3$ (Figure 5.4), the Os isotopic composition of sample 92-LH12 appears

to be significantly different from those of the other Pyrenean samples. Similarly anomalous behaviour is also observed in plots of $^{187}Os/^{188}Os$ as a function of either MgO or Mg# (not shown). The significantly less radiogenic $^{187}Os/^{188}Os$ ratio determined for sample 92-LH12 suggests that this sample may represent mantle material derived from an older source than that which formed the rest of the massifs. On account of its individual character, this sample will be discussed separately from the isotopic data obtained for the other Pyrenean samples.

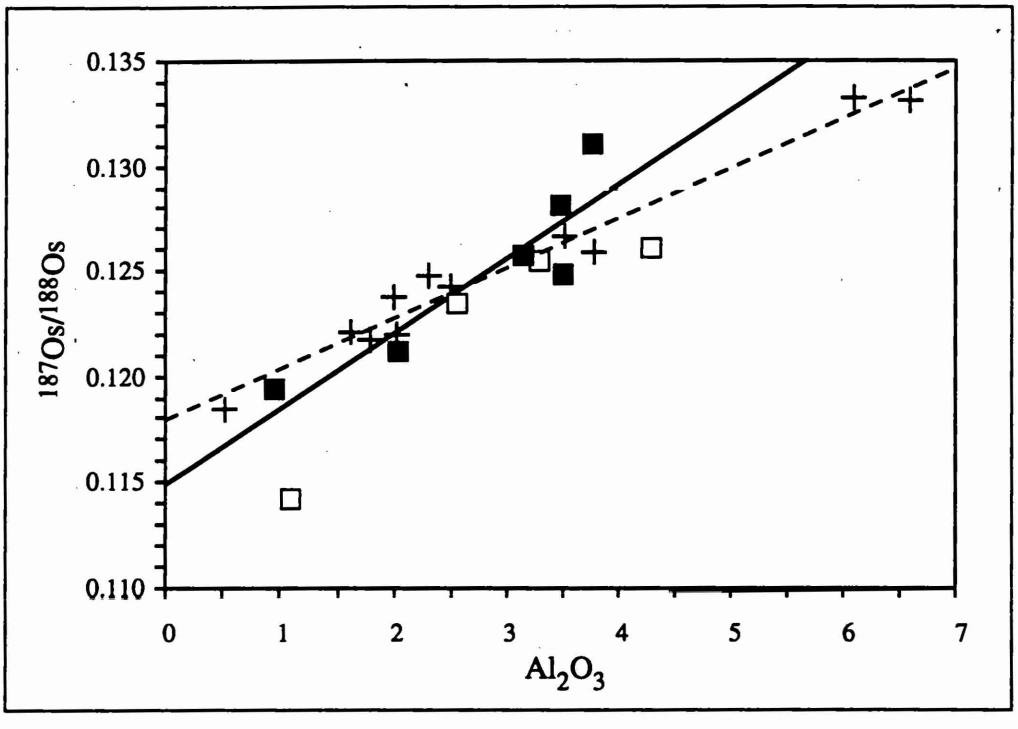


**Figure 5.4** Plot of $^{187}Os/^{188}Os$ as a function of $Al_2O_3$ for the peridotites from N.E. Pyrenean massifs (squares). Peridotites exhibiting anomalous Cu/S ratios and sample 92-LH12 (open squares) excluded from the regression. For comparison, data for the Ronda ultramafic complex (Reisberg *et al.*, 1988, 1991) are also shown (dashed line regressed through all data), illustrating the difference between the gradients defined by the data from the two regions.

When plotted as a function of their depletion in major elements (e.g. MgO or $Al_2O_3$ contents or Mg#), the $^{187}Os/^{188}Os$ ratios of the Pyrenean peridotites (excluding sample 92-LH12) define distinct trends, similar to those reported by Reisberg *et al.* (1991) for peridotites of the Ronda massif. When the data for the two regions are plotted together, however, the trend defined by the $^{187}Os/^{188}Os$ ratios of the Pyrenean peridotites as a function of $Al_2O_3$ is considerably steeper than that shown by the peridotites from the Ronda massif (Figure 5.4).

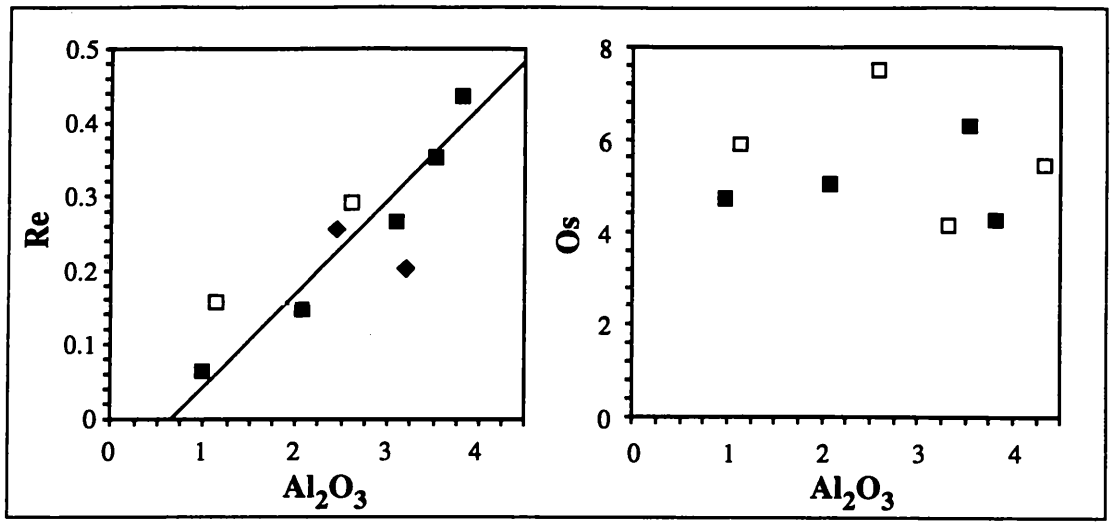


**Figure 5.5** Re and Os abundances as a function of $Al_2O_3$ content in peridotites collected from the N.E. Pyrenean massifs, illustrating the correlation of Re abundances with major element depletion. If the samples with anomalous Cu/S ratios are excluded, then regression yields a line with $R^2 = 0.948$. Also shown are the Re contents of the two Massif Central ultramafic xenoliths for which data were obtained (filled diamonds). Other symbols as in Figure 5.4.

Figure 5.5 shows the variation of the Os and Re concentrations of the Pyrenean samples as functions of their $Al_2O_3$ contents. Whilst the Os contents of the peridotites show no relationship to their depletion in major elements, Re is clearly correlated with $Al_2O_3$ ($R^2 \approx 0.95$), suggesting that the two elements were similarly incompatible in mantle peridotite during melting or refertilisation. Figure 5.6 shows that the Re contents of the peridotites from the N.E. Pyrenean massifs define a similar correlation with S to that shown by the

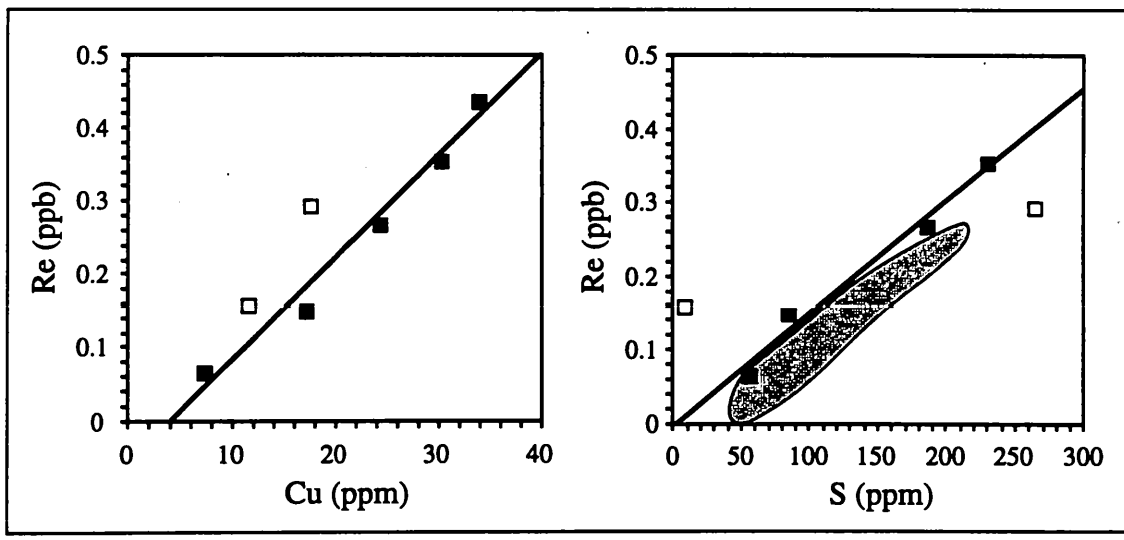


**Figure 5.6** Re *versus* Cu and S in the peridotites collected from the N.E. Pyrenean massifs. In both plots Re exhibits a strong correlation with the chalcophile element compositions of the peridotites. If the two anomalous samples are excluded, regressions through the data give lines with $R^2 = 0.974$ and 0.979 for the plots against Cu and S respectively. Stippled field in plot of Re *vs.* S represents the compositions of the ultramafic xenoliths described by Morgan (1986). Symbols as in Figure 5.4.

ultramafic xenoliths described by Morgan (1986) and discussed in Chapter 2. The trend exhibited by the Pyrenean samples, however, extends to higher Re and S contents than that of the xenoliths. Although the highest S abundances are consistent with a recent estimate of the S concentration of the asthenospheric mantle (~250 ppm, Sun, 1990), the maximum Re concentrations are significantly higher than the concentration estimated for the bulk mantle by Morgan (1986) (~250 ± 20 ppt), using the average Os content of spinel lherzolite xenoliths and the chondritic Re/Os ratio of Allègre & Luck (1980).

| Sample Number | Mg# | Os Conc. (ppb) | Re Conc. (ppt) | $\frac{^{187}Os}{^{188}Os}$ |
|---|---|---|---|---|
| Bo 73 | 90.31 | 2.91‡ | | 0.12698± 43 |
| | 90.31 | 2.23 | 205 | 0.12586± 4 |
| Bt 40 | 89.40 | 1.83 | | 0.13493± 8 |
| RP 68 | 90.87 | 4.05‡ | | 0.12103± 4 |
| | 90.87 | 0.782 | | 0.12205± 8 |
| Ta 19 | 91.00 | 5.55‡ | | 0.11932± 4 |
| | 91.00 | 0.402 | | 0.11943± 7 |
| | 91.00 | 0.398 | | – |
| Ta 39 | 88.75 | 0.925 | 257 | 0.12625± 10 |
| Ta 7 | 90.41 | 0.754 | | 0.12480± 49 |

**Table 5.2** $^{187}Os/^{188}Os$ ratios and Re and Os concentrations for ultramafic xenoliths from the Massif Central. Precision on all Os concentration determinations is better than 3‰. Precision of Re concentrations varied from <0.5% (Bo73) to ~17% (Ta39). Except where indicated, the data were collected using the static collection routine and multiple Faraday collectors and are blank-corrected.
† Data obtained using electron multiplier and dynamic collection routine
‡ Sample prepared by NiS fusion technique

### *Massif Central Xenoliths*

The $^{187}Os/^{188}Os$ ratios determined for the ultramafic xenoliths of the Massif Central vary between 0.1193 and 0.1349. Although the majority of the determined ratios are below that estimated for the present-day chondritic mantle reservoir ($^{187}Os/^{188}Os$ = 0.12711; Walker *et al.*, 1994), the most radiogenic sample (Bt40) is considerably above this value, implying a high time-averaged Re/Os ratio relative to the bulk Earth reservoir. As noted above, the Os concentrations determined for the xenoliths vary according to the method of sample preparation. For samples prepared by fire assay, concentrations of between 2.9 and 5.5 ppb are determined, however, when prepared by acid dissolution, the Os concentrations of the xenoliths lie in the range 0.4 - 2.2 ppb. For only one sample (Bo73) are vaguely similar concentrations determined by the two techniques.

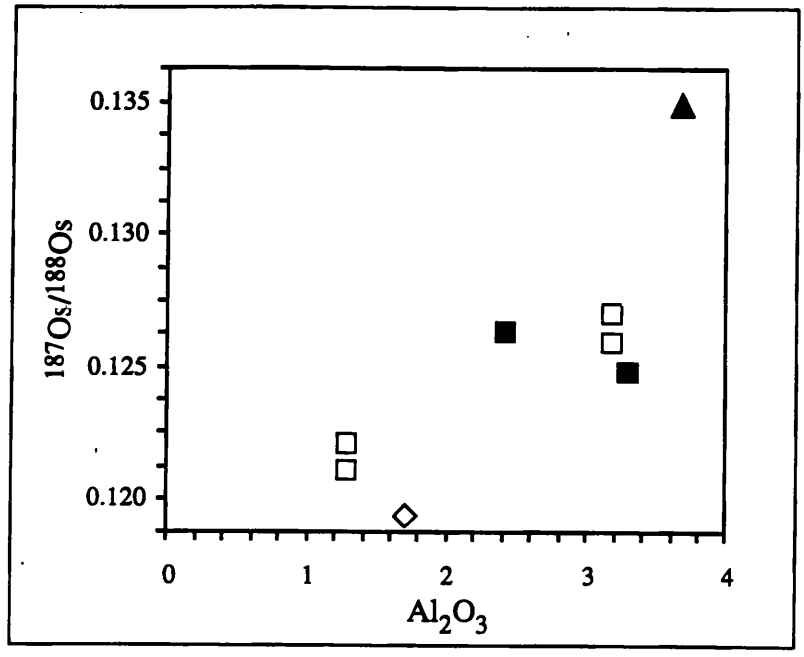


**Figure 5.7** $^{187}Os/^{188}Os$ as a function of $Al_2O_3$ for the ultramafic xenoliths of the Massif Central. Symbols denote xenolith texture: ■, type IA protogranular; □, type IB protogranular; ◇, porphyroclastic; ▲, equigranular. $Al_2O_3$ abundances taken from Downes & Dupuy (1987).

The Re concentrations of the two xenoliths successfully analysed are both greater than 200 ppt, but less than or equal to the concentration estimated by Morgan (1986) for the undepleted mantle. The Re contents of the two xenoliths plot close to, or slightly below, the trends defined by Re as a function of major element depletion in the peridotites collected from the N.E. Pyrénées (Figure 5.5).

When plotted as a function of whole-rock major element depletion, the $^{187}Os/^{188}Os$ ratios of the xenoliths define a similar, but poorer correlation to that observed for the Pyrenean samples. Figure 5.7 illustrates the variation of the xenolith Os isotopic ratios with $Al_2O_3$ content, in which all but the anomalously radiogenic sample (Bt40) plot close to the trend defined by the peridotites of the Pyrenean massifs.

## 5.3 Discussion

### 5.3.1 The Chalcophile Chemistry of the Continental Mantle Lithosphere

In Chapter 2, it was concluded that the abundances and behaviour of Re and Os during mantle processes are predominantly controlled by the base-metal sulphide phases present in the mantle and exsolved from S-saturated melts during transport. Before the Re and Os abundances and Os isotope ratios determined for the orogenic massifs and xenolith suite of this study are interpreted, it is worth discussing the processes which have affected the

chalcophile elements of the analysed samples, in particular the variation of the S content of the peridotites as a function of their major element depletion and the low Cu/S ratios of some of the Pyrenean peridotites.

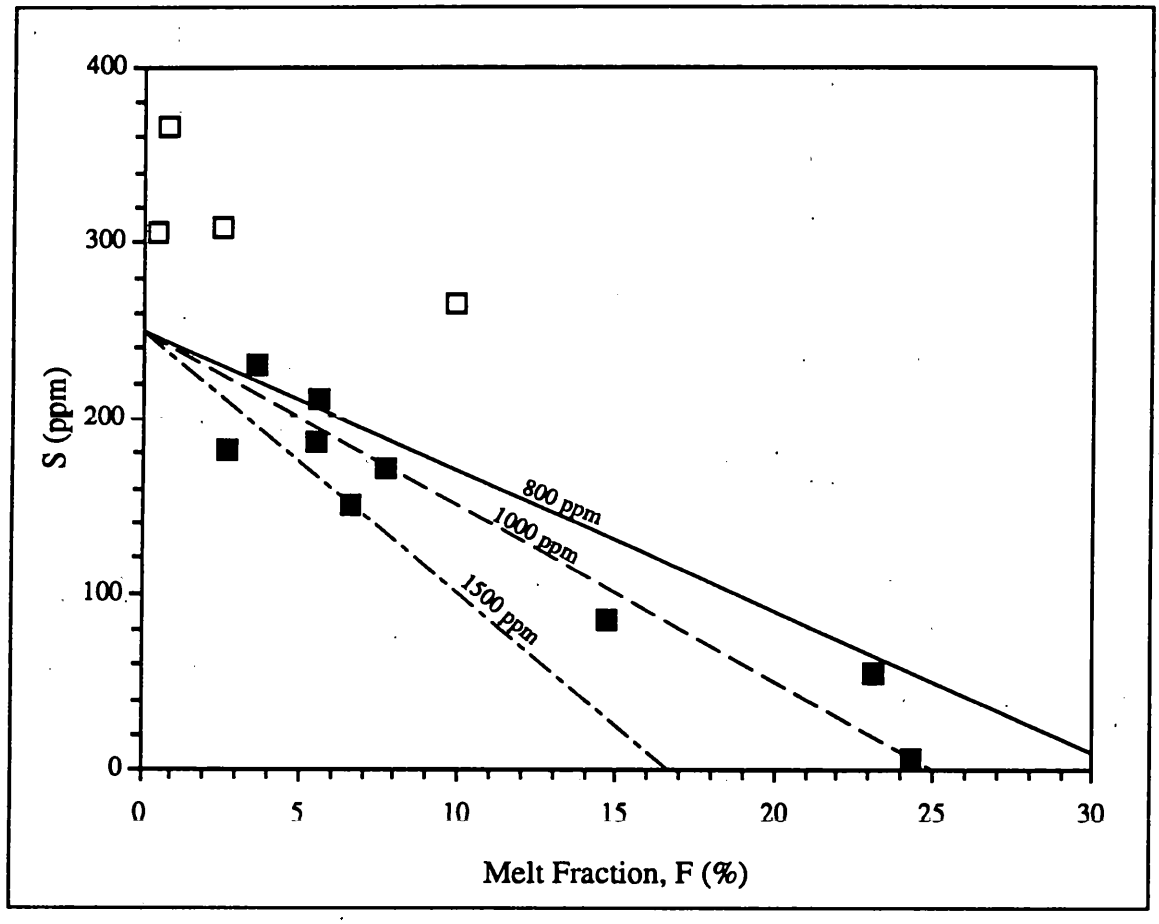


**Figure 5.8** Sulphur contents of the Pyrenean peridotites as a function of melt depletion. Also shown are the trends expected for the extraction of partial melts with a range of dissolved sulphur contents from a mantle source originally containing 250 ppm S (Sun, 1990). Most of the peridotites with "normal" sulphur contents are consistent with the extraction of melts containing 800 - 1000 ppm S (filled symbols), whilst those exhibiting low Cu/S ratios plot above the trends predicted for partial melting (open symbols).

### *Sulphur Content of Mantle Peridotites*

Figure 5.1 shows that the sulphur contents of the peridotites collected from the N.E. Pyrenean massifs are inversely correlated with their whole-rock MgO abundances. A similar plot of S as a function of melt depletion (Figure 5.8) shows that, for the majority of the peridotites, the S abundances are consistent with the partial or complete extraction of a melt containing 900 - 1000 ppm S from a source originally possessing 250 ppm S. Although the solubility of S in basaltic melts varies as a function of several different parameters (primarily $f_{O_2}$, $f_{S_2}$, P, T and the activity of FeO in the partial melt), from the linear regression of

Poulson & Ohmoto (1990) and the experiments of Wendlandt (1982), a sulphur content of ~1000 ppm appears to be within the range expected for a basaltic melt formed by low degrees of melting under upper mantle conditions.

The strong correlation of S abundance with the degree of melt extraction calculated from major and trace element abundances strongly favours the increasingly held view that the mantle sulphide component represents a co-genetic liquid sulphide which persisted throughout a partial melting event, as proposed by Hamlyn & Keays (1986), rather than an exotic immiscible sulphide phase introduced by relatively late "contamination" of the peridotite by a basaltic melt, which was subsequently expelled (e.g. Mitchell & Keays, 1981). Such a contamination process would be expected to result in the heterogeneous distribution of S within the peridotites, as observed in oceanic mantle peridotites, which are believed to have been infiltrated by MORB melts subsequent to the original melt extraction (Lorand, 1987, 1988; Lorand *et al.*, 1993).

If the range of S abundances observed in the Pyrenean peridotites is the result of refertilisation of depleted mantle material by a basaltic melt, as was proposed in Chapter 4 to account for the variation of the major and trace element abundances of the massifs, then a similar degree of heterogeneity would be expected to that observed in oceanic peridotites. In addition, the large degrees of melting needed to produce refertilising melts with the correct major element compositions (Section 4.2.9) would require that melting occurred at temperatures considerably higher than the anhydrous peridotite solidus. Because the solubility of S in basaltic magmas increases with increasing temperature, it is probable that the sulphur contents of such melts would have been considerably greater than the 1000 ppm required to produce the trend of decreasing S with increasing F observed in Figure 5.8. The linear variation of S as a function of major element depletion and the gradient of the sulphur *vs.* F trend, therefore, favour a model involving melt extraction rather than refertilisation for the creation of the range of S compositions observed in the peridotites of the N.E. Pyrénées.

### *Variation of Cu/S ratios*

From the bulk compositions of the sulphide inclusions in the peridotites of the N.E. Pyrenean massifs, Lorand (1989c) concluded that a Cu-rich liquid sulphide phase would have coexisted with the base-metal mono-sulphide solid solution during the latest phase of

plastic deformation recorded by the textures of the peridotites. Although deformation-controlled remobilisation of this Cu-rich liquid, and the chalcopyrite dominated phases which crystallised from it, may account for some of the dispersion observed in the Cu-S trend of Figure 5.2, the considerably lower Cu/S ratios and elevated S abundances observed in several of the peridotites (Figure 5.8) suggest that the whole-rock sulphur abundances of certain samples may have been altered subsequent to the initial removal of S by melt extraction.

Lorand (1991) observed that peridotites collected from the Freychinède and Sem massifs containing high S contents were also characterised by high levels of accessory Ti-pargasite, suggesting that the excess sulphur was introduced during the late-stage metasomatism of the peridotites, coincident with the final phase of deformation. Although no connection is apparent between the $TiO_2$ and S contents of the peridotites analysed in this study, the similarity between the low Cu/S ratios of the anomalous peridotites and those determined for the amphibole-bearing veins found in the Lherz and Freychinède massifs (Bodinier *et al.*, 1990; Figure 5.2) support the suggestion that the S was added by similar small-degree asthenospheric melts.

Because the peridotites sampled in this study were collected from positions far from any visible mafic layers, direct interaction between the peridotites and the pyroxenites may be ruled out as the cause of the elevated S contents. The association between high pargasite contents and the sulphur enrichment in the anomalous peridotites, however, may be accounted for by a process similar to the percolation model proposed by Bodinier *et al.* (1990), in which alkali basalts from the vein conduits infiltrated the peridotite host and were transported by porous-flow percolation along grain boundaries (Figure 5.9). During melting and transport in the vein conduits, the high Fe, Ti and volatile contents of the melts may have led to increased S solubility relative to Cu, leading to low Cu/S ratios in the melt (Haughton *et al.*, 1974; Gorbachev & Kashirceva, 1985). Once the melts entered the peridotites, however, the reduction in temperature and precipitation of Ti-rich phases may have reduced the solubility of sulphur in the melts, leading to sulphur saturation and the precipitation of sulphides with low Cu/S ratios reflecting the composition of the infiltrating melt.

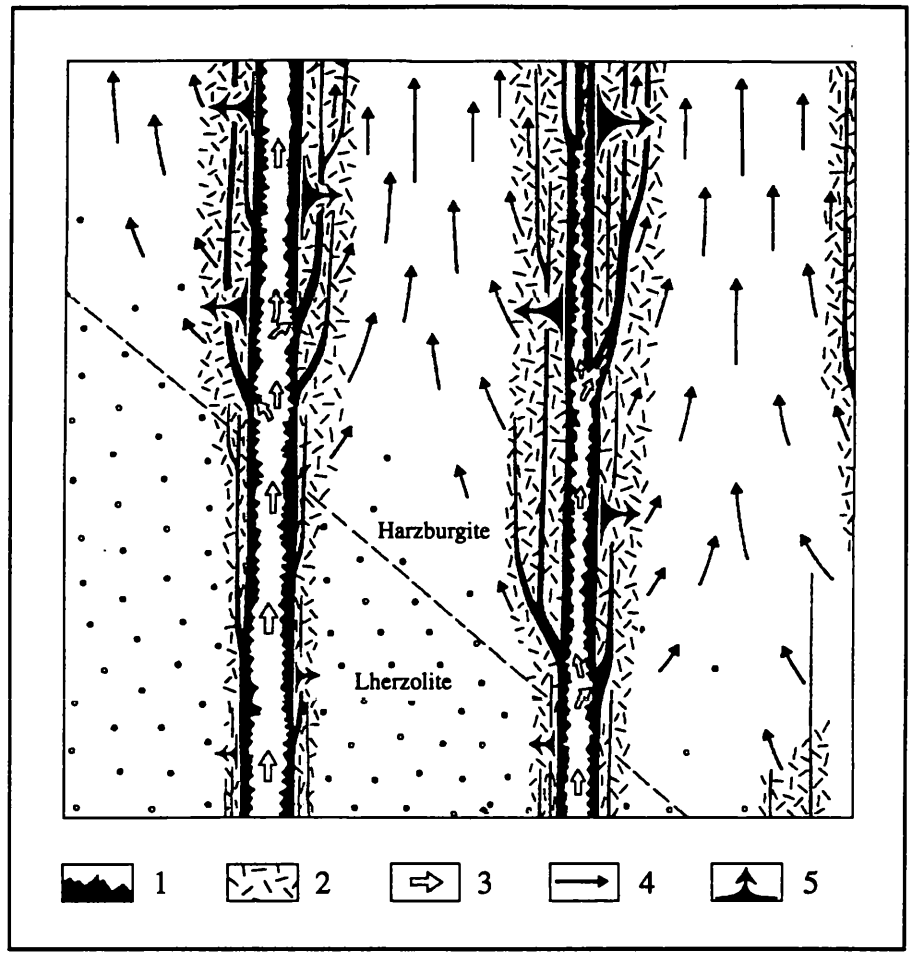


**Figure 5.9** Cartoon illustrating the modal metasomatism of peridotite wall rocks due to the infiltration of alkali basalts from vein-conduits (after Bodinier *et al.*, 1990). Diffusion-controlled, modal metasomatism occurs in the peridotites adjacent to the veining, whilst percolation controlled, cryptic metasomatism occurs in the peridotites at a distance from the veins. 1: Mineral segregates in vein-conduits; 2: amphibole-bearing peridotites; 3: magma flow in vein conduits; 4: porous flow percolation in peridotite host; 5: diffusion through the infiltrated melt phase.

### 5.3.2 Geochemistry of Re and Os in Mantle Peridotites

***Effects of Alteration on Os and Re Abundances***

The peridotite sample sets collected from the N.E. Pyrénées and Massif Central both exhibit evidence of alteration, but of differing types. The Pyrenean massifs show varying degrees of serpentinisation under reducing conditions, as reflected in the losses on ignition determined during major element analysis (Table 4.3) and the buffering of sulphide mineral assemblages at lower sulphur fugacities (Lorand 1989b, 1991). The Massif Central xenoliths, however, appear to have been oxidised by hydrous fluids percolating through the volcanic pile subsequent to their eruption in the alkali basalt, leading to the loss of sulphur and significant alteration of the abundances of the chalcophile elements.

The small degrees of serpentinisation of the N.E. Pyrenean peridotites appear to have had little effect on the abundances of Re in the samples, as demonstrated by the good

correlations between Re and the major element compositions of the samples. The scatter of the Os abundances as a function of major element depletion, however, may reflect the exsolution of the element from the mantle BMS phase under reducing conditions, leading to heterogeneously distributed Os-bearing minerals (either Os-Ir alloys or laurite (Ru, Os, Ir)$S_2$). Such behaviour of Re and Os is consistent with the mineral solubilities suggested by the thermochemical calculations in Chapter 2. Because the majority of the Pyrenean samples were prepared using the NiS fusion technique, however, the occurrence of Os as refractory alloy grains should not have significantly affected the results of the analyses.

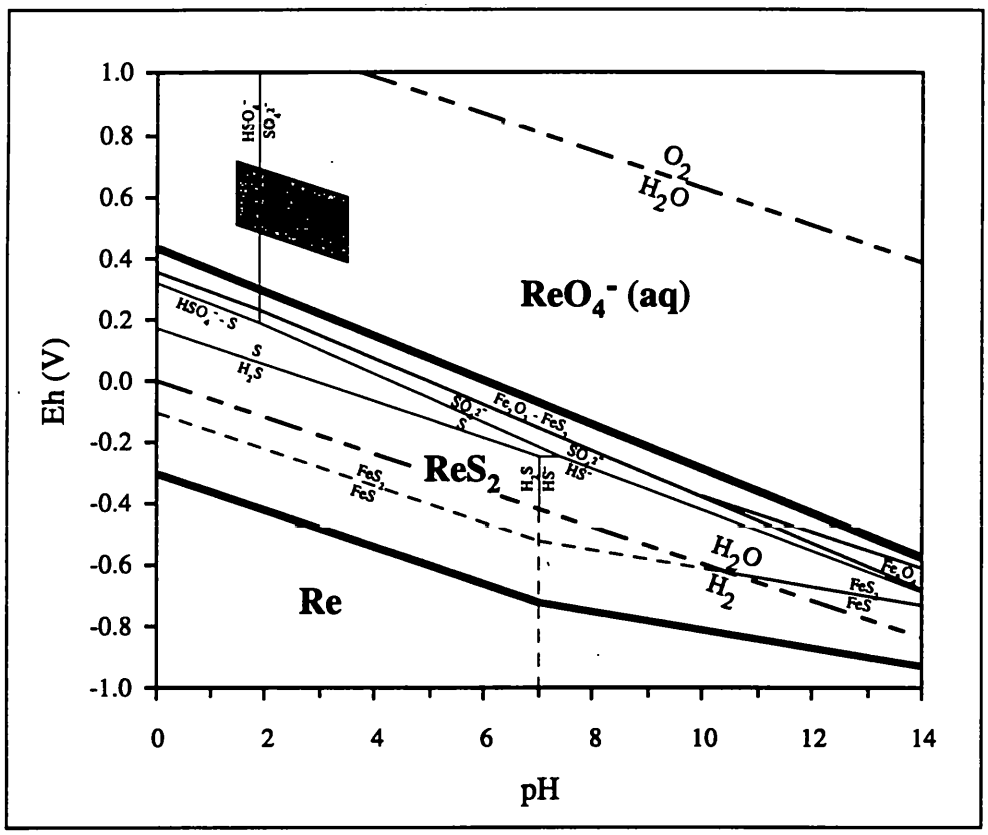


**Figure 5.10** Stability relations of rhenium and its sulphide and oxides in water at 25°C and 1 atmosphere total pressure. Heavy lines enclose the stability field of solid metal compounds. Light lines divide the fields of compounds in the Fe-O-S system and the major sulphide species (after Garrels & Christ, 1965). Dashed lines denote metastable phase boundaries. Dash dot lines delineate the stability fields of water. The activities of sulphide species taken to be 0.1 mol $l^{-1}$, whilst those of the Re species are ~1 nmol $l^{-1}$. Dashed quadrilateral encloses the field of volcanic acid-sulphate waters, estimated from data contained within Mueller & Saxena (1977) and Garrels & Christ (1965). Thermodynamic data for Re and its compounds taken from Weast (1975).

The post-eruptive oxidation of the Massif Central basalts and their xenoliths appears to have removed virtually all of the original BMS phase from the peridotites. Under the highly acidic and oxidising conditions expected during such alteration, neither Re nor Os should be stable as sulphide species, as shown by the Eh-pH diagrams for the elements (Figure 5.10

and 5.11). Both $ReS_2$ and $OsS_2$ should react with the hydrous fluids and release their sulphur into solution as sulphate ions. Whilst the Os may be left as either metal or hydrated oxide grains after alteration, the Re should be soluble in the circulating fluids and so be partially or wholly removed from the xenoliths.

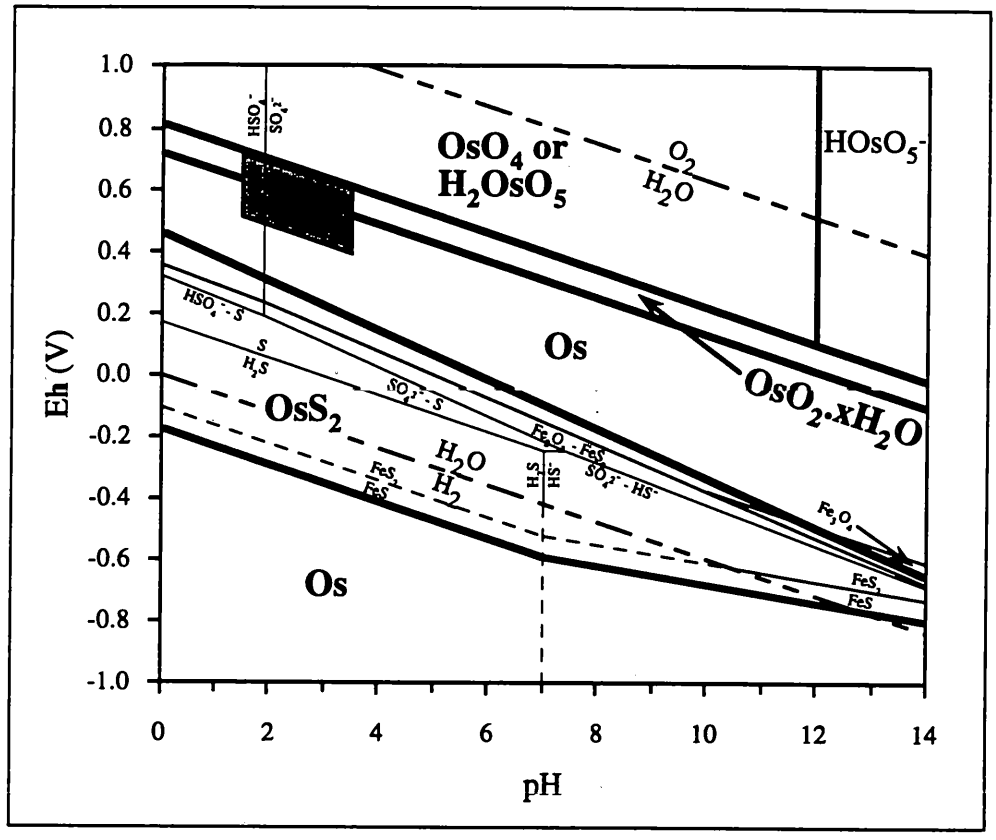


**Figure 5.11** Stability relations of osmium and its sulphide and oxides in water at 25°C and 1 atmosphere total pressure. For details of the fields illustrated, see Figure 5.10. Concentrations of Os species are ~1 nmol $l^{-1}$. Thermodynamic data for Os and its compounds taken from Goldberg & Helper (1968).

The presence of Os in alloy phases in the xenoliths is consistent with the Os concentrations determined in the xenoliths during this study. During acid dissolution under reducing conditions, any Os present in an alloy phase may have been only partially dissolved, leading to the determination of low Os contents in the xenoliths prepared by this technique. If the low concentrations determined in the xenoliths by acid dissolution are related to the presence of Os in insoluble phases, then the discrepancy between the measured and true Os contents should be related to the degree of alteration of the sulphide phase. The similarity between the two Os concentrations determined for the least altered sample (Bo73) when it was prepared by both the acid dissolution and NiS fusion techniques supports this argument.

Although the Re content of sample Bo73 is marginally lower than those of peridotites from the N.E. Pyrenean massifs which exhibit similar degrees of major-element depletion (suggesting some mobilisation of the element may have occurred during alteration), the relatively high Re concentrations determined for the two analysed xenoliths indicate that the dissolution of Re is considerably less than that predicted from the Eh-pH calculations. In the absence of more analyses of the Re content of the xenoliths, however, a thorough discussion of the mobility of Re during the post-eruptive water-rock interaction is not possible.

In conclusion, the heterogeneity observed in the Os abundances determined in the peridotites collected from the N.E. Pyrenean massifs and the dependence of the Os concentrations determined in the Massif Central xenolith samples on the method of sample preparation are interpreted as the results of the alteration processes which have affected the mantle peridotites, rather than any earlier processes in the mantle source. The good correlations observed between the Re abundances of the Pyrenean samples and their major element compositions, however, suggest that during serpentinisation the mantle peridotites behaved as a closed system. Although the oxidation responsible for the removal of S from the Massif Central xenolith samples may have partially mobilised their Re contents, from the two Re concentrations determined in these samples it was not possible to draw any firm conclusions.

***Behaviour of Re and Os During Mantle Melting***

In Chapter 2 it was proposed that the behaviour of Re and Os during mantle melting is primarily controlled by the partitioning of the elements between the base-metal sulphide phase and the silicate liquid. Most of the Os was predicted to remain in the BMS phase of the residual peridotite after melting whilst the Re partially enters the silicate melt, resulting in a decrease in the Re/Os ratio of the mantle during melting. These conclusions are generally supported by the analyses of the peridotites collected from the N.E. Pyrénées.

If the two anomalous samples (92-LH3 and 92-LH12) are excluded from the regressions, the Re abundances of the peridotites show excellent correlations with their depletion in both basaltic elements (e.g. Re vs. $Al_2O_3$, Figure 5.5) and sulphur (Figure 5.6, $R^2 = 0.98$). The linearity of the Re - S relationship verifies the dominant control of the mantle BMS phase on the behaviour of Re during mantle melting, as suggested in Chapter 2.

Although the Re contents of the Pyrenean samples are higher than those described by Morgan (1986) for a collection of spinel peridotite xenoliths (Figure 5.6), on a plot of Re as a function of the degree of melting (Figure 5.12), the linear variation of the Pyrenean Re abundances may be reproduced by a similar non-modal batch-melting model and the same value of $D_{sul/sil}$ (~325) to that determined for the element in Chapter 2, using the xenolith data presented by Morgan. The low value of $D_{sul/sil}$ required to reproduce the Pyrenean Re - F trend confirms that the compatibility of Re in the BMS phase during mantle melting may be similar to those of the moderately chalcophile elements, such as Cu and Ni ($D_{sul/sil} \approx$ 245; Rajamani & Naldrett, 1978), rather than the highly chalcophile Pt-group elements ($D_{sul/sil} \approx 10^3 - 10^5$).

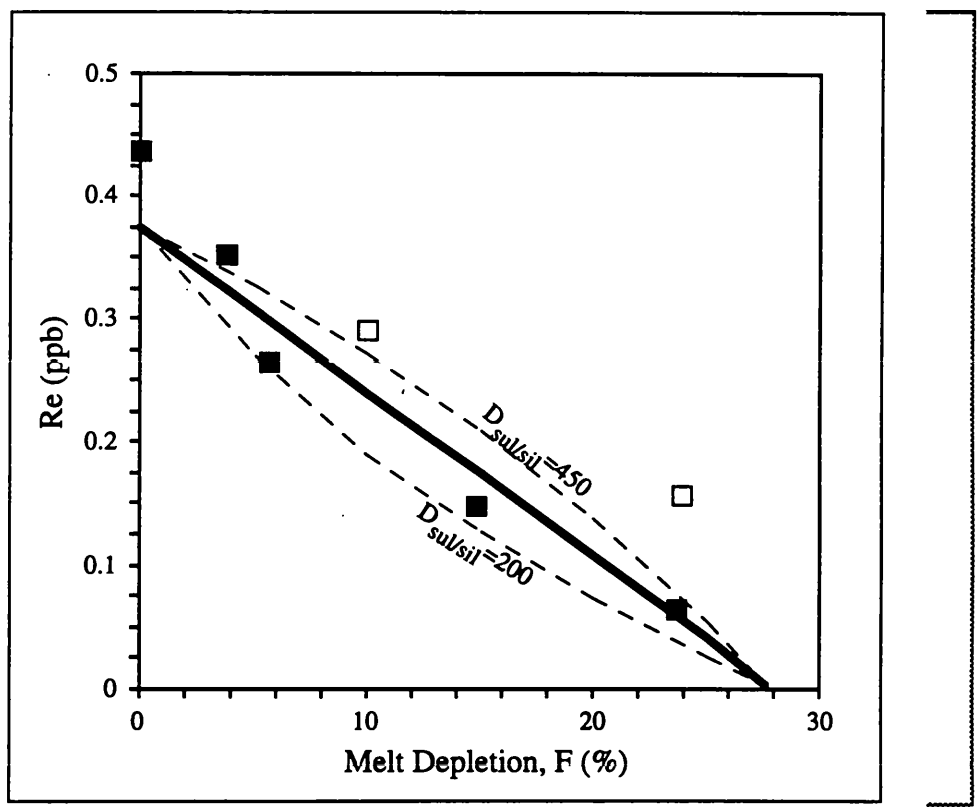


**Figure 5.12** Variation of Re concentration as a function of melt depletion in the peridotites collected from the N.E. Pyrénées. Symbols are the same as in Figure 5.1. Proportion of melt extracted calculated from the Ni contents of the samples (see Section 4.2.7). Also shown are the trends expected for the extraction of a melt containing 900 ppm S, formed by the non-modal melting of a mantle source containing 250 ppm S and 375 ppt Re. The solid line assumes $D_{sul/sil}$ = 325, whilst the dashed lines are calculated using $D_{sul/sil}$ = 450 and 200.

The Os concentrations of the peridotites appear to exhibit a large degree of scatter as a function of both $Al_2O_3$ (Figure 5.5) and S (not shown), with no systematic variations. The high Os contents of the depleted peridotites and the absence of any relation to their major

element compositions indicate that the element is highly compatible in the mantle residue and may be retained in the mantle after the extraction of partial melts. As mentioned above, however, the large degree of scatter as a function of major element composition suggests that Os may be distributed heterogeneously in the samples, leading to poor reproducibility in the determined Os concentrations.

***Interaction of Pyrenean Peridotites with Mafic Melts***

In Section 5.3.1 it was noted that several of the peridotites of the N. E. Pyrenean massifs exhibited S abundances and Cu/S ratios that were inconsistent with a simple origin involving the progressive loss of the sulphide phase by increasing degrees of partial melt extraction. It was concluded that the sulphur contents of these samples had been augmented by the precipitation of base-metal sulphides from low-degree partial melts possessing low Cu/S ratios.

Analysis of the Os and Re contents of these anomalous peridotites suggests that whilst the Os abundances appear to have been unaffected by the addition of the BMS phase (the two analysed samples possessing both high and low Os contents), the Re abundances may have been altered by the metasomatic event. In Figures 5.5 and 5.6, the Re content of sample 92-LH3 plots above the trends defined by the Re contents of the other samples as functions of both Cu and $Al_2O_3$. In Figure 5.6, however, the Re/S ratio of this sample is significantly less than that of the other peridotites, suggesting that whilst the Re/Cu ratio of the infiltrating melt was greater than that of the bulk mantle, like Cu, Re was depleted relative to sulphur in the metasomatising melt.

The single S-rich sample investigated in this study, therefore, indicates that the Re/Os ratios of lithospheric mantle peridotites may be altered by the percolation of the same low-degree partial melts believed to be responsible for the incompatible element enrichment of the continental mantle lithosphere. This observation supports previous observations that the Re/Os ratios of mantle material may be altered by some processes, either within the mantle or during transport in kimberlite melts (Walker *et al.*, 1989a; Pearson *et al.*, 1995b). To understand more fully the influence of such interactions on the Re-Os isotope systematics of the continental mantle lithosphere, a more detailed study is required, in which the pyroxenite veins, their peridotite wall-rocks and the S-rich massive peridotites are investigated.

### 5.3.3 The Re-Os Isotope Systematics of the N.E. Pyrenean Massifs

The correlation of the Os isotope compositions of the peridotites collected for this study with their major element compositions indicates that the Re-Os isotope systematics of the samples were probably established by the same processes that created the range of major element compositions observed in the two sample sets. In the previous chapter, this compositional range was interpreted to be the result of either two-component mixing or unmixing, involving the extraction of variable quantities of basaltic melt from a fertile mantle source or the re-enrichment of depleted mantle material by the addition of a melt formed by partial-melting at relatively low-pressures. Because the nature of these two processes contrast strongly and the interpretation of the Os isotopic compositions of the peridotites depends on the model used for the major element trends, the observed correlations between the $^{187}Os/^{188}Os$ ratios and major element compositions of the peridotites and the significance of the $^{187}Os/^{188}Os$ - $^{187}Re/^{188}Os$ trend will be considered separately for each model.

***Partial Melt Extraction and Lithosphere Evolution***

Within the context of a model for the major element variations involving the extraction of partial melts, the observed range of peridotite $^{187}Os/^{188}Os$ ratios would arise from the in-growth of radiogenic Os in response to variations in the Re/Os ratios of the residues. If the Os isotopic compositions of the peridotites were homogenised during melting and the Re-Os isotope system has remained undisturbed since the melting event, then the correlation of $^{187}Os/^{188}Os$ with $^{187}Re/^{188}Os$ observed for the Pyrenean samples would define an isochron, dating the melt-extraction.

In view of the excellent correlation between the Re contents of most of the samples and their lithophile and chalcophile element compositions, the assumption that the Re-Os system has remained closed since melt extraction may be considered valid for most of the samples used in the regression. However, because the abnormal chalcophile element abundances of sample 92-LH3 suggest that an exotic sulphide phase may have been introduced to the sample since the original melting event (leading to an anomalously high Re content), it fails the necessary criteria and is not included in the regression of the $^{187}Os/^{188}Os$ - $^{187}Re/^{188}Os$ trend. Because the elevated Re content of this sample is accompanied by a high Os content, however, it plots close to the Re-Os isochron, hence exclusion of this sample from the regression has little effect on the determined age and initial $^{187}Os/^{188}Os$ ratio of the Pyrenean

samples, the values becoming 1.97 ± 0.46 Ga and 0.1170 ± 0.0014 respectively for the four-point isochron (Figure 5.3).

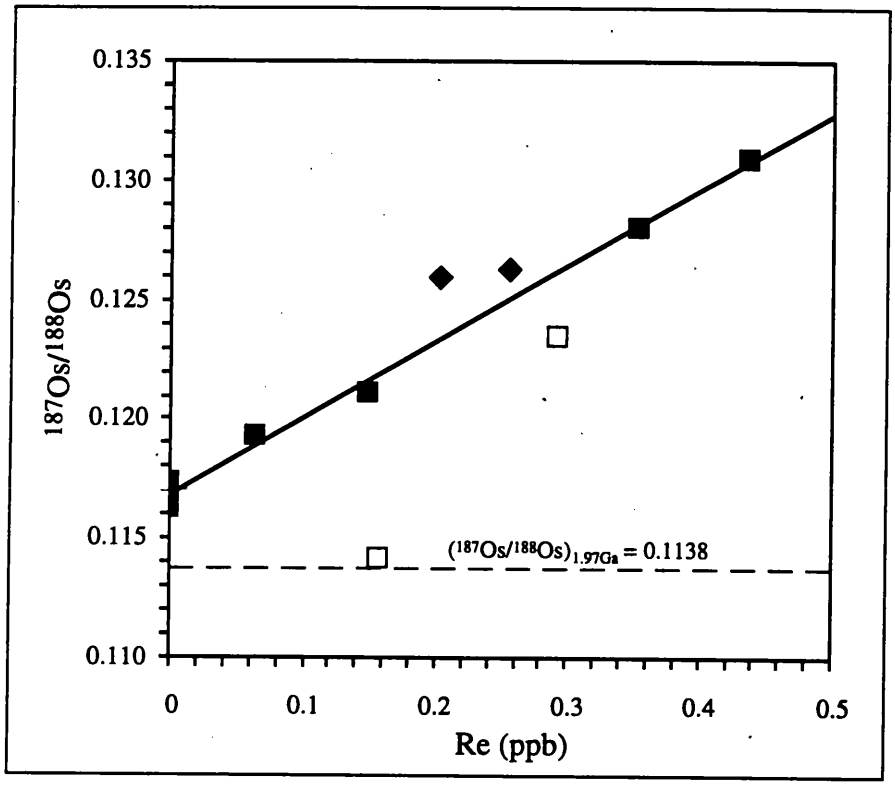


**Figure 5.13** Variation of $^{187}Os/^{188}Os$ as a function of Re content. Symbols as in Figure 5.5. The line shown ($R^2 = 0.995$) is regressed through the data for the peridotites collected from the N.E. Pyrenean massifs only (excluding 92-LH3 and 92-LH12). The bar at zero Re denotes the initial $^{187}Os/^{188}Os$ ratio calculated from the regression, including 2σ errors (0.1168 ± 0.0006). Bulk Earth ratio at 1.97 Ga calculated from the mantle evolution line of Luck & Allègre (1991).

The large errors in the age and initial $^{187}Os/^{188}Os$ ratio calculated from the Re-Os isochron result primarily from the poor reproducibility of the Os concentration determinations, which lead to large uncertainties in the sample Re/Os ratios. In order to by-pass these uncertainties, the $^{187}Os/^{188}Os$ ratios of the peridotites were plotted as a function of their Re content (Figure 5.13), with which they define an excellent correlation ($R^2$ = 0.995). Although the gradient of this correlation has no age-significance, its intercept with the $^{187}Os/^{188}Os$ axis at zero Re (0.1168 ± 0.0006) should be equivalent to the $^{187}Os/^{188}Os$ ratio of the peridotites at the time of melting. The agreement between the initial $^{187}Os/^{188}Os$ ratios calculated from the Re-Os isochron and the $^{187}Os/^{188}Os$ - Re correlation suggests that, despite the large errors on the regression of the Re-Os isochron, the unradiogenic initial $^{187}Os/^{188}Os$ ratio and the early Proterozoic Re-Os isochron age are realistic.

Extraction of melt from the Pyrenean continental mantle lithosphere during the early Proterozoic ties in with crustal ages obtained for the basement exposed in western France and northern Iberia. Guerrot *et al.* (1989) found that the U-Pb isotope systematics of zircons from meta-igneous granulites exposed on the continental shelf of northern Iberia recorded two major events of crustal growth and high-grade metamorphism in the region. The first of these events probably occurred during the Archaean, with upper intercept ages clustering around 2.7 Ga, whilst the second took place in the early Proterozoic (~1.86 Ga), similar to the Re-Os isochron age of the Pyrenean mantle lithosphere. Guerrot *et al.* (1989) suggested that this early Proterozoic event may be related to the "Icartian" event (1.8 - 2.0 Ga) which was responsible for the formation of the high-grade metamorphic basement rocks exposed in northern Brittany and the Channel Islands (Adams, 1976; Calvez & Vidal, 1978).

The early Proterozoic U-Pb ages obtained by Guerrot *et al.* (1989) also coincide with Sm-Nd depleted-mantle model ages for the Hercynian basement and volcanic rocks exposed in the Pyrénées, which lie in the range 1.45 - 2.2 Ga (Ben Othman *et al.*, 1984a; Gilbert *et al.*, 1994). These model ages are in agreement with the crustal evolution model proposed by Liew & Hofmann (1988), based on metamorphic rocks, sediments and granitoids from the Hercynian Fold Belt of central Europe. In their model, most of the crustal protolith of the European Hercynian basement probably separated from a mantle source during the early to mid-Proterozoic, after which it has been recycled, with only minor additions of mantle-derived material during later orogenic events.

Although the coincidence of the crust and mantle stabilisation ages may not be wholly unexpected (given that new continental lithosphere is believed to form by the differentiation of crust at the expense of the underlying mantle), the preservation of the Re-Os isochron recording the stabilisation indicates that, since the original melting event, the mantle source of the Pyrenean massifs has remained relatively stable. It also indicates that the lithospheric mantle underlying the region has not been affected by the processes of thinning or delamination which may have occurred in other regions of post-Archaean mantle lithosphere (Bird, 1978; Houseman *et al.*, 1981; Platt & Vissers, 1989). Because the Pyrenean massifs were probably derived from relatively shallow depths within the mantle (as shown by the absence of garnet in the peridotites and the relatively low pressures estimated for

crystallisation of the mafic layers), such stability can only be inferred for the shallower parts of the mantle lithosphere.

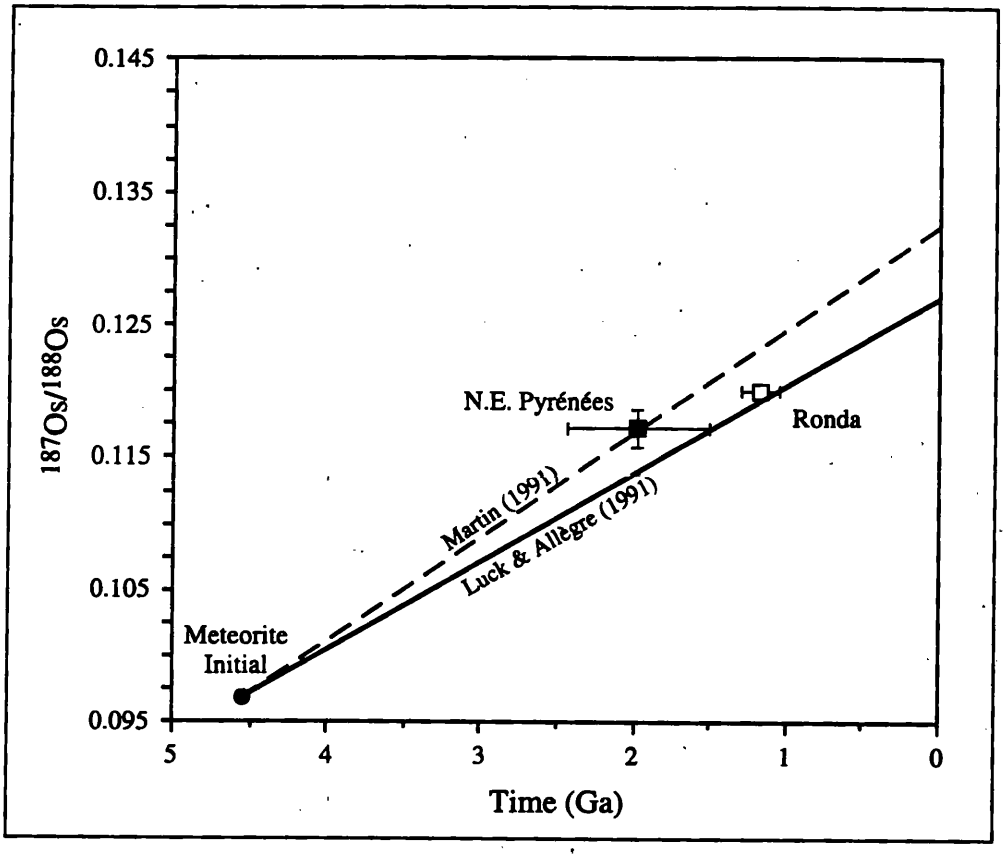


**Figure 5.14** $^{187}Os/^{188}Os$ evolution diagram showing the position of the N.E. Pyrenean massifs relative to the bulk Earth evolution models of Luck & Allègre (1991), solid line, and Martin (1991), dashed line. Also shown is the position of the Ronda ultramafic complex, after Reisberg *et al.* (1991).

Because the initial $^{187}Os/^{188}Os$ ratio of the Pyrenean samples is considerably more radiogenic than the predicted value at ~2.0 Ga using the bulk Earth evolution models of Luck & Allègre (1991) or Walker *et al.* (1994) (~0.1138; Figures 5.3 and 5.14), it is possible that, prior to melt extraction, the mantle protolith of the massifs had evolved with a Re/Os ratio greater than the chondritic ratio used in these models. Such elevated ratios may be created by one of two processes. If a relatively Re-rich component (e.g. recycled oceanic crust or sediments) were added to the mantle protolith during an event significantly earlier than the melting recorded by the Re-Os isochron, then the Os isotope composition of the mantle would have evolved towards $^{187}Os/^{188}Os$ ratios significantly higher than those of the bulk Earth. Alternatively, the Pyrenean massifs may have been derived from an enriched mantle source, similar to that proposed by Martin (1991) to account for the elevated

$^{187}Os/^{188}Os$ ratios of ocean island basalts, which may represent a distinct mantle reservoir, isolated from the mantle source described by the evolution model of Luck & Allègre (1991). Despite the positive values of $\gamma_{Os}$, the derivation of the peridotites of the Pyrenean massifs from a mantle source with a composition similar to that of the bulk Earth evolution curve of Luck & Allègre (1991) cannot be rejected categorically, owing to the poor precision of the determined isochron age, hence large error in $\gamma_{Os}$. Future analyses of the Re-Os isotope systematics of the massifs, in which the Re/Os ratios are determined more precisely, may improve the precision of the isochron age, leading to a better constraint on the mantle source.

In their study of the Re-Os isotope systematics of the Ronda peridotites, Reisberg *et al.* (1991) also observed a "weak positive correlation" between $^{187}Os/^{188}Os$ and $^{187}Re/^{188}Os$ which, when interpreted as an isochron, gave an age of 1.17 ± 0.12 Ga, with an initial $^{187}Os/^{188}Os$ ratio of 0.1199 ± 0.0006. Despite the large errors in the isochron age determined for the Pyrenean samples, the Re-Os isotope systematics of the N.E. Pyrenean massifs demonstrate that depletion of the southern French mantle lithosphere must have occurred during a distinctly earlier event from that which affected the mantle lithosphere underlying southern Spain. An earlier date for the extraction of melt from the Pyrenean lithosphere is supported by the significantly less radiogenic initial $^{187}Os/^{188}Os$ ratio of the French peridotites relative to those from the Ronda massif. Owing to the positive value of $\gamma_{Os}$, however, the difference in age based on the initial $^{187}Os/^{188}Os$ ratios of the two regions is less than that calculated from their isochron ages.

In conclusion, the interpretation of the $^{187}Os/^{188}Os$ - $^{187}Re/^{188}Os$ correlation as an isochron and the age calculated from it are consistent with existing models for the evolution of the western European lithosphere, involving significant crustal growth in the early Proterozoic followed by the recycling of the existing crust during subsequent events. Prior to melting, the mantle protolith of the Pyrenean peridotite massifs may have been marginally more radiogenic than the estimated composition of the convecting mantle at the time. Although this may suggest the existence of "enriched" portions of heterogeneous mantle below western Europe during the early to mid-Proterozoic, owing to the imprecision of the isochron age determination it is not possible to draw any definite conclusions. Both the calculated isochron age and initial $^{187}Os/^{188}Os$ ratio of the Pyrenean peridotite massifs,

however, indicate that the continental mantle lithosphere underlying the region is significantly older than the lithospheric source of the Ronda ultramafic complex.

***Refertilisation***

In the discussion of the whole-rock major and trace element abundances of the peridotite samples collected from the N.E. Pyrenean massifs, it was shown that the compositional trends could be modelled by the refertilisation of depleted mantle material by the addition of variable quantities of basaltic melt. Under such conditions, the linear variations of Re with MgO, $Al_2O_3$ and $Mg^{\#}$ in the Pyrenean peridotites would reflect mixing between a low-Re/Os depleted-mantle end-member and a high-Re/Os melt and the correlation of $^{187}Os/^{188}Os$ with $^{187}Re/^{188}Os$ and the major element compositions would arise from the production of radiogenic $^{187}Os$ in response to the Re/Os ratio created during mixing.

In their discussion of the $^{187}Os/^{188}Os$ - $^{187}Re/^{188}Os$ trend observed in the peridotites of the Ronda ultramafic complex, Reisberg *et al.* (1991) pointed out that linear correlations between the isotope ratios and parent-daughter ratios are a feature of a number of different radiogenic isotope systems in mid-oceanic basalts. Such trends have been interpreted as the result of continuous processes of melt extraction and mixing between different mantle domains, and so to be of no age significance (Allègre *et al.*, 1980). Using a simplified model, Reisberg *et al.* (1991) showed that continuous mixing between depleted mantle material and recycled oceanic crust could account for both the $^{187}Os/^{188}Os$ - $^{187}Re/^{188}Os$ and $^{187}Os/^{188}Os$ - major element correlations observed for the Ronda peridotites. On account of the considerable time required for mantle convection to thin the recycled crust enough for diffusion to homogenise it with the surrounding residual mantle, such trends may be expected to be a mantle-wide phenomenon. The distinctly different slopes and intercepts of the $^{187}Os/^{188}Os$ - $^{187}Re/^{188}Os$ and $^{187}Os/^{188}Os$ - major element trends defined by the peridotites of the Ronda and N.E. Pyrenean massifs, however, demonstrate that the trends defined by these massifs differ significantly, despite the reasonably short distance between the two regions. Therefore, a model involving mantle-wide mixing can probably be ruled out as the cause of the trends shown by the peridotites from either of the orogenic massifs.

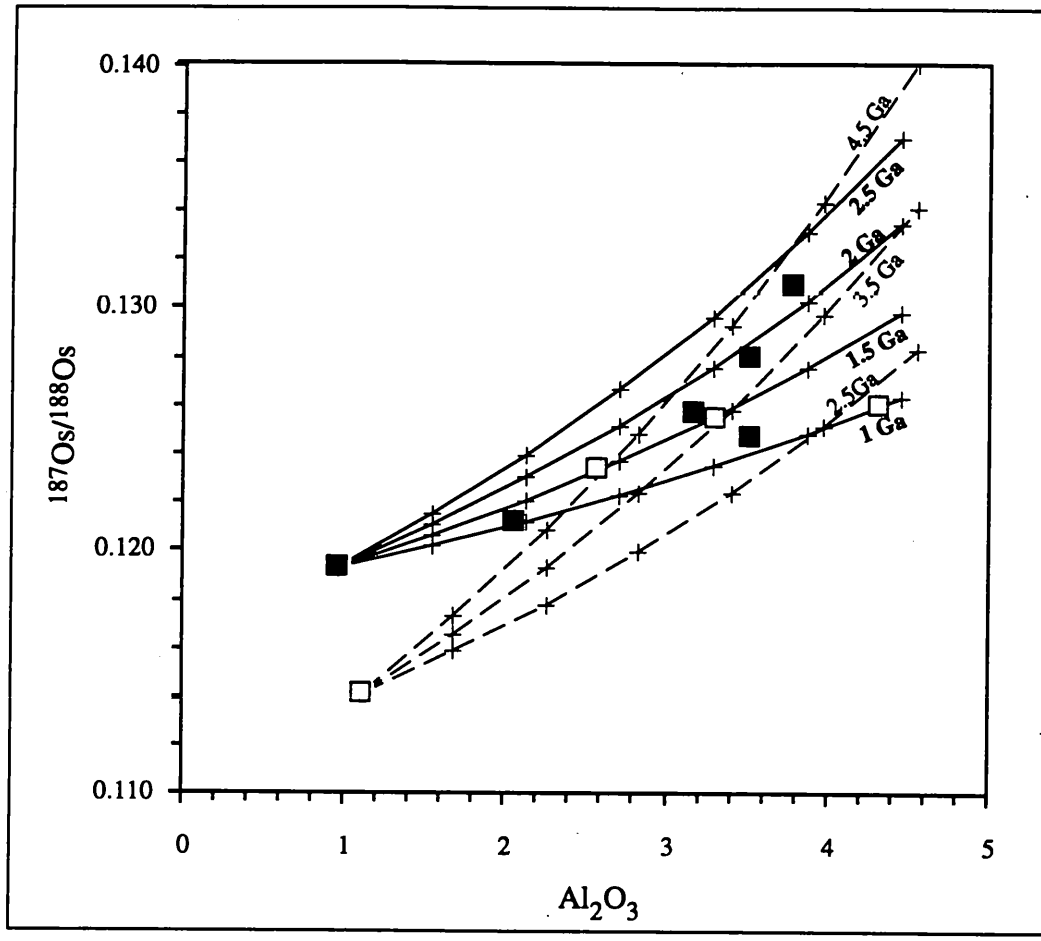


**Figure 5.15** Plot of $^{187}Os/^{187}Os$ vs. $Al_2O_3$ for peridotites collected from the N.E. Pyrenean massifs, illustrating the trends predicted for the refertilisation of depleted mantle material by the addition of basaltic melt of various ages. Refertilisation of two different mantle end-members is shown, using the compositions of samples 92-FT5 (solid lines) and 92-LH12 (dashed lines). Crosses mark 5% melt increments. Although the trends observed for the Pyrenean samples can be reproduced by the addition of 1 - 2 Ga basalts to sample 92-FT5, the addition of melts older than 4.5 Ga would be required for a depleted end-member similar to 92-LH12. For details of the melting model see text. Symbols as in Figure 5.1.

Although mantle-wide processes may be rejected, local refertilisation of depleted mantle material may still account for the observed trends. In such a model the timing and extent of mixing may differ between the N.E. Pyrenean and Ronda massifs, enabling different trends to be produced. The effects of such a process may be calculated using a simple two-component mixing model between the most depleted samples collected from the massifs and a basaltic melt (Figure 5.15).

The elemental and isotopic compositions of the end-members used in the calculations are shown in Table 5.3. For consistency with the results of the modelling performed in Section 4.2.9, the $Al_2O_3$ content of the experimental melt produced by Hirose & Kushiro at ~30% melting and 10 kbar was used in the calculations. The Re and Os contents of the melt were assumed to be similar to those of typical MORB (1 ppb Re, 0.05 ppb Os; Hertogen *et al.*,

1980), with a $^{187}Os/^{188}Os$ ratio similar to that of the bulk mantle at the time of melting. Because the amount of common Os in the melt is so much lower than that of the peridotite end-member, however, the initial Os isotopic composition of the melt has little impact on the $^{187}Os/^{188}Os$ ratio of the mixture.

| Component | Re (ppb) | Os (ppb) | $\left(\frac{^{187}Os}{^{188}Os}\right)_{now}$ | $Al_2O_3$ (wt%) |
|---|---|---|---|---|
| Depleted Mantle Residue (92-FT5) | 0.065 | 4.74 | 0.1193 | 0.96 |
| Depleted Mantle Residue (92-LH12) | 0.157 | 5.92 | 0.1141 | 1.11 |
| Refertilising Melt | 1.0 | 0.05 | – | 12.58 |

**Table 5.3** Parameters used in the modelling of the Re-Os isotope systematics of the mantle following the refertilisation of a depleted mantle residue by the addition of a basaltic melt. Composition of depleted residue taken from the analyses of samples 92-FT5 and 92-LH12. Re and Os contents of the melt from Hertogen *et al.* (1980), MgO contents from melting experiments of Hirose & Kushiro (1993) (see Section 4.2.9). $^{187}Os/^{188}Os$ ratio of melt assumed to be similar to that of the asthenospheric mantle at the time of refertilisation, calculated using $^{187}Re/^{188}Os \approx 0.40076$ and $(^{187}Os/^{188}Os)_{now} = 0.12711$ (Walker *et al.*, 1994).

Whilst the $^{187}Os/^{188}Os$ - $Al_2O_3$ trend defined by the Pyrenean peridotites lies sub-parallel to the trend calculated for the addition of 8 - 30% of a 1 - 2 Ga old basaltic melt to sample 92-FT5, consistent with the conclusions drawn from major element modelling, the calculated mixing trends from sample 92-LH12 cut across the trend of the Pyrenean data and require a melt older than 4.5 Ga to reproduce the $^{187}Os/^{188}Os$ ratios of several samples. Although refertilisation of depleted mantle with a composition similar to 92-FT5 may account for the observed trends of increasing $^{187}Os/^{188}Os$ with decreasing major-element depletion, the considerable scatter about the trend suggests that either the refertilisation occurred over a considerable period of time, or that the depleted mantle was not homogeneous in either its Os isotope or major element compositions prior to refertilisation. Because either of these circumstances would invalidate the conditions necessary for the $^{187}Os/^{188}Os$ - $^{187}Re/^{188}Os$ trend to represent an isochron, neither the "age" nor the initial ratio calculated in Figure 5.3 should have any time significance in a refertilisation model.

In the absence of an isochronous relationship between $^{187}Os/^{188}Os$ and $^{187}Re/^{188}Os$, the time of the initial melting event which created the depleted end-member may be estimated using the Re-depletion model age ($T_{RD}$; Walker *et al.*, 1989a). Because this involves the calculation of the time at which the $^{187}Os/^{188}Os$ ratio of the mantle equalled that of the

sample, it represents a minimum estimate of the age of the original melting event. Although the value of $T_{RD}$ calculated using the $^{187}Os/^{188}Os$ ratio of sample 92-FT5 (1.16 Ga) is indistinguishable from the age determined by Reisberg *et al.* (1991) for the Ronda massif, the considerably less radiogenic $^{187}Os/^{188}Os$ ratio of 92-LH12 indicates that material older than 1.93 Ga may be present in the Pyrenean massifs, supporting the conclusion that the continental mantle lithosphere underlying the N.E. Pyrénées is significantly older than that below southern Spain.

Although local refertilisation of the Pyrenean continental mantle lithosphere by the addition of a basaltic melt, therefore, cannot be discarded as a possible origin for the determined Os isotope systematics of massifs on the basis of the simple modelling above, the well-defined trend of decreasing S contents with increasing degrees of major element depletion and the agreement between the Re-Os isochron age for the peridotites and the timing of crustal growth in the region favour a model in which the range of $^{187}Os/^{188}Os$ ratios and Re abundances of the peridotites result from the extraction of variable degrees of partial melt from an undepleted mantle source. The most likely scenario is that, prior to melting, the continental lithosphere underlying the Pyrénées formed part of the convecting mantle, with Re-Os isotope systematics close to those of the bulk Earth. Following the extraction of variable degrees of partial melt, associated with the formation of continental crust during the early Proterozoic, the mantle source of the massifs became incorporated into the continental lithosphere, where it was isolated from mantle convection.

Whichever model is used to account for the variations in the major-element compositions of the peridotites, the Re-Os isotope systematics of the N.E. Pyrenean massifs suggest that some, if not all, of the continental mantle lithosphere underlying the Pyrénées separated from the mantle prior to 1.9 Ga, indicating a longevity not immediately apparent from other isotope systems.

### 5.3.4 $^{187}Os/^{188}Os$ ratio variations in the Massif Central Mantle Xenoliths

Because only $^{187}Os/^{188}Os$ ratios were obtained for most of the xenoliths examined in this study, their Re-Os isotope systematics cannot be discussed in the same detail as were those of the peridotites from the N.E. Pyrenean massifs. Although Re abundances were

obtained for two of the xenolith samples, the absence of reliable Os abundances and the large errors on one of the Re determinations prevent the $^{187}Os/^{188}Os$ ratios of the xenoliths from being plotted as functions of either the $^{187}Re/^{188}Os$ ratios or whole-rock Re contents.

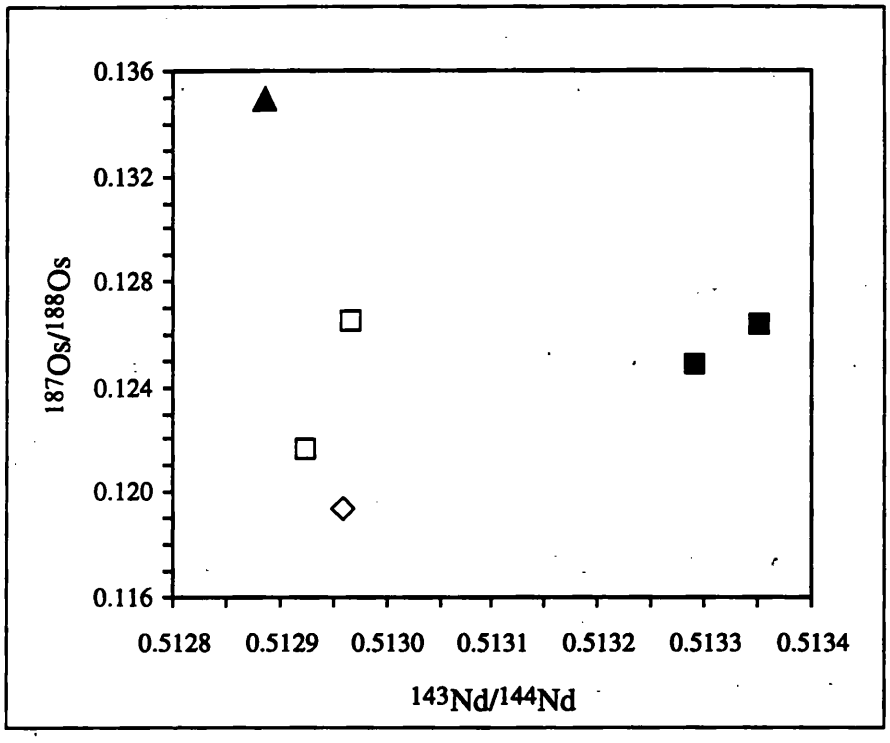


**Figure 5.16** $^{187}Os/^{188}Os$ as a function of $^{143}Nd/^{144}Nd$ for the Massif Central ultramafic xenoliths. Nd data from Downes & Dupuy (1987). Symbols as in Figure 5.7.

Figure 5.16 shows that the $^{187}Os/^{188}Os$ ratios of the xenoliths are unrelated to their $^{143}Nd/^{144}Nd$ ratios, attesting to the resistance of the Re-Os isotope system during the metasomatism which altered the Sm Nd isotope systematics of the type IB xenoliths. This resistance is also displayed by the variation of the Os isotope ratios of the xenoliths as a function of their whole-rock $Al_2O_3$ content (Figure 5.7). Although the correlation between the $^{187}Os/^{188}Os$ ratios and $Al_2O_3$ contents of the xenoliths is relatively poor, the type IA protogranular xenoliths and type IB protogranular and porphyroclastic xenoliths all plot along a similar trend, parallel to that defined by the Pyrenean massifs. If the Re-Os isotope systematics of the Pyrenean massifs are interpreted as the result of ancient melt extraction, associated with the formation of continental crust in the region, then the comparable $^{187}Os/^{188}Os$ - $Al_2O_3$ trend for the mantle xenoliths may indicate a similar origin for the mantle lithosphere beneath the Massif Central.

In the absence of Re abundance data, the time at which the source of the ultramafic xenoliths was incorporated into the continental mantle lithosphere may be estimated using the Re-depletion model-age ($T_{RD}$) of the least radiogenic sample analysed (Ta19). Although the model age calculated for this sample would indicate that the mantle source of the Massif Central xenoliths separated from the convecting mantle at least 1.16 Ga ago, it must be stressed that this date represents the minimum age for the depletion of this sample. The relatively high $Al_2O_3$ content of Ta19 indicates that the degree of melting experienced by the xenolith may have been insufficient to remove all the Re from the sample. Consequently, the determined $^{187}Os/^{188}Os$ ratio may be significantly higher than that of the mantle source at the time of melting, in which case the $T_{RD}$ model-age would considerably underestimate the age of the melting event.

The results of the Os isotope analyses of the Massif Central xenoliths differ from the findings of the REE and Sr-Nd isotope studies discussed in Chapter 4, in which the elemental and isotopic compositions of the type IA protogranular xenoliths were shown to be distinctly different from those of the type IB protogranular and porphyroclastic xenoliths. The difference between the compositions of the two xenolith types was explained by the interaction of the mantle source of the type IB xenoliths with fluids derived from a source exhibiting ancient incompatible-element enrichment. The timing of this interaction, however, was not constrained by the Sr-Nd isotope systematics (Downes & Dupuy, 1987). The formation of a single $^{187}Os/^{188}Os$ - $Al_2O_3$ trend by both the type IA and type IB protogranular xenoliths and the porphyroclastic xenoliths indicates that the Re-Os isotope systematics of the xenoliths were not seriously affected by the incompatible-element enrichment and that, despite their different textures, these xenoliths may originate from a similar mantle source.

The only xenolith to plot off the $^{187}Os/^{188}Os$ - $Al_2O_3$ trend is the equigranular xenolith (Bt40), its high $^{187}Os/^{188}Os$ ratio indicating that it may have been derived from a mantle source which has evolved with a Re/Os ratio greater than that of the convecting mantle. In view of the relatively recent eruption age of the host basalts, the elevated $^{187}Os/^{188}Os$ ratio of the sample cannot be explained by the addition of Re during magma transport. However, it may be consistent with the conclusions of the REE and Sr-Nd isotopic study of the Massif Central xenoliths (Downes & Dupuy, 1987), which suggest that the equigranular and

secondary recrystallised xenoliths sampled from the core of the diapir were derived from an enriched mantle source. Without the Re content of sample Bt40 it is not possible to estimate the age of the Re/Os enrichment, although it may have coincided with the LREE enrichment, for which a mid-Proterozoic age has been proposed (Downes & Dupuy, 1987).

In general, therefore, the Os isotope compositions of the Massif Central mantle xenoliths support the conclusions of the Sr-Nd isotopic study of Downes & Dupuy (1987). The protogranular and porphyroclastic xenoliths originating from outside the main mantle diapir were derived from mantle that has evolved with a range of sub-chondritic Re/Os ratios for a period in excess of ~1.2 Ga, whilst the more deformed equigranular xenoliths may have originated from an enriched mantle source. Although the late-Proterozoic Re-depletion model age of the least radiogenic xenolith is similar to the Re-Os isochron age of the Ronda massif determined by Reisberg *et al.* (1991), the high $Al_2O_3$ content of this sample indicates that the age of the lithosphere may have been significantly underestimated by this calculation and that the continental mantle lithosphere may have separated from the convecting mantle considerably earlier than this date. It is possible that the continental mantle lithosphere underlying both the Massif Central and N.E. Pyrénées stabilised during the same event.

Further work on the Re-Os isotope systematics of the Massif Central xenoliths may help to clear-up some of the ambiguities arising from this study. In particular, analyses of the Re contents of the xenoliths, coupled with Os abundances determined using the Carius tube method of sample preparation, are required in order to determine more accurately the timing of depletion and to investigate the proposed long term enrichment of the equigranular and secondary recrystallised samples.

## 5.4 Conclusions

### 5.4.1 Chalcophile Chemistry of the Pyrenean Massive Peridotites

The sulphur contents of the Pyrenean massifs show a linear variation as a function of the peridotites' major element compositions. This correlation is consistent with the extraction of a sulphur saturated basaltic melt from a fertile peridotite source and favours an origin involving variable degrees of partial melt extraction, rather than refertilisation, for the range of major element compositions observed in the Pyrenean massifs.

Several of the Pyrenean peridotites exhibit low Cu/S ratios owing to their selective enrichment in sulphur. These samples are inferred to have been infiltrated by small-degree partial melts which were enriched in both sulphur and precipitated a Cu-poor sulphide phase on cooling. It is proposed that these melts may have also been responsible for the Ti-pargasite metasomatism which affected the massifs, suggesting that both the sulphide and silicate systems may be affected some metasomatic events.

### 5.4.2 Factors Affecting the Behaviour of Re and Os in Mantle Peridotites

The Re and Os abundances determined in the mantle peridotites of this study confirm the intimate link between the geochemistry of the base-metal sulphide phase and the behaviour of Re and Os in mantle peridotites, as suggested in Chapter 2. The behaviour of Re and Os is controlled by the chalcophile element systematics of the peridotites, both during magmatic events within the mantle lithosphere and during alteration of the peridotites whilst they are either *en route* to, or at the surface.

The apparent incompatibility of Re during mantle melting may be successfully modelled by non-modal batch melting of a peridotite source containing small quantities of accessory base-metal sulphides. The reasonably high compatibility of Re in the base-metal sulphide is balanced by the low modal abundance of the BMS phase, giving rise to bulk distribution coefficients of less than unity.

Whilst the determined Re abundances in the majority of the peridotites collected from the N.E. Pyrénées and Massif Central massifs appear to have been dictated by the original melting event, the variation in the Os abundances of the samples may be a consequence of the alteration of the sulphide inclusions, leading to sample heterogeneity and the presence of the Os in insoluble mineral phases.

The addition of an exotic sulphide component (associated with the small-degree melts responsible for metasomatism of the peridotite massifs) may have supplemented the Re contents of the affected peridotites. Although only one sample was investigated, it would appear that the Re-Os isotope system may not be as resistant to the effects of metasomatism in the mantle lithosphere as previously thought. Further investigation of the Re abundances of sulphur-rich peridotites and the highly metasomatised wall-rocks of pyroxenite layers

occurring in orogenic peridotite massifs is needed, however, in order to establish how common such alteration is in the continental mantle lithosphere.

### 5.4.3 Evolution of the French Continental Mantle Lithosphere

The correlations between the $^{187}Os/^{188}Os$ ratios of the peridotites collected from the N.E. Pyrénées and Massif Central and their major element compositions are interpreted as the result of the radiogenic ingrowth of $^{187}Os$ in response to a range of $^{187}Re/^{188}Os$ ratios produced by variable degrees of melt extraction. If the melting event homogenised the Os isotope compositions of the Pyrenean peridotites, then the correlation of $^{187}Os/^{188}Os$ with $^{187}Re/^{188}Os$ reflects an isochron, yielding an age of ~ 2.0 Ga for the original melting of the mantle source of the massifs and its incorporation into the continental lithosphere.

The coincidence of the early Proterozoic age determined for the stabilisation of the continental mantle lithosphere underlying south-western France with the date of major crustal growth in the region implies that both the crust and mantle components of the European lithosphere may have evolved at a similar time, indicating a possible causative link between the two events. The preservation of the mantle lithosphere source of the Pyrenean massifs for up to 2.0 Ga implies that at least the shallowest mantle lithosphere is sufficiently stable to have resisted removal by the processes of delamination or thermal erosion which are thought to have affected regions of post-Archaean mantle lithosphere elsewhere.

Whilst it was not possible to determine accurately the age of the original melting event responsible for the range of major element compositions observed in the Massif Central xenoliths, the Re depletion model age calculated for the most depleted sample analysed indicates that the continental mantle lithosphere below central France must have separated from the convecting mantle more than 1.2 Ga ago. Considering the incomplete depletion of this sample in major elements, this model-age, in all likelihood, significantly underestimates the time at which the mantle lithosphere stabilised in the region. It is probable that melt extraction occurred during the early Proterozoic, consistent with the age of mantle lithosphere stabilisation determined for the N.E. Pyrenean massifs.

Although the initial $^{187}Os/^{188}Os$ ratio of the Pyrenean samples may indicate that, prior to melting, the source of the N.E. Pyrenean massifs had evolved with a $^{187}Re/^{188}Os$ ratio greater than that of the bulk mantle evolution curve of Luck & Allègre (1991), owing to the

imprecision of the determined isochron age, the observed deviation of the initial $^{187}Os/^{188}Os$ ratio from the bulk Earth evolution curve is not necessarily significant. In order to confirm the suggested enrichment of the original mantle protolith, a more precise date for the mantle melting event would be required.

The contrasting gradients of the correlations between the $^{187}Os/^{188}Os$ ratios and major element compositions of the peridotites of the N.E. Pyrenean massifs and those of the Ronda ultramafic complex not only demonstrate that the $^{187}Os/^{188}Os$ - $^{187}Re/^{188}Os$ and $^{187}Os/^{188}Os$ - major element trends are not the result of mantle-wide mixing processes, but also imply that the lithosphere underlying southern Spain probably formed during a separate and later event from that responsible for the formation of the central and western European lithosphere, consistent with the different Re-Os isochron ages calculated for the two regions.

Although the Re-Os isotope systematics of the N.E. Pyrenean massifs appear to have remained undisturbed until the relatively recent infiltration of S-rich melts, some parts of the continental mantle lithosphere underlying the Massif Central appear to record an ancient enrichment in both incompatible lithophile and chalcophile elements. Whilst this enrichment could not be dated using the Re-Os isotope systematics of the xenoliths, the depleted-mantle model age calculated from its Nd isotopic composition indicates a late Proterozoic age for the incompatible-element enrichment, with which the addition of Re may have coincided.

# Chapter 6

# Summary and Conclusions

## 6.1 Introduction

In this project, the Re-Os isotope systematics of two suites of peridotites derived from the French continental mantle lithosphere have been investigated with the dual aims of:

i) determining the factors which may affect the behaviour of Re and Os, both within the mantle and during the processes associated with the transport of mantle material to the surface.

ii) investigating the link between the stabilisation of continental mantle lithosphere and the formation of the overlying crust.

Because the analytical procedures required to obtain Re and Os abundances and isotopic ratios in unmineralised mantle rocks were far from routine, a significant proportion of the project was also concerned with the development of methods for the analysis of the elements by both ICP-MS and N-TIMS techniques.

The observed behaviour of Re and Os in the peridotite samples was supported by thermochemical calculations of the stabilities of Re, Os and the other Pt-group elements as sulphide or oxide species (either as discrete minerals or dissolved in mantle phases) and the results of a number of published partitioning experiments. The conclusions of the thermochemical calculations were investigated by accurate analyses of the chalcophile element compositions of the mantle peridotite samples.

Before discussing the Re-Os isotope systematics of the French continental mantle lithosphere, the whole-rock compositions of the peridotite samples were investigated, enabling the processes which may have affected the peridotites, either in the mantle or during their emplacement, to be investigated. Two models were proposed to account for the observed range of peridotite whole-rock major-element compositions: depletion of a fertile mantle source by the extraction of partial melts and the refertilisation of refractory mantle

materials by the incorporation of basaltic melts. Whilst it was possible to put constraints on each model, it was not possible to differentiate between the two processes from the lithophile element compositions of the peridotites alone.

## 6.2 Geochemistry of Re and Os

The Re and Os abundances determined in the peridotites collected from the N.E. Pyrenean massifs and Massif Central alkali basalts are consistent with the results of thermochemical calculations which indicated that the behaviour of both elements should be predominantly controlled by the base-metal sulphide phase present in the mantle.

Consistent with the high sulphide-silicate partition coefficients determined for the PGE (e.g. Fleet, *et al.*, 1991; Peach *et al.*, 1994; Bezman *et al.*, 1994), Os appears to be highly compatible in the mantle base-metal sulphide phase, remaining in the mantle residue during melting. Although Re is also located in the BMS phase, it appears to be significantly less compatible than the PGE, with a partition coefficient of ~325, similar to that of Cu (~250, Rajamani & Naldrett, 1978). The differing compatibilities of the two elements in the mantle sulphide phase may be responsible for the extreme fractionation of the Re/Os ratio in mantle-derived melts and the depletion of Re in the residual mantle material.

Evidence from the chalcophile element compositions of peridotites adjacent to pyroxenite layers found in a number of orogenic massifs suggests that, in addition to melt extraction, the Re/Os ratios of mantle peridotites may be affected by interactions with mafic melts in transit through the mantle lithosphere. Although no peridotites collected from such positions within the Pyrenean massifs were analysed during this study, the S, Cu and Re contents of several samples indicate that an exotic sulphide component may have been introduced into the massifs, possibly increasing their Re contents. Further analyses of the Re and Os abundances of peridotites exhibiting high S contents or located adjacent to mafic layers would be required in order to investigate more thoroughly the effects of melt-mantle interactions on the Re-Os isotope system.

Alteration of mantle peridotites, either during transport or at the surface, appears to have negligible effect on the Re-Os isotope systematics of orogenic peridotite massifs or ultramafic xenoliths, although the mineralogy of the Re and Os-bearing phases may be

significantly changed, leading to sample heterogeneity and the production of acid-resistant phases. Under the conditions of low $f_{O_2}$ and $f_{S_2}$ which operate during serpentinisation Os may exsolve from the mantle sulphide phase to form discrete alloy phases, whilst Re may remain dissolved. Whilst Os is probably also present in alloy phases in ultramafic xenoliths following their oxyhydration in volcanic piles after eruption, the Re contents of mantle xenoliths may be altered owing to dissolution in the acidic waters. Because only two xenolith samples were successfully analysed for Re in this study, it was not possible to test this prediction thoroughly.

## 6.3 Evolution of Post-Archaean Continental Mantle Lithosphere

Although the lithophile whole rock elemental compositions of the peridotites of the N.E. Pyrenean massifs may be consistent with an origin by either the extraction of variable amounts of partial melt or the refertilisation of refractory mantle material by a basaltic melt, the chalcophile element contents of the Pyrenean samples could be adequately explained only by a process of melt-extraction The whole-rock elemental compositions of the peridotites are, therefore, interpreted as the residues after the extraction of up to 25% sulphur-saturated basaltic melt from an undepleted peridotite source. In order to explain the incompatible element compositions of the Pyrenean peridotites, subsequent metasomatism of the mantle lithosphere is required. Similar whole rock major element variations are observed in the compositions of the Massif Central ultramafic xenoliths, indicating that the range of compositions observed in these samples may also have originated from variable degrees of melt extraction.

The peridotites analysed from both the N.E. Pyrenean massifs and Massif Central volcanic vents exhibit a wide range of Os isotopic ratios, extending from a value marginally greater than that estimated for the current bulk Earth (0.12711; Walker *et al.*, 1994) to considerably less radiogenic values characteristic of ancient melt depletion (Figure 6.1). Although the range of $^{187}Os/^{188}Os$ ratios observed in the N.E. Pyrenean massifs and Massif Central xenoliths overlaps with that of abyssal peridotites, the lowest values determined in the peridotite samples require a mantle source characterised by long-term Re depletion. Because such depletion is unlikely to be preserved in convecting asthenospheric mantle, the

spinel peridotites from the two regions may be assumed to have been derived from a lithospheric mantle source.

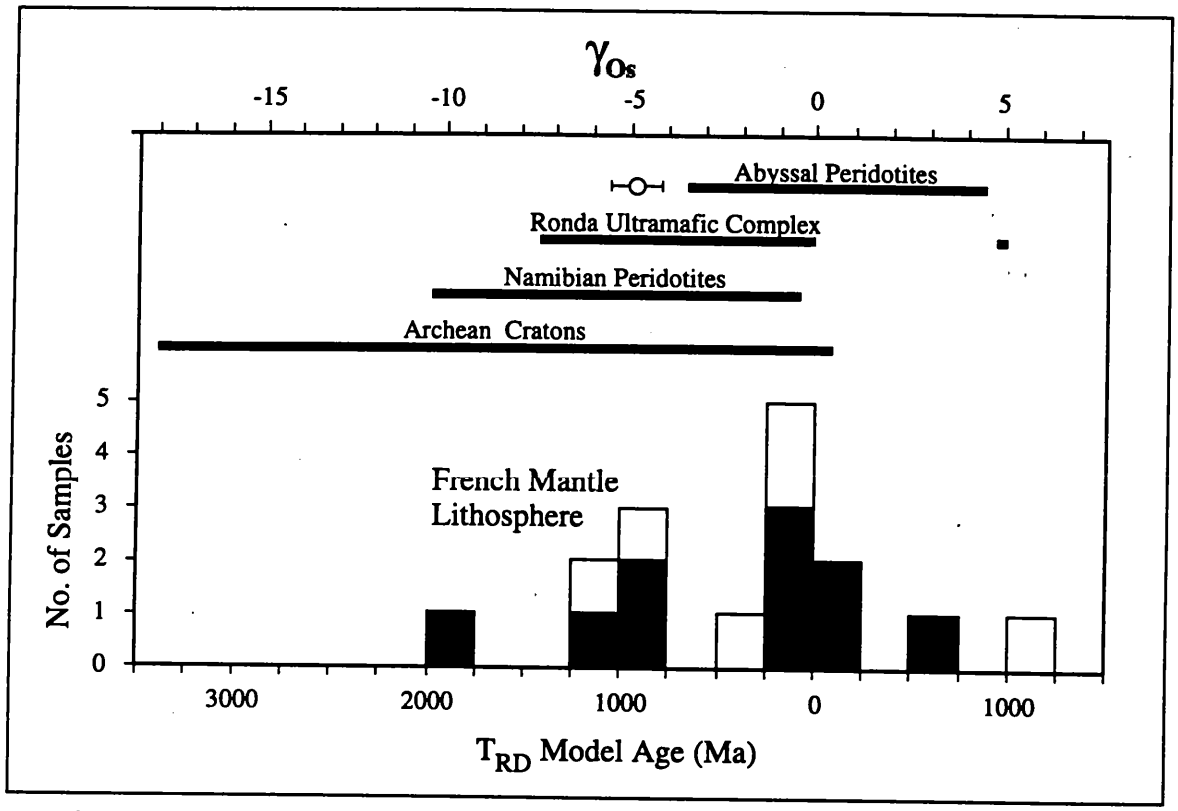


**Figure 6.1** Histograms of Re depletion model ages ($T_{RD}$) for the peridotites from the N.E. Pyrénées (filled columns) and Massif Central (unfilled columns) compared to the range of $T_{RD}$ ages calculated for abyssal peridotites, peridotites from the Ronda Ultramafic Complex, ultramafic xenoliths erupted through Proterozoic crust in Namibia and kimberlite-borne mantle xenoliths from the Archaean Kaapvaal and Siberian cratons. $T_{RD}$ calculated using the mantle evolution line suggested by Walker *et al.* (1994).Data sources: abyssal peridotites, Martin (1991), Luck & Allègre (1991), Roy-Barman & Allègre (1994); Ronda Ultramafic Complex, Reisberg *et al.*, (1991); Namibian xenoliths, Pearson *et al.* (1994); Archaean Craton, Walker *et al.* (1989a), Carlson & Irving (1994), Pearson *et al.* (1995b, 1995c). The anomalously low $T_{RD}$ determined for a single abyssal peridotite in the study by Martin (1991) is indicated by an open circle, with error bars illustrating the uncertainty in the value.

When plotted on an isochron diagram, the Re-Os isotopic compositions of the Pyrenean samples define a linear array. If this is interpreted as an isochron, it yields an age of ~2.0 Ga for the inferred melt depletion event. The Early Proterozoic age of this event is in agreement with the Re-depletion ($T_{RD}$) model age calculated for one of the most depleted peridotites collected from the Pyrenean massifs and coincides with both U-Pb zircon ages and Nd model ages for basement exposed in the region. The similar ages for both the mantle and crustal components of the French continental lithosphere may indicate that the stabilisation of the mantle lithosphere in the region coincided with a period of crustal generation and suggest

a possible causative link between the creation of continental mantle lithosphere and its overlying crust.

Although the oldest $T_{RD}$ model age (~1.2 Ga) determined for the least radiogenic Massif Central xenolith is significantly younger than that observed for the Pyrenean peridotites, the high $Al_2O_3$ and low MgO contents of the most depleted xenoliths indicate that their mantle source was not entirely depleted in Re during melt extraction. Consequently, the model age calculated for the Massif Central xenoliths may considerably underestimate the age of depletion and the underlying mantle lithosphere may have stabilised at a similar time to that below the N.E. Pyrénées.

The range of Os isotopic compositions observed in the French mantle lithosphere closely resembles those found in previous studies of the mantle lithosphere underlying non-cratonic regions (e.g the Ronda Ultramafic Complex, southern Spain, Reisberg *et al.*, 1991 and low-T garnet peridotite xenoliths from Namibian kimberlites, Pearson *et al.*, 1994). Although the low equilibration pressures of the anhydrous pyroxenites occurring within the Pyrenean massifs indicate that the peridotites originated from a source which had been located in the shallow lithospheric mantle for much of its recent history, the peridotite xenoliths collected from the Massif Central alkali basalts and Namibian kimberlites probably originated from greater depths (45 - 75 km (Nicholas *et al.*, 1987) and 100 - 150 km, respectively). The determination of unradiogenic Os isotope ratios in peridotites derived from such depths indicates that a substantial thickness of the mantle lithosphere in these regions may have remained stable since its initial formation and has been resistant to delamination or thermal erosion, despite the regional tectonic deformation associated with the Hercynian and possibly earlier orogenies.

The possibility that regions of relatively fertile continental mantle lithosphere may be preserved since their initial stabilisation in the Early Proterozoic has important implications for the origins of intracontinental volcanic rocks, in particular those of large volume continental flood basalts (CFB). Most of the CFB erupted through the Proterozoic crust of the Gondwana supercontinent (e.g. the Karoo, Parana, Etendeka and Tasmanian basalt provinces) are characterised by negative $\varepsilon_{Nd}$ and positive $\varepsilon_{Sr}$ isotope ratios and require that at least the trace element compositions of the basalts contain a significant contribution from a

component characterised by ancient incompatible element enrichment (Hawkesworth *et al.*, 1990). Although Pb and Nd isotope variations in basalts demonstrated that the source regions of the basalts must be of a similar age to the overlying crust (Hawkesworth *et al.*, 1986; Ellam & Cox, 1989), the derivation of large volumes of basaltic melt from the mantle lithosphere has remained contentious both on thermal grounds and from arguments which claimed that the mantle lithosphere is too depleted in major elements to generate much melt. The observation of stable Proterozoic mantle lithosphere capable of producing basaltic melts, however, supports the suggestions that old continental mantle lithosphere may play a significant role in the petrogenesis of the Gondwana flood basalts, making a substantial contribution to the total volume of basalt produced.

# References


Agiorgitis G. & Wolf R. (1978) Aspects of osmium, ruthenium and iridium contents in some greek ophiolites. *Chem. Geol.*, **23**, 267-272.

Ahern J. L. & Turcotte D. L. (1979) Magma migration beneath an ocean ridge. *Earth Planet. Sci. Lett.*, **45**, 115-122.

Alibert C. (1985) A Sr-Nd isotope and REE study of Late Triassic dolerites from the Pyrénées (France) and the Messejana Dyke (Spain & Portugal). *Earth Planet. Sci. Lett.*, **73**, 81-90.

Alibert C., Michard-Vitrac A., Alberède F. (1983) The transition from alkali basalts to kimberlites. Isotope and trace element evidence from melilitites. *Contrib. Mineral. Petrol.*, **82**, 176-186.

Allègre C. J. & Ben Othman D. (1980) Nd-Sr isotopic relationships in granitoid rocks and continent crust development: a chemical approach to orogenesis. *Nature*, **286**, 335-342.

Allègre C. J. & Luck J.-M. (1980) Osmium isotopes as petrogenetic and geological tracers. *Earth Planet. Sci. Lett.*, **48**, 148-154.

Allègre C. J., Brévart O., Dupré B., Minster J.-F. (1980) Isotopic and chemical effects produced in a continuously differentiating convecting Earth mantle. *Phil. Trans. R. Soc. Lond.*, **A297**, 447-477.

Ancochea E. & Nixon P. H. (1987) Xenoliths in the Iberian Peninsula. In: *"Mantle Xenoliths"*, P. H. Nixon (Ed.), Wiley, Chichester, UK, 119-124.

Ando A., Kamioka H., Terashima S., Itoh S. (1989) 1988 values for GSJ rock reference samples "igneous rock series". *Gechem. J.*, **23**, 143-148.

Arculus R. J. & Delano J. W. (1981) Siderophile element abundances in the upper mantle: evidence for a sulphide signature in equilibrium with the core. *Geochim. Cosmochim. Acta*, **45**, 1331-1343.

Arculus R. J. & Delano J. W. (1987) Oxidation state of the upper mantle: present conditions, evolution and controls. In: *"Mantle Xenoliths"*, P. H. Nixon (Ed.), Wiley, Chichester, UK, 589-598.

Asif M. & Parry S. J. (1989) Elimination of reagent blank problems in the fire assay pre-concentration of the platinum group elements and gold with a nickel sulphide bead of less than one gram mass. *Analyst*, **114**, 1057-1059.

Asif M. & Parry S. J. (1990) Nickel sulphide fire assay for the collection of the platinum group elements and gold from chromitites using reduced bead size. *Mineral. and Petrol.*, **42**, 321-326.

Avé Lallement H. G. (1967) Structural and petrofabric analysis of an "alpine type" peridotite: the lherzolite of the French Pyrénées. *Leidse Geologische Mededelingen*, **42**, 1-57.

Baker M. B. & Stolper E. M. (1994) Determining the composition of high pressure mantle melts using diamond aggregates. *Geochim. Cosmochim. Acta*, **58**, 2811-2827.

Balcerzak M. (1988) Sensitive spectrophotometric determination of osmium with tin (II) chloride and Rhodamine B after flotation using cyclohexane. *Analyst*, **113**, 129-132.

Barin I. & Knacke O. (1973) Thermochemical Properties of Inorganic Substances. Springer-Verlag, New York, 861 pp.

Barin I., Knacke O., Kubaschewski O. (1977) Thermochemical Properties of Inorganic Substances (Supplement). Springer-Verlag, New York, 921 pp.

Barnes I. L., Chang T. L., De Bièvre P., Gramlich J. W., Hageman R. J. Ch., Holden N. E., Murphy T. J., Rosman K. J. R., Shima M. (1991) Isotopic compositions of the elements (1989). *Pure & Appl. Chem.*, **63**, 991-1002.

Barnes S.-J., Naldrett A. J., Gorton M. P. (1985) The origin of the fractionation of platinum group elements in terrestrial magmas. *Chem. Geol.* , **53**, 303-323.

Barnes S. J., Boyd R., Korneliussen A., Nilsson L.-P., Often M., Pedersen R. B., Robins B. (1988) The use of mantle normalisation and metal ratios in discriminating between the effects of partial melting, crystallisation and sulphide segregation on platinum-group elements, gold, nickel and copper: examples from Norway. In: *"Geo-Platinum 87"*, Prichard H. M., Potts P. J., Bowles J. F. W. & Cribb S. J. (Eds.), Elsevier Applied Science, London, 113-143.

Basaltic Volcanism Study Project (1981) Ultramafic xenoliths in terrestrial volcanics and the nature of mantle source regions and magmatic processes. In: *"Basaltic Volcanism on the Terrestrial Planets"*, W. M. Kanka, J. W. Head, R. B. Merrill, R. O. Peppin, S. C. Soloman, D. Walker & C. A. Wood (Eds.), Pergamon Press, New York, 282-310.

Bazan J. M. (1987) Enhancement of Os detection in inductively coupled plasma atomic emission spectrometry. *Anal. Chem.*, **59**, 1066-1069.

Ben Othman D., Fourcade, S., Allègre C. J. (1984a) Recycling processes in granite-granodiorite complex genesis: the Querigut case studied by Nd-Sr isotope systematics. *Earth Planet. Sci. Lett.*, **69**, 290-300.

Ben Othman D., Polvé M., Allègre C. J. (1984b) Nd-Sr isotopic composition of granulites and constraints on the evolution of the lower continental crust. *Nature*, **307**, 510-515.

Berger E. (1981) Enclaves ultramafiques, megacrystaux et leurs basaltes-hôtes en context océanique (Pacifique sud) et continental (Massif Central française). *Thèse Dr. D'Etat*, **University Paris-Sud (Orsay)**.

Berlincourt L. E., Hummel H. H., Skinner B. J. (1981) Phases and phase relations of the platinum-group elements. In: *"Platinum Group Elements: Mineralogy, Geology, Recovery"*, L. J. Cabri (Ed.), Can. Inst. Min. & Metal. Special Vol. No. 23, Harpells Press, Quebec, 19-45.

Bernard A., Symonds R. B., Rose W. I. Jr. (1990) Volatile transport and deposition of Mo, W and Re in high temperature magmatic fluids. *Appl. Geochem.* , **5**, 317-326.

Bezman N. I., Asif M., Brügmann G. E., Romanenko I. M., Naldrett A. J. (1994) Distribution of Pd, Rh, Ru, Ir, Os and Au between sulfide and silicate. *Geochim. Cosmochim. Acta*, **58**, 1251-1260.

Birck J. L & Allègre C. J. (1994) Contrasting Re/Os magmatic fractionation in planetary basalts. *Earth Planet. Sci. Lett.*, **124**, 139-148.

Bird P. (1978) Initiation of intracontinental subduction in the Himalaya. *J. Geophys. Res.*, **83**, 4975-4987.

Bodinier J. L. (1988) Geochemistry and petrogenesis of the Lanzo peridotite body, western Alps. *Tectonophysics*, **149**, 67-88.

Bodinier J. L., Fabriès J., Lorand J.-P., Dostal J., Dupuy C. (1987a) Geochemistry of amphibole pyroxenite veins from the Lherz and Freychinède ultramafic bodies (Ariège, French Pyrénées). *Bull. Minéral.*, **110**, 345-358.

Bodinier J. L., Guiraud M., Fabriès J., Dostal J., Dupuy C. (1987b) Petrogenesis of layered pyroxenites from the Lherz, Freychinède and Prades ultramafic bodies (Ariège, French Pyrénées). *Geochim. Cosmochim. Acta*, **51**, 279-290.

Bodinier J. L., Dupuy C., Dostal J. (1988) Geochemistry and petrogenesis of eastern Pyrenean peridotites. *Geochim. Cosmochim. Acta*, **52**, 2893-2907.

Bodinier J. L., Vasseur G., Vernieres J., Dupuy C., Fabriès J. (1990) Mechanisms of mantle metasomatism: geochemical evidence from the Lherz orogenic peridotite. *J. Petrol.*, **31**, 597-628.

Borisov A. A. & Kadik A. A. (1991) A model for the solubility of metals in a silicate liquid. *Geochem. Intl.*, **28**, 94-104.

Boudreau A. E. & McCallum I. S. (1986) Evidence for mineral reactions and metasomatism by silica undersaturated Cl-rich fluids in the Stillwater Complex (abstr.). In: *4th Intl. Platinum Symp.*, Toronto.*Can. Mineral.*, **23**, 293-294.

Brown G. M., Pinsent R. H., Coisy P. (1980) The petrology of spinel peridotite xenoliths from the Massif Central, France. *Am. J. Science*, **280A**, 471-498.

Brügmann G. E., Arndt N. T., Hofmann A. W., Tobschall H. J. (1987) Noble metal abundances in komatiite suites from Alexo Ontario and Gorgona Island, Columbia. *Geochim. Cosmochim. Acta*, **51**, 2159-2169.

Calvez J. Y. & Vidal P. (1978) Two billion year old relicts in the Hercynian belt of Western Europe. *Contrib. Mineral. Petrol.*, **65**, 395-399.

Campbell I. H., Naldrett A. J., Barnes S. J. (1983) A model for the origin of the platinum rich sulfide horizons in the Bushveld and Stillwater Complexes. *J. Petrol.*, **24**, 133-165.

Capobianco C. J. & Drake M. J. (1990) Partitioning of ruthenium, rhodium and palladium between spinel and silicate melt and implications for PGE fractionation trends. *Geochim. Cosmochim. Acta*, **54**, 869-874.

Capobianco C. J., Hervig R. L., Drake M. J. (1994) Experiments on crystal/liquid partitioning of Ru, Rh and Pd for magnetite and hematite solid solutions crystallized from silicate melt. *Chem. Geol.*, **113**, 23-43.

Carlson R. W. & A. J. Irving A. J. (1994) Depletion and enrichment history of subcontinental lithospheric mantle: an Os, Sr, Nd and Pb isotopic study of the ultramafic xenoliths from the northwestern Wyoming craton. *Earth Planet. Sci. Lett.*, **126**, 457-472.

Carmichael I. S. E. (1991) The redox states of basic and silicic magmas: a reflection of their source regions. *Contr. Mineral. Petrol.*, **106**, 129-141.

Chauvel C. & Jahn B. (1984) Nd-Sr isotope and REE geochemistry of alkali basalts from the Massif Central, France. *Geochim. Cosmochim. Acta*, **48**, 91-110.

Chou C.-L. (1978) Fractionation of siderophile elements in the Earth's upper mantle. *Proc. Lunar Sci. Conf. 9h, Vol. 1*, 219-230.

Chou C.-L., Shaw D. M., Crocket J. M. (1983) Siderophile trace elements in the Earth's oceanic crust and upper mantle. In: "*J. Geophys. Res. Suppl.: Proc. Lunar Sci. Conf. 13th, Part 2*", A507-A518.

Choukroune P. (1992) Tectonic evolution of the Pyrénées. *Ann. Rev. Earth Planet. Sci.*, **20**, 143-158.

Cocherie A., Augé T., Meyer G. (1989) Geochemistry of the platinum-group elements in various types of spinels from the Vourinos ophiolitic complex, Greece. *Chem. Geol.*, **77**, 27-39.

Coisy P. (1977) Structure et chimisme des péridotites en enclaves dans les basalts du Massif Central-modèles géodynamiques du manteau supérieur. *Thèse 3ème cycle*, **University Nantes, France**, 118 pp.

Coisy P. & Nicolas A. (1978) Regional structure and geodynamics of the upper mantle beneath the Massif Central. *Nature*, **274**, 429-432.

Conquéré F. (1971) Les pyroxénolites à amphibole et les amphibolites associées aux lherzolites du gisement de Lherz (Ariège, France): un example du rôle de l'eau au cours de la crystallisation fractionnée des liquides issus de la fusion partielle des lherzolites. *Contrib. Mineral. Petrol.*, **33**, 32-61.

Conquéré F. (1977) Pétrologie des pyroxénites litées dans les complexes ultramafique de l'Ariège (France) et autres gisements de lherzolite à spinelle. Compositions minéralogiques et chimiques, évolution des conditions d'equilibre des pyroxénites. *Bull. Soc. Fr. Minér. Cristal.*, **100**, 42-80.

Conquéré F. (1979) Comments on "The bearing of phase-equilibria in simple and complex systems on the origin and evolution of some well-documented garnet websterites" by C. T. Herzberg. *Contrib. Mineral. Petrol.*, **70**, 219-222.

Conquéré F. & Fabriès J. (1984) Chemical disequilibrium and its thermal significance in spinel peridotites from the Lherz and Freychinède ultramafic bodies (Ariège, French Pyrénées). In: *"Kimberlites II: The mantle and mantle-crust relationships"*, J. Kornprobst (Ed.), Elsevier, Amsterdam, 319-332.

Craig J. R. & Kullerud G. (1989) Abyssal peridotites, very slow spreading ridges and ocean ridge magmatism. In: *"Magmatism in the Oceanic Basins"*, A. D. Saunders & M. J. Norry (Eds.), Geol. Soc. Lond. Sp. Publ. No. 42, 71-105.

Crain J. S., Houk R. S., Eckels O. E. (1989) Noise power spectral characteristics of an inductively coupled plasma mass spectrometer. *Anal. Chem.*, **61**, 606-612.

Creaser R. A., Papanastassiou D. A., Wasserburg G. J. (1991) Negative thermal ion mass spectrometry of osmium, rhenium and iridium. *Geochim. Cosmochim. Acta*, **55**, 397-401.

Crocket J. H. & Kabir A. (1988) PGE in Hawaiian basalt: implications of hydrothermal alteration on PGE mobility on volcanic fluids (abstr.). In: *"Geo-Platinum 87"*, Prichard H. M., Potts P. J., Bowles J. F. W. & Cribb S. J. (Eds.), Elsevier Applied Science, London, p. 29.

Dick H. J. B. (1969) Phase relations in the Cu-Fe-Ni-S system and their applications to magmatic ore deposits. In: *"Magmatic Ore Deposits"*, Econ Geol. Monograph No. 4, 343-358.

Dick H. J. B., Fisher R. L., Bryan W. B. (1984) Mineralogic variability of the uppermost mantle along mid-ocean ridges. *Earth Planet. Sci. Lett.*, **69**, 88-106.

Dickey J. S. (1970) Partial fusion products in alpine-type peridotites: Serrania de la Ronda and other examples. *Miner. Soc. Am. Sp. Paper No. 3*, 33-50.

Dickin A. P., McNutt R. H., McAndrew J. I. (1988) Osmium isotope analysis by inductively coupled plasma mass-spectrometry. *J. Anal. At. Spectrom.*, **3**, 337-342.

Dickin A. P., Richardson J. M., Crocket J. H., McNutt R. H., Peredery W. V. (1992) Osmium isotope evidence for a crustal origin of platinum-group elements in the Sudbury nickel ore, Ontario, Canada. *Geochim. Cosmochim. Acta*, **56**, 3531-3537.

Downes H. (1983) The petrogenesis of coexisting saturated and undersaturated continental alkaline magma series. *PhD. Thesis*, **University of Leeds**, 279 pp.

Downes H. (1984) Sr and Nd isotope geochemistry of coexisting alkaline magma series, Cantal, Massif Central, France. *Earth Planet. Sci. Lett.*, **69**, 321-334.

Downes H. (1987) Relationship between geochemistry and textural type in spinel lherzolites, Massif Central and Languedoc, France. In: *"Mantle Xenoliths"*, P. H. Nixon (Ed.), Wiley, Chichester, UK, 125-133.

Downes H. & Dupuy C. (1987) Textural, isotopic and REE variations in spinel peridotite xenoliths, Massif Central, France. *Earth Planet. Sci. Lett.*, **82**, 121-135.

Downes H. & Leyreloup A. (1986) Granulite xenoliths from the French Massif Central–petrology, Sr and Nd isotope systematics and model age estimates. In: *"The Nature of the Lower Crust"*, Dawson J. B., Carswell D. A., Hall J. & Wedepohl K. H. (Eds.), Geol. Soc. London Sp. Publ. No. 24, 319-330.

Downes H., Bodinier J.-L., Thirlwall M. F., Lorand J.-P., Fabriès J. (1991) REE & Sr-Nd isotopic geochemistry of eastern Pyrenean peridotite massifs: sub-continental lithospheric mantle modified by continental magmatism.. In: *"J. Pet. (Sp. Vol.): Orogenic lherzolites and mantle processes"*, M. A. Menzies, C. Dupuy & A. Nicholas (Eds.), 97-115.

Doyle C. D. & Naldrett A. J. (1986) Ideal mixing of divalent cations in mafic magma and its effect on the solution of ferrous oxide. *Geochim. Cosmochim. Acta*, **50**, 435-443.

Dupuy C., Dostal J., Dautria J. M., Girod M. (1986) Geochemistry of spinel peridotite inclusions in basalts from Hoggar, Algeria. *J. African Earth Sci.*, **5**, 209-215.

Edwards S. J. (1990) Harzburgites and refractory melts in the Lewis Hills Massif, Bay of Islands ophiolite complex: the base metals and precious metals story. *Can. Mineral.*, **28**, 537-552.

Ellam R. M. & Cox K. G. (1989) A Proterozoic lithospheric source for Karoo magmatism: evidence from the Nuanetsi picrites. *Earth Planet. Sci. Lett.*, **92**, 207-218.

Elthon D., Stewart M., Ross D. K. (1992) Compositional trends of minerals in oceanic cumulates. *J. Geophys. Res.*, **97**, 15189-15199.

Esser B. K. & Turekian K. K. (1988) Accretion rate of extraterrestrial particles determined from Os isotope systematics of Pacific pelagic clay and manganese nodules. *Geochim. Cosmochim. Acta*, **52**, 1383-1388.

Esser, B. K. & Turekian K. K (1993) The osmium isotopic composition of the continental crust. *Geochim. Cosmochim. Acta*, **57**, 3093-3104.

Fabriès J. (1979) Spinel-olivine geothermometry in peridotite from ultramafic complexes. *Contrib. Mineral. Petrol.*, **69**, 329-336.

Fabries J., Bodinier J.-L., Dupuy C., Lorand J.-P., Benkerrou C. (1989) Evidence for modal metasomatism in the orogenic spinel lherzolite body from Caussou (north-east Pyrénées, France). *J. Petrol.*, **30**, 199-228.

Fabriès J., Lorand J.-P., Bodinier J.-L., Dupuy C. (1991) Evolution of the upper mantle beneath the Pyénées: evidence from orogenic spinel lherzolite massifs. In: *"J. Pet. (Sp. Vol.): Orogenic lherzolites and mantle processes"*, M. A. Menzies, C. Dupuy & A. Nicholas (Eds.), 55-76.

Farley K. A, Natland J. H., Craig H. (1992) Binary mixing of enriched and undegassed (primitive?) mantle components (He, Sr, Nd, Pb) in Samoan lavas. *Earth Planet. Sci. Lett.*, **111**, 183-199.

Fischer W., Amossé J., Leblanc M. (1989) PGE distribution in some ultramafic rocks and minerals from the Bou-Azzer ophiolite complex. In: *"Geo-Platinum 87"*, Prichard H. M., Potts P. J., Bowles J. F. W. & Cribb S. J. (Eds.), Elsevier Applied Science, London, 199-210.

Fleet M. E., Chryssoulis S. L., Stone W. E., Weisener C. G. (1993) Partitioning of platinum-group elements and Au in the Fe-Ni-Cu-S system: experiments on the fractional crystallization of sulfide melt. *Contr. Mineral. Petrol.*, **115**, 36-44.

Fleet M. E., Stone W. E., Crocket J. H. (1991) Partitioning of palladium, iridium and platinum between sulfide liquid and basaltic melt: effects of melt composition, concentration and oxygen fugacity. *Geochim. Cosmochim. Acta*, **55**, 2545-2554.

Fortané A., Duée G., Lagabrielle Y., Coutelle A. (1986) Lherzolites and the western "Chaînons Bearnais" (French Pyrénées): structural and paleogeographical pattern. *Tectonophysics*, **129**, 81-98.

Frey F. A. & Prinz M. (1978) Ultramafic inclusions from San Carlos, Arizona: petrologic and geochemical data bearing on their petrogenesis. *Earth Planet. Sci. Lett.*, **38**, 129-176.

Frey F. A., Green D. H., Roy S. D. (1978) Integrated models of basalt petrogenesis: a study of quartz tholeiites to olivine melilitites from south eastern Australia utilising geochemical and experimental petrological data. *J. Petrol.*, **19**, 463-513.

Frey F. A., Suen C. J., Stockman H. W. (1985) The Ronda high temperature peridotite: geochemistry and petrogenesis. *Geochim. Cosmochim. Acta*, **49**, 2469-2491.

Furuta N., Monnig C. A., Yang P., Hieftje G. M. (1989) Noise characteristics of an inductively coupled plasma mass spectrometer. *Spectrochim. Acta*, **44B**, 649-656.

Garrels R. M. & Christ C. L. (1965) Solutions, minerals and equilibria. Harper & Row, New York, 450 pp.

Garuti G., Gorgoni C., Sighinolfi G. P. (1984) Sulphide mineralogy and chalcophile and siderophile element abundances in the Ivrea-Verbano mantle peridotites (Western Italian Alps). *Earth Planet. Sci. Lett.*, **70**, 69-87.

Gelinas L., Mellinger M., Trudel P. (1982) Archean mafic metavolcanics from the Rouyn-Noranda district, Abitibi greenstone belt, Quebec. 1. Mobility of the major elements. *Can. J. Earth Sci.*, **19**, 2258-2275.

Gijbels R. H., Millard H. T., Desborough G. A., Bartel A. J. (1974) Osmium, ruthenium, iridium and uranium in silicates and chromite from the eastern Bushveld complex, South Africa. *Geochim. Cosmochim. Acta*, **38**, 319-337.

Gilbert J. S., Bickle M. J., Chapman H. J. (1994) The origin of Pyrenean Hercynian volcanic rocks (France-Spain): REE and Sm-Nd isotope constraints. *Chem Geol.*, **111**, 207-226.

Gillson G. R., Douglas D. J., Fulford J. E., Halligan K. W., Tanner S. D. (1988) Non-spectroscopic interelement interferences in inductively coupled plasma mass spectrometry. *Anal. Chem.*, **60**, 1472-1474.

Gladney E. S. & Roelandts I. (1990) 1988 compilation of elemental concentration data for CCRMP reference rock samples SY-2, SY-3 and MRG-1. *Geostand. Newslett.*, **14**, 373-458.

Gladney E. S., Burns C. E., Roelandts I. (1983) 1982 compilation of elemental concentrations in eleven United States Geological Survey rock standards. *Geostand. Newslett.*, **7**, 3-226.

Goldberg R. N. & Hepler L. G. (1967) Thermochemistry and oxidation potentials of the platinum group metals and their compounds. *Chem. Rev.*, **68**, 229-252.

Gorbachev N. S. & Kashirceva G. A. (1985) Fluid magmatic differentiation of basaltic magma and equilibrium with magmatic sulphides. In: *"Experiments in the study of important problems in geology"*, Nauka 98, Moscow.

Govindaraju K. (1982) Report (1967 - 1981) on four ARNT rock reference samples: diorite DR-N, serpentine UB-N, bauxite BX-N and disthene DT-N. *Geostand. Newslett.*, **6**, 91-159.

Gowing C. J. B. & Potts P. J. (1991) Evaluation of a rapid technique for the determination of precious metals in geological samples based on a selective *aqua regia* leach. *Analyst*, **116**, 773-779.

Gray A. L. (1988) Inductively coupled plasma mass spectrometry. In: *"Inorganic Mass Spectrometry"*, F. Adams, R. Gijbels, R. van Grieken (Eds.), Wiley, New York, 257-300.

Gray A. L., Williams J. G., Ince A. T., Liezers M. (1994) Noise sources in inductively-coupled plasma source mass spectrometry: an investigation of their importance to the precision of isotope ratio measurements. *J. Anal. At. Spectrom.*, **9**, 1179-1181.

Green D. H. (1964) The petrogenesis of the high-temperature peridotite intrusion in the Lizard area, Cornwall. *J. Petrol.*, **5**, 134-188.

Green D. H. & Ringwood A. E (1967) The genesis of basaltic magmas. *Contrib. Mineral. Petrol.*, **15**, 103-190.

Greenough J. D. & Fryer B. J. (1990) Distribution of gold, palladium, platinum, rhodium, ruthenium and iridium in leg 115 hotspot basalts: implications for magmatic processes. In: *"Proc. ODP, Scientific Results, Vol. 115"*, R. A. Duncan, J. Backman & L. C. Peterson *et al.* (Eds.), College Station, Texas, 71-84.

Greenough J. D. & Owen J. V. (1992) Platinum-group element geochemistry of continental tholeiites: analysis of the Long Range dyke swarm, Newfoundland, Canada. *Chem. Geol.*, **98**, 203-219.

Grégoire D. C. (1987) Determination of boron isotope ratios in geological materials by inductively coupled plasma mass spectrometry. *Anal. Chem.*, **59**, 2479-2483.

Grégoire D. C. (1989) Application of isotope ratios determined by ICP-MS to earth science studies. *Prog. Analyt. Spectrosc.*, **12**, 433-452.

Grégoire D. C. (1990) Sample introduction techniques for the determination of osmium isotope ratios by inductively coupled plasma mass-spectrometry. *Anal. Chem.*, **62**, 141-146.

Guerrot C, Peucat J. J., Capdevila R., Dosso L. (1989) Archean protoliths within Early Proterozoic granulitic crust of the west European Hercynian belt: possible relics of the west African craton. *Geology*, **17**, 241-244.

Hamelin B. & Allegre C. J. (1988) Lead isotope study of orogenic lherzolite massifs. *Earth Planet. Sci. Lett.*, **91**, 117-131.

Hamlyn P. R. & Keays R. R. (1986) Sulphur saturation and second stage melts: application to the Bushveld platinum mineral deposits. *Econ. Geol.*, **81**, 1431-1445.

Hanson G. N. & Langmuir C. H. (1978) Modelling of major elements in mantle-melt systems using trace element abundances. *Geochim. Cosmochim. Acta*, **42**, 725-741.

Hart S. R. & Zindler A. (1986) In search of a bulk-Earth composition. *Chem. Geol.*, **57**, 247-267.

Hattori K. & Hart S. R. (1991) Osmium isotope ratios of platinum-group minerals associated with ultramafic intrusions: Os isotopic evolution of the oceanic mantle. *Earth Planet. Sci. Lett.*, **107**, 499-514.

Haughton D. R., Roeder P. L., Skinner B. J. (1974) Solubility of sulfur in mafic magmas. *Econ. Geol.*, **69**, 451-467.

Hauri E. H. & Hart S. R. (1993) Re-Os isotopic systematics of HIMU and EM II oceanic island basalts from the south Pacific Ocean. *Earth Planet. Sci. Lett.*, **114**, 353-371.

Hawkesworth C. J., Kempton P. D., Rogers N. W., Ellam R. M., van Calsteren P. W. (1990) Continental mantle lithosphere, and shallow level enrichment processes in the Earth's mantle. *Earth Planet. Sci. Lett.*, **96**, 256-268.

Hawkesworth C. J., Mantovani M. S. M., Taylor P. N., Palacz Z. (1986) Evidence from the Parana of south Brazil for a continental contribution to DUPAL basalts. *Nature*, **322**, 356-359.

Heath R. L. (1975). In: *"C.R.C. Handbook of Chemistry and Physics (56th Edition)"*, Weast R. C. *et al.* (Eds.), CRC Press, Cleveland, U.S.A., 2350 pp.

Hertogen J., Janssens M.-J., Palme H. (1980) Trace elements in ocean ridge basalt glasses: implications for fractionations during mantle evolution and petrogenesis. *Geochim. Cosmochim. Acta*, **44**, 2125-2143.

Herzberg C. T. (1978a) The bearing of phase equilibria in simple and complex systems on the origin and evolution of some well documented garnet-websterites. *Contr. Mineral. Petrol.*, **66**, 375-382.

Herzberg C. T. (1978b) Pyroxene geothermometry and geobarometry: experimental and thermodynamic evaluation of some subsolidus phase relations involving pyroxenes in the system $CaO$-$MgO$-$Al_2O_3$-$SiO_2$. *Geochim. Cosmochim. Acta*, **42**, 945-957.

Heumann K. G. & Zeininger H., (1985) Boron trace determination in metals and alloys by isotope dilution mass spectrometry with negative thermal ionisation. *Int. J. Mass Spec. Ion Proc.*, **67**, 237-252.

Heumann K. G., Schindlmeier W., Zeininger H., Schmidt M. (1985) Application of an economical and small thermal ionization mass spectrometer for accurate anion trace analyses. *Fres. Z Anal. Chem.*, **320**, 457-462.

Hirata T., Akagi T., Shimizu H., Masuda A. (1989) Determination of osmium and osmium isotope ratios by microthermal vaporization inductively coupled plasma mass spectrometry. *Anal. Chem.*, **61**, 2263-2266.

Hirose K. & Kushiro I. (1993) Partial melting of dry peridotites at high pressures: determination of compositions of melts segregated from peridotite using aggregates of diamond. *Earth Planet. Sci. Lett.*, **114**, 477-489.

Hirt B., Tilton G. R., Herr W., Hoffmeister W. (1963) The half-life of $^{187}Re$. In: *"Earth Sciences and Meteoritics"*, J. Geiss & E. D. Goldberg (Eds.), North Holland Publishing Co., Amsterdam, 273-280.

Hoffman E. L., Naldrett A. J.,van Loon J. C., Hancock R. G. V., Manson A. (1978) The determination of all the platinum group elements and gold in rocks and ore by neutron activation analysis after preconcentration by nickel sulphide fire assay techniques on large samples. *Anal. Chim. Acta.*, **102**, 157-166.

Houk R. S. & Thompson J. J. (1988) Inductively coupled plasma mass spectrometry. *J. Mass Spectrom. Rev.*, **7**, 425-461.

Houseman G. A., McKenzie D. P., Molnar P. (1981) Convective instability of a thickened boundary layer and its relevance for the thermal evolution of continental convergent belts. *Jour. Geophys. Res.*, **86**, 6115-6132.

Hulbert L. J. & Grégoire D. C. (1993) Re-Os isotope systematics of the Rankin Inlet Ni ores: an example of the application of ICP-MS to investigate Ni-Cu-PGE mineralization and the potential use of Os isotopes in mineral exploration. *Can. Mineral.*, **31**, 861-876.

Hurley P. M. & Rand J. R. (1969) Pre-drift continental nuclei. *Science*, **164**, 1229-1242.

Hutchinson R., Chambers A. L., Paul D. K., Harris P. G. (1975) Chemical variation amoung French ultramafic xenoliths - evidence for a heterogeneous upper mantle. *Min. Mag.*, **40**, 153-170.

Ince A. T., Williams J. G., Gray A. L. (1993) Noise in inductively-coupled plasma mass spectrometry: some preliminary measurements. *J. Anal. At. Spectrom.*, **8**, 899-903.

Ito K. & Kennedy G. C. (1968) Melting and phase relations in the plane tholeiite-lherzolite-nepheline basanite to 40 kilobars with geological implications. *Contrib. Mineral. Petrol.*, **19**, 177-211.

Ito K., White W. M., Göpel C. (1987) The O, Sr, Nd and Pb isotopic geochemistry of MORB. *Chem. Geol.*, **62**, 157-176.

Jackson S. E., Fryer B. J., Gosse W., Healey D. C., Longerich H. P., Strong D. F. (1990) Determination of the precious metals in geological samples by inductively coupled plasma mass spectrometry with nickel sulphide fire-assay collection and Te coprecipitation. *Chem. Geol.*, **83**, 119-132.

Jacques A. L. & Green D. H. (1980) Anhydrous melting of peridotite at 0-15 kb pressure and the genesis of tholeiitic basalts. *Contrib. Mineral. Petrol.*, **73**, 287-310.

Jagoutz E., Palme H., Baddenhausen H., Blum K., Cendales M., Dreibus G., Spettel B., Lorenz V., Wänke H. (1979) The abundances of major, minor and trace elements in the Earth's mantle as defined from primitive ultramafic nodules. *Proc. Lunar Planet. Sci. Conf. 10th*, 2031-2050.

Johnson K. T. M., Dick H. J. B., Shimizu N. (1990) Melting in the oceanic upper mantle: an ion microprobe study of diopsides in abyssal peridotites. *J. Geophys. Res.*, **95**, 2661-2678.

Jones E. A., Kruger M. M., Wilson A. (1971) The determination of osmium. *Nat. Inst. Met., Johannesburg.* **Report 1232**, 11 pp.

Jones J. H. & Drake M. J. (1986) Geochemical constraints on core formation in the Earth. *Nature*, **322**, 221-228.

Jonson B. (1616) The Alchemist. William Stansby, London.

Jordan T. H. (1978) Composition and development of continental tectosphere. *Nature*, **274**, 544-548.

Jordan T. H. (1988) Structure and formation of the continental tectosphere. In: "*J. Pet Sp. Vol.: Oceanic and continental lithosphere: similarities and differences*", *M. A. Menzies & K. G. Cox (Eds.)*, 1-37.

K. E. Jarvis, A. L. Gray, I. Jarvis, J. Williams (1990) Plasma Source Mass Spectrometry. Royal Soc. Chem., Cambridge, 172 pp.

Kaneda H., Takenouchi S., Shoji T. (1986) Stability of pentlandite in the Fe-Ni-Co-S system. *Mineral. Deposita*, **21**, 169-180.

Keays R. R. & Campbell I. H. (1981) Precious metals in the Jimberlana intrusion, Western Australia: implications for the genesis of platiniferous ores in layered intrusions. *Econ. Geol.*, **76**, 1118-1141.

Kelemen P. B., Johnson K. T. M., Kinzler R. J., Irving A. J. (1990) High-field-strength element depletions in arc basalts due to mantle-magma interaction. *Nature*, **345**, 521-524.

Kilinc A., Carmichael I. S. E., Rivers M. L., Sack R. O. (1983) Ferric-ferous ratio of natural silicate liquids equilibrated in air. *Contrib. Mineral. Petrol.*, **83**, 136-140.

Kimura K., Lewis R. S., Anders E. (1974) Distribution of gold and rhenium between nickel-iron and silicate melts: implications for the abundance of siderophile elements on the Earth and Moon. *Geochim. Cosmochim. Acta*, **38**, 683-701.

Kobetich E. J. & Katz R. (1968) Energy deposition by electron beams and ∂-rays. *Phys Rev.*, **170**, 391-396.

Koide M., Hodge V., Yang J. S., Goldberg E. D. (1987) Determination of rhenium in marine waters and sediments by graphite furnace atomic absorbtion spectrometry. *Anal. Chem.*, **58**, 1802-1805.

Kornprobst J. & Vielzeuf D. (1984) Transcurrent crustal thinning: a mechanism for the uplift of deep continental crust/upper mantle associations. In: *"Kimberlites II: The mantle and mantle-crust relationships"*, J. Kornprobst (Ed.), Elsevier, Amsterdam, 347-359.

Kullerud G., Yund R. A., Mohr G. (1969) Phase relationships in the Cu-Fe-S, Cu-Ni-S and Fe-Ni-S systems. In: *"Magmatic Ore Deposits"*, Econ Geol. Monograph No. 4, 232-343.

Kutznetsov A. P., Kukushkin Y. N., Makarov D. (1974) Use of nickel mattes as a collector for the noble metals in analysis of poor materials. *Anal. Khim.*, **29**, 2155-2160.

Lacroix A. (1901) Sur les ariége, nouveau types de roches éruptives. *Musée Histoire Naturelle, Bulletin*, **7**, 238-240.

Lacroix A. (1917) Les péridotites des Pyrénées et les autres roches intrusives non feldspathiques qui les accompagnent. *C. R. Acad. Sci. Paris*, **165**, 381-387.

Liew T. C. & Hofmann A. W. (1988) Precambrian crustal components, plutonic associations, plate environment of the Hercynian Fold Belt of central Europe: indications from a Nd and Sr isotopic study. *Contrib. Mineral. Petrol.*, **98**, 129-138.

Lindner M., Leich D. A., Borg R. J., Russ G. P., Bazan J. M., Simons D. S., Date A. R. (1986) Direct laboratory determination of the $^{187}$Re half life. *Nature*, **320**, 246-248.

Lindner M., Leich D. A., Russ G. P., Bazan J. M., Borg R. J. (1989) Direct determination of the half-life of $^{187}$Re. *Geochim. Cosmochim. Acta*, **53**, 1597-1606.

Lloyd F. E. & Bailey D. K. (1975) Light element metasomatism of the continental mantle: the evidence and the consequences. *Phys. Chem. Earth*, **9**, 389-416.

Lodders K. (1988) Neutronenaktivierungsanalyse von Edelmetal, Rhenium, Molybdan and Wolfram mit Hilfe der Nickelsulphidextraktion. *Diplomarbeit*, **University of Mainz**, 67 pp.

Longerich H. P., Fryer B. J., Strong D. F. (1987) Determination of lead isotope ratios by inductively coupled plasma mass spectrometry (ICP-MS). *Spectrochim. Acta*, **42**, 39-48.

Lorand J.-P. (1987) Cu-Fe-Ni-S mineral assemblages in upper mantle peridotites from the Table Mountain and Blow-Me-Down Mountain massifs (Bay of Islands area, Newfoundland): their relationships with fluids and silicate melts. *Lithos*, **20**, 59-76.

Lorand J.-P. (1988) Fe-Ni-Cu sulphides in tectonite peridotites from the Maqsad district, Sumail ophiolite, southern Oman: implications for the origin of the sulfide component in the oceanic upper mantle. *Tectonophysics*, **151**, 57-73.

Lorand J.-P. (1989a) Sulphide petrology of spinel and garnet pyroxenite layers from mantle derived spinel lherzolite massifs of Ariège, north eastern Pyrénées, France. *J. Petrol.*, **30**, 987-1015.

Lorand J.-P. (1989b) Mineralogy and chemistry of Cu-Fe-Ni sulphides in orogenic-type spinel peridotite bodies from Ariège (north eastern Pyrénées). *Contr. Mineral. Petrol.*, **103**, 335-345.

Lorand J.-P. (1989c) Abundance and distribution of Cu-Fe-Ni sulfides, sulfur, copper and platinum group elements in orogenic-type spinel lherzolite massifs of Ariège (north eastern Pyrénées, France). *Earth Planet. Sci. Lett.*, **93**, 50-64.

Lorand J.-P. (1989d) The Cu-Fe-Ni sulfide component of the amphibole-rich veins from the Lherz and Freychinède spinel peridotite massifs (northeastern Pyrénées, France): a comparison with mantle-derived megacrysts from alkali basalts. *Lithos*, **23**, 281-298.

Lorand J.-P. (1990) Are spinel lherzolite xenoliths representative of the abundance of sulfur in the upper mantle? *Geochim. Cosmochim. Acta*, **54**, 1487-1492.

Lorand J.-P. (1991) Sulphide petrology and sulphur geochemistry of orogenic lherzolites: a comparative study of the Pyrenean bodies (France) and the Lanzo Massif (Italy). In: *"J. Pet. (Sp. Vol.): Orogenic lherzolites and mantle processes"*, M. A. Menzies, C. Dupuy & A. Nicholas (Eds.), 77-95.

Lorand J. P., Keays R. R., Bodinier J. L. (1993) Copper and noble metal enrichments across the lithosphere-asthenosphere boundary of mantle diapirs: evidence from the Lanzo lherzolite massif. *J. Petrol.*, **34**, 1111-1140.

Loubet M. & Allègre C. J. (1982) Trace elements in orogenic lherzolites reveal the complex history of the upper mantle. *Nature*, **298**, 809-814.

Luck J.-M. & Allègre C. J. (1983) $^{187}Re$-$^{187}Os$ systematics in meteorites and cosmochemical consequences. *Nature*, **302**, 130-132.

Luck J.-M. & Allègre C. J. (1991) Osmium isotopes in ophiolites. *Earth Planet. Sci. Lett.*, **107**, 406-415.

Luck J.-M., Birck J. L., Allègre C. J. (1980) $^{187}Re$-$^{187}Os$ systematics in meteorites: early chronology of the solar system and the age of the galaxy. *Nature*, **283**, 256-259.

Maaloe S. & Aoki K. (1977) The major element composition of the upper mantle estimated from the composition of lherzolites. *Contrib. Mineral. Petrol.*, **63**, 161-173.

Malevskiy A. Yu., Laputina I. P., Distler V. V. (1977) Behavior of the platinum group metals during crystallization of pyrrhotite from a sulfide melt. *Geochem. Intl.*, **61**, 177-184.

Mallett R. C., Royal S. J., Steele T. W. (1979) Determination of osmium by atomic absorption spectrophotometry. *Anal. Chem.*, **51**, 1617-1620.

Marcantonio F., Zindler A., Reisberg L., Mathez E. A. (1993) Re-Os isotopic systematics in chromitites from the Stillwater Complex, Montana, U.S.A. *Geochim. Cosmochim. Acta*, **57**, 4029-4037.

Marcantonio F., Reisberg L., Zindler A., Wyman D., Hulbert L. (1994) An isotopic study of the Ni-Cu-PGE rich Wellgreen intrusion of the Wrangellia Terrane: evidence for hydrothermal mobilisation of rhenium and osmium. *Geochim. Cosmochim. Acta*, **58**, 1007-1017.

Martin C. E. (1989) Re-Os isotopic investigation of the Stillwater Complex, Montana. *Earth Planet. Sci. Lett.*, **93**, 336-344.

Martin C. E. (1990) Rhenium-osmium isotope geochemistry of the mantle. *PhD Thesis*, **Yale University**, 170 pp.

Martin C. E. (1991) Os isotope characteristics of mantle-derived rocks. *Geochim. Cosmochim. Acta*, **55**, 1421-1434.

Masuda A., Hirata T., Shimizu H. (1986) Determinations of osmium isotope ratios in iron meteorites and iridosmines by ICP-MS. *Geochem J.*, **20**, 233-239.

Mattioli G. S., Baker M. B., Rutter M. J., Stolper E. M. (1989) Upper mantle oxygen fugacity and its relationship to metasomatism. *J. Geol.* , **97**, 521-536.

McDonough W. F. (1990) Constraints on the composition of the continental lithospheric mantle. *Earth Planet. Sci. Lett.*, **101**, 1-18.

McDonough W. F. & Frey F. A. (1989) Rare-earth elements in upper mantle rocks. In: *"Geochemistry and mineralogy of rare-earth elements"*, B Lipin & G. R McKay (Eds.), Mineralogical Society of America, **21**, Washington, 99-145.

McKenzie D. (1984) The generation and compaction of partially molten rock. *J. Petrol.*, **25**, 713-765.

McKenzie D. (1985) The extraction of magma from the crust and mantle. *Earth Planet. Sci. Lett.*, **74**, 81-91.

Menzies M. A. (1983) Mantle ultramafic xenoliths in alkaline magmas: evidence for mantle heterogeneity modified by magmatic activity. In: *"Continental basalts and mantle xenoliths"*, C. J. Hawkesworth & M. J. Norry (Eds.), Shiva, Nantwich, UK, 92-110.

Menzies M. A. & Hawkesworth C. J. (Eds.) (1987) Mantle Metasomatism. Academic Press, London, 472 pp.

Mercier J. C. (1972) Structure des péridotites en enclaves dans quelque basalts d'Europe et d'Hawaii. Regards sur la consitution du manteau supérieur. *Thèse 3ème cycle*, **University of Nantes, France**, 229 pp.

Mercier J. C. & Nicholas A. (1975) Textures and fabrics of upper mantle peridotites as illustrated by xenoliths from basalts. *J. Petrol.*, **16**, 454-487.

Minnigh L. D., van Calsteren P. W. C., den Tex E. (1980) Quenching: an additional model for emplacement of the lherzolite at Lers (French Pyrénées). *Geology*, **8**, 18-21.

Mitchell R. H. & Keays R. R. (1981) Abundance and distribution of gold, palladium and iridium in some spinel and garnet lherzolites: implications for the nature and origin of precious metal rich intergranular components in the upper mantle. *Geochim. Cosmochim. Acta*, **45**, 2425-2442.

Monchoux P. (1970) Les lherzolites Pyrénées: contribution à l'étude de leur mineralogie, de leur genèse et leur transformation. *PhD.Thesis*, **Université Paul Sabatier, Tolouse, France**, 180 pp.

Montigny R., Azambre B., Rossy M., Thuizat R. (1982) Etude K/Ar du magmatisme basique lié au Trias supérieur des Pyrénées. Conséquences méthodologiques et paléogéographiques. *Bull. Minéral.*, **105**, 673-680.

Montigny R., Azambre B., Rossy M., Thuizat R. (1986) K-Ar study of Cretaceous magmatism and metamorphism in the Pyrénées: age and length of rotation of the Iberian peninsula. *Tectonophysics*, **129**, 257-273.

Morgan J. W. (1986) Ultramafic xenoliths: clues to Earth's late accretionary history. *J. Geophys. Res.*, **91**, 12375-12387.

Morgan J. W. & Walker R. J. (1989) Isotopic determinations of rhenium and osmium in meteorites by using fusion, distillation and ion-exchange separations. *Anal. Chim. Acta.*, **222**, 291-300.

Morgan J. W., Wandless G. A., Petrie R. K., Irving A. J. (1981) Composition of the earths upper mantle-I) Siderophile trace elements in ultramafic nodules. *Tectonophysics*, **75**, 47-67.

Morgan J. W., Walker R. J., Grossman J. N. (1992) Rhenium-osmium isotope systematics in meteorites I: Magmatic iron meteorite groups IIAB and IIIAB. *Earth Planet. Sci. Lett.*, **108**, 191-202.

Mueller R. F. & Saxena S. K. (1977) Chemical Petrology. Springer-Verlag, New York, 394 pp.

Mukasa S. B., Shervais J. W., Wilshire H. G., Nielson J. E. (1991) Intrinsic Nd, Pb and Sr isotopic heterogeneities exhibited by the Lherz alpine peridotite massif, French Pyrénées. In: *"J. Pet. (Sp. Vol.): Orogenic lherzolites and mantle processes"*, M. A. Menzies, C. Dupuy & A. Nicholas (Eds.), 117-134.

Mysen B. O. (1979) Trace element partitioning between garnet peridotite minerals and water-rich vapour: experimental data from 5 to 30 kbar. *Am. Mineral.*, **64**, 274-287.

Mysen B. O. & Seitz M. G. (1975) Trace element partitioning determined by beta track mapping: an experimental study using carbon and samarium as examples. *J. Geophys. Res.*, **80**, 2627-2635.

Naldrett A. J. & Duke J. M. (1980) Platinum metals in magmatic sulphide ores. *Science*, **208**, 1417-1424.

Naldrett A. J., Hoffman E. L., Green A. H., Chou C.-L., Naldrett S. R. (1979) The composition of Ni-sulphide ores, with particular reference to their content of PGE and Au. *Can. Mineral.*, **17**, 403-415.

Naldrett S. N & Libby W. F. (1948) Natural radioactivity of Re. *Phys. Rev.*, **73**, 487-493.

Nicholas A., Lucazeau F., Bayer R. (1987) Peridotite xenoliths in Massif Central basalts, France: textural and geophysical evidence for asthenospheric diapirism. In: *"Mantle Xenoliths"*, P. H. Nixon (Ed.), Wiley, Chichester, UK, 563-574.

Nicolas A. (1985) Novel type of crust produced by continental rifting. *Nature*, **315**, 112-115.

Nier A. O. (1937) The isotopic constitution of osmium. *Phys. Rev.*, **52**, 885.

Nier A. O. (1950) A redetermination of the relative abundances of the isotopes of carbon, nitrogen, oxygen, argon and potassium. *Phys. Rev.*, **77**, 789-793.

O'Hara M. J. (1968) The bearing of phase equilibria studies in synthetic and natural systems on the origin and evolution of basic and ultrabasic rocks. *Earth Sci. Rev.*, **4**, 69-133.

O'Hara M. J., Richardson S. M., Wilson G. (1971) Garnet peridotite stability and occurence in the crust and mantle. *Contrib. Mineral. Petrol.*, **32**, 48-68.

Obata M. (1980) The Ronda peridotite: garnet-, spinel- and plagioclase-lherzolite facies and the P-T trajectories of a high temperture mantle intrusion. *J. Petrol.*, **21**, 533-572.

Oshin I. O. & Crocket J. H. (1982) Noble metals in Thetford Mines ophiolites, Quebec, Canada. Part I: distribution of gold, iridium, platinum and palladium in the ultramafic and gabbroic rocks. *Econ. Geol.*, **77**, 1556-1570.

Page N. J. & Talkington R. W. (1984) Palladium, platinum, rhodium, ruthenium and iridium in peridotites and chromitites from ophiolite complexes in Newfoundland. *Can. Mineral.*, **22**, 137-149.

Page N. J., Cassard D., Haffty J. (1982) Palladium, platinum, rhodium, ruthenium and iridium in chromitites from the Massif du Sud and Tiebaghi Massif, New Caledonia. *Econ. Geol.*, **77**, 1571-1577.

Palmer R. & Watterson J. I. W. (1971) The recovery of noble metals for analysis. A radiotracer investigation of losses. *Nat. Inst. Met., Johannesburg.* **Report 1185**, 11 pp.

Parthé E., Hohnke D., Hulliger F. (1967) A new structure type with octahedron pairs for $Rh_2S_3$, $Rh_2Se_3$ and $Ir_2S_3$. *Acta Cryst.*, **23**, 832-840.

Peach C. L., Mathez E. A., Keays R. R. (1990) Sulfide melt-silicate melt distribution coefficients for noble metals and other chalcophile elements as deduced from MORB: implications for partial melting. *Geochim. Cosmochim. Acta*, **54**, 3379-3389.

Peach C. L., Mathez E. A., Keays R. R., Reeves S. J. (1994) Experimentally determined sulfide melt-silicate melt partition coefficients for iridium and platinum. *Chem. Geol.* , **117**, 361-377.

Pearson D. G. (1989) The petrogenesis of pyroxenites containing octahedral graphite and associated mafic and ultramafic rocks of the Beni Bousera massif, N. Morroco. *PhD. Thesis*, **University of Leeds**, 412 pp.

Pearson D. G., Boyd F. R., Hoal K. E. O., Hoal B. G., Nixon P. H., Rogers N. W. (1994) A Re-Os isotopic and petrological study of Namibian peridotites: contrasting petrogenesis and composition of on- and off-craton lithospheric mantle. *Min. Mag.*, **58A**, 703-704.

Pearson D. G., Shirey S. B., Carlson R. W., Boyd F. R., Pokhilenko N. P., Shimizu N. (1995a) Re-Os, Sm-Nd and Rb-Sr isotope evidence for thick Archaean lithospheric mantle beneath the Siberia craton modified by multistage metasomatism. *Geochim. Cosmochim. Acta*, **59**, 959-977.

Pearson D. G., Snyder G. A., Shirey S. B., Taylor L. A., Carlson R. W., Sobolev N. V. (1995b) Archaean Re-Os age for Siberian eclogites and constraints on Archean tectonics. *Nature*, **374**, 711-713.

Pearson D. G., Carlson R. W., Shirey S. B., Boyd F. R., Nixon P. H. (1995c) The stabilisation of Archaean lithospheric mantle: a Re-Os isotope study of peridotite xenoliths from the Kaapvaal and Siberian cratons. *Earth Planet. Sci. Lett. (in press).*

Perrier G. & Ruegg J. C. (1973) Structure profonde du Massif Central français. *Ann. Geophys.*, **29**, 435-502.

Platt J. P., Vissers R. L. M. (1989) Extensional collapse of thickened continental lithosphere: a working hypothesis for the Alboran sea and Gibraltar arc. *Geology*, **17**, 540-543.

Potts P. J. (1984) Neutron activation-induced beta autoradiography as a technique for locating minor phases in thin sections: application to rare earth element and platinum group element mineral analysis. *Econ. Geol.*, **79**, 738-747.

Potts P. J. (1987) A handbook of silicate rock analysis. Blackie & Son, 622 pp.

Potts P. J. & Prichard H. M. (1986) Mineralogical applications of neutron activation-induced beta autoradiography: the search for gold mineralisation in thin section. In: *"Metallogeny of Basic and Ultrabasic Rocks"*, M. J. Gallagher, R. A. Ixer, C. R. Neary & H. M. Pritchard (Eds.), Inst. Min. & Metal., London, 455-465.

Poulson S. R. & Ohmoto H. (1990) An evaluation of the solubility of sulfide sulfur in silicate melts from experimental data and natural samples. *Chem. Geol.*, **85**, 57-75.

Presnall D. C., Dixon J. R., O'Donnell T. H., Dixon S. A. (1979) Generation of mid-ocean ridge tholeiites. *J. Petrol.*, **20**, 3-35.

Prichard H. M, Potts P. J., Neary C. R. (1981) Platinum-group minerals in the Unst chromite, Shetland Isles. *Trans. Inst. Min. Metall.*, **90**, B186-B188.

Prinzhofer A. & Allègre C. J. (1985) Residual peridotites and the mechanisms of partial melting. *Earth Planet. Sci. Lett.*, **74**, 251-265.

Quick J. E. (1981) Petrology and petrogenesis of the Trinity Peridotite, an upper mantle diapir in the eastern Klamath Mountains, northern California. *J. Geophys. Res.*, **86**, 11837-11863.

Rajamani V. & Naldrett A. J. (1978) Partitioning of Fe, Co, Ni and Cu between sulfide liquid and basaltic melts and the composition of Ni-Cu sulfide deposits. *Econ. Geol.*, **73**, 82-93.

Ravier J. (1959) Le métamorphisme des terrains secondaires des Pyrénées. *Mém. Soc. Géol. France*, **38**, 250 pp.

Ravizza G., Turekian K. K., Hay B. J. (1991) The geochemistry of rhenium and osmium in recent sediments from the Black Sea. *Geochim. Cosmochim. Acta*, **55**, 3741-3752.

Reisberg L. C. (1988) The isotopic and geochemical systematics of the Ronda ultramafic complex of southern Spain. *PhD. Thesis*, **Columbia University**, 232 pp.

Reisberg L., Zindler A., Jagoutz E. (1989b) Further Sr & Nd isotopic results from peridotites of the Ronda Ultramafic Complex. *Earth Planet. Sci. Lett.*, **96**, 161-180.

Reisberg L. C., Allègre C. J., Luck J.-M. (1991) The Re-Os systematics of the Ronda Ultramafic Complex of southern Spain. *Earth Planet. Sci. Lett.*, **105**, 196-213.

Reisberg L., Zindler A., Marcantonio F., White W., Wyman D., Weaver B. (1993) Os isotope systematics in ocean island basalts. *Earth Planet. Sci. Lett.*, **120**, 149-167.

Ringwood A. E. (1975) Composition and petrology of the Earth's mantle. McGraw-Hill, New York, 618 pp.

Ringwood A. E. (1977) Basaltic magmatism and the bulk composition of the moon, I, Major and heat producing elements. *Moon*, **16**, 425-464.

Robért R. V. D., van Wyk E., Palmer R. (1971) Concentration of the noble metals by a fire assay technique using nickel sulphide as the collector. *Nat. Inst. Met., Johannesburg* **Report 1371**, 14 pp.

Roeder P. L & Emslie R. F (1970) Olivine-liquid equilibrium. *Contrib. Mineral. Petrol.*, **29**, 276-289.

Roy-Barman M. & Allègre C. J. (1994) $^{187}Os/^{186}Os$ ratios of mid-ocean ridge basalts and abyssal peridotites. *Geochim. Cosmochim. Acta*, **58**, 5043-5054.

Roy-Barman M. & Allègre C. J. (1995) $^{187}Os/^{186}Os$ in oceanic island basalts: tracing oceanic crust recycling in the mantle. *Earth Planet. Sci. Lett.*, **129**, 145-161.

Russ G. P. & Bazan J. M. (1987) Isotopic ratio measurements with an inductively coupled plasma source mass spectrometer. *Spectrochim. Acta*, **42B**, 49-62.

Russ G. P., Bazan J. M., Date A. R. (1987) Osmium isotopic ratio measurements by inductively coupled plasma source mass-spectrometry. *Anal. Chem.*, **59**, 984-989.

Sautter V. & Fabriès J. (1990) Cooling kinetics of garnet websterites from the Freychinède orogenic lherzolite massif, French Pyrénées. *Contr. Mineral. Petrol.*, **105**, 533-549.

Schilling J.-G., Zajac M., Evans R., Johnston T., White W., Devine J. D., Kingsley R. (1983) Petrologic and geochemical variations along the Mid-Atlantic Ridge from 29°N to 73°N. *Am. J. Science*, **283**, 510-586.

Shannon R. D. (1976) Revised effective ionic radii and systematic studies of interatomic distances in halides and chalcogenides. *Acta Crystal.*, **A32**, 751-767.

Shaw D. M. (1970) Trace element fractionation during anatexis. *Geochim. Cosmochim. Acta*, **34**, 237-243.

Shazali I., Van't Dack L., Gijbels R. (1987) Determination of precious metals in ores and rocks by thermal neutron activation/ γ-spectrometry after preconcentration by nickel sulphide fire assay and coprecipitation by tellurium. *Anal. Chim. Acta.*, **196**, 49-58.

Shazali I., Van't Dack L., Gijbels R. (1988) Preconcentration of precious metals by tellurium sulphide fire assay followed by instrumental neutron activation analysis. In: *"Geo-Platinum 87"*, Prichard H. M., Potts P. J., Bowles J. F. W. & Cribb S. J. (Eds.), Elsevier Applied Science, London, 29-42.

Shi P. (1992) Fluid fugacities and phase equilbria in the Fe-Si-O-H-S system. *Am. Mineral.*, **77**, 1050-1066.

Shi P. & Saxena S. K. (1992) Thermodynamic modeling of the C-H-O-S fluid system. *Am. Mineral.*, **77**, 1038-1049.

Shirey S. B & Walker R. J. (1994) Improved spike-sample equilibration for Re-Os isotopic analysis at low blank levels using Carius tubes. *Spring AGU Meeting (abstr.).*

Smith D. (1977) The origin and interpretation of spinel-pyroxene clusters in peridotite. *J. Geol.*, **85**, 476-482.

Steele T. W. & Hansen R. G. (1979) Major element data (1966 - 1978) for the six "NIMROC" reference samples. *Geostand. Newslett.*, **3**, 135-172.

Steele T.W., Levin J., Copelowitz I. (1975) The preparation and certification of a reference sample of a precious metal ore. *Nat. Inst. Met., Johannesburg.* **Report 1686**, 42 pp.

Stockman H. W. & Hlava P. F. (1984) Pt group minerals in alpine chromite from south west Oregon. *Econ. Geol.*, **79**, 491-508.

Stosch H.-G. & Seck H. A. (1980) Geochemistry and mineralogy of two spinel peridotite suites from Dreiser Weiher, West Germany. *Geochim. Cosmochim. Acta*, **44**, 457-470.

Suen C. J. &.Frey F. A. (1987) Origins of the mafic and ultramafic rocks in the Ronda peridotite. *Earth Planet. Sci. Lett.*, **85**, 183-202.

Summerhays K. D., Lamothe P. J., Fries T. L. (1983) Volatile species in inductively coupled plasma atomic emission spectroscopy: implications for enhanced sensitivity. *Appl. Spectroscopy*, **37**, 25-28.

Sun S.-S. (1982) Chemical composition and origin of the Earth's primitive mantle. *Geochim. Cosmochim. Acta*, **46**, 179-192.

Sun S.-S. (1990) Mantle plume and melting of refractory mantle: implications for PGE and Au mineralisation *(abstr.)*. 10th Australian Geol. Convention, Hobart, Tasmania. *Geol. Soc. Aust.*, 130-131.

Sun S.-S. & McDonough W. F. (1989) Chemical and isotopic systematics of oceanic basalts: implications for mantle compositions and processes. In: *"Magmatism in the Oceanic Basins"*, A. D. Saunders & M. J. Norry (Eds.), Geol. Soc. Lond. Sp. Publ. No. 42, 313-345.

Sun X. F., Ting B. T. G., Zeisel S. H., Janghorbani M. (1987) Accurate measurement of stable isotopes of lithium by inductively coupled plasma mass spectrometry. *Analyst*, **112**, 1223-1228.

Takahashi E. (1986) Melting of dry peridotite KLB-1 up to 14 GPa: implications for the origin of peridotitic upper mantle. *J. Geophys. Res.*, **91**, 9367-9382.

Takahashi E. & Kushiro I. (1983) Melting of a dry peridotite at high pressures and basalt magma genesis. *Am. Mineral.*, **68**, 859-879.

Takahashi E., Shimazaki T., Tsuzaki Y., Yoshida H. (1993) Melting study of a peridotite KLB-1 to 6.5 GPa and the origin of basaltic magmas. *Phil. Trans R. Soc. Lond. (A)*, **342**, 105-120.

Tarkian M., Naidenova E., Zhelyaskova-Panayotova M. (1991) Platinum-group minerals in chromitites from the Eastern Rhodope Ultramafic Complex, Bulgaria. *Miner. & Petrol.*, **44**, 73-87.

Thirlwall M. F. (1982) A triple filament method for rapid and precise analysis of rare-earth elements by isotope dilution. *Chem. Geol.*, **35**, 155-166.

Turekian K. K. & Wedepohl K. H. (1961) Distribution of the elements in some major units of the Earth's crust. *Bull. Geol. Soc. Am.*, **72**, 175-191.

Vielzeuf D. & Kornprobst J. (1984) Crustal splitting and the emplacement of Pyrenean lherzolites and granulites. *Earth Planet. Sci. Lett.*, **67**, 87-96.

Völkening J., Walczyk T., Heumann K. G. (1991) Osmium isotope ratio determinations by negative thermal ionisation mass spectrometry. *Intl. J. Mass Spectrom Ion Processes*, **105**, 147-159.

Wachsmann M. (1991). *PhD. Thesis*, **University of Regensburg**.

Walczyk T., Hebeda E. H., Heumann K. G. (1991) Osmium isotope ratio measurements by negative thermal ionization mass spectrometry (NTI-MS). Improvement in precision and enhancement in emission by introducing oxygen or freons into the ion source. *Fres. J. Anal. Chem.*, **341**, 537-541.

Walczyk T., Hebeda E. H., Heumann K. G. (1994) Low blank rhenium isotope ratio determinations by $V_2O_5$ coated nickel filaments using negative thermal ionization mass spectrometry. *Int. J. Mass Spec. Ion Proc.*, **130**, 237-246.

Walder A. J. & Freedman P. A. (1992) Isotopic ratio measurement using a double focusing magnetic sector mass analyser with an inductively coupled plasma as an ion source. *J. Anal. At. Spectrom.*, **7**, 571-575.

Walder A. J., Platzner I., Freedman P. A. (1993) Isotope ratio measurement of lead, neodymium and neodymium-samarium mixtures, hafnium and hafnium-lutetium mixtures with a double focusing multiple collector inductively coupled plasma mass spectrometry. *J. Anal. At. Spectrom.*, **8**, 19-23.

Walker R. J. (1988) Low-blank separation of rhenium and osmium from gram quantities of silicate rock for measurement by resonance ionisation mass-spectrometry. *Anal. Chem.*, **60**, 1231-1234.

Walker R. J. & Fasset J. D. (1986) Isotopic measurement of subnanogram quantities of Re and Os by resonance ionisation mass-spectrometry. *Anal. Chem.*, **56**, 2923-2927.

Walker R. J. & Morgan J. W. (1989) Rhenium-osmium isotope systematics of carbonaceous chondrites. *Science*, **243**, 519-521.

Walker R. J., Shirey S. B., Stecker O. (1988) Comparative Re-Os, Sm-Nd, Rb-Sr isotope and trace element systematics for Archean komatiite flows from Munro Township, Abitibi Belt, Ontario. *Earth Planet. Sci. Lett.*, **87**, 1-12.

Walker R. J., Carlson R. W., Shirey S. B., Boyd F. R. (1989a) Os, Sr, Nd and Pb isotope systematics of southern African peridotite xenoliths: implications for the chemical evolution of subcontinental lithosphere. *Geochim. Cosmochim. Acta*, **53**, 1583-1595.

Walker R. J., Shirey S. B., Hanson G. N., Rajamani V., Horan M. F. (1989b) Re-Os, Rb-Sr and O isotopic systematics of the Archean Kolar schist belt, Karnataka, India. *Geochim. Cosmochim. Acta*, **53**, 3005-3013.

Walker R. J., Morgan J. W., Naldrett A. J., Li C., Fassett J. D. (1991) Re-Os isotope systematics of Ni-Cu sulfide ores, Sudbury Igneous Complex, Ontario: evidence for a major crustal component. *Earth Planet. Sci. Lett.*, **105**, 416-429.

Walker R. J., Morgan J. W., Horan M. F., Czmanske G. K. (1994) Re-Os isotopic evidence for an enriched mantle source for the Noril'sk-type, ore-bearing intrusions, Siberia. *Geochim. Cosmochim. Acta*, **58**, 4179-4197.

Wasserburg G. J., Jacobsen S. B., DePaolo D. J., McCulloch M. T., Wen T. (1981) Precise determination of Sm/Nd ratios, Sm and Nd isotopic abundances in standard solutions. *Geochim. Cosmochim. Acta*, **45**, 2311-2323.

Watson E. B., Ben Othman D., Luck J.-M., Hofmann A. W. (1987) Partitioning of U, Pb, Cs, Yb, Hf, Re and Os between chromian diopsidic pyroxene and haplobasaltic liquid. *Chem. Geol.*, **62**, 191-208.

Weast R. C. *et al* (Eds.) (1975) C.R.C. Handbook of Chemistry and Physics (56th Edition). CRC Press, Cleveland, U.S.A, 2350 pp.

Wendlandt R. F. (1982) Sulfide saturation of basalt and andesite melts at high pressures and temperatures. *Am. Mineral.*, **67**, 877-885.

Westland A. D. & Beamish F. E. (1954) Study of osmium and ruthenium distillations. *Anal. Chem.*, **26**, 739-741.

White D. E., Hem J. D., Waring G. A. (1963) Chemical composition of sub-surface waters. In: "*Data of Geochemistry (6th Edition)*", E. D. Fleischer (Ed.), U.S. Geol. Surv. Bull..

Wilson B. J. (Ed.) (1966) The Radiochemical Manual. The Radiochemical Centre, Amersham, U.K.

Wilson G. C., Kilius L. R., Rucklidge J. C. (1991) *In situ* analysis of precious metals in polished mineral samples and sulphide "standards" by accelerator mass spectrometry at concentrations of parts per billion. *Geochim. Cosmochim. Acta*, **55**, 2241-2251.

Witt G. & Seck H. A. (1987) Temperature history of sheared mantle xenoliths from the west Eifel, West Germany: evidence for mantle diapirism beneath the Rhenish Massif. *J. Petrol.*, **28**, 475-493.

Wood B. J. & Virgo D. (1989) Upper mantle oxidation state: ferric iron contents of lherzolite spinels by $^{57}$Fe Mössbauer spectroscopy and the resultant oxygen fugacities. *Geochim. Cosmochim. Acta*, **53**, 1277-1291.

Wood B. J., Bryndzia L. T., Johnson K. E. (1990) Mantle oxidation state and its relationship to tectonic environment and fluid speciation. *Science*, **248**, 337-345.

Wood S. A. (1987) Thermodynamic calculations of the volatility of the platinum group elements (PGE): the PGE contents of fluids at magmatic temperatures. *Geochim. Cosmochim. Acta*, **51**, 3041-3050.

Zeininger H. & Heumann K. G. (1983) Boron isotope ratio measurement by negative thermal ionization mass spectrometry. *Int. J. Mass Spectrom. Ion Phys.*, **48**, 377-380.

Zindler A. & Hart S. (1986) Chemical geodynamics. *Ann Rev. Earth Planet Sci.*, **14**, 493-571.

# Appendix A

# Whole-Rock Elemental Analytical Techniques

## A1 Sample Preparation

The whole-rock powders of the peridotite samples collected from the Eastern Pyrénées and the ultramafic xenolith samples from the volcanics of the Massif Central were prepared for analysis by similar techniques. The mass of sample used to prepare the powders was dictated by the amount of material available: for the Pyrenean samples, large samples were collected in the field, enabling 1 - 2 kg of material to be used, however, owing to the smaller sizes of the xenoliths, the amount of material available for crushing was limited to approximately 25 - 100 g. After a slab had been taken out of each sample for the production of thin sections and a sub-sample had been removed as archive material, the weathered crust and any basaltic material were removed from the remaining peridotite and the samples reduced to ~2 cm cubes, either using a hydraulic splitter (Pyrenean samples) or circular saw, depending on the size of the samples. To eliminate the possibility of contamination all veins of basalt, pyroxenite or carbonate were removed from the massive peridotites either using the circular saw, or by discarding the peridotite cubes prior to crushing.

The cubes were reduced to < 5 mm chips using a hardened steel jaw crusher, from which representative sub-samples were obtained by a cone and quartering technique. Three 80 g sub-samples of each rock were powdered to < 125 μm in an agate tema for 15 minutes. Experiments using longer periods in the tema and smaller aliquots of crushate were carried out in an attempt to reduce the grain size of the powder further, but with little success, possibly due to the lubrication of the grain surfaces by a layer of serpentine. Between samples the tema barrel was cleaned using compressed air followed by scrubbing in water. Final cleaning of the barrel was performed by crushing a sample of optically clear quartz, then repeating the cleaning with air and water.

# A2 X-Ray Fluorescence (XRF)

## A2.1 Major and Trace Element Analysis

All major and trace element whole-rock x-ray fluorescence analyses were performed at the Open University using an ARL 8420+ wave-length dispersive XRF spectrometer. In total ten major elements and seventeen trace elements were analysed in the peridotite samples, however the low concentrations of incompatible elements present in the samples resulted in many elements being below the instrumental detection limits.

## A2.2 Sample Preparation

For trace element analysis ~9 g of powder were thoroughly mixed with 0.6 - 0.7 g of polyvinylpyrollidone (P.V.P.) - methyl cellulose binder in a resealable plastic bag and transferred to a hydraulic press in which the bound powder was formed into 3 cm diameter pellets by applying a pressure of 10 tons per sq. inch (~15.4 MPa) for a few moments. After gently removing the pressure (so as not to crack the pellet), the pellet was removed from the press and dried at 105 °C overnight.

Glass discs for the determination of major element compositions were prepared by fusing the samples with a flux composed of a 4:1 mixture of lithium metaborate and lithium tetraborate (Spectroflux 100B). The sample was dried overnight at ~105 °C to remove any moisture and mixed in a 5:1 ratio with the flux in a Pt/5%Au crucible. The mixture was fused at 1100 °C for 15 - 20 minutes, swirling every 5 minutes to ensure thorough mixing. The fused mixture was poured into a pre-heated 3 cm diameter mould, pressed down with a heated plunger to produce the correct surface texture and allowed to cool slowly to prevent cracking of the disc.

Loss on ignition (LOI) was determined by heating an accurately weighed aliquot of each sample to 1000 °C in air for 20 minutes within clean silica crucibles and measuring the percentage loss of mass. The calculated LOI value reflects the quantity of volatile components present in the sample. For the peridotite samples this is principally $H_2O$, but some $CO_2$ and $SO_2$ will also be lost, owing to the decomposition or oxidation of any carbonate or sulphides present.

## A2.3 Precision and Accuracy

Instrumental detection limits and the results of the analysis of reference materials and monitor samples are displayed in Tables A.1 to A.3.

| Element | OUAC | | | OUBE | | |
|---|---|---|---|---|---|---|
| | 9/12/92[a] | 13/5/93[b] | Range | 9/12/92[a] | 13/5/93[b] | Range |
| $SiO_2$ | 70.15 ± 10 | 69.99 ± 1 | 70.05 - 70.32 | 38.63 ± 5 | 38.35 ± 5 | 38.54 - 38.81 |
| $TiO_2$ | 0.106 ± 3 | 0.109 ± 4 | 0.104 - 0.110 | 2.63 ± 2 | 2.64 ± 2 | 2.609 - 2.634 |
| $Al_2O_3$ | 14.73 ± 2 | 14.54 ± 8 | 14.66 - 14.74 | 10.15 ± 2 | 9.96 ± 6 | 10.10 - 10.17 |
| $Fe_2O_3$ | 2.53 | 2.53 | 2.51 - 2.54 | 12.95 ± 1 | 12.99 ± 3 | 12.89 - 12.97 |
| MnO | 0.059 ± 1 | 0.059 | 0.057 - 0.062 | 0.202 ±3 | 0.203 | 0.199 - 0.204 |
| MgO | 0.06 ± 1 | 0.08 ± 1 | 0.05 - 0.07 | 13.24 ± 3 | 13.19 ± 3 | 13.19 - 13.28 |
| CaO | 0.38 | 0.38 | 0.37 - 0.39 | 14.11 ± 5 | 14.13 ± 1 | 14.08 - 14.15 |
| $Na_2O$ | 6.54 ± 1 | 6.49 ± 1 | 6.48 - 6.57 | 3.24 ± 2 | 3.24 ± 4 | 3.21 - 3.27 |
| $K_2O$ | 4.53 ± 3 | 4.55 ± 1 | 4.50 - 4.54 | 1.42 ± 1 | 1.41 ± 1 | 1.39 - 1.42 |
| $P_2O_5$ | 0.017 ± 3 | 0.021 | *0.014 - 0.02* | 1.079 ± 6 | 1.076 ± 7 | 1.067 - 1.084 |
| Ba | 63 ± 6 | 57 | 44 - 71 | 1023 ± 16 | 1025 ± 13 | 1007 - 1060 |
| Cr | 6 ± 4 | 5 ± 4 | 0 - 9 | 357 ± 5 | 359 ± 7 | 348 - 367 |
| Ni | 6 ± 3 | 8 ± 4 | 1 - 9 | 266 ± 8 | 286 ± 11 | 256 - 270 |
| S | 200 | 200 | 100 | 400 | 500 | 500 |

**Table A.1** Major and trace element concentrations determined from glass discs of the monitor samples OUAC and OUBE analysed during the course of this study. Italics indicate measurements close to or below detection for an element. Ranges reflect 95% confidence limits on the two materials from previous analyses at the Open University. [a] Mean and 2 sigma on four analyses. [b] Mean and 2 sigma on two analyses.

The calibration of the instrument for major element determinations was checked by the analysis of a number of international reference materials (UB-N, NIM-D, NIM-P), covering the range of concentrations and matrices present in the samples. Two internal monitors (OUAC and OUBE) were also analysed to assess instrumental drift, providing a second check on the reproducibility of the measurements. Almost all of the major elements are within 1 to 3% of the literature values of the reference materials, at the concentrations encountered in the peridotite samples. Such variation is well within the range quoted for these materials. At low concentrations some elements appear to differ significantly from the reference values (e.g. $Al_2O_3$ in NIM-D and both $TiO_2$ and $Na_2O$ in UB-N), however these values remain within the range expected for the reference materials. From replicate analyses of both the reference materials and the internal monitor samples, the relative precision of the

| Element | Detection Limit | Range in Massive Peridotites | Range in Pyroxenite layers | Reference Materials JP-1 (Peridotite) | Ref | UB-N (Serpentinite) | Ref | NIM-D (Dunite) | Ref | NIM-P (Pyroxenite) | Ref |
|---|---|---|---|---|---|---|---|---|---|---|---|
| Routine Major Elements (wt %) | | | | | | | | | | | |
| $SiO_2$ | 0.106 | 41.98 - 45.75 | 42.86 - 48.28 | 42.65 | 42.56 | 39.67±2 | 39.93±0.54 | 38.76±8 | 38.96±0.62 | 50.58±4 | 51.1±0.8 |
| $TiO_2$ | 0.083 | 0.013 - 0.141 | 0.15 - 2.021 | 0.009 | - | 0.099±2 | 0.11±0.05 | 0.0217±12 | - | 0.191±7 | 0.2 |
| $Al_2O_3$ | 0.094 | 0.94 - 4.25 | 7.7 - 14.52 | 0.65 | 0.62 | 2.81±2 | 2.94±0.3 | 0.24 | 0.3±0.3 | 4.09±2 | 4.18±0.38 |
| $Fe_2O_3$ | 0.071 | 7.95 - 9.33 | 4.8 - 6.22 | 8.35 | 8.37 | 8.34±2 | 8.45±0.36 | 17.20±8 | 17.0±0.7 | 12.42±12 | 12.7±0.96 |
| MnO | 0.065 | 0.118 - 0.135 | 0.1 - 0.115 | 0.12 | 0.12 | 0.124±2 | 0.12±0.03 | 0.219±2 | 0.22 | 0.222±2 | 0.22 |
| MgO | 0.050 | 36.69 - 44.54 | 17.92 -28.36 | 45.23 | 44.9 | 35.26±14 | 35.66±0.63 | 43.28 | 43.51±1.56 | 25.00±8 | 25.33±1.1 |
| CaO | 0.014 | 0.42 - 3.43 | 7.63 -13.04 | 0.54 | 0.56 | 1.213±13 | 1.22±0.11 | 0.28 | 0.28±0.14 | 2.67±2 | 2.66±0.3 |
| $Na_2O$ | 0.054 | 0.02 - 0.31 | 0.53 - 1.71 | 0.00 | 0.02 | 0.13±2 | *0.1* | 0 | 0.04±0.05 | 0.366±12 | 0.37±0.14 |
| $K_2O$ | 0.012 | 0 - 0.02 | 0 - 0.25 | 0.01 | 0.00 | 0.02 | *0.02* | *0.01* | *0.01* | 0.09 | 0.09±0.03 |
| $P_2O_5$ | 0.023 | *0.011 - 0.019* | *0.01 - 0.032* | *0.012* | *0.000* | *0.015±1* | *0.04* | *0.0126±12* | *0.009* | *0.024±2* | *0.02* |
| Additional Minor Elements (ppm) | | | | | | | | | | | |
| Ba | 20 | 1 - 18 | 11 - 36 | 19 | 17 | 38±7 | 30 | 8±4 | 2.2 | 43±7 | 35 |
| Cr | 10 | 2225 - 2777 | 517 - 10224 | 2992 | 2970 | 2326±7 | 2300 | 2921±16 | 2900 | 23350±50 | 24000 |
| Ni | 10 | 1770 - 2401 | 616 - 1193 | 2419 | 2460 | 2018±9 | 2000 | 2068±19 | 2040 | 556±16 | 555 |
| S | - | 100 - 300 | 0 - 1900 | 100 | 0 | 200 | 200 | 200 | 200 | 200 | 200 |

**Table A.2** XRF instrumental detection limits and range of major and selected trace element concentrations determined from glass discs of the massive peridotites and pyroxenite layers collected for this study (Mean and 2 sigma of three separate measurements). Italics indicate that most samples are close to or below detection for an element. Data for reference materials, recommended values and 2 sigma limits: UB-N, Govindaraju (1982); NIM-D and NIM-P, Steele & Hansen (1979); JP-1, Ando *et al.* (1989).

determinations ranges from better than 1% for most of the major elements (e.g. $SiO_2$, $Al_2O_3$, $Fe_2O_3$, MgO, CaO) to approximately 5% for the other elements over the range of concentrations considered.

| Element | Detection Limit (ppm) | Range in Massive Peridotites | Range in Pyroxenite layers | S-2 Open University | S-2 UK Labs Average |
|---|---|---|---|---|---|
| Rb | 2 | *0 - 1* | *0 - 1.5* | *1.8 ± 9* | *2± 2* |
| Sr | 2 | 1.2 - 18.5 | 14.1 - 179 | 89 ± 1 | 91 ± 5 |
| Y | 2 | 0.9 - 4.5 | 7.8 - 27.6 | 10 ± 1 | 10 ± 1 |
| Zr | 2 | 5 - 12 | 11 - 81 | 28 ± 1 | 28 ± 6 |
| Nb | 1.5 | 0.9 - 2.4 | 1.4 - 6.4 | *2 ± 1.5* | *2± 2* |
| Ba | 12 | *0 - 12* | 0 - 31 | 84 ± 8 | 70 ± 15 |
| Pb | 5 | *0 - 1* | *0 - 2* | *1 ± 2* | *1 ± 2* |
| Th | 4 | *0* | *0 - 1* | *1 ± 1* | *1 ± 1* |
| U | 3 | *0 - 2* | *0 - 2* | *0* | *1 ± 1* |
| Sc | 5 | 5 - 17 | 27 - 41 | 21 ± 4 | 19 ± 2 |
| V | 5 | 26 - 79 | 145 - 295 | 115 ± 7 | 104 ± 16 |
| Cr | 4 | 1462 - 2791 | 528 - 10922 | 884 ± 5 | 898 ± 58 |
| Co | 2 | 89 - 118 | 32 - 55 | 108 ± 2 | 114 ± 6 |
| Ni | 3 | 1960 - 2489 | 716 - 1348 | 1127 ± 11 | 1150 ± 183 |
| Cu | 3 | 7 - 33 | 4 - 154 | 140 ± 1 | 145 ± 8 |
| Zn | 3 | 40 - 53 | 53 - 118 | 67 ± 2 | 69 ± 8 |
| Ga | 3 | 2 - 6 | 8 - 20 | 9 ± 1 | 8 ± 2 |

**Table A.3** XRF instrumental detection limits and range of trace element concentrations measured from powder pellets of the massive peridotites and pyroxenite layers collected for this study. Data for monitor sample S-2 is the mean and 2 sigma of three measurements taken during the measurements of the peridotite samples, with similar data for a compilation from a number of other UK laboratories. Italics indicate measurements close to or below detection for an element.

The quality of the trace element data was checked by the routine analysis of monitor samples representing a range of common rock types. Although these are not true reference materials, by comparison with the mean values variation obtained for these samples by a number of UK laboratories (mostly by XRF), they provide a quantitative check on both the precision and consistency of the data with those of other workers. Only one of the trace element monitor samples (S-2) had elemental concentrations similar to those occurring in the peridotite and pyroxenite samples, so only these data are reported. For the elements above detection limit in the peridotites (Sr, Y, Zr, Sc, V, Cr, Co, Ni, Cu, Zn) the data for S-2 are within the range obtained by other laboratories. Relative precisions vary from 1% or better for Sr, Cr, Ni and Cu to 2 - 6% for Zr, V, Co and Zn. The low levels of both Sc and Y present in S-2 are responsible for the considerably poorer reproducibility (10 - 20%) in their determined concentrations.

## A3 REE Element Determination by ID-MS

REE element compositions were determined by isotope dilution mass-spectrometry (ID-MS) on a VG-Isomass 54E solid-source mass spectrometer, using a LREE-spike (La, Ce, Nd, Sm, Eu and Gd) and a HREE-spike (Dy, Er and Yb). Computer software was designed by D. W. Wright and P. W. C. van Calsteren.

### A3.1 Sample Dissolution

200 - 300 mg of sample powder was weighed into a clean teflon bomb and 20 - 50 µl of the two REE spikes added. (Separate spikes were used for the LREE and HREE). A couple of drops of 15M teflon distilled (TD) $HNO_3$ were added to wet the powder, followed by ~5 ml 40% TD HF. The bombs were then sealed in metal jackets and placed in an oven overnight at 180 °C. The $HNO_3$ / HF solution was then evaporated under heat lamps over which an air flow was maintained. To prevent the formation of insoluble fluorides (particularly $CaF_2$), evaporation was stopped when the samples attained a jelly-like consistency, at which point a further ~2 ml of 15M TD $HNO_3$ were added and the samples evaporated to incipient dryness. After a second addition of ~2 ml of 15M TD $HNO_3$ and evaporation to complete dryness, ~6 ml 6M TD HCl were added to the sample, the bomb resealed and heated at 180 °C overnight again. At this point the sample was not normally completely dissolved in the HCl, with variable quantities of insoluble spinels remaining. Repetition of the sequence of 15M TD $HNO_3$ and 6M TD HCl dissolutions and evaporations was unsuccessful at dissolving these grains, however the contribution of spinels to the REE abundances of the samples is likely to be small, enabling their non-dissolution to be overlooked.

### A3.2 Ion-exchange Chromatography

To separate the REE from the residues after digestion, the samples were redissolved in 2 - 3 ml 2.5M QD HCl, transferred to a clean centrifuge tube and centrifuged for 5 minutes, following which, they were ready for the ion-exchange columns.

For the initial separation of the REE from the rock matrix, the sample was passed through a column of 200 - 400 mesh AG 50W-X8 resin, similar to those used at the Open University for the separation of Rb and Sr for radiogenic isotope work. Prior to loading the

sample onto the column, the resin was cleaned with several column volumes of 6M QD HCl followed by a similar amount of RO $H_2O$. The resin was then pre-conditioned with 10 ml 2.5M QD HCl, after which 1 ml of the dissolved sample was added to the top of the resin, taking care not to disturb the top of the resin bed. After the sample had passed onto the resin column, it was washed on with two batches of 1 ml QD 2.5M HCl. To remove the majority of the major elements, 36 ml QD 2.5M HCl were then eluted to waste through the column. The REE were then stripped from the column and collected using 30 ml QD HCl.

After evaporating the sample solution to dryness, it was transferred to a set of reverse chromatography columns for the separation of the REE. The sample was redissolved in 0.5 ml 0.2M QD HCl and loaded onto the top of a column composed of 1 g teflon powder coated with 100 mg of di-(2-ethylhexyl) phosphate (DEHP). After washing the sample onto the column with two batches of 0.5 ml 0.2M HCl and eluting a further 3 ml 0.2M HCl (containing the majority of the Ba), the REE were collected in 30 ml 6M QD HCl, which was evaporated to dryness for storage. Total procedural blanks for the sample preparation are shown in Table A.5.

### A3.3 Sample Loading and Analysis

The samples were redissolved in 2µl RO water and loaded onto Ta-Re-Ta triple filaments. 1 µl of the solution was loaded onto each of the two Ta side filaments in turn and a current of 0.8 - 0.9 A allowed to pass through the filament until the solution had evaporated to dryness. Prior to loading, all filaments were outgassed for 5 minutes at 4.5 A in a vacuum ~$10^{-6}$ torr.

The rare earth elements were analysed following the technique of Thirlwall (1981), in which the sample is evaporated off the Ta side filaments and ionised by the central Re filament. By progressively increasing the current through the Ta filament, the REE are evaporated in order of decreasing volatility. For each element, the signal at between four and six different masses were measured, enabling the signal intensities at the masses of interest to be corrected for both background noise and possible interfering peaks. Table A.4 shows details of the running conditions.

Although the software enabled completely automated analysis, most samples were run manually. The determination of REE concentrations for a single sample required between 4

and 6 hours, during which time considerable Re was evaporated off the ionisation filament onto the glass bead. If not thoroughly removed between samples, the Re coating enabled a current to flow over the surface of the bead, apparently affecting the operation of the barrel motor. As a consequence the barrel occasionally tried to reset itself during the determination of the later elements in the sequence, allowing high filament currents to pass through unanalysed filaments, "flashing" off the most volatile REE, leading to poor precision on the Eu and Yb data obtained in some of the early analyses.

| Element | Filament Currents (A) | | Peaks Measured | | | |
|---|---|---|---|---|---|---|
| | Evaporation | Ionisation | Spike | Ref | Background | Interference |
| La | 2.5 -2.8 | 2.5 | 139 | 138 | 136.5 | 140 (Ce) |
| Ce | 2.0 -2.2 | 4.5 | 140 | 142 | 143.5 | 143, 145 (Nd) |
| Nd | 2.2 - 2.4 | 4.6 | 145 | 146 | 143.5 | |
| Sm | 2.0 - 2.2 | 4.4 | 149 | 147, 152 | 152.5 | 156 (CeO) |
| Eu | 1.5 - 1.8 | 4.3 | 151 | 153 | 147.5 | 152 (BaO) |
| Gd(O) | 2.8 - 3.5 | 2.8 | 171 | 172, 173 | 170.5 | |
| Dy | 4.7 - 4.8 | 4.8 | 161 | 162,163 | 165.5 | 166 (NdO-Er)<br>167 (NdO) |
| Er | 4.6 - 4.8 | 4.75 | 167 | 168 | 170.5 | 170, 171 (Yb) |
| Yb | 1.75 - 2.0 | 4.3 | 171 | 173,174 | 172.5 | |

**Table A.4** Running conditions and peaks measured for each element. Gd analysed as its oxide GdO.

### A3.4 Interferences

Although the samples were spiked for the determination of nine REE, it was not always possible to obtain reliable data for all the elements, principally owing to interference from metal or metal-oxide ions of Ba or other REE. Despite efforts to ensure that the majority of the Ba had been eluted prior to the collection of the REE from the columns, the relatively high concentration of Ba in the samples and the proximity of its elution peak to that of La meant that the fraction collected for REE analysis often contained traces of Ba.

The determination of La concentrations were particularly affected by the presence of $Ba^+$, with $^{138}Ba$ often swamping the minor $^{138}La$ peak (~0.09% of natural La). In many cases it was possible to correct for Ba interference, however, leading to constant $^{138}La/^{139}La$ ratios after correction.

The presence of Ba during the analysis of the REE also affected the determination of Eu abundances, with direct interference of $BaO^+$ on both $^{151}Eu$ and $^{153}Eu$. Correction of the measured $^{153}Eu/^{151}Eu$ ratio for BaO required the $^{136}BaO^+$ ion to be monitored using the peak at mass 152, to which a second correction had to be applied for $^{152}Sm$, measured at 147. Comparison of the chondrite normalised REE profiles obtained for the peridotite samples with the measured $^{153}Eu/^{151}Eu$ ratios and relative contribution of BaO to the two Eu peaks shows that, where the calculated Ba interference was relatively high, the determined Eu concentrations are anomalously low in comparison to the measured Sm and Dy abundances (i.e. Eu/Eu* < 1). These Eu anomalies are particularly pronounced when the samples were underspiked, indicating that the correction for BaO may be overestimated in some cases. Repeated analysis of sample 92-LH11, which initially exhibited high Ba interference and anomalously low Eu concentrations, displayed no such anomaly when the Ba interference was reduced following improvements to the ion-exchange procedure (Table A.5). The Eu anomalies are therefore considered consequences of the analytical procedure and do not require a geological interpretation.

| Element | Procedural Blank | Reference Materials | | | | Duplicate Samples | | | |
|---|---|---|---|---|---|---|---|---|---|
| | | BHVO-1 (ppm) | Ref. | PCC-1 (ppb) | Ref. | 92-LH11 (ppb) | | 92-FT5 (ppb) | |
| La | 0.53 ng | n.d | 15.8±1.3 | 72±24 | 90 | 224 ± 8 | n.d. | 99 ± 10 | 135 ± 8 |
| Ce | 0.54 ng | 45.5±3 | 39±4 | 87.1±2 | 100 | 783 ± 4 | n.d. | 265.4 ± 1 | 273 ± 1 |
| Nd | 0.31 ng | 31.4±1 | 25.2±2 | 41.7±3 | 44 | 766 ± 1 | 767 ± 2 | 117.8 ± 4 | 112.6 ± 6 |
| Sm | 0.07 ng | 8.03±1 | 6.2±3 | 7.12±6 | 7.4 | 276 ± 1 | 277.7 ± 2 | 22.4 ± 1 | 24.24 ± 6 |
| Eu | 0.05 ng | 2.45±4 | 2.06±8 | 1.8±8 | 1.8 | 102.8 ± 4 | 72.7 ± 2† | 7.57 ± 8 | 8.54 ± 6 |
| Gd | n. d. | *5±1* | 6.4 | n.d | - | | | | |
| Dy | 0.13 ng | 5.51±3 | 5.2±3 | *24±12* | 10 | 534 ± 8 | 547 ± 60 | 25 ± 3 | 26 ± 7 |
| Er | 0.18 ng | 2.860±8 | 2.4±2 | 9±1 | 8 | 371 ± 7 | 393 ± 22 | 19.2 ± 2 | 25.2 ± 5 |
| Yb | 2.04 ng | 2.25±5 | 2.0±2 | *25.6±4* | 6 | 377 ± 2 | 392 ± 2 | 38.7 ± 1 | 39.4 ± 3 |

**Table A.5** Total procedural blank and results for the reference materials analysed in this study. Errors are 2 sigma. Figures in italics denote poorer data resulting from erratic values either due to poor beam intensity or high interferences. n.d. element not determined successfully. Reference data: BHVO-1, Gladney & Roelandts (1988); PCC-1, Gladney *et al.* (1983).
† Negative Eu anomaly associated with high $BaO^+$ interference.

### A3.4 Accuracy and Precision

The accuracy and precision of the analyses may be estimated from the analyses of the reference material PCC-1, included in the study, and duplicate analyses of the two peridotite samples 92-FT5 and 92-LH11, Table A.5. Although individual concentrations exhibit better than 1% precision, calculated by propagating the error on the isotopic ratio, the reproducibility of the data varies from 0.2 - 5% to 2 - 12% over the range of concentrations present in the samples. The concentrations determined for the reference material PCC-1 are consistently 5 - 8% lower than their recommended values. Although the determination of consistently low REE concentrations in PCC-1 may be due to systematic errors introduced from the calibration of the spike concentrations, without an estimate of the uncertainties in the certified values for PCC-1, heterogeneity of the reference material cannot be ruled out.

## A4 Total Sulphur and Carbon Determination

### A4.1 Method of Analysis

The total sulphur and carbon contents of the peridotite samples were measured at the University of Leicester, using a Leco CS-125 Carbon and Sulphur determinator. Approximately 0.5 - 1 g of sample powder was mixed with two accelerating reagents in a low-carbon crucible: ~ 0.8 g "Lecocell II" (a W/Sn based compound) and ~ 0.7 g "Iron chip". The crucible was then placed in the instrument, where it was surrounded in an atmosphere of 99.5% pure oxygen and heated to > 1500 °C in a high frequency induction furnace. At this temperature, the samples are fused and any C and S oxidised to $CO_2$ and $SO_2$. The gases produced by the decomposition of the sample were passed through a moisture trap to an IR detector tuned to detect $SO_2$ then through a catalyst, in which any $SO_3$ was trapped and CO converted to $CO_2$. The $CO_2$ was then measured in a second IR detector. The detector measurements were adjusted for weight and displayed as concentrations. Every 4 - 5 samples the filter which formed the furnace wall required cleaning to remove fine powder formed during the oxidation of the sample.

The instrument was calibrated by analysing a blank and instrumental standards composed of C and S in iron metal. These standards were also analysed following the furnace cleaning, to monitor drift. Each analysis of the standard or peridotite samples

consisted of between three and five measurements, using fresh material for each measurement. The weighted mean of the determined concentrations was then calculated, enabling the C and S contents of 2 - 3 g of each peridotite to be determined.

### A4.2 Accuracy and Precision

Whilst the accuracy of the technique was determined by analysing two different reference materials (a peridotite,GSJ: JP-1, and a gabbro, CCRMP:MRG-1; Table A.6), the precision was estimated from both the repeatability of the replicate analyses performed for each sample and the reproducibility of the values determined for two of the peridotite samples analysed on different days.

Table A.6 shows that the values determined for the reference materials are (with the exception of the S content of JP-1) within 5 - 10% of the reference values. Although this is marginally greater than the accuracy suggested by the manufacturers (i.e. ± 5% or 10 ppm, whichever is greater, for ≤ 1000 ppm S or C), the considerable uncertainties in the reference values can easily account for the differences.

| Element | JP-1 | | MRG-1 | |
|---|---|---|---|---|
| | Measured | Reference | Measured | Reference |
| S (ppm) | 0 ± 8 | 30 | 663 ± 4 | 610 ± 100 |
| C (ppm) | 807 ± 3 | 764 | 3110 ± 30 | 2930 ± 230 |

**Table A.6** Total sulphur and carbon contents measured for the reference samples JP-1 and MBG-1 using the Leco CS-125 Carbon and Sulphur Determinator. Reference values were obtained from Ando *et al.* (1989) (JP-1) and Gladney & Roelandts (1990) (MRG-1). No estimates were available of the uncertainties in the reference values of JP-1.

It is not clear why no S was detected in JP-1. It is possible that the sulphides contained in the sample are heterogeneous on the gram scale or that, since preparation, the sulphides in the reference material have been oxidised. In the absence of an estimate of the uncertainty in the reference value, however, it is not possible to draw any definite conclusions, once more. Following the determination of the low S concentration for JP-1, the technique was checked by analysing an instrumental Fe-metal standard, containing 14 ± 4 ppm S and 9 ± 3 ppm C. The agreement between the values obtained by these analyses (17 ppm S and 16 ppm C) and those quoted for the metal suggested that the technique was reliable at the low concentrations present in some samples, despite the erroneous values determined for JP-1.

| Analysis | 92-PG2 | | 92-FT5 | |
|---|---|---|---|---|
| Date | S | C | S | C |
| 21/1/93 | 85 | 189 | 55 ± 10 | 1400 ± 20 |
| 26/2/93 | 87 ± 10 | 206 ± 7 | – | – |
| 13/7/93 | – | – | 60 ± 3 | 1580 ± 30 |

**Table A.7** Replicate analyses of samples 92-PG2 and 92-FT5, demonstrating the reproducibility of the total sulphur and carbon contents determined during this study.

Table A.7 shows that, although the S contents of the peridotites were reproducible within the precision of the individual analyses, the determined C content appeared to vary between analytical sessions. However, because great precision was not required for the total C contents determined in this study, such variation was tolerated.

# Appendix B

# Thermodynamic Data and Equations used in the Calculation of Mineral Solubilities

## B1. Equations to Calculate the Activities of PGE or Re Species

The $f_{O_2}$ - $f_{S_2}$ conditions necessary to stabilise each of the PGE and Re as either oxide or sulphide minerals and the activities of PGE and Re compounds under mantle conditions were calculated from the standard Gibbs free energies of formation of the compounds, $\Delta G_f°$, (where the superscript ° denotes standard conditions of temperature and pressure and the presence of the compounds at unit activity).

For reactions of the form $M + xY_2 = MY_{2x}$ (where M is one of the PGE or Re and Y is either oxygen or sulphur), the change in the free energy of the system under standard conditions ($\Delta G_r°$) is given by the difference between the standard free energies of formation of the reagents. Under non-standard conditions, the free energy change during the reaction, $\Delta G_r$, may be related to $\Delta G_r°$ by the equation:

$$\Delta G_r(p,T)=\Delta G_r°(p,T)+RT \ln \frac{a_{MY_{2x}}}{a_M . f_{Y_2}{}^x} \qquad \textbf{(Eqn. B.1)}$$

where $a_i$ is the activity of component i (the fugacities of sulphur and oxygen being the equivalent of their activities, $f_{Y_2}$) and R is the gas constant. At equilibrium $\Delta G_r$ is zero and Equation B.1 becomes:

$$x.\log f_{Y_2} + \log a_M - \log a_{MY_{2x}} = \frac{\Delta G_r°(p,T)}{RT \ln 10} \qquad \textbf{(Eqn. B.2)}$$

The values of $f_{O_2}$ or $f_{S_2}$ required for the coexistence of the pure PGE or Re compounds and the metal or the activities of the PGE and Re compounds in equilibrium with the pure metals under mantle conditions may be calculated by rearranging Equation B.2 to give Equations B.3a and B.3b, respectively, assuming unit activities for the pure metals.

$$\log_{10} f_{Y_2} = \frac{\Delta G_r^\circ(T)}{x.RT\ln 10} \qquad \textbf{(Eqn. B.3a)}$$

$$a_{MY_{2x}} = \exp\left(\frac{-\Delta G_r^\circ(T)}{RT}\right).f_{Y_2}{}^x \qquad \textbf{(Eqn. B.3b)}$$

## B2. Equations for the Calculation of $D_{spinel/BMS}$

To calculate a partition coefficient for the PGE and Re between spinel and the base metal phase required the free energy change ($\Delta G_r^\circ$) during the reaction

$$MS_{2x}\ (BMS) + xO_2 = MO_{2x}\ (spinel) + xS_2 \qquad \textbf{(Eqn. B.4)}$$

at the p-T conditions of interest.

$\Delta G_r^\circ$ is related to the activities of the two dissolved species ($a_{MS_{2x}}$ and $a_{MO_{2x}}$), $f_{S_2}$ and $f_{O_2}$ by the equation:

$$\exp\left(\frac{-\Delta G_r^\circ}{RT}\right) = \ln\left(\frac{a_{MO_{2x}}.f_{S_2}{}^x}{a_{MS_{2x}}.f_{O_2}{}^x}\right) \qquad \textbf{(Eqn. B.5)}$$

The concentration of the element in each phase was calculated from its activity via the activity coefficient, $\gamma_{MY_{2x}}$, which relates the activity of the element present in the phase to its mole fraction ($X_{MY_{2x}}$) by the relation

$$a_{MY_{2x}} = \gamma_{MY_{2x}}.X_{MY_{2x}} \qquad \textbf{(Eqn B.6)}$$

Any non-ideality during mixing is contained within $\gamma_{MY_{2x}}$, which may vary as a function of composition. Two similar equations were written for the PGE and Re oxide and sulphide species, relating their activities to the concentration of the metals in the host phase

$$a_{MS_{2x}} = \gamma_{MS_{2x}}.X_{MS_{2x}} = \gamma_{MS_{2x}}.C_M^{BMS}.\frac{MW_M}{MW_{BMS}} \qquad \textbf{(Eqn. B.7)}$$

$$a_{MO_{2x}} = \gamma_{MO_{2x}}.X_{MO_{2x}} = \gamma_{MO_{2x}}.C_M^{spinel}.\frac{MW_M}{MW_{spinel}} \qquad \textbf{(Eqn. B.8)}$$

where $C_M^i$ is the concentration of the metal in phase i and $MW_j$ is the molecular or atomic weight of component j.

Combining Equations B.5, B.7 and B.8 and rearranging the terms produces the equation:

$$D_{spinel/BMS} = \frac{C_M^{spinel}}{C_M^{BMS}} = \exp\left(\frac{-\Delta G_r}{RT}\right)\frac{\gamma_{MS_{2x}}.MW_{spinel}.f_{O_2}^{x}}{\gamma_{MO_{2x}}.MW_{BMS}.f_{S_2}^{x}} \quad \textbf{(Eqn. B.9)}$$

from which the partition coefficients were calculated.

## B3. Calculation of Free Energies of Formation ($\Delta G_f$)

In order to calculate the changes in the free energy during the reactions, it was first necessary to calculate the free energies of formation of the reagents and reaction products at the temperatures and pressures of interest. Because the free energies of chemical species are conventionally reported as those at standard temperature and pressure (~1 bar and 298.15 K), values of $G_f°$ under different p-T conditions had to be calculated using

$$G_f°(p,T) = H_f°(T) - T.S_f°(T) + \int_1^p V_m \, dp \quad \textbf{(Eqn. B.10)}$$

where $H_f°(T)$ and $S_f°(T)$ are the standard enthalpy and entropy of formation for the element or compound at a pressure of 1 bar and temperature T, and $V_m$ is its molar volume.

### B3.1 Effect of Temperature on $G_f°$

$H°(T)$ and $S°(T)$ may be obtained from the expressions:

$$H°(T) = H°(298.15) + \int_{298.15}^{T} C_p \, dT + \sum \Delta H_{tr} \quad \textbf{(Eqn. B.11)}$$

and

$$S°(T) = S°(298.15) + \int_{298.15}^{T} C_p/T \, dT + \sum \Delta H_{tr}/T_{tr} \quad \textbf{(Eqn. B.12)}$$

where $C_p$ is the specific heat capacity at constant pressure, $\Delta H_{tr}$ is enthalpy change of any phase transition which may occur in the integrated temperature range and $T_{tr}$ is the temperature at which the phase transition occurs.

$C_p$ may be expressed as a function of temperature and is frequently formulated according to a power law of the type:

$$C_p = a + b.T + c.T^{-2} + d.T^{2} + e.T^{-3} + f.T^{-1/2} + g.T^{-1} \quad \textbf{(Eqn. B.13)}$$

in which the coefficients a, b, c, d, e, f and g vary between the compounds and their different phases.

| Compound | Temp. Range (K) | $V_m$ $cm^3/mol$ | $H°_{1,298}$ cal/mol | $S°_{1,298}$ cal/mol | $C_p = a + b.T + c.T^{-2} + d.T^2 + e.T^{-3} + f.T^{-1/2} + g.T^{-1}$ | | | | | | |
|---|---|---|---|---|---|---|---|---|---|---|---|
| | | | | | a ($10^2$) | b ($10^{-3}$) | c ($10^6$) | d ($10^{-6}$) | e ($10^8$) | f | g ($10^4$) |
| Ir | 298-600 | 8.58 | 0 | 8.49 | 0.0558 | 1.2890 | 0 | 0 | 0 | 0 | 0 |
| | 600- | | | | 0.0510 | 1.9130 | 0.0397 | -0.036 | 0 | 0 | 0 |
| $Ir_2S_3$ | 298-1400 | 49.85 | -58400 | 23.20 | 0.2636 | 7.8800 | -0.2300 | 0 | 0 | 0 | 0 |
| $IrO_2$ | 298-1300 | 19.22 | -57400 | 13.70 | 0.0917 | 15.2000 | 0.0000 | 0 | 0 | 0 | 0 |
| $IrO_3$ | 298-1800 | | 3200 | 69.40 | 0.1964 | 0.4200 | -0.1320 | 0 | 0 | 0 | 0 |
| $IrS_2$ | 298-1400 | 30.39 | -34600 | 14.70 | 0.1639 | 3.7700 | -0.1570 | 0 | 0 | 0 | 0 |
| Os | 298- | 8.46 | 0 | 7.80 | 0.0563 | 0.9200 | 0 | 0 | 0 | 0 | 0 |
| $OsO_2$ | 298-1200 | 19.54 | -70400 | 12.40 | 0.1672 | 2.4800 | -0.3390 | 0 | 0 | 0 | 0 |
| $OsO_4$ | 404-1000 | | -77823 | 76.97 | 0.2055 | 4.8800 | -0.3820 | 0 | 0 | 0 | 0 |
| $OsS_2$ | 298-1400 | 26.84 | -35300 | 13.00 | 0.1638 | 2.8300 | -0.2100 | 0 | 0 | 0 | 0 |
| Pd | 298-400 | 8.85 | 0 | 9.04 | 0.0568 | 1.7670 | 0 | 0 | 0 | 0 | 0 |
| | 400-1400 | | | | 0.0587 | 1.2740 | 0 | 0 | 0 | 0 | 0 |
| PdO | 298-1143 | 14.07 | -36900 | 9.40 | 0.0330 | 14.2000 | 0 | 0 | 0 | 0 | 0 |
| PdS | 298-1243 | 20.9 | -16900 | 13.50 | 0.0997 | 4.1100 | -0.0730 | 0 | 0 | 0 | 0 |
| Pt | 298- | 9.10 | 0 | 9.95 | 0.0580 | 1.2850 | 0 | 0 | 0 | 0 | 0 |
| $PtO_2$ | 298-2000 | | 40300 | 61.15 | 0.1325 | 0.5000 | -0.2750 | 0 | 0 | 0 | 0 |
| PtS | 298-1500 | 22.62 | -19860 | 13.16 | 0.0997 | 4.1100 | -0.0730 | 0 | 0 | 0 | 0 |
| Re | 298- | 9.08 | 0 | 8.73 | 0.0566 | 1.3020 | 0 | 0 | 0 | 0 | 0 |
| $Re_2O_7$ | 298-636 | | -270643 | 105.79 | 0.2915 | 44.0000 | -0.2250 | 0 | 0 | 0 | 0 |
| $ReO_2$ | 298-1300 | 19.14 | -103400 | 15.00 | 0.1610 | 3.0300 | -0.3090 | 0 | 0 | 0 | 0 |
| $ReS_2$ | 298-1500 | 33.36 | -42700 | 15.50 | 0.1639 | 3.7700 | -0.1570 | 0 | 0 | 0 | 0 |
| Rh | 298- | 8.3 | 0 | 7.53 | 0.0497 | 3.2140 | 0.0081 | -0.5420 | 0 | 0 | 0 |
| $Rh_2O_3$ | 298-1300 | 30.95 | -91500 | 22.00 | 0.2074 | 13.8000 | 0 | 0 | 0 | 0 | 0 |
| Ru | 298-1600 | 8.22 | 0 | 6.82 | 0.0525 | 1.1780 | 0.0109 | 0.2660 | 0 | 0 | 0 |
| $RuO_2$ | 298-1300 | 19.09 | -72800 | 14.50 | 0.1670 | 2.5000 | -0.3550 | 0 | 0 | 0 | 0 |
| $RuO_4$ | 298-2000 | | -44000 | 69.47 | 0.1880 | 0.6000 | -0.4250 | 0 | 0 | 0 | 0 |
| $RuS_2$ | 298-1500 | 23.63 | -49200 | 13.00 | 0.1638 | 2.8300 | -0.2100 | 0 | 0 | 0 | 0 |

**Table B.1** Thermodynamic properties of the metals, oxides and sulphides of the PGE and Re. H°, S° and $C_p$ obtained from Barin *et al.* (1977), except $IrO_2$ Os and Pt (Barin & Knacke, 1973). Molar volumes, $V_m$, calculated from the molecular or atomic weights and densities given by Weast *et al.* (1975).

The data used in the calculation of $G_f°$ for the PGE and Re species of interest, as well as the solid phases in the Fe-O-S-Si system are shown in Tables B.1 and B.2.

## B3.2 Effect of Pressure on $G_f°$

For solid phases, the molar volume ($V_m$) is a function of both temperature and pressure owing to the thermal expansion and compressibility of the solid. However, under most

| Compound | Temp. Range (K) | $V_m$ $cm^3$/mol | $H°_{1,298}$ cal/mol | $S°_{1,298}$ cal/mol | $C_p = a + b.T + c.T^{-2} + d.T^2 + e.T^{-3} + f.T^{-1/2} + g.T^{-1}$ a ($10^2$) | b ($10^{-3}$) | c ($10^6$) | d ($10^{-6}$) | e ($10^8$) | f | g ($10^4$) |
|---|---|---|---|---|---|---|---|---|---|---|---|
| Fe | 298-848 | 7.15 | 0 | 27.28 | -0.28567 | 53.34 | -5.893 | 0 | 4.754 | 0 | 25630 |
| | 848-1000 | | 499 | | -2.4828 | 249.2 | 66.09 | 0 | -5.011 | 0 | -12310 |
| | 1000-1042 | | | | -6.3974 | 695.4 | 0.667 | 0 | -0.837 | 0 | -1864 |
| | 1042-1060 | | | | 19.172 | -1775 | -8.495 | 0 | 10.43 | 0 | 24370 |
| | 1060-1184 | | | | -5.5363 | 332 | 2.93 | 0 | -2.236 | 0 | -4774 |
| | 1184- | | 899.6 | | 0.23819 | 8.416 | -0.07295 | 0 | 0.1005 | 0 | 178.6 |
| 1/4 $Fe_3O_4$ | 298-848 | 11.131 | -278739 | 37.56 | 0.18343 | 56.67 | 0.2384 | 0 | 0.01747 | 0 | 38.69 |
| | 848-1300 | | 391 | | -0.02828 | 2.451 | 31.14 | 0 | 0.1861 | 0 | 383.4 |
| | 1300- | | | | 0.86812 | 15.82 | 19.74 | 0 | 889 | 0 | -144800 |
| 1/2 $Fe_2O_3$ | 298-956 | 15.137 | -412795 | 44.03 | 0.39874 | 46.44 | -1.642 | 0 | 1.402 | 0 | 3575 |
| | 956-1250 | | 335 | | -0.69915 | 72.45 | 78.24 | 0 | -0.07284 | 0 | -175.8 |
| | 1250- | | | | 1.974 | 4.323 | 61.97 | 0 | 2404 | 0 | -432700 |
| FeS | 298-411 | | -100416 | 60.291 | 0.00502 | 167.36 | 0 | 0 | 0 | 0 | 0 |
| | 411-598 | | 2384 | | 0.728 | 0 | 0 | 0 | 0 | 0 | 0 |
| | 598-1468 | | 502 | | 0.5104 | 9.95792 | 0 | 0 | 0 | 0 | 0 |
| $Fe_{0.877}S$ | 298-598 | 17.58 | -99440 | 60.799 | 0.13305 | 75.826 | -1.3588 | 0 | 0.60498 | 0 | 8039.4 |
| | 598-1000 | | 398 | | 0.71653 | -10.605 | 3.9706 | 0 | 11.782 | 0 | -14193 |
| | 1000- | | | | -2.2837 | 147.15 | 450.57 | 0 | -2500.9 | 0 | -68808 |
| $FeS_2$ | 298- | 23.94 | -171544 | 52.93 | 0.72148 | 0.00179 | -2.0421 | 3.4213 | 1.2495 | -0.378 | 2778.2 |
| 1/2 $Fe_2SiO_4$ | 298- | 23.14 | -739085 | 75.5 | 1.0957 | 1.832 | 2.963 | 0 | -1.862 | 0 | -2.01 |
| $SiO_2$ | 298-848 | 22.69 | -910700 | 41.46 | 1.0149 | 2.782 | 4.353 | 0 | -1.913 | 0 | -29610 |
| | 848- | | | | 0.62684 | 21.039 | -2.5826 | 0 | 52.92 | 0 | -4803 |
| $O_2$ | 298- | | 0 | 205.03 | 0.3945 | 0.5609 | 0.9067 | 0 | 0.00060 | 0 | -6101 |
| | $T_{cr}$ = 154.75 | | $P_{cr}$ = 50.764 | | | | | | | | |
| $S_2$ | 298- | | 128365 | 228.07 | 0.38408 | -0.0463 | -0.4635 | 0 | 0.693 | 0 | -993.6 |
| | $T_{cr}$ = 208.15 | | $P_{cr}$ = 72.954 | | | | | | | | |
| S(l)z | 388-440 | | 4263.5 | 43.664 | -20.64 | 3467 | 113.1 | 0 | 0 | 0 | 0 |
| | 440-718 | | | | -0.2556 | 57.78 | 8.863 | 0 | 0 | 0 | 0 |

**Table B.2** Thermodynamic properties of the phases in the Fe-O-S-Si system. Data obtained from the compilation of Shi (1992), except $O_2$ and $S_2$ ($H°$, $S°$, $T_{cr}$, $P_{cr}$ and $C_p$, Shi & Saxena, 1992), FeS and liquid S ($H°$, $S°$ and $C_p$, Barin *et al.*, 1977; $V_m$ calculated from molecular weights and densities from Weast, 1978). Critical temperatures and pressure are in K and bar, respectively.

geological conditions, the free energy change during a reaction due to the compression of solid reagents is small relative to that arising from the change in molar volume, hence may be overlooked without significant loss of accuracy, enabling $\int_1^p V_m(p,T)\,dp$ to be simplified to $V_m\,(p-1)$ in Equation B.10.

For volatile reagents (such as $O_2$ and $S_2$), the change in the free energy of the reagent with changing pressure does not follow such a simple relationship, on account of the non-ideal behaviour of the vapour phase. For volatile reagents, the fugacity, $f_{Y_2}$, is related to the true pressure of the reagent, p, by the relationship $f_{Y_2} = \gamma_{Y_2}.p$, where $\gamma_{Y_2}$ is the fugacity

coefficient of the volatile phase and is analogous to the activity coefficient of Equation B.6. Although the pressure exerted by a mole of gas is constant at constant temperature, regardless of changes in the confining pressure, the fugacity coefficient is not. Hence, for a mole of fluid

$$\int_1^p V_m(p,T)\,dp = RT(\ln f_{Y_2}(p, T) - \ln f_{Y_2}(1, T))$$

$$= RT(\ln \gamma_{Y_2}(p, T) - \ln \gamma_{Y_2}(1, T)) \qquad \textbf{(Eqn B.14)}$$

| | A(T) | B(T) | C(T) | D(T) |
|---|---|---|---|---|
| <1 kbar | | | | |
| $Q_1$ | 1 | 0 | 0 | |
| $Q_2$ | 0 | 0.09827 | 0 | |
| $Q_3$ | 0 | 0 | -0.00103 | |
| $Q_4$ | 0 | -0.2709 | 0 | |
| $Q_5$ | 0 | 0 | 0.01427 | |
| 1-5 kbar | | | | |
| $Q_1$ | 1 | 0 | 0 | |
| $Q_2$ | 0 | 0 | 0 | |
| $Q_3$ | 0 | 0.09122 | 0 | |
| $Q_4$ | 0 | 0 | 0 | |
| $Q_5$ | -0.5917 | 0 | -0.0001416 | |
| $Q_6$ | 0 | 0 | 0 | |
| $Q_7$ | 0 | 0 | $-2.835 \times 10^{-6}$ | |
| $Q_8$ | 0 | 0 | 0 | |
| >5 kbar | | | | |
| $Q_1$ | 2.0614 | 0 | 0 | 0 |
| $Q_2$ | 0 | 0 | 0 | 0 |
| $Q_3$ | 0 | 0.05513 | $-1.894 \times 10^{-6}$ | $5.053 \times 10^{-11}$ |
| $Q_4$ | 0 | 0 | 0 | 0 |
| $Q_5$ | -2.235 | 0.03934 | $-1.109 \times 10^{-5}$ | 0 |
| $Q_6$ | 0 | 0 | 0 | $-6.303 \times 10^{-21}$ |
| $Q_7$ | 0 | 0 | $-2.189 \times 10^{-5}$ | 0 |
| $Q_8$ | -0.3941 | 0 | 0 | 0 |

**Table B.3** Coefficients used in Equation B.17 to calculate the functions A(T), B(T), C(T) and D(T) used in the modelling of super-critical $S_2$ and $O_2$ under mantle conditions. Values of $Q_i$ taken from Shi & Saxena (1992).

The variation of the fugacity coefficient as a function of pressure may be calculated using the compressibility factor, Z(p,T), using the integral

$$\ln \gamma_{Y_2}(p, T) = \int_1^p Z(p,T)\,dp - \ln p + \ln \gamma_{Y_2}(p, T) \qquad \textbf{(Eqn B.15)}$$

where $\int_{p_o}^{P} Z(P,T)dP = A(T).\ln p_r/p_{or} + B(T).(p_r - p_{or}) + C(T).(p_r^2 - p_{or}^2) + D(T).(p_r^3 - p_{or}^3)$ **(Eqn B.16)**

in which $p_r$ is the reduced pressure ($p/p_{cr}$) and A(T), B(T), C(T) and D(T) are each a function of temperature, with the form

$$Q(T)_{p\geq 1\ kbar} = Q_1 + Q_2T_r + Q_3T_r^{-1} + Q_4T_r^2 + Q_5T_r^{-2} + Q_6T_r^3 + Q_7T_r^{-3} + Q_8.\ln T_r$$

or $$Q(T)_{p<1\ kbar} = Q_1 + Q_2T_r^{-1} + Q_3T_r^{-1.5} + Q_4T_r^{-3} + Q_5T_r^{-4} \quad \textbf{(Eqn B.17)}$$

where $T_r$ is the reduced temperature ($T/T_{cr}$) and $Q_1$ - $Q_8$ are constants (Saxena & Shi, 1992). The values of $T_{cr}$ and $Q_1$ - $Q_8$ used in the calculation of $\gamma_{S_2}$ and $\gamma_{O_2}$ are given in Tables B.2 and B.3.

# Appendix C

# Whole-Rock Geochemical Data

Table C.1 presents the whole-rock elemental data for the peridotites analysed during this study, uncorrected for loss on ignition (LOI) and the presence of iron as FeO. It contains the data obtained by XRF (major and trace elements), isotope-dilution mass spectrometry (REE) and pyrometry (S and C).

The magnesium numbers of the samples are also presented, calculated using

$$Mg^{\#} = \left( \frac{\frac{MgO}{40.32}}{\frac{MgO}{40.32} + \frac{Fe_2O_3}{79.85}} \right) x\ 100 \qquad \textbf{(Eqn. C.1)}$$

Replicate major element analyses of samples 92-FT4, 92-FT5 and 92-LH12 and trace element analyses of 92-PR1 are also reported. Analytical methods are described in detail in Appendix A. Petrographic descriptions of the samples are given in Appendix D, whilst their locations are illustrated in Figure 4.1.

| Sample | 92-FR3 | 92-FR4 | 92-FR4b | 92-FT5 | 92-FT5b | 92-FT6 | 92-FT7 |
|---|---|---|---|---|---|---|---|
| Locality | Freychinède | Freychinède | Freychinède | Fontête Rouge | Fontête Rouge | Fontête Rouge | Fontête Rouge |
| **XRF Glass Discs** | | | | | | | |
| $SiO_2$ | 44.48 | 43.92 | 44.1 | 42.43 | 42.86 | 44.49 | 44.39 |
| $TiO_2$ | 0.119 | 0.113 | 0.114 | 0.014 | 0.013 | 0.118 | 0.087 |
| $Al_2O_3$ | 4.25 | 2.97 | 3.06 | 0.94 | 0.96 | 3.49 | 3.05 |
| $Fe_2O_3$ | 8.19 | 8.62 | 8.65 | 8.73 | 8.8 | 9.33 | 8.84 |
| MnO | 0.124 | 0.126 | 0.126 | 0.124 | 0.126 | 0.135 | 0.128 |
| MgO | 37.68 | 38.3 | 38.07 | 44.17 | 44.42 | 38.46 | 39.89 |
| CaO | 3.43 | 2.59 | 2.63 | 1.15 | 1.18 | 3.2 | 2.7 |
| $Na_2O$ | 0.31 | 0.24 | 0.23 | 0.05 | 0.05 | 0.22 | 0.25 |
| $K_2O$ | 0.01 | 0 | 0.01 | 0.01 | 0.01 | 0.01 | 0.02 |
| $P_2O_5$ | 0.015 | 0.016 | 0.016 | 0.012 | 0.012 | 0.012 | 0.014 |
| LOI | 1.35 | 3.36 | 3.14 | 2.25 | 2.08 | 0.19 | 0.58 |
| Cr (ppm) | 2777 | 2290 | 2341 | 2336 | 2416 | 2413 | 2666 |
| Ni (ppm) | 1770 | 1939 | 1965 | 2224 | 2401 | 1890 | 2042 |
| Total | 100.43 | 100.26 | 100.15 | 100.34 | 100.51 | 100.11 | 99.949 |
| $Mg^{\#}$ | 90.11 | 89.80 | 89.71 | 90.93 | 90.91 | 89.09 | 89.94 |
| **Powder Pellets** | | | | | | | |
| Ba | <12 | <12 | | <12 | | <12 | <12 |
| Co | 91 | 98 | | 113 | | 102 | 99 |
| Cr | 2791 | 2292 | | 2196 | | 2442 | 2595 |
| Cu | 28 | 19 | | 7 | | 30 | 24 |
| Ga | 5 | 5 | | 3 | | 5 | 5 |
| Nb | <1.5 | 2.1 | | <1.5 | | <1.5 | <1.5 |
| Ni | 1960 | 1997 | | 2489 | | 2068 | 2106 |
| Pb | <5 | <5 | | <5 | | <5 | <5 |
| Rb | <2 | <2 | | <2 | | <2 | <2 |
| Sc | 15 | 11 | | 11 | | 16 | 17 |
| Sr | 14.4 | 7 | | 7.2 | | 2.9 | 5.8 |
| Th | <4 | <4 | | <4 | | <4 | <4 |
| U | <3 | <3 | | <3 | | <3 | <3 |
| V | 74 | 66 | | 32 | | 77 | 69 |
| Y | 3.9 | 3.9 | | <2 | | 3.7 | 3.9 |
| Zn | 53 | 44 | | 43 | | 49 | 48 |
| Zr | 10 | 10 | | 5 | | 8 | 8 |
| **ID-MS** | | | | | | | |
| La | 0.076 | | | 0.099 | | 0.007 | |
| Ce | 0.445 | | | 0.265 | | 0.095 | 0.135 |
| Nd | 0.539 | | | 0.118 | | 0.343 | 0.279 |
| Sm | 0.230 | | | 0.022 | | 0.202 | 0.152 |
| Eu | 0.085 | | | 0.008 | | 0.078 | 0.056 |
| Gd | | | | | | | |
| Dy | 0.502 | | | 0.025 | | 0.534 | 0.408 |
| Er | 0.346 | | | 0.019 | | 0.394 | 0.324 |
| Yb | 0.367 | | | 0.039 | | 0.404 | 0.339 |
| **Pyrometry** | | | | | | | |
| S | 290 | 181 | | 55 | | 229 | 186 |
| C | 640 | 384 | | 1400 | | 184 | 126 |

**Table C.1** Whole-rock geochemical analyses of the N.E. Pyrenean peridotites

| Sample | 92-LH11 | 92-LH12 | 92-LH12b | 92-LH14 | 92-LH16 | 92-LH17 | 92-LH18 |
|---|---|---|---|---|---|---|---|
| Locality | Lherz | Lherz | Lherz | Lherz | Lherz | Lherz | Lherz |
| **XRF** | | | | | | | |
| **Glass Discs** | | | | | | | |
| $SiO_2$ | 45.73 | 42.19 | 42.7 | 44.84 | 43.82 | 44.74 | 43.78 |
| $TiO_2$ | 0.137 | 0.033 | 0.036 | 0.141 | 0.114 | 0.123 | 0.118 |
| $Al_2O_3$ | 3.46 | 1.08 | 1.15 | 3.7 | 3.27 | 3.51 | 3.2 |
| $Fe_2O_3$ | 7.95 | 9.13 | 9.2 | 8.51 | 8.43 | 8.91 | 8.24 |
| MnO | 0.12 | 0.122 | 0.123 | 0.128 | 0.123 | 0.13 | 0.122 |
| MgO | 37.59 | 44.26 | 44.54 | 36.69 | 38.49 | 39.19 | 38.1 |
| CaO | 3.1 | 0.42 | 0.43 | 3.39 | 2.91 | 2.98 | 2.82 |
| $Na_2O$ | 0.29 | 0.02 | 0.02 | 0.3 | 0.23 | 0.24 | 0.25 |
| $K_2O$ | 0 | 0 | 0 | 0.01 | 0.01 | 0 | 0.02 |
| $P_2O_5$ | 0.017 | 0.019 | 0.016 | 0.017 | 0.016 | 0.018 | 0.017 |
| LOI | 1.31 | 3.24 | 2.49 | 1.96 | 2.17 | 0.29 | 3.14 |
| Cr (ppm) | 2675 | 2552 | 2679 | 2492 | 2627 | 2454 | 2534 |
| Ni (ppm) | 1778 | 2356 | 2368 | 1770 | 1897 | 1890 | 1823 |
| Total | 100.17 | 100.51 | 100.71 | 100.13 | 100.05 | 100.58 | 100.27 |
| $Mg^{\#}$ | 90.35 | 90.57 | 90.56 | 89.52 | 90.04 | 89.70 | 90.16 |
| **Powder Pellets** | | | | | | | |
| Ba | <12 | <12 | | <12 | <12 | <12 | <12 |
| Co | 89 | 118 | | 92 | 96 | 100 | 92 |
| Cr | 2684 | 2376 | | 2564 | 2619 | 2541 | 2481 |
| Cu | 29 | 11 | | 33 | 27 | 32 | 25 |
| Ga | 5 | 3 | | 5 | 5 | 4 | 6 |
| Nb | 1.8 | 1.9 | | 2.4 | 2.1 | 2 | 1.9 |
| Ni | 1985 | 2489 | | 1960 | 2089 | 2117 | 1989 |
| Pb | <5 | <5 | | <5 | <5 | <5 | <5 |
| Rb | <2 | <2 | | <2 | <2 | <2 | <2 |
| Sc | 15 | 5 | | 14 | 14 | 16 | 14 |
| Sr | 12.9 | 1.2 | | 11.1 | 8.7 | 8.9 | 12.9 |
| Th | <4 | <4 | | <4 | <4 | <4 | <4 |
| U | <3 | <3 | | <3 | <3 | <3 | <3 |
| V | 79 | 26 | | 78 | 75 | 75 | 66 |
| Y | 3.9 | <2 | | 4.5 | 3.2 | 2.8 | 3.1 |
| Zn | 46 | 45 | | 47 | 49 | 50 | 45 |
| Zr | 12 | 6 | | 11 | 10 | 10 | 12 |
| **ID-MS** | | | | | | | |
| La | 0.224 | 0.018 | | 0.138 | | 0.053 | |
| Ce | 0.783 | 0.075 | | 0.725 | | 0.344 | |
| Nd | 0.766 | 0.064 | | 0.698 | | 0.483 | |
| Sm | 0.276 | 0.023 | | 0.273 | | 0.217 | |
| Eu | 0.103 | 0.009 | | 0.088 | | | |
| Gd | | | | | | 0.373 | |
| Dy | 0.534 | 0.059 | | 0.600 | | 0.514 | |
| Er | 0.371 | 0.048 | | 0.418 | | 0.363 | |
| Yb | 0.376 | 0.068 | | | | | |
| **Pyrometry** | | | | | | | |
| S | 304 | 7 | | | 149 | 210 | 307 |
| C | 301 | 420 | | | 670 | 205 | 945 |

**Table C.1 (cont.)** Whole-rock geochemical analyses of the N.E. Pyrenean peridotites

| Sample | 92-LH19 | 92-LH3 | 92-PG1 | 92-PG2 | 92-PR1 | 92-PR1b |
|---|---|---|---|---|---|---|
| Locality | Lherz | Lherz | Pic de Géral | Pic de Géral | Prades | Prades |
| **XRF** | | | | | | |
| **Glass Discs** | | | | | | |
| $SiO_2$ | 44.4 | 43.88 | 41.98 | 44.12 | 43.78 | |
| $TiO_2$ | 0.126 | 0.084 | 0.097 | 0.063 | 0.114 | |
| $Al_2O_3$ | 3.51 | 2.52 | 3 | 2.04 | 3.1 | |
| $Fe_2O_3$ | 8.38 | 8.28 | 8.2 | 8.49 | 8.66 | |
| MnO | 0.127 | 0.118 | 0.12 | 0.124 | 0.128 | |
| MgO | 37.06 | 40.52 | 37.3 | 42.57 | 39.13 | |
| CaO | 3.16 | 2.14 | 2.46 | 1.78 | 2.71 | |
| $Na_2O$ | 0.28 | 0.18 | 0.21 | 0.12 | 0.22 | |
| $K_2O$ | 0.01 | 0.02 | 0 | 0 | 0.01 | |
| $P_2O_5$ | 0.016 | 0.016 | 0.015 | 0.011 | 0.018 | |
| LOI | 2.9 | 2.39 | 6.54 | 0.68 | 2.17 | |
| Cr (ppm) | 2704 | 2225 | 2345 | 2627 | 2434 | |
| Ni (ppm) | 1801 | 1937 | 1928 | 2026 | 1931 | |
| Total | 100.45 | 100.59 | 100.36 | 100.47 | 100.5 | |
| $Mg^{\#}$ | 89.75 | 90.65 | 90.01 | 90.85 | 89.95 | |
| **Powder Pellets** | | | | | | |
| Ba | <12 | <12 | <12 | <12 | <12 | <12 |
| Co | 92 | 97 | 95 | 104 | 99 | 99 |
| Cr | 2666 | 2180 | 2160 | 2554 | 2512 | 2470 |
| Cu | 28 | 17 | 26 | 17 | 31 | 30 |
| Ga | 4 | 5 | 4 | 4 | 4 | 4 |
| Nb | <1.5 | <1.5 | <1.5 | <1.5 | <1.5 | 1.6 |
| Ni | 1965 | 2166 | 2038 | 2309 | 2120 | 2141 |
| Pb | <5 | <5 | <5 | <5 | <5 | <5 |
| Rb | <2 | <2 | <2 | <2 | <2 | <2 |
| Sc | 15 | 11 | 14 | 10 | 15 | 15 |
| Sr | 12.9 | 18.5 | 8.7 | 4.8 | 7.2 | 6.7 |
| Th | <4 | <4 | <4 | <4 | <4 | <4 |
| U | <3 | <3 | <3 | <3 | <3 | <3 |
| V | 77 | 55 | 59 | 49 | 68 | 68 |
| Y | 3.5 | <2 | 3.3 | <2 | 3.9 | 2.6 |
| Zn | 48 | 43 | 42 | 44 | 44 | 46 |
| Zr | 11 | 9 | 8 | 7 | 10 | 10 |
| **ID-MS** | | | | | | |
| La | | | | 0.080 | | |
| Ce | | 0.355 | | 0.264 | | |
| Nd | | 0.345 | | 0.256 | | |
| Sm | | 0.134 | | 0.097 | | |
| Eu | | 0.042 | | 0.038 | | |
| Gd | | | | | | |
| Dy | | 0.290 | | 0.217 | | |
| Er | | 0.209 | | 0.155 | | |
| Yb | | 0.228 | | 0.175 | | |
| **Pyrometry** | | | | | | |
| S | 365 | 264 | – | 85 | 170 | |
| C | 786 | 1062 | 435 | 204 | 500 | |

**Table C.1 (cont.)** Whole-rock geochemical analyses of the N.E. Pyrenean peridotites

# Appendix D

# Petrography of the N.E. Pyrenean Peridotite Samples

The mineral abundances were estimated from thin sections and hand specimens of the samples collected from the N.E. Pyrenean massifs. In all samples the olivine and orthopyroxene content lay in the range 60 - 70% and 20 - 25% respectively. Textures are given according to the classification scheme of Mercier & Nicholas (1975).

Abbreviations: Cpx = clinopyroxene, Sp = spinel, Amph = amphibole

## Freychinède

92-FR3 Protogranular, cpx-rich lherzolite containing relatively abundant intergranular sulphides, green-brown spinel and rare amph. Slight serpentinisation has destroyed much of the finer detail. (15% cpx, 5% sp, trace amph)

92-FR4 Intensely serpentinised lherzolite, possibly originally possessing a protogranular texture. Common intergranular sulphide grains and green-brown spinel. Alteration obscures much of the detail. (7% cpx, 3% sp)

## Fontête Rouge

92-FT5 Protogranular harzburgite containing rare brown spinels. No visible intergranular sulphides. Rare 2 mm thick serpentinite veins containing abundant angular mineral fragments. (3% cpx, <1% sp)

92-FT6 Protogranular lherzolite containing abundant sulphide grains, both as intergranular minerals and inclusions within silicate mineral grains. Brown-green spinels, often associated with more pyroxene-rich regions. (12% cpx, 5% sp)

92-FT7 Protogranular lherzolite containing olive-green spinels and relatively fresh intergranular sulphide grains. Rare, pale-brown amphiboles. (10% cpx, 5% sp)

## Lherz

92-LH3 Slightly altered porphyroclastic cpx-poor lherzolite with serpentine and calcite-filled veins. Olive-green spinel and abundant oxide or hydroxide grains, possibly after sulphides. (5% cpx, 3% sp)

92-LH11 Porphyroclastic lherzolite containing common sulphide grains, both as an intergranular component and as mineral inclusions, rare green-brown spinels and occasional serpentine veins. (10% cpx, 2% sp)

92-LH12 Moderately altered harzburgite, possibly originally possessing a protogranular texture. (3% cpx, 2% sp)

92-LH14 Porphyroclastic lherzolite containing intergranular sulphides and relatively rare, pale brown spinels in distinct groups. Mineral grains commonly ≥ 2 mm. (10 - 15% cpx, 2% sp)

92-LH16 Moderately altered porphyroclastic lherzolite containing common serpentine veins. Predominantly coarse-grained, but common strained or fragmented grains (10% cpx, 3% sp)

92-LH17 Moderately fresh porphyroclastic lherzolite containing green-brown spinels and rare amph. Sulphide minerals common, both as intergranular grains and as inclusions (7% cpx, 5% sp, trace amph)

92-LH18 Porphyroclastic lherzolite exhibiting intense alteration and common serpentine veins. (10% cpx, 3% sp)

92-LH19 Moderately altered, protogranular cpx-rich lherzolite containing brown-green spinel and relatively abundant intergranular sulphide grains. (12% cpx, 5% sp)

## Pic de Géral

92-PG1 Intensely altered lherzolite with abundant green spinels and rare amph. Possible protogranular texture prior to alteration. (10% cpx, 7% sp, trace amph)

92-PG2 Protogranular cpx-poor lherzolite containing dark-brown spinels and common sulphide inclusions. Very fresh. (5% cpx, 5% sp)

## Prades

92-PR1 Protogranular cpx-rich lherzolite containing dispersed mid-brown spinel grains and common pale-brown amphibole. Moderately altered. (15% cpx, 5% sp, 1% amph)

# Appendix E

# Sample Management Table

Table E.1 summarises the details of the rocks collected for this study and currently being held at the Open University. It includes data concerning the date of collection, the sampling location and the important petrological features. Although other samples of peridotite and pyroxenite from the Pyrenean massifs were also collected as part of this study, their details are not reported in Table E.1, either on account of their large degrees of alteration (leading their not being analysed), or because no study of the pyroxenites was eventually undertaken.

| Sample Identifier | Rock Type | Rock Sub-type | Description and Special Features of Sample |
|---|---|---|---|
| 92-FR 3 | Peridotite | Lherzolite | Protogranular texture, trace amphibole |
| 92-FR 4 | Peridotite | Lherzolite | Intensely serpentinised |
| 92-FT 5 | Peridotite | Lherzolite | Cpx-poor, protogranular texture |
| 92-FT 6 | Peridotite | Lherzolite | Protogranular texture |
| 92-FT 7 | Peridotite | Lherzolite | Protogranular texture |
| 92-LH 3 | Peridotite | Lherzolite | Porphyroclastic with calcite-filled veins |
| 92-LH 11 | Peridotite | Lherzolite | Porphyroclastic texture |
| 92-LH 12 | Peridotite | Lherzolite | Cpx-poor, possibly originally protogranular |
| 92-LH 14 | Peridotite | Lherzolite | Cpx-rich |
| 92-LH 16 | Peridotite | Lherzolite | Porphyroclastic with abundant serpentine veins |
| 92-LH 17 | Peridotite | Lherzolite | Porphyroclastic texture |
| 92-LH 18 | Peridotite | Lherzolite | Intensely altered, with porphyroclastic texture |
| 92-LH 19 | Peridotite | Lherzolite | Moderately altered, with protogranular texture |
| 92-PG 1 | Peridotite | Lherzolite | Intensely altered, with metasomatic amphibole |
| 92-PG 2 | Peridotite | Lherzolite | Cpx-poor, with protogranular texture |
| 92-PR 1 | Peridotite | Lherzolite | Moderately altered, protogranular texture |

| Sample Identifier | Place of Origin | Description of Locality | Date Collected |
|---|---|---|---|
| 92-FR 3 | 42°48'N 1°26'E | Freychinède (200 m NNW of glade) | Jul-1992 |
| 92-FR 4 | 42°48'N 1°26'E | Freychinède (250 - 300 m N of glade) | Jul-1992 |
| 92-FT 5 | 42°48'N 1°24'E | Fontête Rouge (at peak) | Jul-1992 |
| 92-FT 6 | 42°48'N 1°24'E | Fontête Rouge (50 m W of peak) | Jul-1992 |
| 92-FT 7 | 42°48'N 1°24'E | Fontête Rouge (20 m SW of peak) | Jul-1992 |
| 92-LH 3 | 42°48'N 1°23'E | Lherz (NE part of massif below zone of harzburgite / amphibole pyroxenite layering) | Jul-1992 |
| 92-LH 11 | 42°48'N 1°23'E | Lherz (300 m due S of island) | Jul-1992 |
| 92-LH 12 | 42°48'N 1°23'E | Lherz (400 m SW of island) | Jul-1992 |
| 92-LH 14 | 42°48'N 1°23'E | Lherz (200 m E of l'Estagnon) | Jul-1992 |
| 92-LH 16 | 42°48'N 1°23'E | Lherz (E shore of l'Estagnon) | Jul-1992 |
| 92-LH 17 | 42°48'N 1°23'E | Lherz (150 m S of bridge over stream) | Jul-1992 |
| 92-LH 18 | 42°48'N 1°23'E | Lherz (next to road, on bend) | Jul-1992 |
| 92-LH 19 | 42°48'N 1°23'E | Lherz (next to road, close to café) | Jul-1992 |
| 92-PG 1 | 42°47'N 1°51'E | Pic de Géral (S slope) | Jul-1992 |
| 92-PG 2 | 42°47'N 1°51'E | Pic de Géral (crest of ridge) | Jul-1992 |
| 92-PR 1 | 42°47'N 1°51'E | Prades (SW end of massif) | Jul-1992 |

**Table E.1** Simplified sample management table for the Pyrenean samples used during this study